UNIVERSIDAD DE GRANADA

ADAMTS proteases and uveal melanoma: unveiling the contribution of ADAMTS1 to the plasticity of tumor cells.

PROGRAMA DE DOCTORADO EN BIOMEDICINA (B11.56.1)

Doctoral Thesis

Tesis Doctoral

Carlos Peris Torres

Thesis supervisor // Director de Tesis

Juan Carlos Rodríguez-Manzaneque Escribano

Granada, XX de XX de 20XX

Genyo PFIZER-UNIVERSIDAD DE GRANADA-JUNTA DE ANDALUCÍA
CENTRE FOR GENOMICS AND ONCOLOGICAL RESEARCH

Editor: Universidad de Granada. Tesis Doctorales
Autor: Carlos Peris Torres
ISBN: 978-84-1306-752-0
URI: http://hdl.handle.net/10481/66398

TABLE OF CONTENTS

FIGURES INDEX

TABLES INDEX

BOXES INDEX

ABBREVIATIONS AND ACRONYMS

SHORTENED FORM	DEFINITION
2D	bidimensional
3D	tridimensional
ACAN	aggrecan
ADAM	a disintegrin and metalloprotease
ADAMTS	a disintegrin and metalloprotease with thrombospondin motifs
ADAMTS1	a disintegrin and metalloprotease with thrombospondin motifs 1
ATS1-KO	ADAMTS1-knock out
BM	basement membrane
CAFs	cancer-associated fibroblasts
CD133	cluster of differentiation molecule 133
CDH5	cadherin-5
cDNA	complementary deoxyribonucleic acid
CM	conditioned medium
CRISPR/Cas9	Clustered Regularly Interspaced Short Palindromic Repeats/CRISPR-associated 9
CRISPR	Clustered Regularly Interspaced Short Palindromic Repeats
CSC	cancer stem cell
Ct	cycle threshold
DAPI	4′,6-diamidino-2-phenylindole
ddH2O	double-distilled water
DEG	differentially expressed gene
DNA	deoxyribonucleic acid
DSB	double strand break
ECM	extracellular matrix
EGF	epidermal growth factor
EL	endothelial-like
EMCN	endomucin
ENG	endoglin
EPC	endothelial precursor cell
EPHA2	ephrin type-A receptor 2
EtOH	ethanol
FBS	fetal bovine serum
FDR	false discovery rate
FGF-2	fibroblast growth factor 2

GEO	Gene Expression Omnibus
GFP	green fluorescent protein
GO	Gene Ontology
GSC	glioma stem cell
HEK293T	human embryonic kidney 293T (cell line)
HOPP	Heuristic Online Phenotype Prediction algorithm
HR	homologous recombination
HUVEC	human umbilical vein endothelial cell
IF	immunofluorescence.
IGFBP2	insulin like growth factor binding protein 2
IHC	Immunohistochemistry
IIC	infiltrating immune cell
IIH	intertumor or intrapatient heterogeneity
IPH	interpatient heterogeneity
iPSCs	induced pluripotent stem cells
IQR	interquartile range
ITH	intratumor heterogeneity
kDa	kiloDalton
KDR	vascular endothelial growth factor 2
KO	knockout
LAMC2	laminin subunit gamma-2
MMP	matrix metralloprotease
mRNA	messenger ribonucleic acid
NANOG	Nanog homeobox
NHEJ	non-homologous end joining
NID1	nidogen 1
NID2	nidogen 2
NK	natural killer
NSG	NOD scid gamma
p	p-value
PAS	periodic acid-Schiff
PBS	Phosphate-buffered saline
PBS-T	PBS 0,5 % tween
PCR	polymerase chain reaction
PECAM1	platelet endothelial cell adhesion molecule
Pen-Strep	Penicillin-Streptomycin solution
POU5F1	POU class 5 homeobox 1
PROM1	prominin-1
Q1	quartile 1
Q3	quartile 3

qPCR	quantitative polymerase chain reaction
RCF	relative centrifugal force
rhATS1	recombinant human ADAMTS1
RNA	ribonucleic acid
RNA-Seq	ribonucleic acid sequencing
RT	room temperature
SD	standard deviation
SEM	standard error of the mean
shRNA	short hairpin ribonucleic acid
SKCM	skin cutaneous melanoma
SOX2	Sex-determining region Y-box transcription factor 2
STR	short tandem repeat
SwN	Swiss Nude
TCGA	The Cancer Genome Atlas
TCGA-UVM	The Cancer Genome Atlas Uveal Melanoma project
TEK	angiopoietin-1 receptor
TFPI	tissue factor pathway inhibitor
THBD	thrombomodulin
TIE1	tyrosine kinase with immunoglobulin like and epidermal growth factor like domains 1
TME	tumor microenvironment
TSR	thrombospondin motif
UCSC Xena	University of California, Santa Cruz, Xena data portal
UGR	University of Granada
UVM	uveal melanoma
VCAN	versican
VM	vasculogenic mimicry
vWF	von-Willebrand factor
WT	wild type

RESUMEN

Los tumores están compuestos no sólo por una masa de células heterogéneas que crecen sin control, sino también por el entorno que crean durante su crecimiento, conocido todo ello como microambiente tumoral. El componente no celular de este microentorno, constituido mayoritariamente por la matriz extracelular, ha sido reconocido como un elemento dinámico crucial debido a su íntima relación con las células cancerosas, afectando al desarrollo tumoral y a la metástasis. De manera particular, el estudio de la remodelación de esta matriz, mediada por proteasas extracelulares, sigue revelando una amplia gama de acciones tanto pro- como anti-tumorigénicas.

El conocimiento de las acciones de la proteasa extracelular ADAMTS1 (del inglés "*A Disintegrin And Metalloproteinase with ThromboSpondin motifs 1*") ejemplifica ese doble papel. En línea con la experiencia de este laboratorio en la proteasa ADAMTS1, la presente tesis es un paso más en la comprensión de sus funciones, con la particularidad de desarrollarse en torno al melanoma y, más concretamente, un subtipo raro: el melanoma uveal. Con tal objetivo global, este trabajo presenta diferentes aproximaciones.

En primer lugar, se realizó una completa caracterización *in vitro* e *in silico* de líneas celulares de melanoma humano, con especial atención a la relación de ADAMTS1 y la adquisición por parte de las células cancerosas de un fenotipo similar al de células endoteliales, denominado *endothelial-like*. Este fenómeno reflejaría la capacidad de células tumorales para transdiferenciarse y "mimetizar" las células endoteliales, y está correlacionado con tumores más agresivos y de peor pronóstico clínico. Resultados de esta tesis confirman una correlación positiva de la expresión de ADAMTS1 con el fenotipo *endothelial-like* de células de melanoma humano, así como la estrecha asociación que esta proteasa muestra con genes clave en dicho fenotipo como la cadherina endotelial *CDH5*.

Además, este trabajo demuestra que ADAMTS1 es esencial para el crecimiento tumoral, ya que su inhibición mediante la tecnología CRISPR/Cas9 en células de melanoma uveal (MUM-2B) provocó un bloqueo drástico de la progresión de xenógrafos tumorales en diferentes modelos

murinos. Los tumores deficientes en ADAMTS1 mostraron importantes alteraciones de su vasculatura, y de manera más relevante se encontró una reducción en la expresión de *CDH5* en las células tumorales. Adicionalmente esta alteración se encontró asociada con la expresión de marcadores de células madre del cáncer o *stemness*. En este punto es importante destacar que las características *stemness* están íntimamente ligadas al fenotipo *endothelial-like* y a las capacidades de iniciación de los tumores, por lo que aquí se revela un papel esencial de ADAMTS1 para ambos procesos. De hecho, la realización de reconocidos ensayos con esferas derivadas de células de melanoma mostró una capacidad insuficiente para formar tales esferas en ausencia de ADAMTS1. Igualmente, este trabajo muestra una correlación directa de la deficiencia en estos procesos con la disminución de marcadores *stemness* y, notablemente, también de *CDH5*.

Por último, haciendo uso de herramientas bioinformáticas avanzadas y beneficiándose de datos disponibles públicamente sobre melanomas uveales (proyecto *The Cancer Genome Atlas*, TCGA), en esta tesis se han identificado nuevos factores de pronóstico destacando moléculas endoteliales como *CDH5* y *KDR* y varios miembros de la familia de proteasas ADAMTS. Un análisis detallado también reveló una alta expresión de *ADAMTS1* en estadios iniciales del melanoma uveal, confirmando la contribución de esta proteasa en fenómenos de inducción de las capacidades *stemness* y del fenotipo *endothelial-like* de células tumorales. De manera adicional, un estudio más amplio de proteasas ADAMTS sugirió el papel de otros miembros de la familia a lo largo de toda la progresión de este agresivo tipo tumoral.

Todos estos resultados conducen a la conclusión general de que ADAMTS1 es necesaria para un desarrollo adecuado del melanoma uveal, ya que contribuye a la adquisición de un fenotipo *endothelial-like* y afecta a los rasgos *stemness*, sin ignorar su función principal como moduladora de la matriz extracelular. El trabajo mostrado en esta tesis representa el primer testimonio que apoya el desarrollo de dianas terapéuticas dirigidas a la matriz extracelular en la lucha contra el melanoma uveal.

ABSTRACT

Tumors are composed not only by a mass of heterogeneous cells that grow out of control, but also by the environment created during their growth, everything commonly known as tumor microenvironment. The non-cellular component of this microenvironment, constituted mostly by the extracellular matrix, has been recognized as a crucial dynamic element due to its intimate crosstalk with cancer cells, affecting tumor development and metastasis. Particularly, the study of the remodeling of this matrix, mediated by extracellular proteases, keeps revealing a wide range of both pro- and anti-tumorigenic actions.

The knowledge of the actions of the extracellular protease ADAMTS1 (A Disintegrin And Metalloproteinase with ThromboSpondin motifs 1) exemplifies this dual role. In line with the experience of this laboratory in ADAMTS1 protease, the present thesis is a further step for the comprehension of its functions, with the particularity of being developed in relation to melanoma and, more precisely, to a rare subtype: uveal melanoma. With such global objective, this work reports different approaches.

First of all, a complete *in vitro* and *in silico* characterization of human melanoma cell lines was conducted, with special attention to the relationship of ADAMTS1 with the acquisition by cancer cells of an endothelial-like phenotype. This phenomenon would reflect the capacity of tumor cells to transdifferentiate and "mimic" endothelial cells, and it is correlated with more aggressive and worse clinical prognosis tumors. Results included in this thesis confirms a positive correlation of ADAMTS1 expression with the endothelial-like phenotype of human melanoma cells, as well as the close association that this protease shows with key genes for that phenotype such as endothelial cadherin *CDH5*.

Furthermore, this work demonstrates that ADAMTS1 is essential for tumor growth, since its inhibition by CRISPR/Cas9 technology in uveal melanoma cells (MUM-2B) caused a drastic blockade of tumor xenograft progression in different murine models. ADAMTS1-deficient tumors showed significant alterations in their vasculature, and most relevantly they revealed the downregulation of *CDH5* in tumor cells. Additionally, this alteration was

found to be associated with the expression of cancer stemness markers. At this point it is important to remark that stemness features are closely linked to endothelial-like phenotype and tumor-initiating capacities, so an essential role of ADAMTS1 for both processes is revealed here. Indeed, recognized assays with spheres derived from melanoma cells also showed an insufficient capacity to form such spheres in the absence of ADAMTS1. Likewise, this work demonstrates a direct correlation of the deficiency in these processes with the decrease of stemness markers and, remarkably, also of *CDH5*.

Finally, using advanced bioinformatics tools and taking advantage of publicly available data of uveal melanomas (The Cancer Genome Atlas, TCGA), new prognostic factors were identified in this thesis, highlighting endothelial molecules such as *CDH5* and *KDR* and several members of the ADAMTS family of proteases. A detailed analysis also uncovered a high expression of *ADAMTS1* at early stages of uveal melanoma, confirming the contribution of this protease to phenomena of induction of stemness features and of endothelial-like phenotype in tumor cells. Additionally, a broader study of ADAMTS proteases suggested the role of other members of the family throughout the progression of this aggressive cancer subtype.

All these results lead to the general conclusion that ADAMTS1 is necessary for an adequate development of uveal melanoma, since it contributes to the acquisition of an endothelial-like phenotype and affects stemness features, without ignoring its main function as an extracellular matrix modulator. The work shown in this thesis represents the first evidence that supports the development of therapeutic targets directed to the extracellular matrix in the fight against uveal melanoma.

INTRODUCTION

1. The heterogeneity of cancer

Cancer is a very heterogeneous disease. Nevertheless, although it is now widely considered, the heterogeneity of cancer has only been considered during the last three decades. Accordingly, the previous paradigm about tumors being mere clusters of relatively homogeneous cancer cells has been deeply reviewed (Hanahan and Weinberg, 2000, 2011). It has been extensively described that tumors are conformed by different types of cells (Figure 1), comprising specific genomes, epigenomes, transcriptomes, proteomes, different angiogenic, proliferative, immunogenic and metastatic potentials and other phenotypic features (Marusyk and Polyak, 2010).

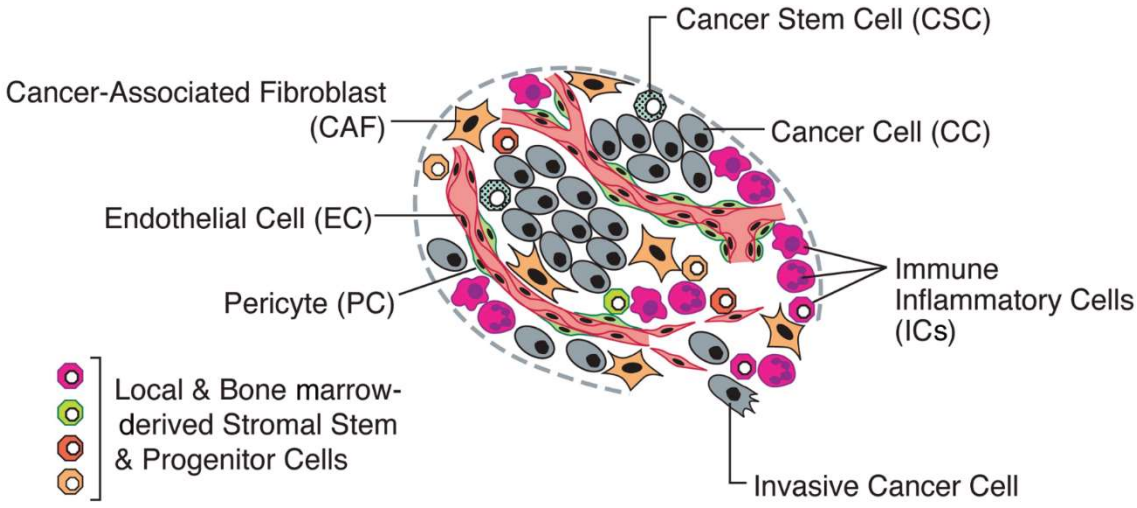

Figure 1. Tumors are conformed by different types of cells.
Most solid tumors are composed by different cell types that contribute to tumor progression and metastasis. Besides cancer and cancer stem cells it is important to note the infiltrated immune inflammatory cells and cancer-associated fibroblasts, as well as endothelial cells that generate tumor vasculature and pericytes that support it. Modified from (Hanahan and Weinberg, 2011)

This conception of tumors as heterogeneous and complex tissues composed of multiple cell types that interact between them was the base for Hanahan and Weinberg to propose the hallmarks of cancer in their two seminal works (Hanahan and Weinberg, 2000, 2011). To date, these hallmarks comprise ten functional capabilities that tumors acquire during tumorigenesis that will be summarized in the following lines (and illustrated in Figure 2). In their first work, these authors proposed six hallmarks (Hanahan and Weinberg, 2000),

initiating the list with the fundamental *sustaining proliferative signaling*. Cancer cells reach this hallmark either by growth factor production or sending signals to stimulate normal cells within the supporting tumor-associated stroma. Cancer cells also need to inactivate tumor suppressors which limit cell growth and proliferation, therefore *evading growth suppressors*. *Resisting cell death* is a third hallmark, characterized by the attenuation of apoptosis (which serves as a natural barrier to cancer development), as well as *enabling replicative immortality*, which allows cancer cells to evade cell senescence and death by affecting the telomere function. Since tumors need an associated vasculature to provide nutrients and oxygen and evacuate metabolic wastes and carbon dioxide, the fifth hallmark is their capacity of *inducing angiogenesis*. A whole section will subsequently be dedicated to this hallmark according to its relevance for this work. The last of these hallmarks correspond to *activating invasion and metastasis* through the invasion-metastasis cascade i. e., alterations in cell shape, attachment to other cells and to the extracellular matrix. In 2011, Hanahan and Weinberg updated their original contribution with two emerging hallmarks and two enabling characteristics (causally associated with the acquisition of hallmarks capabilities) (Hanahan and Weinberg, 2011). The first group includes *deregulating cellular energetics* through energy metabolism adjustments that support cell growth and division, and *avoiding immune destruction*, which implies the still unsolved major issue of the dichotomous role of the immune system in cancer development (sometimes enhancing and sometimes preventing it). Finally, these authors added two enabling characteristics that were crucial to the acquisition of all the aforementioned hallmarks. They were *genome instability and mutation*, which could confer selective advantages and dominance of certain subclones of cells in a local tissue environment, and *tumor-promoting inflammation*, which supplies bioactive molecules to the tumor microenvironment and therefore contributes to multiple hallmark capabilities.

These and many other works have contributed to the current understanding of cancer, enabling the identification of three different levels of tumor heterogeneity named intratumor, intertumor and interpatient (Figure 3).

Intratumor heterogeneity (ITH) refers to the coexistence of cells with different phenotypic and molecular features within a tumor (Grzywa et al., 2017) (Figure 3a). It rises through a Darwinian-like tumor evolution, accumulating stochastic mutations as a result of cell proliferation and increased genomic instability, as well as through the selective pressure that tumor microenvironment exerts over tumor cells (Marusyk and Polyak, 2010; Polyak et al., 2009).

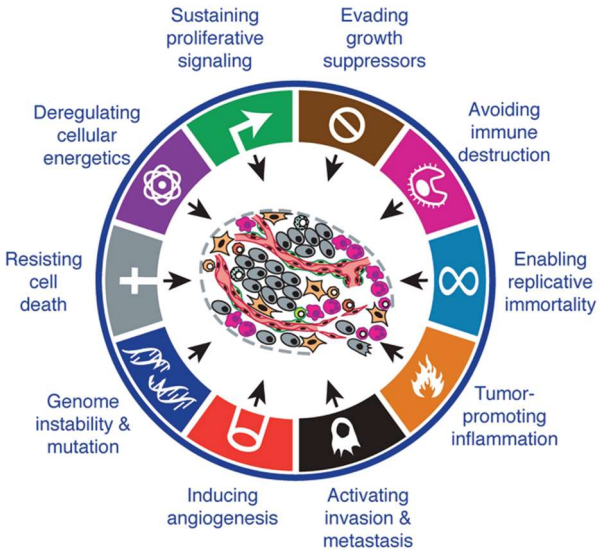

Figure 2. The hallmarks of cancer.
Hanahan and Weinberg defined ten capabilities that tumors acquire during tumorigenesis. In an initial work they proposed six of them: sustaining proliferative signaling, evading growth suppressors, enabling replicative immortality, activating invasion and metastasis, inducing angiogenesis and resisting cell death. More than ten years after, they completed this list of ten hallmarks of cancer with avoiding immune destruction, tumor-promoting inflammation, genome instability and mutation and deregulating cellular energetics. Modified from (Hanahan and Weinberg, 2011)

Intertumor or intrapatient heterogeneity (IIH) refers to the presence, in one patient, of significantly different tumors that came from the same origin (Grzywa et al., 2017) (Figure 3b). It is particularly relevant in metastatic lesions, since the higher rate of intermetastatic heterogeneity makes it difficult to eradicate all metastatic lesions by surgery and therefore to ensure patient survival (Vogelstein et al., 2013). In reality, this intertumor heterogeneity is caused and enhanced by intratumor variations, since every metastatic tumors may arise from different subpopulations of founder tumor cells (Grzywa et al., 2017).

The third level is interpatient heterogeneity (IPH), that includes the differences among tumors between different patients (Grzywa et al., 2017) (Figure 3c). It provokes that different patients with the same tumor type may show different imaging and histological features, as well as different response to the same treatment (Alessandrino et al., 2019).

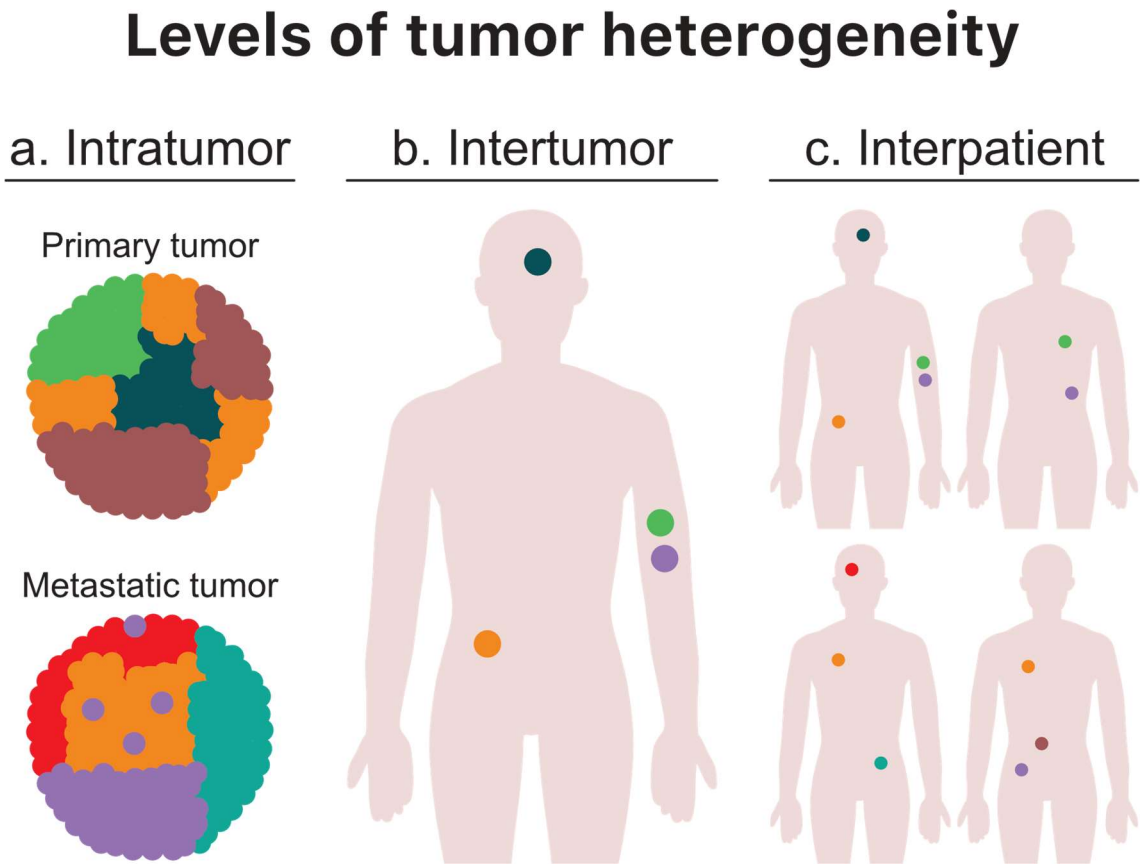

Figure 3. The three levels of tumor heterogeneity.
Three levels of heterogeneity have been described for solid tumors: (**a**) intratumor (differences among tumor cells), (**b**) intertumor or intrapatient (differences between primary tumor and metastases or among metastases), and (**c**) interpatient (differences among tumors from distinct patients). Adapted from (Grzywa et al., 2017) with the help of macrovector (Freepik).

Intratumor heterogeneity, and therefore the rest of heterogeneity levels, have been widely pointed as the consequence of proposing two different models (Thankamony et al., 2020). On one hand, the clonal evolution theory explains that the fitter tumor clones are selected and generate tumor heterogeneity (Figure 4a). In this clonal selection, tumor microenvironment (TME) is critical since it could influence the outcome of tumor clones, depending on the specific niche in which they develop. On the other hand,

the Cancer Stem Cell model proposes that there exists a subset of tumor cells with stem-like properties which are the main drivers of tumor progression (Figure 4b). These highly plastic cancer stem cells (CSCs) are able to differentiate into different cell types supporting tumor heterogeneity.

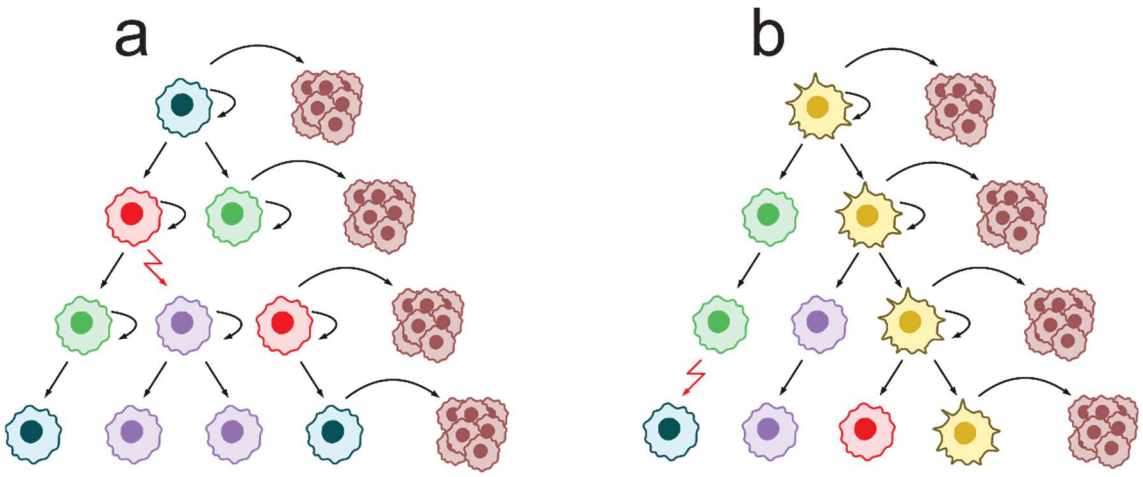

Figure 4. Two general models to explain the origin of heterogeneity of solid tumors.

(**a**) Clonal evolution model of heterogeneity, according to which all cancer cells are highly proliferative and are able to initiate tumors if the microenvironment is appropriate. (**b**) Cancer Stem Cell (CSC) model, which proposes that only a subpopulation of stem-like cells (represented here in yellow) is responsible for tumor cell heterogeneity and the initiation of new tumors. Modified from (Reya et al., 2001).

Both clonal selection and CSC models are not mutually exclusive. In fact, in this work they will be studied together as two interconnected possibilities that take part of the same overall tumor growth process. However, the main features of these complex models will be introduced separately, starting with the tumor microenvironment, the molecules and processes related with it, and the effect that it exerts on tumor growth. Afterwards, the concept and characteristics of CSCs will be introduced, to finally describe the aforementioned connection with the TME that occurs in the phenomenon known as vasculogenic mimicry.

2. Tumor microenvironment

As previously described, the conception of tumors as complex heterotypic organs changed the paradigm of cancer research, since it helped to understand the tumor biology not only by the study of the specialized cells that shape them, but also by the evaluation of the tumor microenvironment that they create during tumor growth (Hanahan and Weinberg, 2011). It is composed by cells of different types and extracellular components which surround them (Figure 5), and whose intimate crosstalk is a key player during tumor development and metastasis (Vitale et al., 2019; Wu and Dai, 2017).

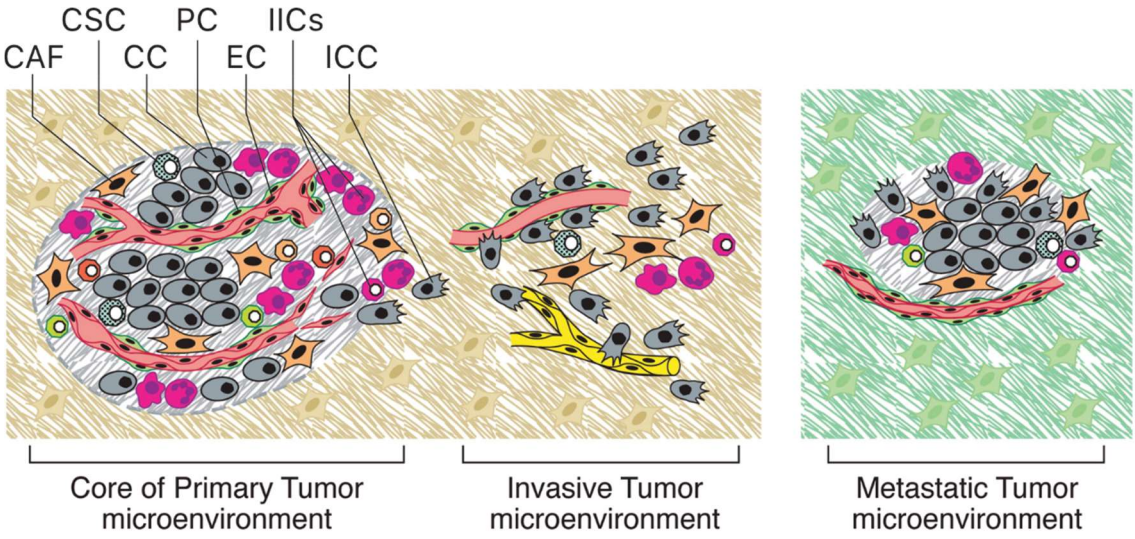

Figure 5. Different types of tumor microenvironments.
Tumor microenvironment is modulated by the changes exerted by tumor cells. The primary tumor microenvironment changes when cancer cells invade normal tissue and also when they further colonize distant locations (metastasis). CAF: cancer-associated fibroblast. CSC: cancer stem cell. CC: cancer cell. PC: pericyte. EC: endothelial cell. IICs: infiltrating immune cells. ICC: invasive cancer cell. Modified from (Hanahan and Weinberg, 2011).

This important function could not be developed without the vascular network that supports and feeds the tumor and removes its waste, as it will be described in later sections of this work. Tumor microenvironment is extremely dynamic, providing specific signals that support cell invasion, proliferation and phenotypic plasticity (Arozarena and Wellbrock, 2019) during tumor initiation, progression, and metastasis. The continuous crosstalk between tumor cells and the surrounding microenvironment also mediates drug resistance and affects therapeutic efficacy, so its full

understanding requires a multilayered research to identify new targets and biomarkers (Mushtaq et al., 2018; Wu and Dai, 2017). In 2012, Hanahan and Coussens reviewed the contribution of the cellular component of tumor microenvironment to cancer development (Hanahan and Coussens, 2012). They grouped the stromal component into three classes which will be briefly described next: angiogenic vascular cells, infiltrating immune cells and cancer-associated fibroblastic cells (Figure 6). In addition, these authors also reviewed the roles that these stromal cells play on the different hallmarks of cancer (Figure 7).

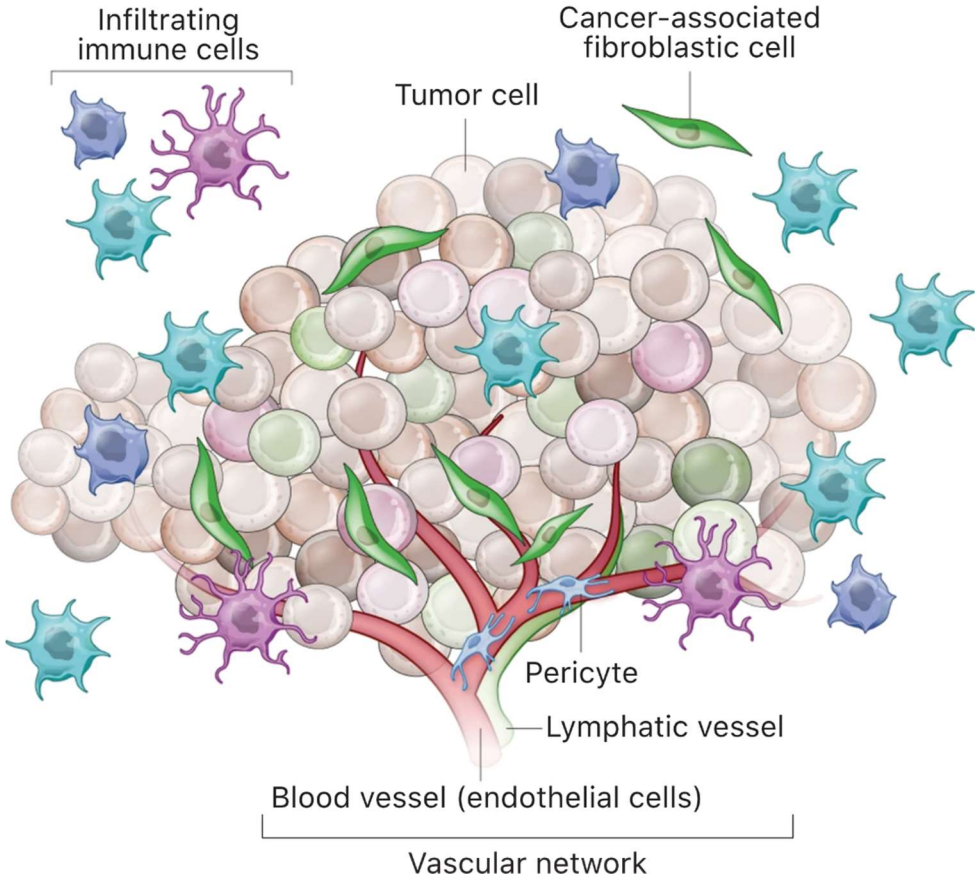

Figure 6. Cellular components of the tumor stroma.
The stromal cell component of the TME can be classified into three types: angiogenic vascular cells (endothelial cells and pericytes), infiltrating immune cells and cancer-associated fibroblastic cells). Modified from (Junttila and De Sauvage, 2013).

Angiogenic vascular cells

This class included endothelial cells, which constitute the vasculature, and pericytes that support it. Although vascularization prevents cell death from hypoxia or lack of nutrients, tumors usually present an aberrant vasculature

which also contributes to tumor progression. For example, impaired vascular integrity, often caused by loss of pericytes coverage, facilitates dissemination of cancer cells from primary human tumors (Cooke et al., 2012). This tumor aberrant vasculature also alters the arrival of immune cells that would be necessary to end up with the tumor (Hanahan and Coussens, 2012).

Infiltrating immune cells

Virtually all solid tumors present infiltrates of both innate (macrophages, mast cells, neutrophils, dendritic cells, myeloid derived suppressor cells and natural killer cells) and adaptive (T and B lymphocytes) immune cells which affect tumor microenvironment either by direct contact or by chemokines and cytokines releasing (Hanahan and Coussens, 2012; Wu and Dai, 2017). Tumor-associated macrophages are probably the most studied population of infiltrating immune cells (IICs), being involved in protection against chemotherapy, regulation of tumor angiogenesis through VEGF-A production and subsequent resistance to anti-angiogenic therapies, expression of immune-suppressive markers or implication in the altered metabolism of tumors, among other actions (Hanahan and Coussens, 2012). IICs also affect tumor microenvironment by extracellular matrix (ECM) remodeling, since for example mast cells and macrophages can secrete proteases which cleave cell-cell and cell-ECM adhesion molecules and therefore facilitate ectopic tissue invasion (van Kempen et al., 2006).

Cancer-associated fibroblastic cells

Cancer-associated fibroblasts (CAFs) comprise a large proportion of stromal cells with a wide range of effects over tumor development, notably tumor-promoting functions. Moreover, CAFs can produce a variety of ECM proteins and enzymes which are able to modify tumor microenvironment and release angiogenic factors, as well as chemoattractants for proangiogenic macrophages, neutrophils and other myeloid cells (Vong and Kalluri, 2011). A metabolic relationship has also been described between CAFs and cancer cells, based on the exchange of energy sources to optimize metabolic efficiency and tumor growth (Hanahan and Coussens, 2012).

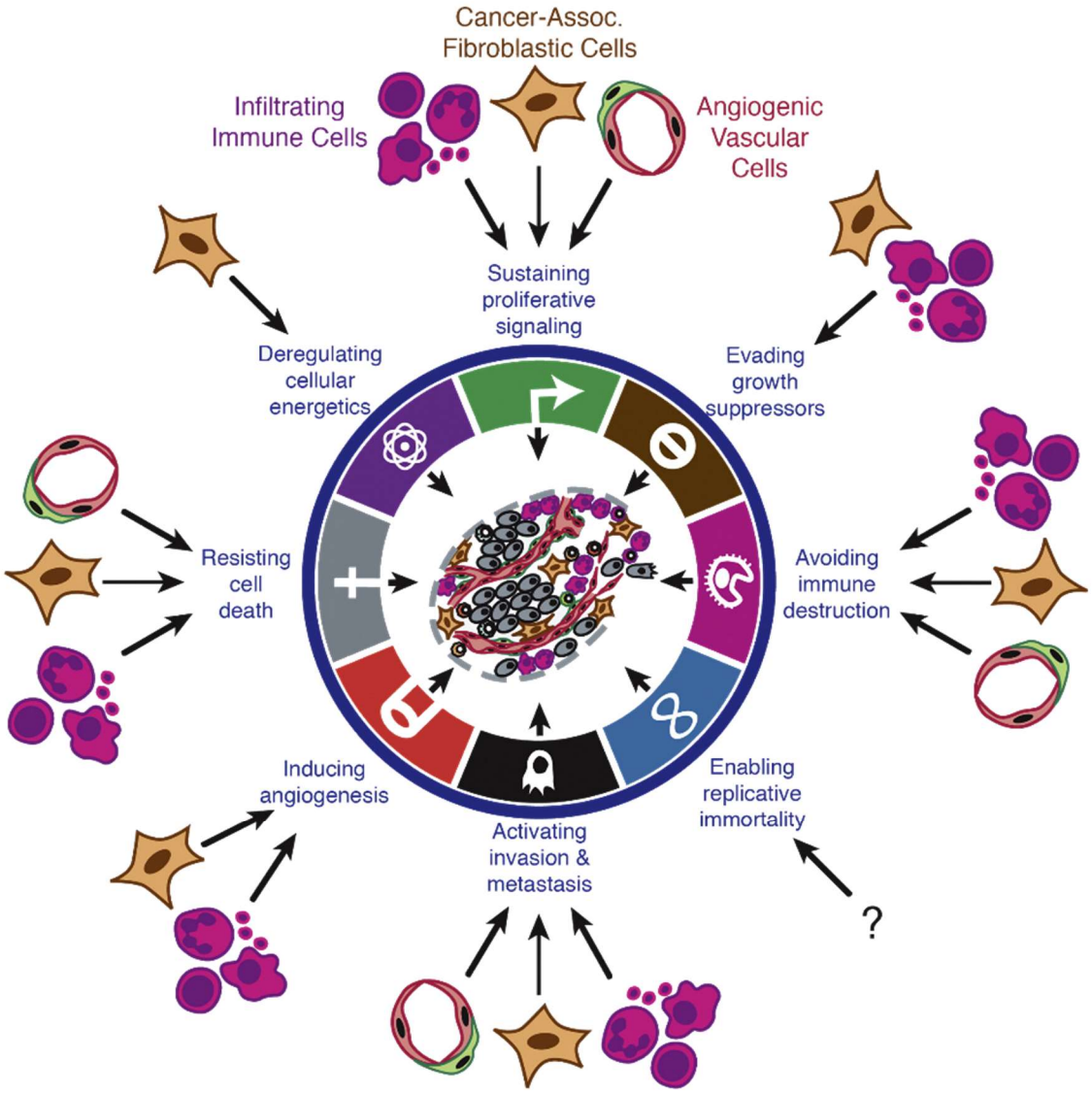

Figure 7. TME stromal cells contribution to the Hallmarks of Cancer.
Of the eight hallmark capabilities (without taking under consideration the two enabling characteristics), seven demonstrated to receive the influence of the stromal cells of the TME. The three stromal cell types are illustrated: angiogenic vascular cells (endothelial cells and pericytes), infiltrating immune cells and cancer-associated fibroblastic cells. Modified from (Hanahan and Coussens, 2012).

As previously mentioned, all these cellular components are associated with the non-cellular extracellular matrix. This ECM is produced by all cell types within the tumor microenvironment and plays a very important role in tumor development, as it will be described in the next section.

3. Extracellular matrix

The extracellular matrix is a non-cellular three-dimensional complex network of macromolecules which is present in all tissues and is essential for life. For many years, it has been considered as a mere inert scaffold which provides structure to cells. However, this view has changed in the past two or three decades. The extracellular matrix is an extremely dynamic element that suffers a continuous remodeling. This dynamism includes the cleavage of its components, which regulates ECM abundance, composition and structure in a tissue-specific manner (Bonnans et al., 2014; Poltavets et al., 2018).

In mammals, extracellular matrix is composed by approximately 300 proteins (named the core matrisome) including collagens, proteoglycans (PGs) and glycoproteins (Hynes and Naba, 2012). Structurally, extracellular matrix could be divided in interstitial matrix and basement membrane (BM). Interstitial matrix is highly charged and contribute to the strength of tissues, and its main components are fibrillary collagens, proteoglycans and glycoproteins such as tenascin C and fibronectin (Lu et al., 2012). The basement membrane is a specialized extracellular matrix, more compact and less porous than interstitial matrix. It is mainly composed by collagen IV, laminins, fibronectin, the heparan sulphate proteoglycan perlecan and linker proteins such as nidogens (Figure 8) (Lu et al., 2012; Sorokin, 2010). The main function of basement membrane is to provide a physical barrier between epithelial cells and the stroma (Poltavets et al., 2018).

Among its functions, extracellular matrix regulates cell growth, survival, proliferation, motility and differentiation (Pickup et al., 2014), and its constant remodeling contributes to control tissue homeostasis and development (Bonnans et al., 2014; Walker et al., 2018). The study of the interconnected physical (rigidity, porosity, insolubility, etc.), biochemical (growth factor binding, ligand-receptor signaling, etc.) and biomechanical (softness, stiffness, etc.) properties of the extracellular matrix is necessary for the understating of its role in maintaining homeostasis. In addition, several diseases, including cancer, are associated with an altered extracellular matrix, which justifies the necessity of deepening in its study.

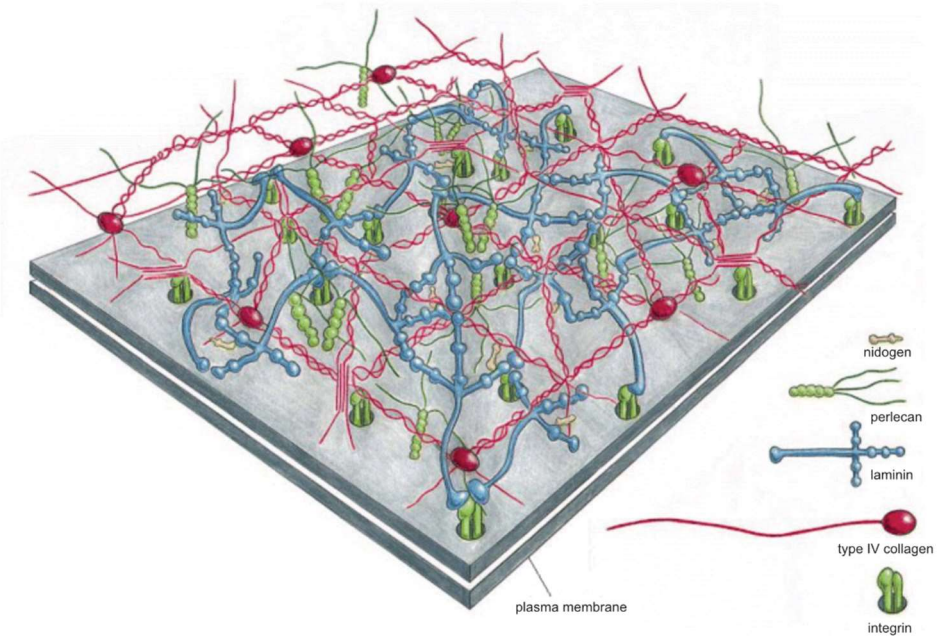

Figure 8. Molecular composition of the basement membrane.
Basement membrane is a specialized type of extracellular matrix, and it formed by the specific interactions between ECM molecules such as type IV collagen, laminins, perlecan and linker proteins such as nidogens. Modified from (Alberts et al., 2002).

The importance of biochemical and biophysical properties of extracellular matrix during tumor development has been widely studied, influencing the acquisition and maintenance of all ten hallmarks of cancer (Hanahan and Weinberg, 2011; Pickup et al., 2014). In addition, extracellular matrix also plays an important role in the sensitivity of tumors to drug treatment (Wu and Dai, 2017). The study of the ECM remodeling is equally important, since this process generates physical and chemical changes that influence tumor development and plasticity. Epithelial cells, as an example, need the rupture of the basement membrane to undergo epithelial-to-mesenchymal transition, an important sign of cancer plasticity (Poltavets et al., 2018).

Cancer cells are able to condition extracellular matrix through the deregulation and/or production of enzymes that modify it. Indeed, many extracellular proteases have demonstrated to play a role on tumor development through their impact on ECM remodeling (Figure 9) (Hillebrand and Reinheckel, 2019). They also affect multiple pathways during all stages of neoplasias and they have been even recognized as

prognostic factors in different tumor types. Among the high number of such proteases, this thesis will focus on the less studied members of the ADAMTS family, introduced in the next section.

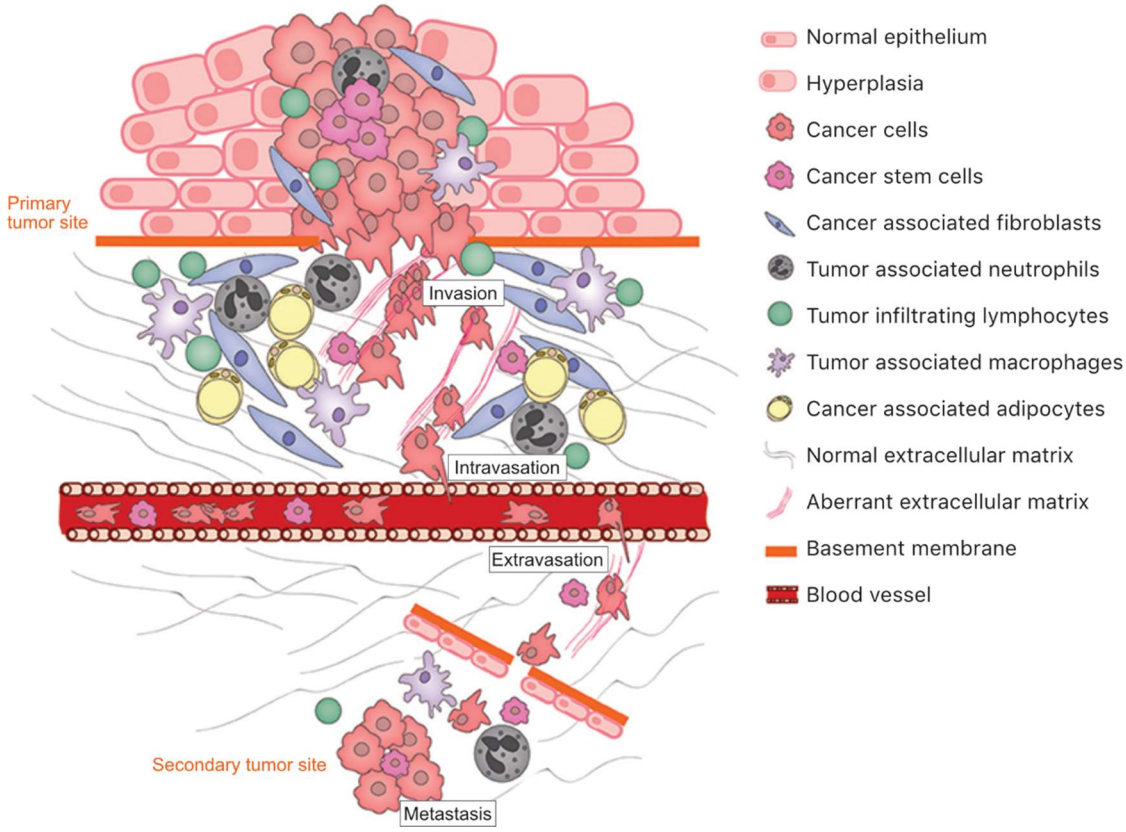

Figure 9. ECM is critical in cancer development.
Extracellular matrix plays an essential role in all the processes that a tumor needs to grow and also to metastasize. Its complex nature and its continuous remodeling allow tumor cells to invade healthy tissues, intravasate into blood vessels, extravasate from them and colonize distant tissues in which a secondary tumor (metastasis) will develop. Modified from (Poltavets et al., 2018).

4. ADAMTS proteases

ADAMTS family (A Disintegrin And Metalloproteinase with ThromboSpondin motifs) encloses a group of secreted zinc-dependent endopeptidases with essential roles preserving normal organ and tissue homeostasis (Malemud, 2019). They belong to the superfamily of the metzincin proteases, in which all contain a proteolytic domain with a zinc-binding site and a conserved methionine (Gomis-Rüth, 2003). Matrix MetalloProteinases (MMPs) and A Disintegrin And Metalloproteinases (ADAMs) also belong to this superfamily. All of them, together with ADAMTSs, are considered key players in tissue microenvironment regulation, not only under physiological conditions but also in a wide range of pathological settings such as cancer (Cal and López-Otín, 2015; Fontanil et al., 2019; Rossi et al., 2020). ADAMTS is the most recently described family, and they were initially considered a subfamily of the ADAMs.

The first ADAMTS member was identified in 1997 in a mouse cell model of colon cancer cachexia (Kuno et al., 1997). It was named ADAMTS-1 remarking the presence of thrombospondin type I repeats (TSR) that differentiate it from the closely related ADAM family. The human ortholog for ADAMTS1 was described in 1999 and it was initially named METH-1, due to its metalloprotease (ME) and thrombospondin (TH) motifs (Vazquez et al., 1999). Since then, 19 human members have been identified for this family, which exhibit a common multi-domain structure including both protease and ancillary domains. The N-terminal protease domain contains a prodomain, a metalloproteinase (catalytic) motif and a disintegrin-like motif. The C-terminal ancillary domain is comprised by a conserved region (composed by a TSR, a cysteine-rich domain and a spacer fragment) and a variable region, which may or may not contain additional TSR domains and other motifs (Apte, 2004; Rodríguez-Manzaneque et al., 2015). To date, the 19 members of this family can be classified into five groups based on their proteolytic activity: (a) aggrecanases and proteoglycanases (ADAMTS1, 4, 5, 8, 9, 15 and 20); (b) pro-collagen N-propeptidases (ADAMTS2, 3 and 14); (c) von-Willebrand factor (VWF)-cleaving protease (ADAMTS13); (d) cartilage oligomeric matrix protein proteinases (ADAMTS7 and 12); and (e) “orphan”

proteinases (ADAMTS6, 10, 16, 17, 18 and 19) with unknown substrates (Kelwick et al., 2015a).

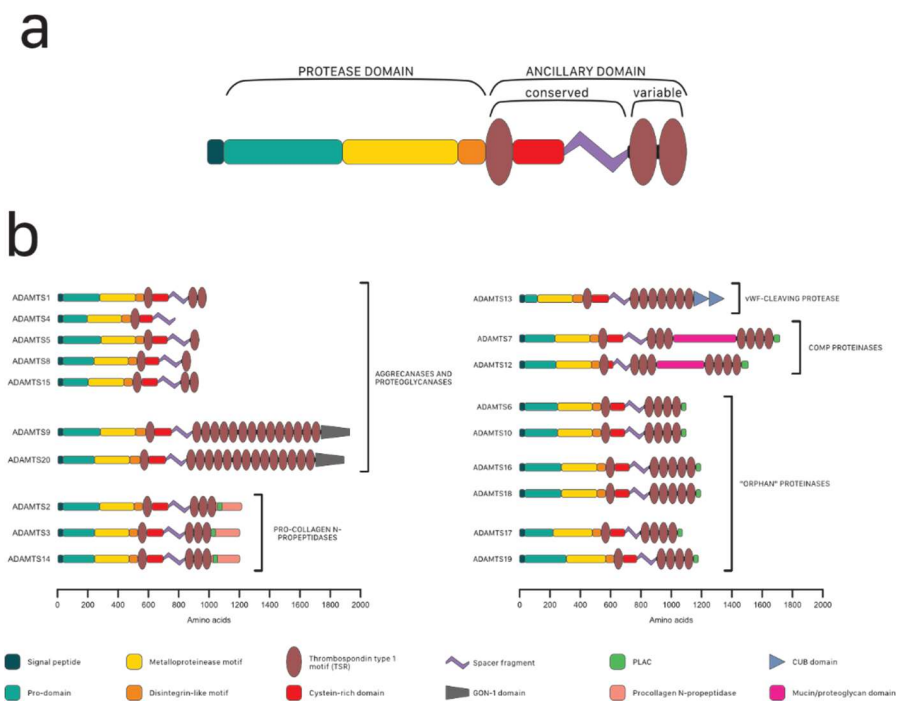

Figure 10. ADAMTS family of proteases.
(**a**) General scheme of the multi-domain structure of ADAMTS extracellular proteases, composed by a N-terminal protease domain (containing a prodomain, a metalloproteinase domain motif and a disintegrin-like motif) and an C-terminal ancillary domain (divided in a conserved region which is composed by a thrombospondin type I motif [TSR], a cysteine-rich domain and a spacer fragment; and a variable region). (**b**) Schemes of the 19 human members of ADAMTS family, classified by clades: aggrecanases and proteoglycanases, pro-collagen N-propeptidases, von-Willebrand factor (VWF)-cleaving protease, cartilage oligomeric matrix protein (COMP) proteases and "orphan" proteases. The different motifs that they show in their variable ancillary domain can be observed: GON-1 domain, protease and lacunin (PLAC) module, procollagen N-propeptidase, CUB domain and mucin/proteoglycan domain. Adapted from (Kelwick et al., 2015a; Rodríguez-Manzaneque et al., 2015).

ADAMTS1 could be considered as the prototype of the ADAMTS family, and it has demonstrated to be involved in a wide range of biological processes. It is also the main object of study of this thesis, so it will be introduced in more detail in the next section. Until then, other ADAMTSs that also appear in this work will be briefly presented.

Human ADAMTS1 belongs to the aggrecanases group of ADAMTSs, and it shares a high sequence homology with ADAMTS4, 5, 8 and 15 (Kuno, 2013), as well as the capacity to cleave extracellular proteoglycans such as

aggrecan, versican, brevican or neurocan. They have also been designated as "angioinhibitory" ADAMTS because some of them showed this effect, such as ADAMTS1 and 8 (Vazquez et al., 1999), ADAMTS4 (Hsu et al., 2012) and ADAMTS5 (Kumar et al., 2012). However, this name would later be discarded since some of these ADAMTS also showed pro-angiogenic effects.

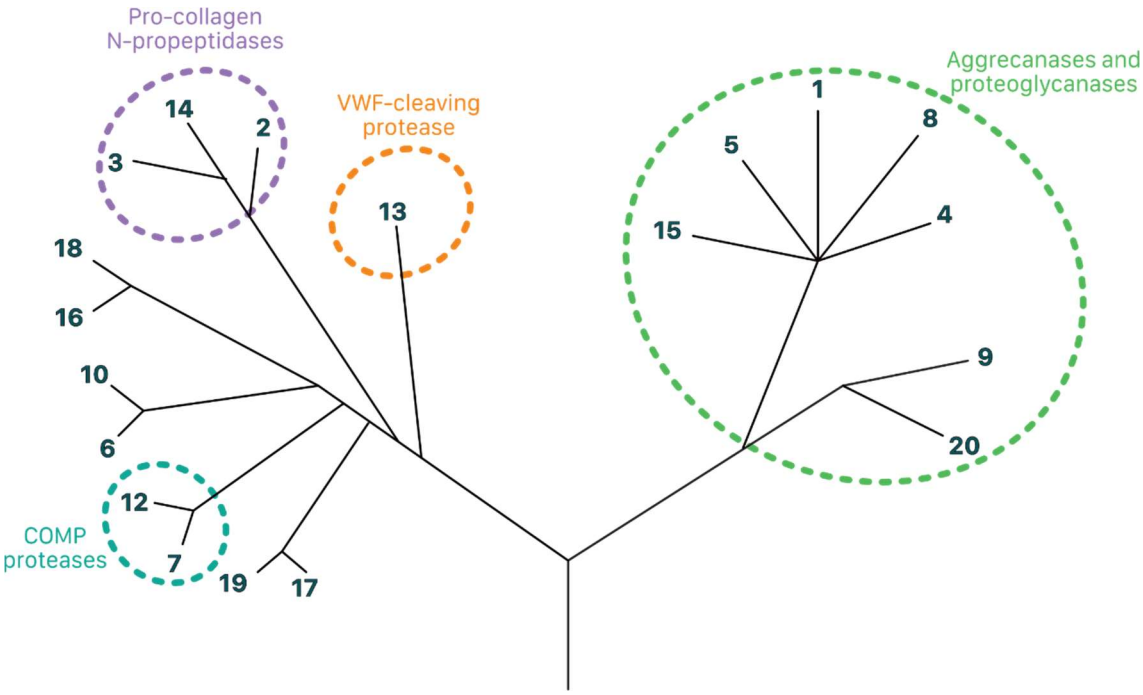

Figure 11. Evolution of the ADAMTS family.
Schematic representation of the relationships between the different clades of ADAMTS proteases, including aggrecanases and proteoglycanases (ADAMTS1, 4, 5, 8, 15, 19 and 20), von-Willebrand factor (VWF)-cleaving protease (ADAMTS13), pro-collagen N-propeptidases (ADAMTS2, 3 and 14) and cartilage oligomeric matrix protein (COMP) proteases (ADAMTS7 and 12) and the four clades known as "orphans". The scheme is not scaled according to evolutionary distance. Modified from (Kelwick et al., 2015a)

The name "aggrecanase" was originated in the arthritis field, according to the relevant and progressive loss of aggrecan from cartilage. ADAMTS4 and ADAMTS5 were originally named aggrecanase-1 and aggrecanase-2, respectively, although this activity has been furtherly shown for ADAMTS1 (Rodríguez-Manzaneque et al., 2002), ADAMTS8 (Collins-Racie et al., 2004), ADAMTS9 (Somerville et al., 2003) and ADAMTS15 (Kelwick et al., 2015b). Together with aggrecan, the extracellular matrix chondroitin sulfate proteoglycan versican is the other major substrate of aggrecanases. Versican has demonstrated to play an important role in many contexts,

including cancer, involving in many cases its interaction with aggrecanases (Binder et al., 2020; Gueye et al., 2017; Kern et al., 2010).

Besides these actions attributed to the proteolytic activity of aggrecanases, there are other scenarios in which there are no evidences of the requisite of their proteolytic activity. For example, atherosclerotic plaques have shown a high expression of ADAMTS1, 4, 5 and 8 (Ashlin et al., 2013; Wågsäter et al., 2008), as well as an increased expression of ADAMTS4 was detected in brains of patients suffering from ischemic stroke (Lemarchant et al., 2016). In a similar context, ADAMTS1, 5 and 9 were up-regulated after spinal cord injury (Demircan et al., 2013), the same as other ADAMTSs for different neurodegenerative diseases, as recently reviewed (Mohamedi et al., 2020).

Aggrecanases are also very present in tumor biology studies. Accordingly, the effect of ADAMTS4 and 5 on glioma through their cleavage of brevican (Matthews et al., 2000; Nakada et al., 2005), or on laryngeal carcinoma through aggrecan (Filou et al., 2013) are examples in which their proteolytic activity affect cancer development. Alternatively, proteolytic independent-actions have been reported for ADAMTS4, 5 and 9 in colorectal cancer (Chen et al., 2017; Haraguchi et al., 2017; Shang et al., 2020); ADAMTS5 in gastric cancer (Huang et al., 2019) and ADAMTS4 in melanoma (Rao et al., 2013).

5. ADAMTS1

Human *ADAMTS1* gene is mapped in chromosome 21 and translates into a 967 amino acids extracellular protein. Its distinguishing structural feature consists of two thrombospondin type 1 motifs (TSR) in its ancillary domain and the full and proactive molecule has a molecular weight of 110 kDa. ADAMTS1 could be found in different forms that have been named relative to their molecular weight as p110, p87 and p65 (110, 87 and 65 kDa, respectively), (Figure 12) (Rodríguez-Manzaneque et al., 2000). As other metalloproteases, ADAMTS1 is synthetized as an inactive zymogen (Figure 12a) which is processed after secretion and with the N-terminal prodomain acting as a proteolytic activity blocker (Rodríguez-Manzaneque et al., 2000). Functional activation therefore requires the removal of the prodomain, that in this case is performed by furin, resulting the p87 form (of 715 amino acids length, approximately) which can be found anchored to the extracellular matrix (Figure 12b). Finally, the p65 form, of approximately 520 amino acids length, arises after a second proteolytic event which in this case is conducted by MMPs. It removes the two TSR motifs and a part of the spacer region from the C-terminus and changes its extracellular distribution from ECM-anchored to soluble (Figure 12c) (Rodríguez-Manzaneque et al., 2000).

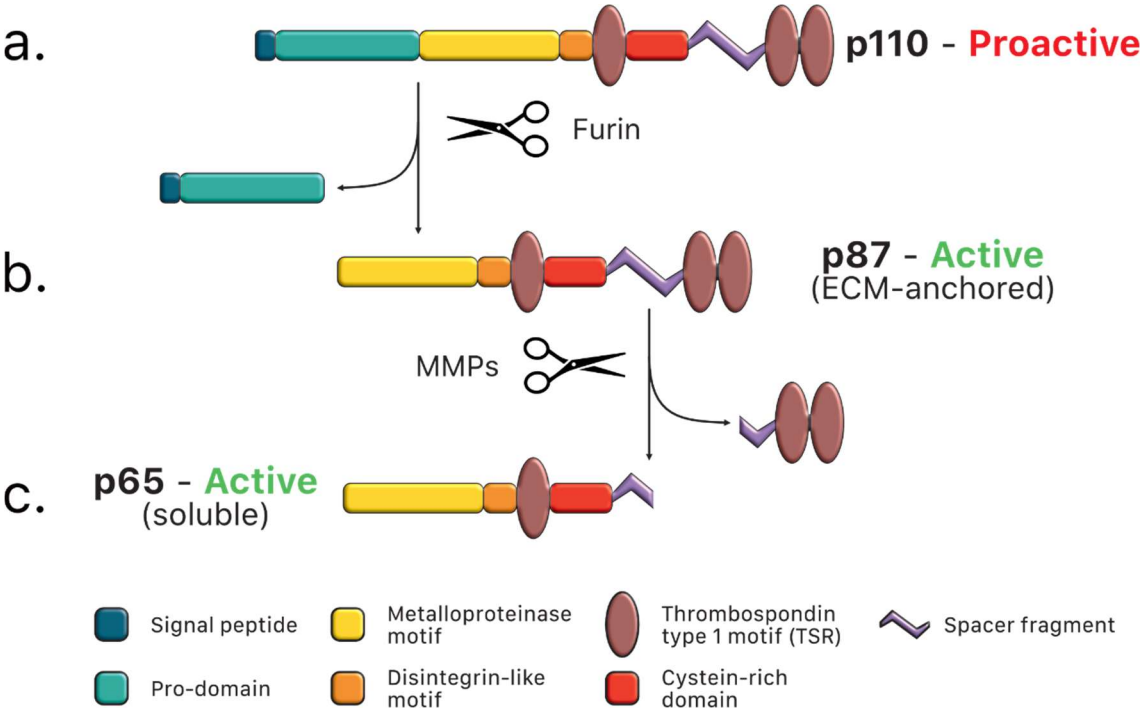

Figure 12. ADAMTS1 maturation reveals different forms of the protease.
(a) ADAMTS1 is synthetized as an inactive (proactive) zymogen which is named p110. (b) ADAMTS1 p87 form results from the removal of the pro-domain by furin and appears anchored to the ECM. (c) Finally, a secondary proteolytic event results in the ADAMTS1 p65 form, which has lost two TSR motifs and a part of the spacer fragment and changes its extracellular distribution to soluble. Modified from (Rodríguez-Manzaneque et al., 2000) with the help of Freepik.

ADAMTS1 is involved in many different biological processes and diseases, including cancer. Its functions can be both dependent or independent of its proteolytic activity, and some of them will be briefly introduced before deepening into a tumor context.

The first function attributed to ADAMTS1 concerned angiogenesis. In fact, its initial cloning resulted from the search of human proteins that contained the TSR motif (Vazquez et al., 1999), according to its intrinsic anti-angiogenic properties (Iruela-Arispe et al., 1999; Tolsma et al., 1993). Indeed, the anti-angiogenic function of ADAMTS1 was first attributed to the C-terminal TSR motifs-containing region of the protein, which sequesters VEGF and impedes its binding to KDR (also named VEGFR2) and consequently suppresses endothelial cell proliferation (Luque et al., 2003). This action was also reported in a model of oxygen-induced murine retinopathy (Xu et al., 2006). Alternatively, pro-angiogenic functions have also been attributed to

ADAMTS1, which showed to be necessary for endothelial cell invasion in an *in vitro* 3D model of angiogenesis (Su et al., 2008).

ADAMTS1 is also involved in other diseases without apparent relationship to angiogenesis. These are the cases of acute myocardial infarction, in which the expression of ADAMTS1 is induced in the ischemic endothelium (Nakamura et al., 2004), or of neurodegenerative diseases, in which this protease has been proposed as a marker due to its overexpression in Alzheimer, Pick's disease and Down syndrome (Miguel et al., 2005), as well as after spinal cord injury in mice (Demircan et al., 2013).

ADAMTS1 has also been described as an immune system modulator. Indeed, it was associated with inflammatory processes since its initial description (Kuno et al., 1997). Importantly, ADAMTS1 expression appeared induced during the differentiation of monocytes into macrophages in a atherosclerosis context (Ashlin et al., 2013). Furthermore, a previous study by this laboratory demonstrated alterations in immune-related organs in *Adamts1*-deficient mice, such as a pro-inflammatory setting in the spleen (Rodríguez-Baena et al., 2018a). Moreover, we also observed an increase of T cells and myeloid populations in the bone marrow of *Adamts1*-deficient mice, therefore proposing a modulatory role of the protease in the immune response.

So far, the mentioned studies reflect the functions of ADAMTS1 independently of its catalytic regions or activities. However, this may be a limited view of the biological functions of this and other ADAMTSs, so it is necessary to know their proteolytic activity and substrates to determine their functions more appropriately. To date, a wide range of molecules with heterogeneous nature have been identified as ADAMTS1 substrates (Table 1). Their cleavage by ADAMTS1 has been related with diverse effects, like anti-angiogenic properties during wound healing by the release of TSR fragments from THBS1 and 2 (Lee et al., 2006), or the disruption of cell adhesion and promotion of cell migration by cleaving syndecan 4 (Rodríguez-Manzaneque et al., 2009). Again related with the immune system, ADAMTS1 expression appears induced in aortic aneurysm and

dissections (AAD) tissues, which may promote its progression by versican degradation and macrophage invasion (Ren et al., 2013).

The relationship of ADAMTS1 with cancer has barely been addressed yet in this thesis, and it will be introduced in the next paragraphs. This connection is present from the very beginning, since ADAMTS1 was initially described in a model of colon cancer cachexia (Kuno et al., 1997). As with non-oncological pathologies, the effects of ADAMTS1 on cancer may involve its proteolytic activity and substrates although it is unknown in many cases. This is the case of the examples in which ADAMTS1 has been proposed as a tumor suppressor element, such as in lung (Choi et al., 2008) or prostate (Gustavsson et al., 2009) cancers. This laboratory has also reported an anti-tumorigenic role for ADAMTS1 in breast cancer, both in xenograft experiments and patient samples (Martino-Echarri et al., 2013).

Alternatively, ADAMTS1 has been widely described as a tumor-promoting metalloprotease. Very soon after its discovery, ADAMTS1 expression was reported in pancreatic cancer and involved in local tumor invasion and lymph node metastasis (Masui et al., 2001). Since then, not only its pro-tumorigenic role but also its pro-metastatic effect have been reported, as described in MMTV-PyMT mouse spontaneous mammary tumor model (Ricciardelli et al., 2011), or in studies with human samples such as with ovarian (Lima et al., 2016) or renal (Wen et al., 2020) cancer. The latest investigations developed by this laboratory have also pointed to this pro-tumorigenic effect of ADAMTS1. Regarding the origin of the protease within a tumor, we demonstrated that the stroma-derived ADAMTS1 also contributes to tumor development and metastasis (Fernández-Rodríguez et al., 2016). The interesting findings of that work triggered the research that culminated in the identification of ADAMTS1 as a regulator of the immune system and which helped to explain the tumor development blockade that was observed in its absence (Rodríguez-Baena et al., 2018a).

Confirmed substrates

Versican	(Sandy et al., 2001)
Aggrecan	(Rodríguez-Manzaneque et al., 2002)
Nidogens 1 and 2	(Canals et al., 2006)
Thrombospondin 1 and 2	(Lee et al., 2006)
Gelatin (type I collagen)	(Lind et al., 2006)
Tissue factor pathway inhibitor 2	(Torres-Collado et al., 2006)
EGF-like ligands (AR and HB-EGF)	(Liu et al., 2006)
Syndecan 4	(Rodríguez-Manzaneque et al., 2009)
Semaphorin 3C	(Esselens et al., 2010)
IGF-binding protein 2	(Martino-Echarri et al., 2014)

Candidate substrates

Desmocolin 3	(Canals et al., 2006)
Dystroglycan 1	(Canals et al., 2006)
Galectin-3-binding protein	(Canals et al., 2006)

Table 1. ADAMTS1 substrates.
Several molecules have reported to be cleaved by ADAMTS1. In this table they are compiled in chronological order of their uncovering as ADAMTS1 substrates.

As previously mentioned, the proteolytic activity of ADAMTS1 in these cancer studies is absent or unknown, which highlights the importance of deepening in the knowledge of extracellular proteases and their roles. Indeed, research on ADAMTS1 and its proteolytic activity has provided,

within its substrates, a subset with different roles in cancer development. Some of them will be considered in this thesis and they are briefly introduced in Box 1.

Box 1. ADAMTS1 substrates in cancer

IGFBP2. Insulin-like growth factor-binding protein 2 has been correlated with poor prognosis in a wide range of tumors. This laboratory identified it as an ADAMTS1 substrate in a glioma model, attributing its pro-tumorigenic role to its proteolytic cleavage (Martino-Echarri et al., 2014). More recently, IGFBP2 showed to contribute to VM in glioblastoma by increasing CDH5 and MMP2 expression (Liu et al., 2019).

Nidogens. Previously known as entactins, both nidogens (1 and 2) are triglobular extracellular glycoproteins which act as main components and linkers of the BM. Their cleavage by ADAMTS1 was described by this laboratory (Canals et al., 2006), as well as the resulting anti-angiogenic and anti-tumorigenic effect in a mouse breast cancer model (Martino-Echarri et al., 2013).

Versican. This is the largest member of the hyalectan family of proteoglycans and it was described as an ADAMTS1 substrate in a human aorta model (Sandy et al., 2001). Accumulation of ADAMTS1-cleaved versican promotes cancer cell motility and invasion in breast cancer (Ricciardelli et al., 2011), and it may be relocated to endothelial cells, affecting angiogenesis and tumor growth (Asano et al., 2017).

In line with the introduced actions of ADAMTS1 related to angiogenesis, such relationship has also been studied in cancer. Again, both anti- and pro-angiogenic functions have been reported in a tumor context, even showing the two roles depending on whether the full-length or fragments were present (Liu et al., 2006). Tumor angiogenesis inhibition effects of ADAMTS1 were described in the Tc1 mouse model of Down's syndrome with the participation of some members of this laboraytory (Reynolds et al., 2010), as well as in fibrosarcoma, ovarian and prostate cancer models in a proteolytic-independent manner (Obika et al., 2012). In addition, thrombospondin 1 (THBS1) cleavage by ADAMTS1 and its anti-angiogenic consequences have also been described in various tumor models, such as in prostate cancer xenografts (Gustavsson et al., 2010) and metastatic models for melanoma, colon and renal carcinomas (Lee et al., 2010).

Regarding the pro-angiogenic role of ADAMTS1 in a tumoral context, it has been suggested that VEGF-A-induced tumor angiogenesis is initiated by the expression of ADAMTS1 and is facilitated by its cleavage of versican (Fu et al., 2011). This laboratory also demonstrated the contribution of the protease to acquire an endothelial-like phenotype by aggressive plastic tumor cells

(Casal et al., 2010). These findings, which also included the inhibition of ADAMTS1 and its consequences on the endothelial-like phenotype, triggered the development of this thesis project and the publication that supports it, where the contribution of the protease to this phenotype in melanoma is studied in depth (Peris-Torres et al., 2020a).

Nevertheless, the effect on tumor angiogenesis of ADAMTS proteases is not exclusive to ADAMTS1. Other members of the family have also demonstrated an angiogenic-related role, either stimulating or inhibiting or both. For example, while full-length ADAMTS4 showed a pro-angiogenic effect in melanoma, a truncated fragment containing only the ancillary domain suppresses tumor growth and angiogenesis. (Rao et al., 2013), ADAMTS5, 8 and 9 demonstrated anti-angiogenic properties in melanoma, glioma and esophageal carcinoma, respectively (Dunn et al., 2006; Kumar et al., 2012; Lo et al., 2010). According to the relevant references of ADAMTs in this field and its global importance in tumor microenvironment, a following section is dedicated to tumor angiogenesis.

6. Tumor angiogenesis

As aforementioned, tumor angiogenesis, i.e. the *de novo* formation of tumor-associated blood vessels from preexisting ones, serves as a support to the high proliferative rate of tumors and it has been considered as one of the hallmarks of cancer (Hanahan and Weinberg, 2011) (Figure 2). Angiogenesis, in adulthood, is activated only transiently (e.g. in wound healing processes), but in a tumor context, the so-called "angiogenic switch" is relevantly sustained (Hanahan and Folkman, 1996), causing a continuous sprouting of new vessels that allows neoplastic growth. Indeed, tumor vasculature becomes aberrant, different from normal tissue vessels, as it is characterized by dilated, tortuous and disorganized blood vessels, erratic blood flow, leakiness and poor perfusion (Hanahan and Weinberg, 2011; Viallard and Larrivée, 2017). In addition, pericytes are loosely attached or absent and the basement membrane is often abnormal (Jain, 2005).

Several therapeutic strategies have been implemented to abolish tumor angiogenesis, including the more widespread use of bevacizumab, an anti-VEGF-A monoclonal antibody (Crawford and Ferrara, 2009). The combination of bevacizumab (and other VEGF-A receptor KDR/VEGFR2 inhibitors) with conventional chemotherapies or radiotherapies has had varying success among different tumor types. In this pursuit of an adequate anti-tumor vasculature therapy is important to highlight the concept of vascular normalization (

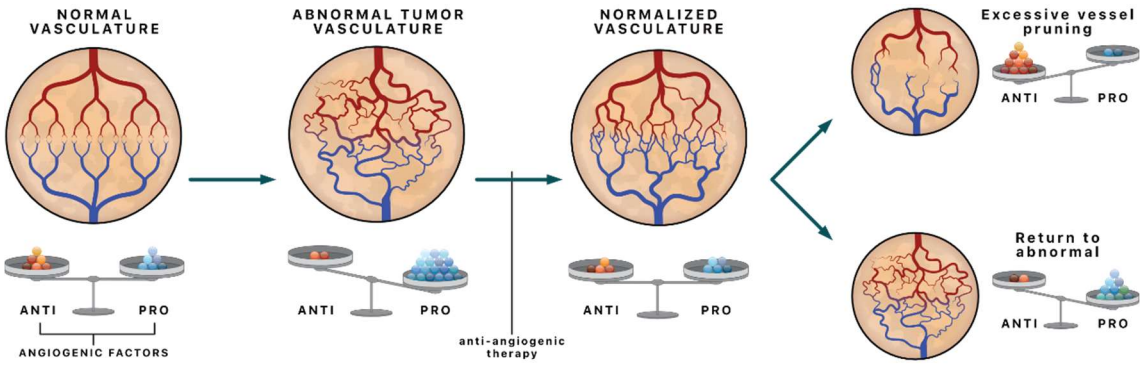

Figure 13). A tumor "normalized vasculature" displays a balance of pro- and anti-angiogenic factors similar to normal healthy vasculature and away from the aberrant vasculature of the tumor. This would increase the delivery of drugs and oxygen, improving the response to therapy and avoiding hypoxic

areas in order to ultimately eliminate the tumor (Jain, 2005). However, this is a very delicate balance, since an excess of anti-angiogenic factors could cause an excessive vessel pruning affecting tumor regression but, alternatively, tumors may switch to using other pro-angiogenic factors and begin to create an abnormal vasculature again (Jain and Carmeliet, 2012).

The principal mechanism of new vessel formation is named sprouting angiogenesis. The process starts from quiescent vessels that are formed by

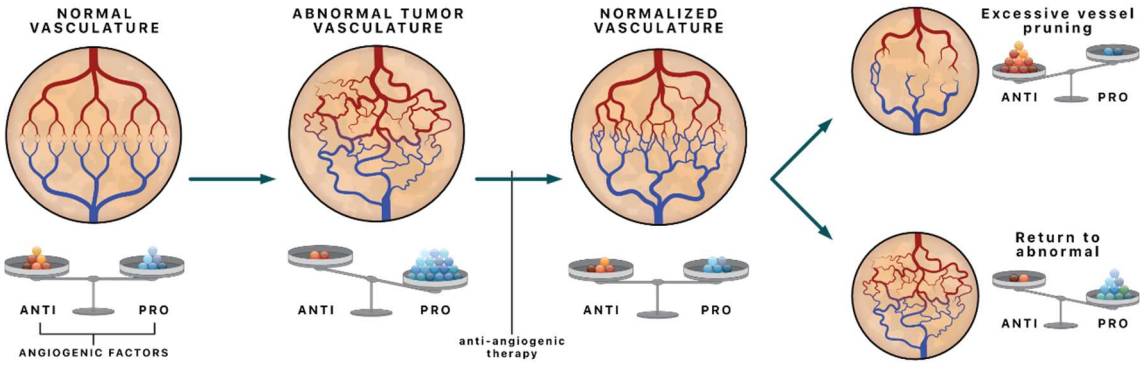

Figure 13. Scheme of the tumor vasculature normalization.
A normal vasculature presents a balance between anti- and pro-angiogenic factors. On the contrary, this balance is lost in tumors, becoming an abnormal tumor vasculature with an excess of pro-angiogenic factors. Anti-angiogenic therapy restores this balance and a normalized vasculature is obtained. However, an excess of anti-angiogenic therapy could lead to an excessive vessel pruning which will affect tumor regression. Alternatively, tumors may switch to using another pro-angiogenic factors and thus return to the abnormal vasculature initially shown. Modified from (Jain and Carmeliet, 2012).

a monolayer of interconnected endothelial cells. This monolayer is surrounded by pericytes, and together they conform a common vascular basement membrane which is a critical component of blood vessel integrity (Carmeliet and Jain, 2011; Viallard and Larrivée, 2017). When a quiescent vessel senses an angiogenic signal, pericytes detach from the vessel wall and endothelial cells loosen their junctions, processes which are facilitated by the basement membrane remodeling conducted by metalloproteinases (Figure 14a). In consequence, the extravasation of plasma proteins and endothelial cells generate a provisional ECM scaffold, whose remodeling establish an angio-competent milieu. Then, the tip (endothelial cell provided with filopodia that lead the new vessel formation) and stalk (neighbor endothelial cells to the tip cell that divide to elongate de new vessel) cells selection occurs and the new lumen is established (Figure 14b). To become

functional, the new vessel needs the recovery of the quiescent phalanx formed by endothelial cells and pericytes, the deposition of the basement membrane and the reestablishment of cell junctions to ensure optimal blood flow (Carmeliet and Jain, 2011), (Figure 14c).

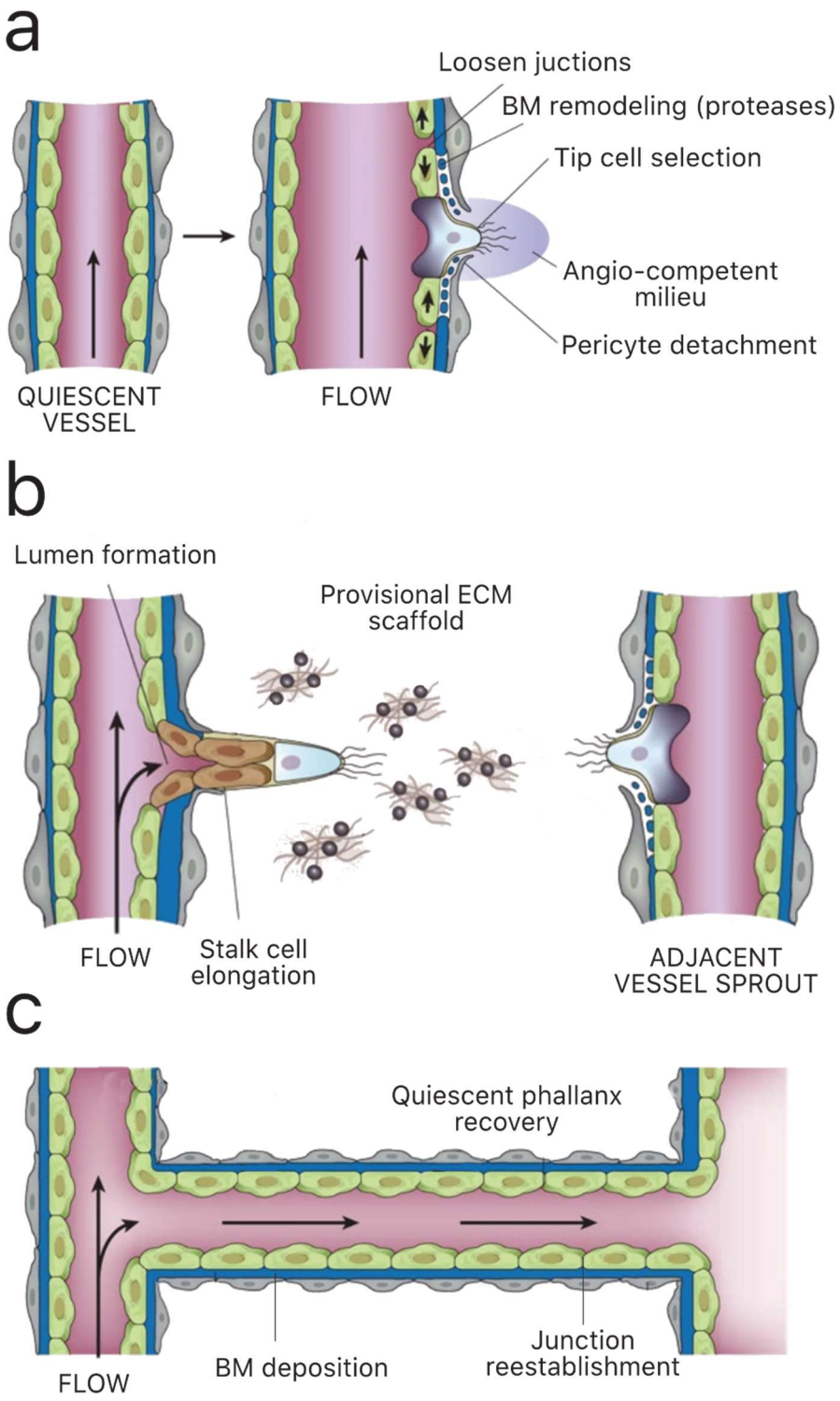

Figure 14. New blood vessel formation mechanism by sprouting angiogenesis.
When a quiescent blood vessel senses an angiogenic signal, (**a**) the ECM remodeling allows the selection of a tip cell, which (**b**) triggers the lumen formation with the help of stalk cells and the

deposition of a provisional ECM. (**c**) Finally, the new vessel needs the recovery of the quiescent phalanx and ECM to become functional Modified from (Carmeliet and Jain, 2011)

Although sprouting angiogenesis is the principal mechanism of new vessel formation, a deeper study of tumors has shown the existence of alternative mechanisms of neovascularization which appearance has been directly related with resistance episodes to antiangiogenic therapies. Intussusceptive angiogenesis, vessel co-option, vasculogenesis and vasculogenic mimicry are the most studied of these mechanisms. With the exception of vasculogenic mimicry, that receives a special attention in this thesis, a brief description of the remaining mechanisms follows next (Figure 15).

Intussusceptive angiogenesis

Also known as splitting angiogenesis, it is characterized by the insertion of connective tissue pillars into the lumen of preexisting vessels, splitting them into two new functional ones (Figure 15a) (Kurz et al., 2003; Viallard and Larrivée, 2017), (Figure 15). Intussusceptive angiogenesis is faster than sprouting angiogenesis, and its independence from EC proliferation would imply resistance to anti-angiogenic treatments (Döme et al., 2007). It has been shown in different tumor types, including melanoma where VEGF expression correlates with the appearance of these tissue pillars (Ribatti et al., 2005).

Vessel co-option

First described in 1999, it is characterized by the ability of tumor cells to "hijack" the preexisting vessels in the surrounding tissues growing along these existing vessels and integrating them during tumor expansion (Figure 15b) (Holash et al., 1999; Viallard and Larrivée, 2017). Although it was initially suggested that vessel co-option only occurred during early stages of tumorigenesis, later evidence showed that it might persist during all the process of tumor growth, both primary and metastatic (Döme et al., 2007)

Vasculogenesis

The term "vasculogenesis" defines the formation of primitive blood vessels from mesoderm through angioblast differentiation (Risau and Flamme,

1995). In the context of tumors, it could be divided into two different but related mechanisms, named bone marrow-derived vasculogenesis and cancer stem cell-derived vasculogenesis (Figure 15c). Bone marrow derived vasculogenesis includes the recruitment of endothelial precursor cells (EPCs) from the bone marrow, their incorporation into growing vessels and their in situ differentiation into ECs (Luo et al., 2020; Viallard and Larrivée, 2017), (Figure 15). After incorporation, the local endothelium is activated to express adhesion molecules and recruit more EPCs (Döme et al., 2007). It has been shown that EPCs share a common precursor with hematopoietic stem cells (HSCs), named hemangioblast, and that they express several interesting markers for this thesis, such as *KDR*, *TEK, NANOG*, *POU5F1* or *PROM1* at initial stages of EPCs and *CDH5* when they become tissue ECs (Asahara and Kawamoto, 2004; Peichev et al., 2000; Romagnani et al., 2005).

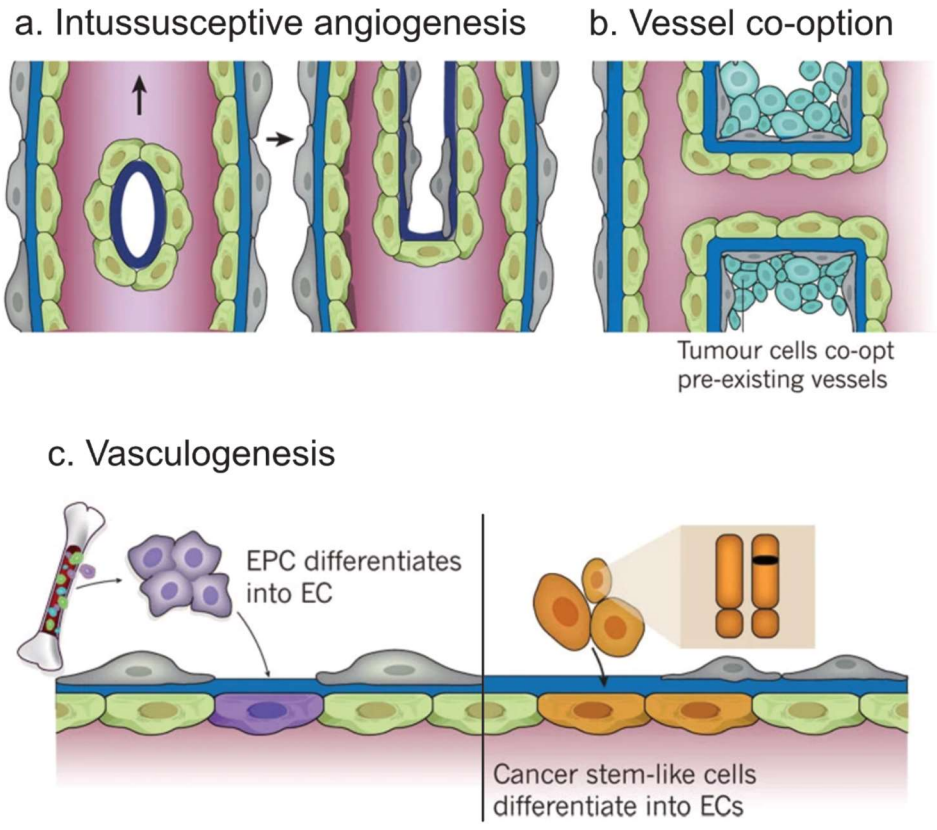

Figure 15. Mechanisms of neovascularization alternative to sprouting angiogenesis. (**a**) Intussusceptive angiogenesis, the insertion of connective tissue pillars to split the lumen of preexisting vessels into two new functional ones. (**b**) Vessel co-option, preexisting vessels "hijacking" by tumor cells in the surrounding tissues. (**c**) Vasculogenesis, the generation of blood

vessels through differentiation that can be generated either by endothelial precursor cells (EPCs) or cancer stem cells (CSCs) differentiation. Modified from (Carmeliet and Jain, 2011).

Cancer stem cells have also been pointed as a source of progenitor cells responsible for vasculogenesis (Wang et al., 2010). In fact, the difference between stem and progenitor cells has proved to be diffuse in some investigations, to the extent that the nomenclature has been considered confusing and to exhaustively characterize each cell type to avoid any confusion (Medina et al., 2017). The capacity of CSCs to contribute to tumor vasculature by integrating into the vascular wall and transdifferentiating into endothelial cells was reported by two independent groups in 2010 in glioblastoma models (Ricci-Vitiani et al., 2010; Wang et al., 2010) (Figure 15). These CSCs have been shown to retain their genetic alterations and to express endothelial markers (such as *CDH5*), therefore being candidate participants of VM (Viallard and Larrivée, 2017; Wang et al., 2010).

As remarked in this last section, CSCs play a crucial role on tumor angiogenesis. However, this is not the only scenario where they are relevant, since their existence supported the basis for the intratumor heterogeneity model introduced above (Figure 4). Furthermore, CSCs are key players on vasculogenic mimicry, already mentioned as another alternative mechanism of vascularization. Accordingly, a brief portrayal of CSCs follows now prior to a deeper description of vasculogenic mimicry.

7. Cancer Stem Cells

Taking into account that the definition and identity of these cells has been accompanied of many controversies, CSCs represent a subpopulation of neoplastic cells within tumors that are defined by their capacity to self-renew, to initiate and repopulate tumors and to differentiate into different cell types (Brown et al., 2019). In fact, some authors refer to them as cancer initiating cells. These features support their responsibility on the Cancer Stem Cell model of intratumor heterogeneity (Figure 4). CSCs were firstly identified in 1994 in leukemia (Lapidot et al., 1994), but it was not until 2001 when the CSC term was coined (Reya et al., 2001). Their characterization revealed similar transcriptional profiles and cell surface markers to normal tissue stem cells (Brown et al., 2019; Hanahan and Weinberg, 2011). Relevant for this work, CSC subpopulations were also identified in human melanomas (Fang et al., 2005), and some progress has been reported with uveal melanoma cells (Kalirai et al., 2011).

CSCs are closely involved in the complexity of the tumor microenvironment, to the extent that the concept of cancer stem cell niche was coined. In such niche the extracellular matrix supports the acquisition and maintenance of stem cell properties as well as CSC differentiation (Lu et al., 2012). It is therefore very relevant to understand the cellular and molecular mechanisms that allow CSCs to interact with the tumor microenvironment, thus giving them adaptive and survival advantages (Brown et al., 2019). Furthermore, recent investigations in colon cancer have proposed that CSC functionality may depend more on their microenvironment than on the expression of stem cell markers, and the propensity of cancer cells to become CSC depends on their location (Lenos et al., 2018).

Whether these latter findings can be applied to other tumors remain to be investigated. According to the development of this thesis, CSCs are considered in the "more classical" point of view, i.e. as highly plastic cells that express cancer stem cell markers and are able to initiate tumor or grow as nonadherent tumor spheres. Among such stemness makers, *NANOG*, *POU5F1*, *PROM1* and *SOX2* (Box 2) have been considered in this thesis.

Box 2. Stemness markers

NANOG. Nanog (from Irish mythology Tír na nÓg, Land of Eternal Youth) homeobox is a key transcription factor regulating pluripotency in mammalian early embryos, pluripotent stem cells, tumor growth and metastasis (Garza Treviño et al., 2019; Hayashi et al., 2015). *NANOG* also plays an important role in regulating the self-renewal capacity and proliferation of CSCs (Yang et al., 2020).

POU5F1. POU class 5 homeobox 1, also named *OCT4*, is a transcription factor involved in stem cell maintenance and embryogenesis, CSCs self-renewal capacity, tumor growth and metastasis (Bradshaw et al., 2016; van Schaijik et al., 2018). *POU5F1* is one of the pluripotency Yamanaka factors that generated induced pluripotent stem cells (iPSCs) (Takahashi and Yamanaka, 2006).

PROM1. Prominin-1, also named CD133, is a cell surface glycosylated transmembrane protein extensively used as CSC marker (Wang et al., 2010). It was discovered in human hematopoietic stem and progenitor cells (Miraglia et al., 1997), related to a worse clinical outcome in several types of tumors (Liou, 2019). PROM1+ cells also showed to express endothelial CDH5 and extracellular proteases MMP2 and 9, showing characteristics of endothelial progenitors and contributing to VM (Liu et al., 2013; Wang et al., 2010).

SOX2. Sex-determining region Y-box transcription factor 2 is other Yamanaka factor (Takahashi and Yamanaka, 2006). It is involved in the early development and maintenance of undifferentiated embryonic stem cells, as well as in promoting of self-renewal, undifferentiation of CSCs, tumor growth and metastasis (Garza Treviño et al., 2019; Yang et al., 2020).

These four CSC markers have shown to act in an interconnected manner in different contexts. For instance, *SOX2* and *PROM1* co-expression is essential for sphere-forming ability in glioblastoma cells (Song et al., 2016), *PROM1* expression is directly proportional to *NANOG* and *POU5F1* in head and neck cancer (Chen et al., 2011), and *PROM1* requires for its expression in human lung cancer that *POU5F1* and *SOX2* bind to its promoter 1 (Iida et al., 2012). In addition, the co-expression of these CSC markers is usually associated with higher aggressiveness and worse clinical prognosis, as it was observed for glioblastoma (Bradshaw et al., 2016), rectal (Saigusa et al., 2009) or pancreatic cancer (Nomura et al., 2015).

Among the plethora of markers that CSCs express, it results very interesting for this thesis the identification of endothelial related genes such as *CDH5*, *EPHA2*, *LAMC2* and *KDR* (Yao et al., 2013). The expression of these molecules corroborates once again the relevance of CSCs in vasculogenic mimicry, phenomenon that will finally be introduced in the following section.

8. Vasculogenic mimicry

The term vasculogenic mimicry (VM) was coined in 1999 to describe a mechanism of tumor neovascularization characterized by the formation of fluid-conducting channels by highly aggressive and genetically dysregulated melanoma cells (Folberg and Maniotis, 2004; Maniotis et al., 1999). Accordingly, these highly invasive melanoma cells would act in absence of endothelial cells, mimicking the vasculature pattern and acquiring the so-called endothelial-like (EL) phenotype (Figure 16).

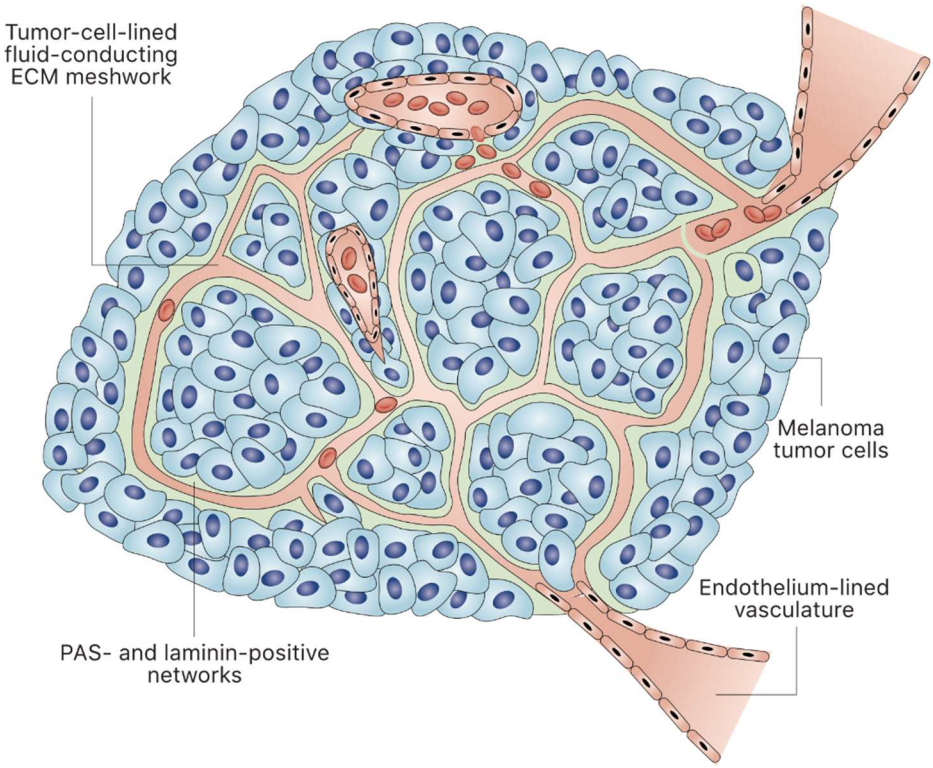

Figure 16. Schematic diagram of vasculogenic mimicry formation.
Vasculogenic mimicry describes the ability of melanoma tumor cells to line and create fluid-conducting networks. These networks are independent but close to endothelium-lined vasculature, and ECM plays a crucial role in their formation. VM has been detected in vivo by the identification of PAS- and laminin-positive networks. Modified from (Hendrix et al., 2003a)

Vasculogenic mimicry has been described both *in vitro* and *in vivo* and, in addition to melanoma (Seftor et al., 2001), it has been identified in several cancer types associated with poor overall survival, including osteosarcoma (Cai et al., 2004), breast (Shirakawa et al., 2002), prostate (Sharma et al.,

2002), ovarian (Sood et al., 2001, 2002), lung cancers, glioma and hepatocellular carcinoma (Luo et al., 2020), among others.

In vivo vasculogenic mimicry was originally identified by the appearance of periodic acid-Schiff (PAS)-positive laminin-rich looping patterns in tumor histological sections (Maniotis et al., 1999). Although the functionality of vasculogenic mimicry has been criticized (McDonald et al., 2000), subsequent works revealed the 3D structure of these structures (Chen et al., 2003) and demonstrated blood circulation in VM tubes (Frenkel et al., 2008), confirming it as an actual mechanism of vascularization. The appearance of these PAS-positive patterns correlated with an increased occurrence of metastasis and poor prognosis outcome (Thies et al., 2001; Warso et al., 2001). Indeed, in a very recent review, Valdivia et al. compiled and compared the presence of vasculogenic mimicry and the survival time of patients across 20 cancer types, revealing that vasculogenic mimicry has a very negative impact on the overall survival of oncological patients (Valdivia et al., 2019) (Figure 17).

As already introduced, cancer stem cells are directly involved in vasculogenic mimicry. In one side, it has been reported the ability of aggressive melanoma cells to revert to a stem-like state and express CSC- or stemness-related genes (Yao et al., 2011). Later investigations suggested that such pluripotent CSCs are the basis of vasculogenic mimicry formation in tumors (Luo et al., 2020), according to their capacity to differentiate into endothelial-like cells and align to create VM channels (Kirschmann et al., 2012; Yao et al., 2011).

However, the expression of those stemness-related genes are not the only feature that characterizes VM cells. Indeed, it is necessary to emphasize the importance of an endothelial-related signature in these cells. There exists a plethora of endothelial markers which are related with angiogenesis and vasculogenesis which are also involved. In addition, they are also usually closely related with CSC- or stemness-related features, comprising the complex and intricate mechanism that underlies vasculogenic mimicry. A subset of these endothelial-related markers, as well as their known involvement

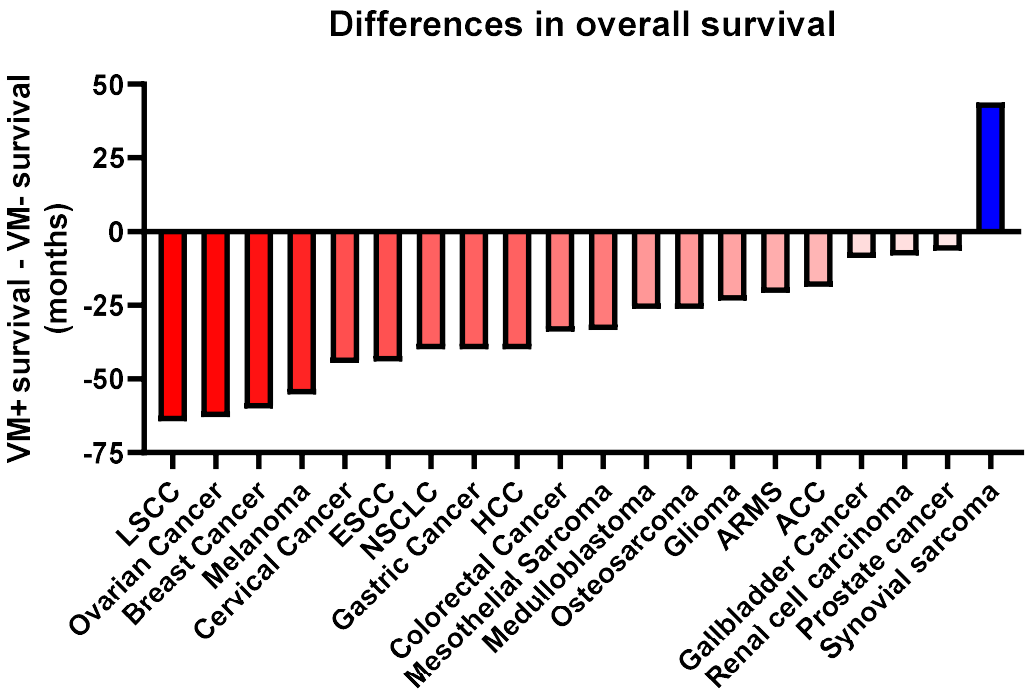

Figure 17. Vasculogenic mimicry negatively contributes to patient survival.
Waterfall plot representing the differences in survival time (months) between patients that have shown VM in their tumor samples and patients that do not (VM+ survival – VM- survival). Data of 2229 patients were collected, with a VM incidence of 29,7%. LSCC: laryngeal squamous cell carcinoma; esophageal squamous cell carcinoma; NSCLC: non-small cell lung cancer; HCC: hepatocellular carcinoma; ARMS: alveolar rhabdomyosarcoma; ACC: adrenocortical carcinoma. Modified from (Valdivia et al., 2019).

Regarding the therapeutic targeting of vasculogenic mimicry, it is remarkable that antiangiogenic therapies targeting endothelial cells failed against it (Rybak et al., 2003; van der Schaft et al., 2004). In contrast, promising results have been reported with compounds designed to target some of its molecular regulators, such as CDH5 and EPHA2 (Mabeta, 2020).

A critical step for the development of vasculogenic mimicry is the remodeling of the extracellular matrix, mainly conducted by extracellular proteases. MMPs, for instance, have demonstrated to induce vasculogenic mimicry through LAMC2 cleavage, and the use of some MMPs inhibitors resulted in a dramatic reduction of VM-associated genes such as *CDH5* and *TIE1* (Hendrix et al., 2003b; Seftor et al., 2001). Importantly, previous research conducted by this laboratory already studied the relationship between extracellular protease ADAMTS1 and vasculogenic mimicry (Casal et al., 2010). Such work reported an increased expression of ADAMTS1 in

melanoma and Ewing sarcoma cells correlating with an endothelial-like phenotype, as well as an impaired capacity to generate endothelial-like networks when ADAMTS1 was knocked down. This study also showed that the overexpression of ADAMTS1 caused an increased tumor growth and the acquisition of the endothelial-like phenotype by plastic tumor cells, which acquired a specific gene signature that included *CDH5*, *TIE1* and *LAMC2* (Casal et al., 2010).

Indeed, this previous work established the bases for this current thesis in an attempt to unveil the relationships between endothelial-like phenotype and CSC features, regulated by an ECM modifying enzyme such as ADAMTS1. Importantly, these studies will be developed in the tumor type in which vasculogenic mimicry was initially described, i.e. melanoma (Maniotis et al., 1999), and more specifically this thesis will focus in the rare uveal melanoma, also a paradigm in the investigation on vasculogenic mimicry.on vasculogenic mimicry, is briefly presented in Box 3.

Box 3. Endothelial genes related to vasculogenic mimicry

CDH5. Cadherin-5, also named VE-Cadherin and CD144, is a junctional transmembrane protein which promotes homotypic cell-to-cell interaction (Hendrix et al., 2001). It promotes vessel stabilization in quiescent endothelial cells by inhibiting KDR, and it is essential for the formation of VM networks (Carmeliet and Jain, 2011; Hendrix et al., 2001, 2003b). CDH5 colocalizes and interacts with EPHA2, promoting VM in aggressive melanoma (Hess et al., 2006). It is a poor prognosis factor for glioblastoma multiforme, where it has shown to be specifically activated in glioma stem cells (GSCs) (Mao et al., 2013).

EPHA2. Ephrin type-A receptor 2 is a receptor protein tyrosine kinase involved in angiogenesis and tumor growth (Dobrzanski et al., 2004; Hendrix et al., 2003c). It is often overexpressed in melanoma, and it displays an essential role in VM (Demou and Hendrix, 2008; Hess et al., 2001; Maniotis et al., 1999). It has also shown to be expressed in GSCs that are involved in VM (El Hallani et al., 2010).

ENG. Endoglin, also named CD105, is a transmembrane homodimer glycoprotein associated with vascular endothelium proliferation and angiogenic properties in several cancer types (Gougos and Letarte, 1990). Considered a poor prognosis factor in high grade gliomas and Ewing sarcoma, ENG is closely related to CSC features, particularly to PROM1+ cells and POU5F1 overexpression in GSCs (El Hallani et al., 2010; Pardali et al., 2011; Smith et al., 2012, 2015). In addition, it is overexpressed in aggressive melanoma VM+ cells, correlating with VM structures.

KDR. Vascular endothelial growth factor 2, also named VEGFR2 or FLK1, is involved in blood vessel permeability, endothelial cell proliferation and tube formation. It has been associated with malignant transformation of melanoma cells and with VM (Francescone et al., 2012; Halaban and Neufeld, 1993). KDR is co-expressed with PROM1 in GSCs, promoting VM (Wu et al., 2017; Yao et al., 2013).

LAMC2. Laminin subunit gamma-2 is a major component of BM involved in cell attachment and migration, angiogenesis and tumor metastasis. It is highly expressed in aggressive VM+ melanoma cells, correlating with the activity of extracellular proteases MMP2 and 14 (Hendrix et al., 2003b; Seftor et al., 2001). LAMC2 is also found overexpressed in GSCs derived from tumors exhibiting VM (El Hallani et al., 2010).

TIE1 and TEK. Both TIE1 (tyrosine-protein kinase receptor Tie-1) and TEK (angiopoietin-1 receptor, also named TIE2) belong to the Tie family of endothelial-specific receptor tyrosine kinases, involved in tumor angiogenesis and growth (Masiero et al., 2013; Seegar et al., 2010). They are also expressed in aggressive VM+ cells (Hendrix et al., 2001; Maniotis et al., 1999; Sood et al., 2002), as well as being related to stem-like features (Ricci-Vitiani et al., 2010).

9. Uveal melanoma

Uveal melanoma (UVM) is a malignant tumor that arises in melanocytes of any location of the uveal tract, the pigmented layer of the eye encompassing the iris, ciliary body and choroid (Chattopadhyay et al., 2016) (Figure 18). It is the most common primary intraocular malignancy in adults (Castet et al., 2019; Thornton et al., 2020). Uveal melanoma is considered a rare cancer, with an incidence of 4,9 – 5,2 cases per million in the United States and 2 – 8 in Europe (Castet et al., 2019).

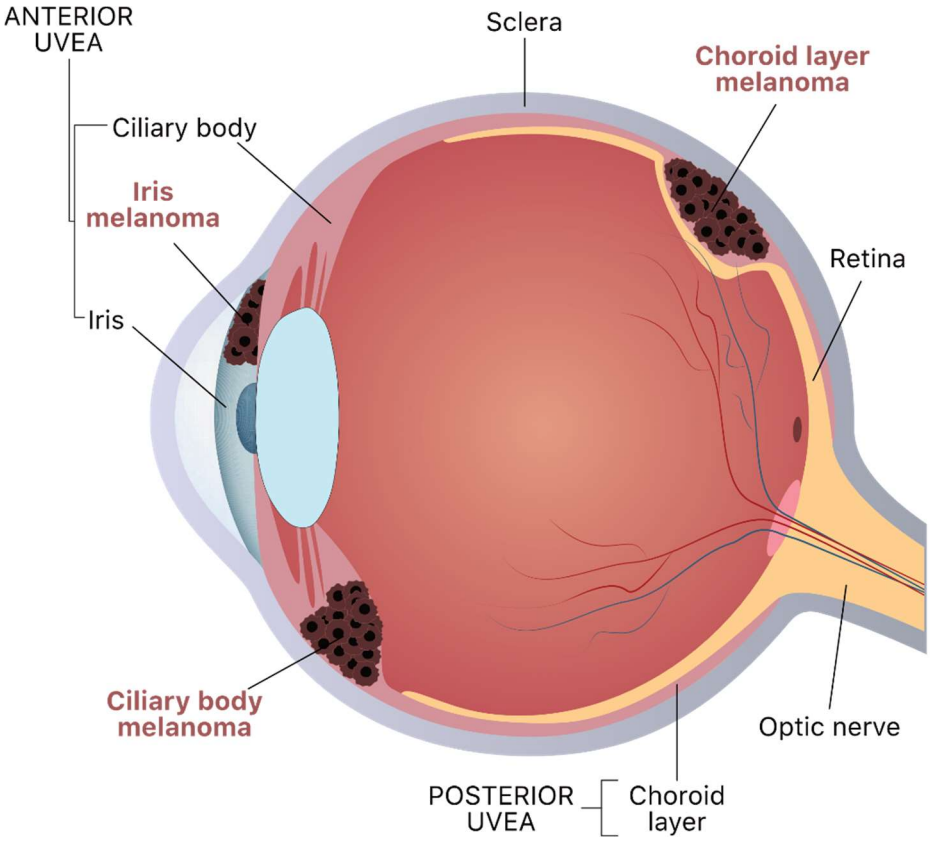

Figure 18. Illustration of the uveal tract and different uveal melanomas.
Uveal melanoma can be developed in any location of the uveal tract: iris, ciliary body and choroid layer. Designed with the help of Freepik.

While primary uveal melanoma is treated with surgery or radiation and it has a low local recurrence (95 % of success), up to 50 % of patients will develop metastasis, mainly to the liver, in a median time of 5 years after the treatment of the primary tumor (Blum et al., 2016; Robertson et al., 2017). In

addition, it is a very appropriate model to study the hematogenous dissemination of cancer, since the eye lacks lymphatic vessels (Seftor et al., 2002). Another peculiar aspect of uveal melanoma is that continuously evolves from primary tumors to metastases, displaying more oncogenic mutations in the metastatic stages than in the earlier ones, in contrast to most other tumor types that usually show genetic similarities between these two time points (Shain et al., 2019).

Several large-scale sequencing works have uncovered the genomic landscape of uveal melanoma, revealing genetic alterations distinctive from other melanoma subtypes (Shain et al., 2019). Those analyses reported the existence of different subsets of uveal melanomas with specific genomic profiles, and served to established an initial clustering division into two prognostic subgroups. This analysis discriminated low metastatic risk (low-grade) or class 1 uveal melanomas from high metastatic risk (high-grade) or class 2, based on a 15 gene expression profile (GEP) (Table 2) (Harbour, 2014; Onken et al., 2004).

This initial subdivision supported further studies with several, and more recent, large-scale techniques, including next-generation sequencing (NGS) (Afshar et al., 2019; Thornton et al., 2020), whole exome sequencing (WES) (Royer-Bertrand et al., 2016) and multiplatform analyses (Robertson et al., 2017; Shain et al., 2019).

Significantly, the high amount of publicly available data allowed the *in silico* analysis included in this thesis, complementary to its experimental approaches, not requiring the use of fresh samples, something of crucial importance given the scarce availability of samples of this rare cancer. Such *in silico* tools will be briefly presented in the next section.

Up-regulated in class 2 uveal melanoma	
CDH1	Cadherin 1 (E-cadherin)
ECM1	Extracellular matrix protein 1
HTR2B	5-Hydroxytryptamine (serotonin) receptor 2B
RAB31	RAB21, member of RAS oncogene family
Down-regulated in class 2 uveal melanoma	
EIF1B	Eukaryotic translation initiation factor 1B
FXR1	Fragile X mental retardation, autosomal homolog 1
ID2	Inhibitor of DNA binding 2
LMCD1	LIM and cysteine-rich domains 1
LTA4H	Leukotriene A4 hydrolase
MTUS1	Microtubule associated scaffold protein 1
ROBO1	Roundabout guidance receptor 1
SATB1	SATB homeobox 1
Control genes	
MRPS21	Mitochondrial ribosomal protein S21
RBM23	RNA-binding motif protein 23
SAP130	Sin3A associated protein 130

Table 2. Differentially expressed genes between low and high metastatic risk uveal melanomas.
Genes included in the 15-gene expression profile that allowed an initial clustering of uveal melanomas in class 1 (low metastatic risk) and class 2 (high metastatic risk). Modified from (Harbour, 2014)

10. *In silico* tools to study cancer

Bioinformatics and its applications on cancer research is a rising field, becoming a very powerful tool in the attempt of deciphering cancer behavior. The enormous quantity of downloadable data of different nature (gene expression, mutation, clinical records, etc.) is continuously growing, and these data may support and give strength to results obtained directly from the bench. The wide variety of available data allows researchers to conduct a multitude of different analyses. In addition, the large number of samples allows testing hypotheses with greater statistical strength that would otherwise be impossible, either due to limited availability, separation of the originating laboratories, elevated economic costs, etc. Moreover, it becomes easier to share data and results between different laboratories and researchers, improving collaborations so that investigation can progress more rapidly.

Along with the outbreak of bioinformatics, there has also been a large increase of platforms that facilitate the understanding of big data for not specialized users. This thesis has taken advantage of some of these platforms to conduct a modest bioinformatics analysis on some parameters of interest related to melanoma, and they will be introduced in the same order as they are developed in the *Results* section.

Heuristic Online Phenotype Prediction

Heuristic Online Phenotype Prediction (HOPP) platform is an online gene expression analysis tool that allows the user to predict the phenotype of a desired cell sample by comparing its gene expression data with two previously established signatures (Widmer et al., 2012). These two gene signatures are strongly related with either a proliferative or an invasive phenotype of melanoma cells, so HOPP will help to predict which phenotype will display a queried cell sample. It also facilitates the comparison of the expression of a given gene between these two phenotypes. HOPP allows the user to analyze its own data, explore the National Center for Biotechnology Information Gene Expression Omnibus (NCBI GEO) database or browse the HOPP database. The expression data analyzed in this work came from a

combination of HOPP database with additional gene expression data from NCBI GEO database.

NCBI Gene Expression Omnibus

NCBI GEO is a public repository of genomics data that contains approximately 4 million of array- and sequence-based samples. It was used in this thesis to obtain RNA-Seq data of the cell lines considered in it, being an essential part of the *in silico* analysis. Once these RNA-Seq data were obtained, they were classified into two groups according to whether the corresponding cells were capable of exhibiting an endothelial-like phenotype or not. Then, an analysis of differentially expressed genes (DEGs) identification was conducted with them with the help of the Bioinformatics Unit of GENyO.

Once the DEGs were identified, they were subjected to Gene Ontology (GO) enrichment analysis to determine in which biological processes are they involved. The interpretation of these results benefited from the utilization of the REViGO platform (Supek et al., 2011). REViGO is an online tool that removes redundant GO biological processes (named GO terms) from a given list and summarizes the others.

All these determinations could not have been conducted without the existence of a repository such as the NCBI GEO. Similarly, The Cancer Genome Atlas database was used to perform further *in silico* analyses, in this case with samples from uveal melanoma patients.

The Cancer Genome Atlas

The Cancer Genome Atlas (TCGA) is a massive database of over 20.000 primary cancer samples among 33 cancer types which is publicly available. It was launched in 2006 and, since then, TCGA has generated over 2.5 petabytes of genomic, epigenomic, transcriptomic and proteomic data. Among this huge amount of data, this thesis was focused on the TCGA-UVM project, which contains mRNA expression data and clinical parameters of 80 human uveal melanomas (https://portal.gdc.cancer.gov/projects/TCGA-UVM) (Robertson et al., 2017). Two different online platforms were used to facilitate the interpretation of the raw data offered by the TCGA.

On one hand, UCSC Xena Functional Genomics Explorer platform (Goldman et al., 2020) allowed the identification of genes that behave as prognostic factors in human uveal melanoma, and facilitated gene expression comparisons between different tumor clinical stages. On the other hand, cBioPortal platform (Cerami et al., 2012; Gao et al., 2013) helped in the evaluation of co-expressed genes across the TCGA-UVM cohort of patients, constituting the basis for further analyses.

All these data provided by these platforms and the analyses that were conducted with them complemented the experimental contribution of this thesis. The large amount of cell line and tumor samples that were analyzed strengthened the results obtained from both cell lines experiments and *in vivo* assays.

OBJECTIVES

The main objective of this thesis was to study the contribution of the extracellular protease ADAMTS1 to the plasticity phenomena on uveal melanoma. For that purpose, both endothelial-like and stemness features were evaluated in different contexts, and the information of other ADAMTSs contributed to a more comprehensive understanding. Four specific objectives could be extracted from the main one, composed by the following tasks:

Objective 1. To develop a general characterization of human melanoma cell lines.

1.1. *In vitro* analyses of the expression levels of genes that are involved in uveal melanoma plasticity and *in silico* prediction of their phenotype.

1.2. Assessment of their endothelial-like phenotype and identification of specific genes associated with it.

1.3. Study of the loss of function of ADAMTS1, focusing on its consequences on the endothelial-like phenotype of melanoma cell lines.

Objective 2. To analyze the contribution of ADAMTS1 to tumor development using in vivo xenograft models of human uveal melanoma.

2.1. Evaluation of the effect of ADAMTS1 inhibition on tumor growth in different models of xenografts.

2.2. Identification of the consequences of ADAMTS1 inhibition on tumor vasculature.

Objective 3. To study the role of ADAMTS1 over stemness features.

3.1. Analysis of the effect of ADAMTS1 over the *in vivo* stemness features of tumor xenografts.

3.2. Study of the contribution of ADAMTS1 to the *in vitro* stemness features of melanoma spheres.

Objective 4. To in silico assess the relevance of the endothelial-like plasticity and ADAMTS proteases in human uveal melanoma samples.

4.1. Identification of endothelial-related markers and extracellular matrix molecules as poor prognosis factors for uveal melanoma.

4.2. Evaluation of the contribution of ADAMTS proteases and substrates to clinical outcomes of uveal melanoma.

RESULTS

1. Characterization of human melanoma cell lines

According to the interest of this thesis to study the extracellular protease ADAMTS1 in human melanoma, an initial characterization of human melanoma cell lines was approached. The cell line panel used in this work includes uveal (MUM-2B and MUM-2C) and skin cutaneous (A-375, C8161, G-361, SK-MEL-28, SK-MEL-103 and SK-MEL-147) melanoma cells. Previous research conducted by this laboratory with some of these human melanoma cells served as basis for this initial characterization (Casal et al., 2010; Fernández-Rodríguez et al., 2016). It included expression analyses of several genes of interest, evaluation of their endothelial-like (EL) phenotype and *in silico* analyses to strengthen the experimentally obtained results.

1.1. Gene expression analyses of human melanoma cell lines

The initial characterization of the expression levels of genes of interest among human melanoma cell lines was determined by quantitative PCR (qPCR). The analyzed genes were divided into three groups, attending to their roles in different processes.

The first group included genes involved in the extracellular matrix (ECM) regulation. They were the extracellular protease *ADAMTS1*, main objective of this study, and some of its substrates with a role in ECM functionality and cancer, namely *IGFBP2, NID1*, *NID2* and *VCAN*. Our qPCR analysis showed a high heterogeneity for all these genes among cell lines (Figure 19). However, it was observed that, except *NID2*, the rest of these ECM molecules were medium or highly expressed in these cell lines. Moreover, in the case of *IGFBP2* there were two groups of cell lines with clearly differentiated expression levels. Something that began to be perceived already within this first group of genes and that would be more evident with later analyses was the dichotomy observed between MUM-2B and MUM-2C lines. These two related cell lines are traditionally classified as highly (MUM-2B) and poorly aggressive (MUM-2C) uveal melanoma cell lines (Maniotis et al., 1999), and their differences in terms of gene expression resulted very interesting for this thesis. In addition, an evident similarity was detected between gene

expression of uveal MUM-2B and cutaneous C8161, both described as highly aggressive melanoma cell lines (Hendrix et al., 2001).

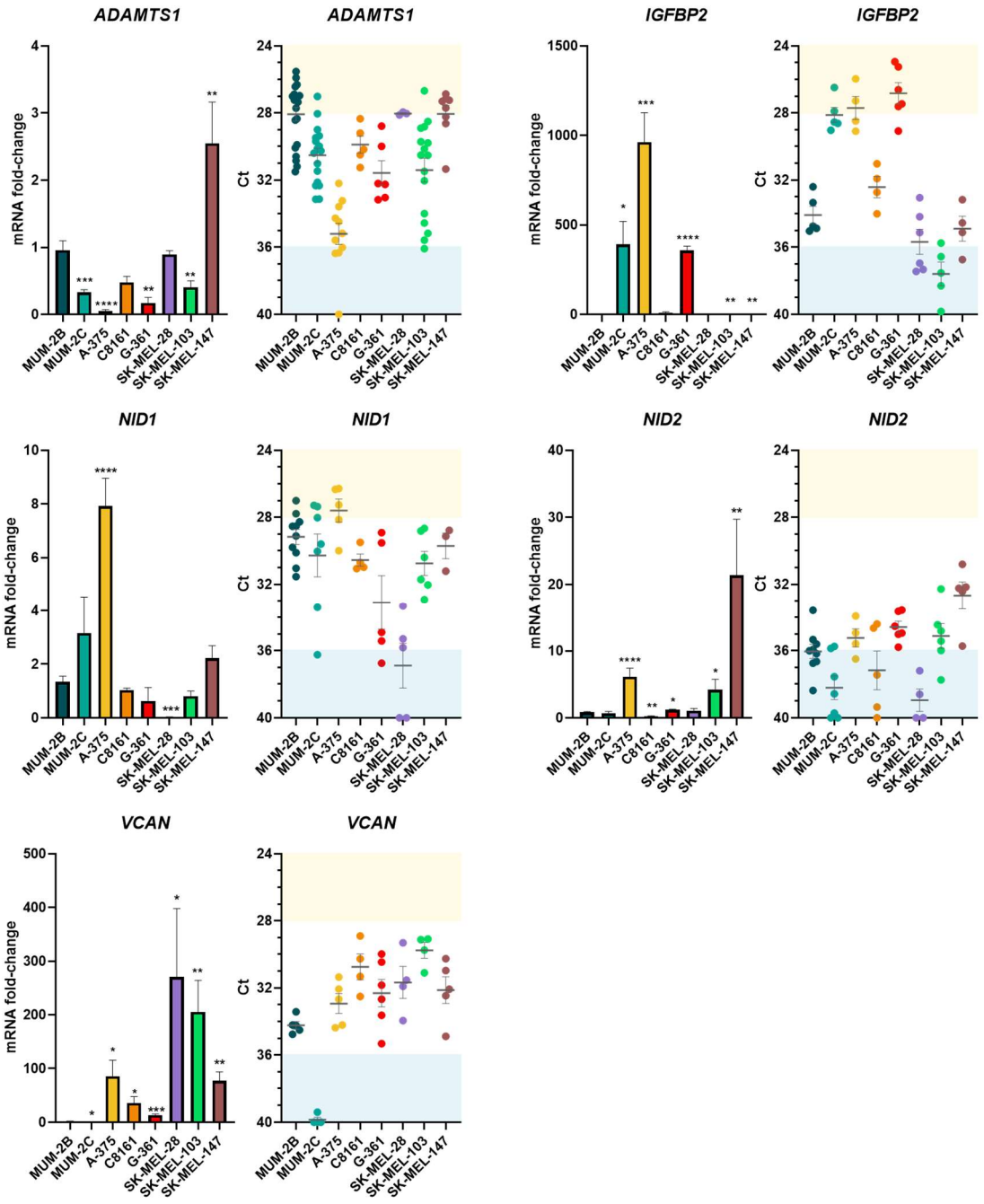

Figure 19. qPCR analysis of genes involved in ECM remodeling.
Graphs representing mRNA fold change expression and Ct values of ADAMTS1, IGFBP2, NID1, NID2 and VCAN in human melanoma cell lines. High and low gene expression is depicted in Ct graphs with yellow and blue backgrounds, respectively (n = 5-21 for MUM-2B, n = 4-17 for MUM-2C, n = 4-11 for A-375, n = 4-5 for C8161, n = 5-6 for G-361, n = 3-6 for SK-MEL-28, n = 4-16 for SK-MEL-103 and n = 3-8 for SK-MEL-147) (****, $p < 0.0001$; ***, $p < 0.001$; **, $p < 0.01$; *, $p < 0.05$. MUM-2B cell line was used as control for statistical analyses).

The second group of genes included those involved in the acquisition of an endothelial-like phenotype and closely related with VM. They are *CDH5*, *ENG*, *EPHA2*, *KDR*, *LAMC2*, *TEK* and *TIE1*. As mentioned in the *Introduction*, the acquisition of an endothelial-like phenotype by cancer cells represents a paradigm of their plasticity. In line with the previous group of genes, this analysis showed even more heterogeneity (Figure 20). Some genes were highly expressed in all cell lines, like *ENG*, others were very low, like *TEK*, and others depended on the particular cell line. Again, similar expression patterns of uveal MUM-2B and cutaneous C8161 cells could be detected for *CDH5*, *ENG*, *KDR* and *LAMC2* genes, as well as the clear differences between highly aggressive MUM-2B and poorly aggressive MUM-2C, observed here for all markers except *TIE1*.

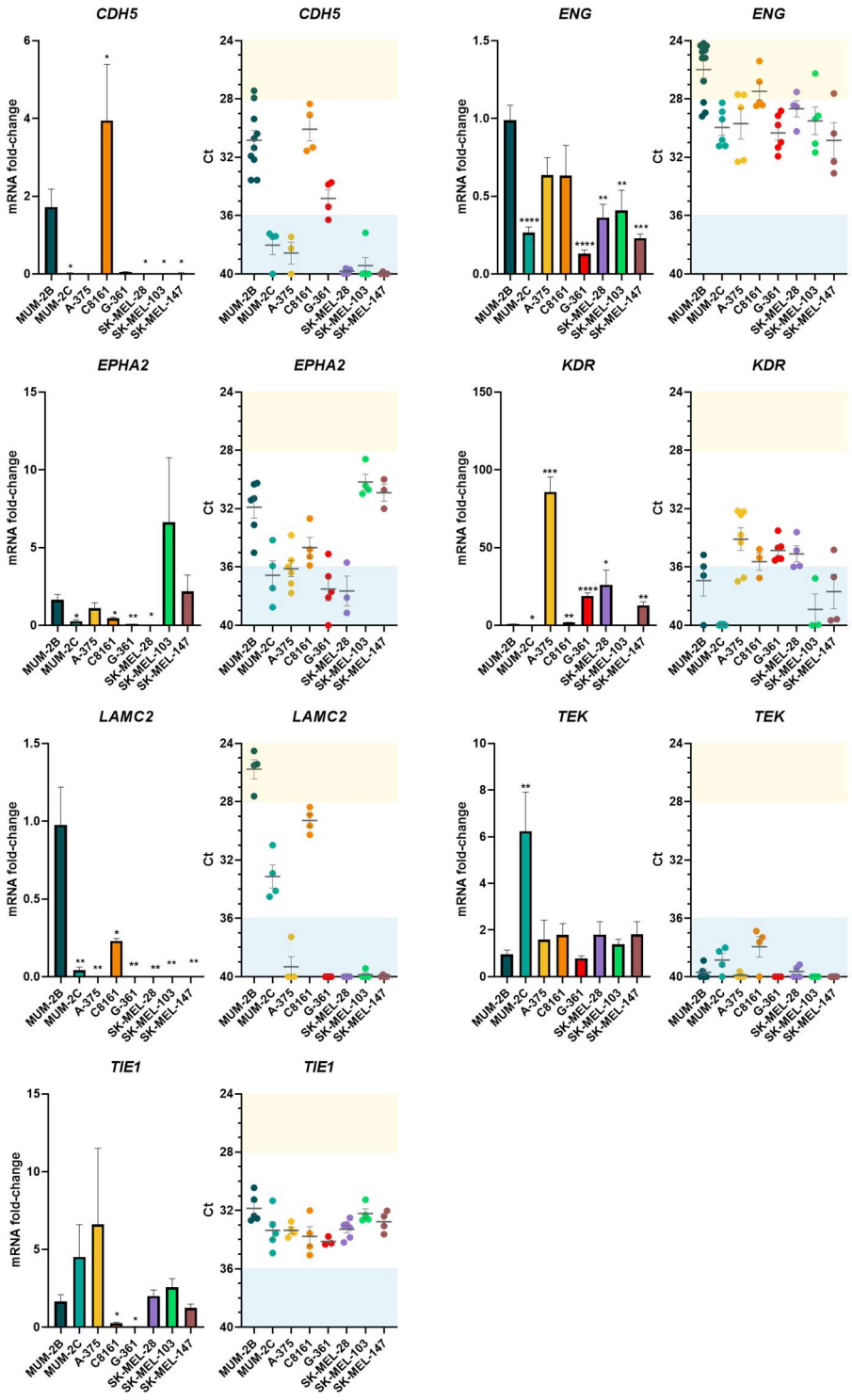

Figure 20. qPCR analysis of genes related to the endothelial-like phenotype.
Graphs representing mRNA fold change expression and Ct values of CDH5, ENG, EPHA2, KDR, LAMC2, TEK and TIE1 in human melanoma cell lines. High and low gene expression is depicted in Ct graphs with yellow and blue backgrounds, respectively (n = 11-4 for MUM-2B, n = 4-6 for MUM-2C, n = 3-7 for A-375, n = 3-5 for C8161, n = 3-6 for G-361, n = 3-6 for SK-MEL-28, n = 3-5 for SK-MEL-103 and n = 3-5 for SK-MEL-147) (****, $p < 0.0001$; ***, $p < 0.001$; **, $p < 0.01$; *, $p < 0.05$. MUM-2B cell line was used as control for statistical analyses).

Finally, a third group included genes classically related with stemness and cancer stem cells (CSC): *NANOG*, *POU5F1*, *PROM1* and *SOX2*. In general they displayed low expression levels in all cell lines (Figure 21), despite the stemness features already attributed to melanoma and more particularly to aggressive uveal melanoma (Djirackor et al., 2019; Kalirai et al., 2011; Thill et al., 2011). Moreover, these low levels suggest that cells under standard culture conditions are not adequate to study CSC features and not meaningful conclusions can be drawn at this point.

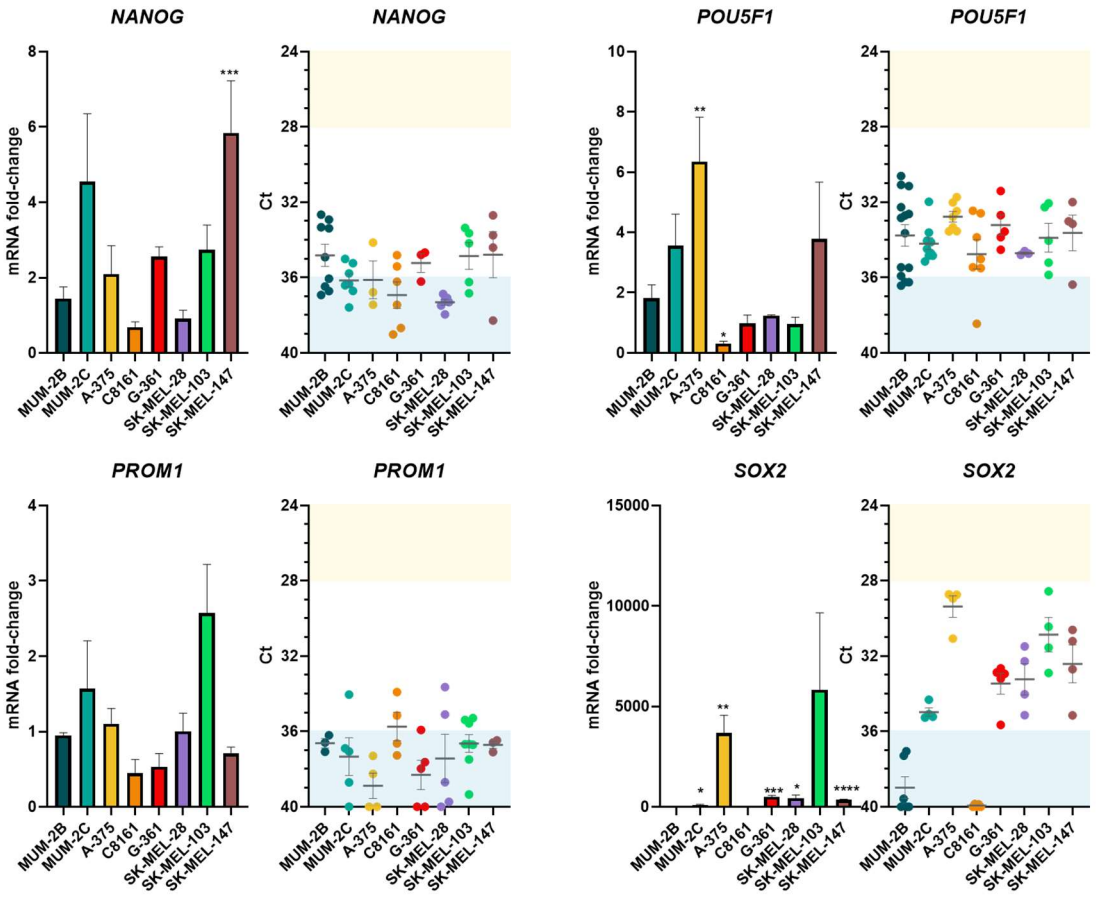

Figure 21. qPCR analysis of genes related to stemness features.
Graphs representing mRNA fold change expression and Ct values of NANOG, POU5F1, PROM1 and SOX2 in human melanoma cell lines. High and low gene expression is depicted in Ct graphs with yellow and blue backgrounds, respectively (n = 3-14 for MUM-2B, n = 4-9 for MUM-2C, n = 3-7 for A-375, n = 4-7 for C8161, n = 3-5 for G-361, n = 4-6 for SK-MEL-28, n = 4-8 for SK-MEL-103 and n = 3-5 for SK-MEL-147) (****, $p < 0.0001$; ***, $p < 0.001$; **, $p < 0.01$; *, $p < 0.05$. MUM-2B cell line was used as control for statistical analyses).

The initial characterization of the gene expression divided by groups allowed to obtain a preliminary overview of main biological processes of interest for this work. A remarkable observation was the great heterogeneity

shown among all the melanoma cell lines. To reach a complete picture of all the evaluated genes, a heatmap representation was conducted with the expression data obtained from qPCR analyses (Figure 22). Apart from heterogeneity, this representation helped visualizing some suggestions already remarked, such as the closer expression pattern between uveal MUM-2B and cutaneous C8161, or the evident differences between highly aggressive MUM-2B and poorly aggressive MUM-2C.

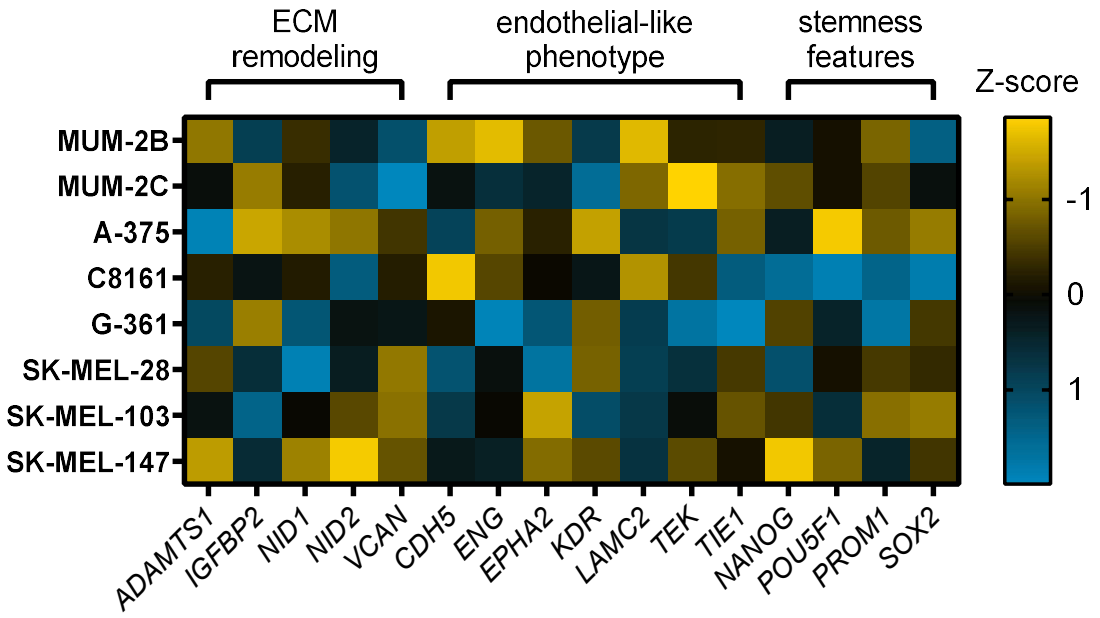

Figure 22. Heatmap representation of gene expression levels among human melanoma cell lines.
Expression levels of the 16 genes of interest for the 8 human melanoma cell lines included in this work were represented together. Gene expression data were scaled by columns, obtaining the Z-score by genes to allow the comparison between cell lines. Since heatmap representation was obtained from ΔCt data, a negative Z-score is equivalent to high expression levels and a positive Z-score to low levels (number of samples is the same as in Figures 19-21).

In addition to the heatmap, not separating the genes by groups allowed correlation analyses between them even though they were involved in different processes. Although these analyses were conducted in a low number of melanoma cell lines, the finding of significant correlations may help to interpret further results. Particularly here we highlighted three correlations (Figure 23). First, the positive correlation *CDH5* vs. *LAMC2* genes was appealing according to the endothelial-related nature of both genes and also the relevance of *LAMC2* as a key element of the ECM. Second,

the positive correlation *EPHA2 vs. NID1* also included a main endothelial marker with the BM component *NID1*, indeed recognized as an ADAMTS1 substrate. A third correlation was the negative one that resulted between extracellular protease *ADAMTS1* and one of its substrates *IGFBP2*. It resulted very interesting for this thesis, since it was opposite to previous reports by this laboratory (Martino-Echarri et al., 2014), and it will be furtherly discussed.

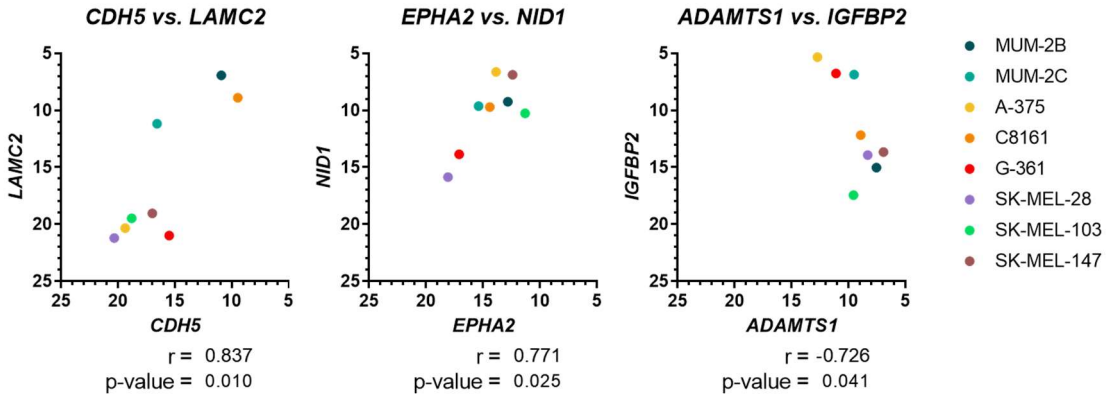

Figure 23. Correlation analyses of gene expression between melanoma cell lines. Scatter plot representing Pearson correlation analysis of gene expression levels between CDH5 and LAMC2, EPHA2 and NID1, and ADAMTS1 and IGFBP2. Axes represent gene expression by ΔCt (r = Pearson correlation coefficient).

1.2. Heuristic Online Phenotype Prediction (HOPP) of melanoma cell lines

As introduced above, the in silico tool Heuristic Online Phenotype Prediction (HOPP) allows to predict the behaviour of melanoma cells towards a proliferative or invasive phenotype (Widmer et al., 2012). Accordingly, RNA-Seq data of the human melanoma cells considered in this thesis were extracted from Gene Expression Omnibus (GEO) database (

Table 4) and were subjected to HOPP analysis (Figure 24).

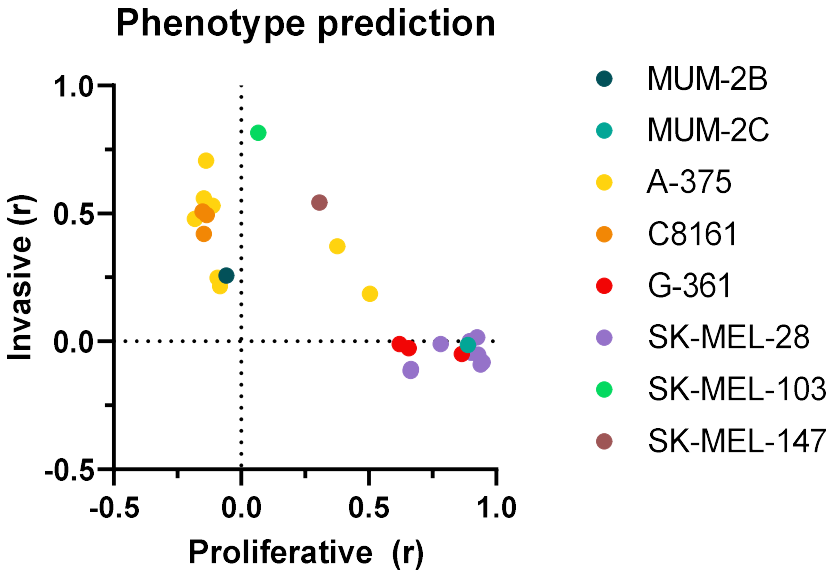

Figure 24. HOPP analysis of human melanoma cell lines.
Widmer plot representing HOPP analysis results, where the x- and y-axis describe the correlation with the proliferative and invasive phenotype signature standards, respectively. GEO accession numbers and proliferative and invasive coefficients for every cell line are listed in

Table 4.

This study revealed the existence of two different clusters among these melanoma cell lines corresponding with invasive and proliferative phenotypes. With the exception of A-375 cells, the rest could be clearly included in one or the other group. As occurred with the gene expression analyses showed in previous section, a clear dichotomy was observed between highly aggressive MUM-2B and poorly aggressive MUM-2C cell lines, which now were classified as invasive and proliferative, respectively. In addition, uveal MUM-2B and cutaneous C8161 confirmed their similarity being both identified as invasive cells.

In addition to phenotype prediction, a second feature of HOPP tool allowed the evaluation of the expression of certain genes in all invasive and proliferative cells included in the platform. Importantly, the analysis of genes of interest revealed that ADAMTS1 was significantly upregulated in invasive melanoma cells in comparison with proliferative ones (Figure 25a), suggesting the importance of the protease for this phenotype as it would be furtherly studied. In addition, endothelial-related genes *ENG*, *EPHA2*, *KDR* and *LAMC2* were also upregulated in invasive cells supporting the putative contribution of an endothelial-like phenotype for melanoma invasive properties (Figure 25b).

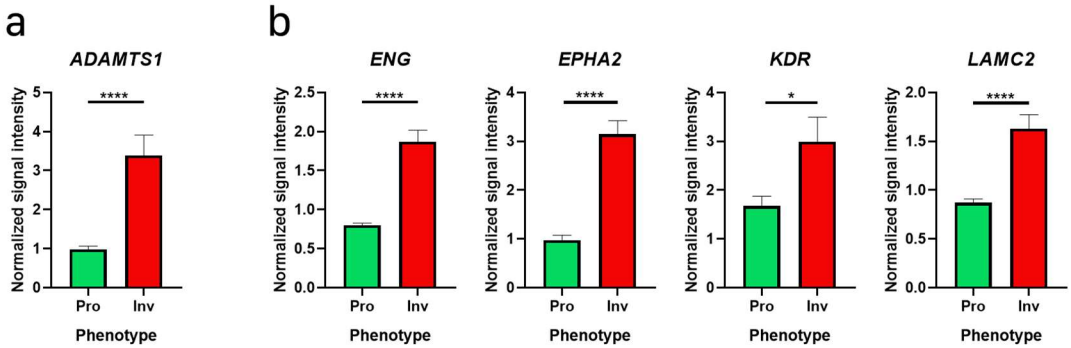

Figure 25. Differentially expressed genes between HOPP phenotypes.
Graph representing gene expression comparison of (a) ADAMTS1 and (b) ENG, EPHA2, KDR and LAMC2, between proliferative (Pro) and invasive (Inv) melanoma cells from HOPP database. Analyzed probesets were 222162_s_at (ADAMTS1), 201809_s_at (ENG), 203499_at (EPHA2), 203934_at (KDR) and 202267_at (LAMC2) (n = 101 for Pro and n = 90 for Inv) (****, $p < 0.0001$; *, $p < 0.05$).

This connection between endothelial-related genes and invasive capacity was detected in vasculogenic mimicry (VM) as a relevant mechanism of tumor neovascularization studied in this thesis. It initial description already associated vasculogenic mimicry with aggressive melanoma cells that were able to acquire an endothelial-like phenotype (Maniotis et al., 1999). Moreover, the endothelial-related genes considered in this thesis have demonstrated their involvement in vasculogenic mimicry, and their upregulation in invasive melanoma cells support it. Furthermore, initial reports of vasculogenic mimicry included the study of MUM-2B and C8161 cells (Maniotis et al., 1999), triggering here the evaluation of the endothelial-like phenotype in all human melanoma cell lines considered in this thesis, as follows.

1.3. Assessment of endothelial-like phenotype of melanoma cells

After these characterizations, the study of melanoma cell lines included the performance of Matrigel assays to evaluate their endothelial-like phenotype. Matrigel is a solubilized basement membrane preparation which has been widespread used for studying angiogenesis and cancer research, since it allows cells to grow in an *in vitro* 3D setting (Benton et al., 2014). Moreover, the initial description of vasculogenic mimicry already included the use of Matrigel as a method to detect its characteristic tumor vascular-like networks (Maniotis et al., 1999). Human umbilical vein endothelial cells (HUVECs) were used as positive control for these experiments, clearly showing the called "vascular-like network" (Figure 26). Indeed these cells in Matrigel have been extensively used for testing pro- or anti-angiogenic compounds (Quesada-Gómez et al., 2015; Vailhé et al., 2001).

The endothelial-like phenotype of the eight melanoma cell lines used in this thesis was therefore evaluated. Previous Matrigel assays developed in the laboratory already revealed the different endothelial-like phenotype for MUM-2B and MUM-2C, EL+ and EL-, respectively (Casal et al., 2010), so this work aimed to expand this knowledge to other human melanoma cell lines.

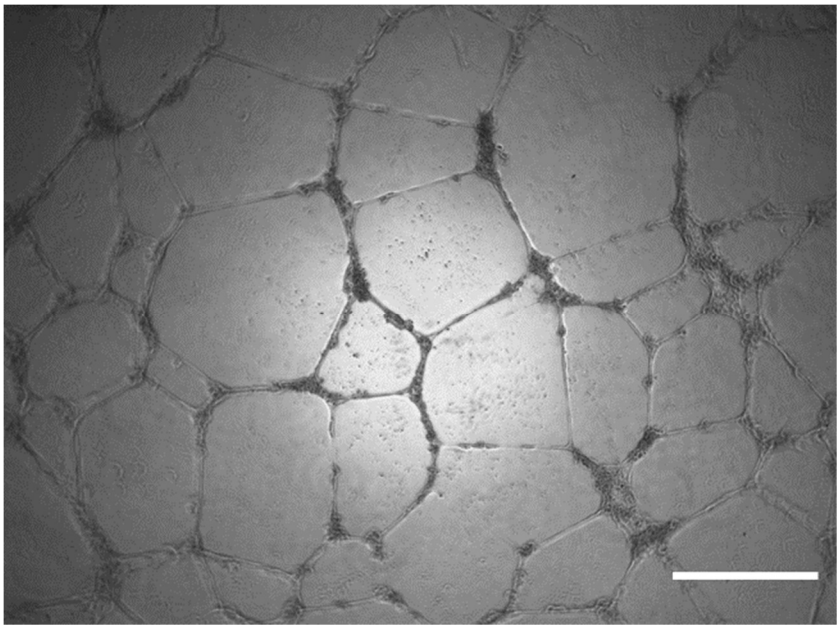

Figure 26. Matrigel experiment using HUVEC cell line.
Representative images of 3D Matrigel-based assay of human umbilical vein endothelial cells (HUVECs), 24 h after seeding. 20.000 cells/well were cultured (white scale bar = 500 µm).

Matrigel assays not only confirmed the different endothelial-like phenotype for uveal MUM-2B and MUM-2C cell lines that was previously demonstrated (Casal et al., 2010), but also allowed the classification of all cells into EL+ (MUM-2B, C8161, SK-MEL-28, SK-MEL-103 and SK-MEL-147) and EL- (MUM-

2C, A-375 and G-361), depending on whether they were able to form an endothelial-like network or just cell clusters (Figure 27).

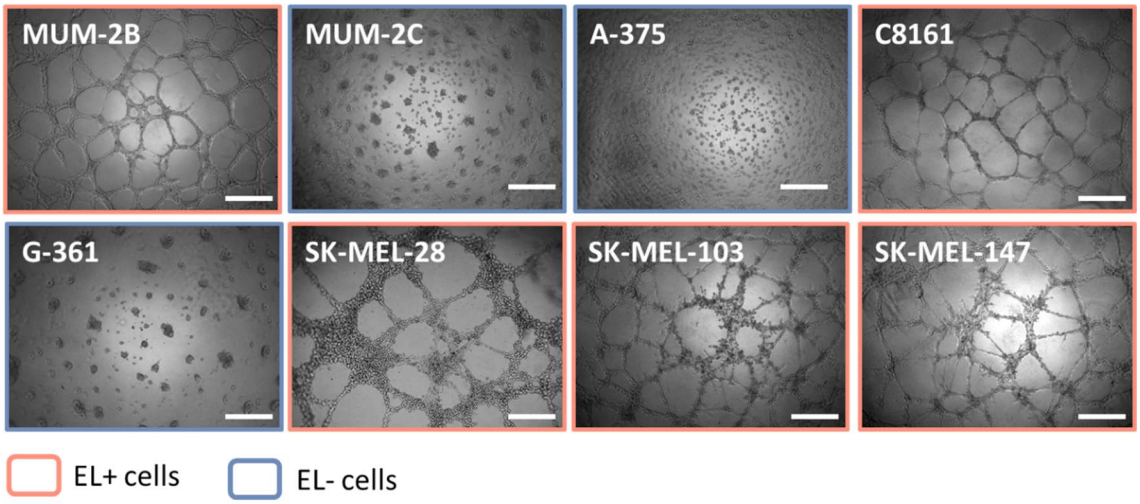

Figure 27. Human melanoma cell line classification in EL+ and EL- cells.
Representative images of 3D Matrigel-based assay of human melanoma cell lines, 24 h after seeding. 20.000 cells/well were cultured for MUM-2B, MUM-2C, C8161, SK-MEL-103 and SK-MEL-147; and 30.000 cells/well for A-375, G-361 and SK-MEL-28 (white scale bar = 500 µm).

It is remarkable that the distribution of cell lines in this experimental approach revealed a parallel classification to the observed using HOPP analysis (Figure 24). Suggestively, these results are consistent with the fact that EL+ cancer cells are typically more aggressive and invasive than EL- (Maniotis et al., 1999; Sood et al., 2001).

1.4. Identification of an endothelial-like phenotype-dependent differential gene expression

According to the EL+ and EL- classification of melanoma cell lines, a study of differentially expressed genes (DEGs) between these groups was approached. Such task included a first qPCR analysis followed by an evaluation of available RNA-seq data to identify DEGs between EL+ and EL- cells.

Analysis of differentially expressed genes between EL+ and EL- cell lines

ADAMTS1 was the first gene analyzed and further identified as a DEG between EL+ and EL- cells. Previous work by this laboratory reported its

significant upregulation in EL+ MUM-2B cell line compared to EL- MUM-2C (Casal et al., 2010). The results obtained now confirmed not only that *ADAMTS1* was upregulated in EL+ MUM-2B cells, but also that it was significantly upregulated in all EL+ cells compared to EL- (Figure 28).

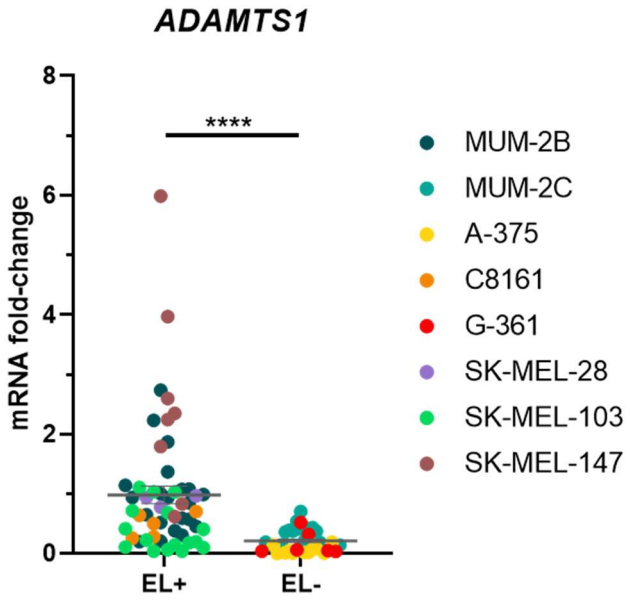

Figure 28. Different expression of ADAMTS1 between EL+ and EL- cell lines.
Graph representing mRNA fold change expression of ADAMTS1 in human melanoma cell lines, according to their EL+ or EL- phenotype (values are based in same data that Figure 19).

These higher levels of ADAMTS1 supported its involvement in the acquisition of the endothelial-like phenotype in human melanoma cell lines. Moreover, these results coincided with the *in silico* HOPP analysis, where ADAMTS1 was identified as an invasive phenotype-associated gene (Figure 25a). Indeed, those cells in which *ADAMTS1* was upregulated resulted at the same time EL+ (through Matrigel assays, Figure 28) and invasive (trough HOPP analysis, Figure 24), suggesting the contribution of this protease on melanoma endothelial-like phenotype and deserving further studies to uncover it.

Encouraged by the results obtained for *ADAMTS1*, a similar analysis was performed for the endothelial VM-related genes. Importantly, *CDH5* and *ENG* resulted DEGs between EL+ and EL- cells, being both significantly upregulated genes in EL+ cells (Figure 29). These differences in terms of

gene expression are consistent with previous reports, in which these endothelial-related genes have shown to be associated with aggressive and VM+ cells (Hendrix et al., 2001; Pardali et al., 2011).

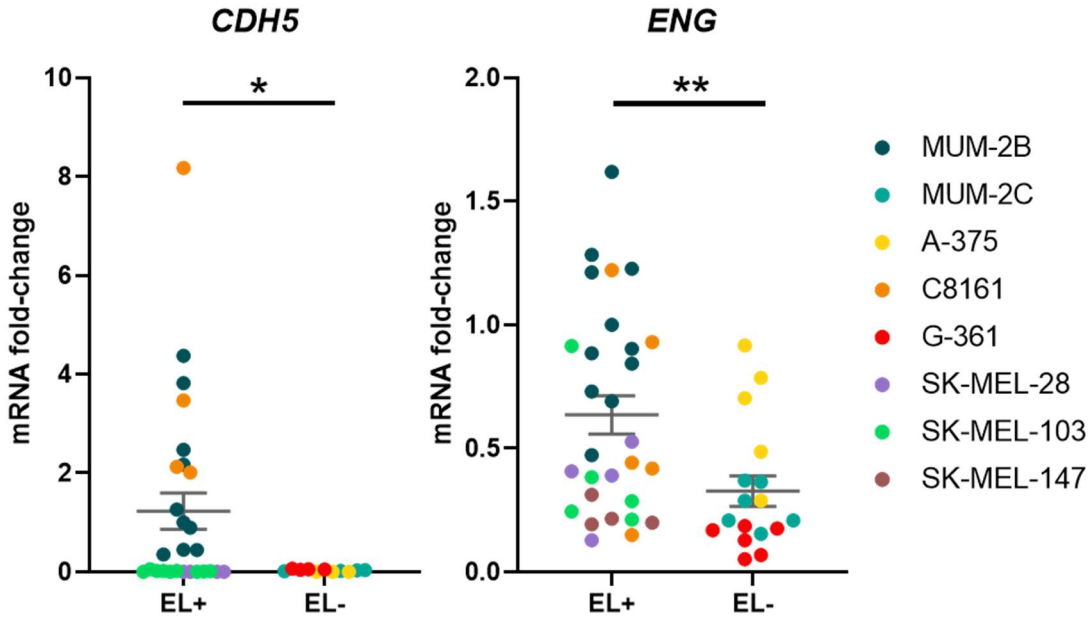

Figure 29. Different expression of CDH5 and ENG between EL+ and EL- melanoma cell lines.
Graph representing mRNA fold change expression of CDH5 and ENG in human melanoma cell lines, according to their EL+ or EL- phenotype (values are based in same data that Figure 20).

In silico analysis of differentially expressed genes between EL+ and EL- cells

RNA-Seq data of the melanoma cell lines used in this study were collected from GEO and an *in silico* comparison of their gene signatures was executed in an attempt to identify DEGs between EL+ and EL- cells. Human umbilical vein endothelial cells (HUVECs) RNA-Seq data were also included to ponder the phenotype towards EL+ cells. 467 DEGs were obtained from a total of 9572 analyzed genes, of which 47 were upregulated and 420 downregulated in EL+ cells (including HUVECs) (Figure 30, Table 5).

Remarkably, endothelial-related *CDH5* and ECM *NID1*, two of the genes of interest for this work, were among the upregulated DEGs in EL+ cells. Besides them, which will be deeply studied throughout this thesis, it should be noted the appearance of two genes related to anticoagulation processes

as are *TFPI* (tissue factor pathway inhibitor) and *THBD* (thrombomodulin). Both have been shown to be involved in relevant processes such as vasculogenic mimicry, stemness or metastasis (El Hallani et al., 2010; Horowitz et al., 2011; Seftor et al., 2002), and the relevance of their appearance as DEGs in EL+ cells will be furtherly discussed.

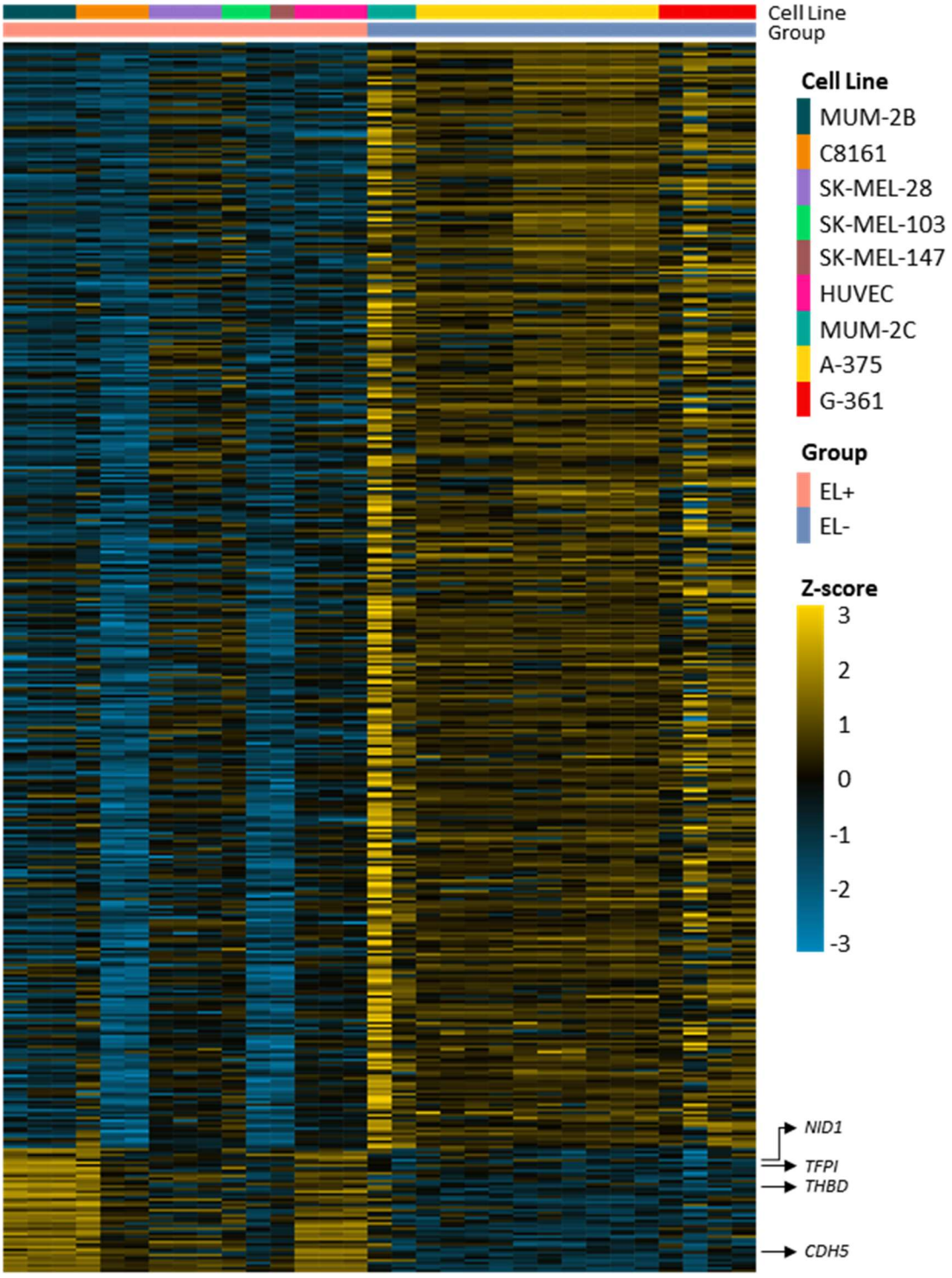

Figure 30. Differentially expressed genes between EL+ and EL- cell lines.
Heatmap showing significant DEGs between EL+ (including HUVECs) and EL- cell lines (47 upregulated and 420 downregulated, FDR < 0.05). Gene Expression Omnibus (GEO) accession numbers of cell samples are listed and color coded in Table 4 ***¡Error! No se encuentra el origen de la referencia.*** *and the full list of DEGs is compiled in Table 5.*

In addition to DEGs identification, Gene Ontology (GO) enrichment analysis was conducted in an attempt to know in which specific biological processes

were involved the 47 upregulated genes in EL+ cells. This analysis revealed the prevalence of biological processes that are strongly related with vascular functionality and ECM organization, such as regulation of coagulation, hemostasis and wound healing. Indeed, these processes include some of the genes mentioned above (Figure 31, Table 6).

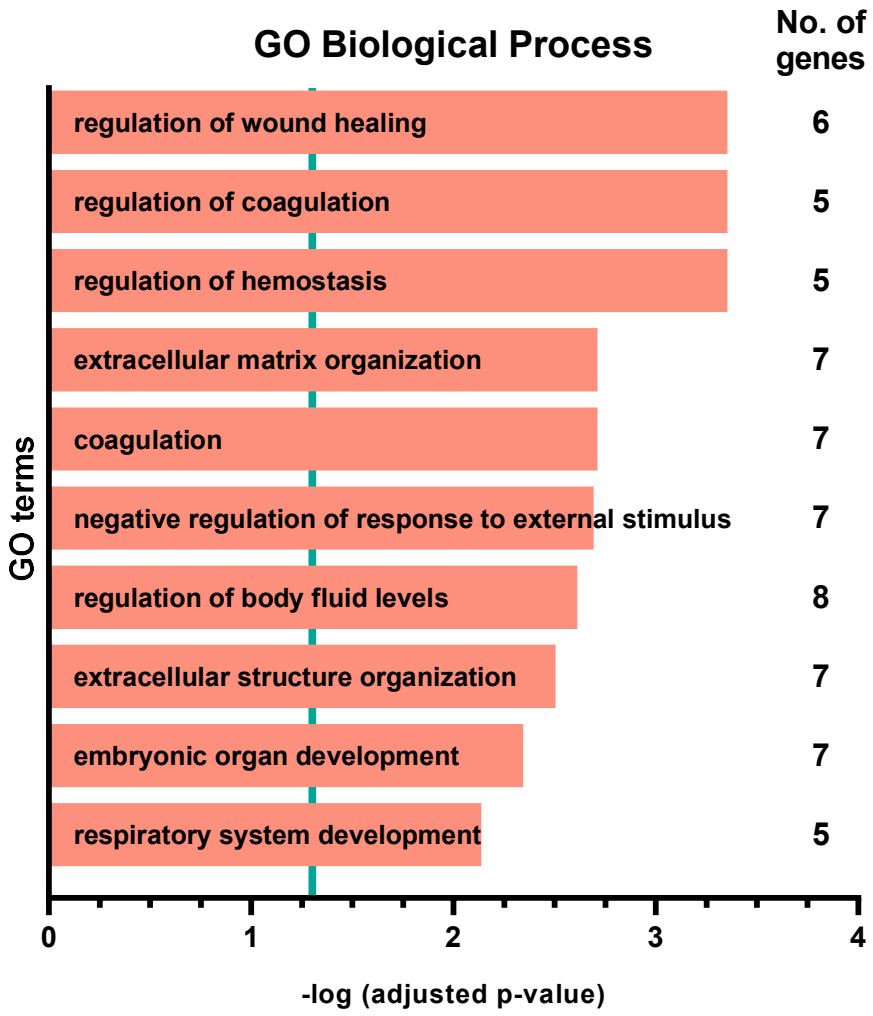

Figure 31. GO enrichment analysis of the upregulated DEGs in EL+ cells
Representation of top ten GO Biological Processes that resulted from the GO enrichment analysis of upregulated DEGs in EL+ cells. Turquoise line determined the limit of significance: -log (0.05). More data in Table 6.

Overall, these results encouraged additional studies of the endothelial-like phenotype of these melanoma cells and the contribution of ADAMTS1.

2. Loss of function of ADAMTS1 in human melanoma cells

In line with the promising results revealed by the cell line characterization, our main objective to determine the role of ADAMTS1 in human melanoma would be studied accomplishing its inhibition.

A first approach was short hairpin RNA (shRNA) technology, generating ADAMTS1 knockdown in MUM-2B, SK-MEL-103 and SK-MEL-147 cells. However, although initial knocking down was successful, *ADAMTS1* expression was recovered over time and passages, even at original expression levels. Accordingly, this technique to inhibit ADAMTS1 was dismissed and CRISPR/Cas9 technology was pursued.

2.1. *ADAMTS1* inhibition by CRISPR/Cas9

CRISPR/Cas9 (Clustered Regularly Interspaced Short Palindromic Repeats/CRISPR-ASsociated 9) has emerged in the last few years as a novel breakthrough for gene editing. The CRISPR/Cas9 system used in this thesis relies on the non-homologous end joining (NHEJ) mechanism of DNA repair to obtain ADAMTS1-KO cells. The whole protocol is described in *Materials and Methods* section and it was also compiled in a book chapter published by this laboratory (Peris-Torres et al., 2020b). Briefly, after lentiviral infection and cell selection and expansion, *ADAMTS1* edition and inhibition was confirmed by Sanger DNA sequencing and Western blot, respectively (Figure 32). Two ADAMTS1-KO clones were successfully obtained for uveal MUM-2B (named ATS1-KO1 and ATS1-KO2) and other two for cutaneous C8161 (ATS1-KO3 and ATS1-KO4) (Figure 32). *ADAMTS1* edition was also conducted in SK-MEL-103 and SK-MEL-147 cells, but they were not fully confirmed before the completion of this thesis, so they will be useful for future research.

a

		611				614		624				628
	Consensus seq:	g	g	c	-	g	...	g	t	g	t	c
	WT	G	G	C	-	G	...	G	T	G	T	C
MUM-2B	ATS1-KO1	G	G	C	C	G	...	G	T	G	T	C
MUM-2B	ATS1-KO2	G	C	T	-	G	...	G	T	G	T	C
C8161	ATS1-KO3	G	G	-	-	G	...	G	T	-	-	C
C8161	ATS1-KO4	G	G	-	-	G	...	G	-	G	T	C

b

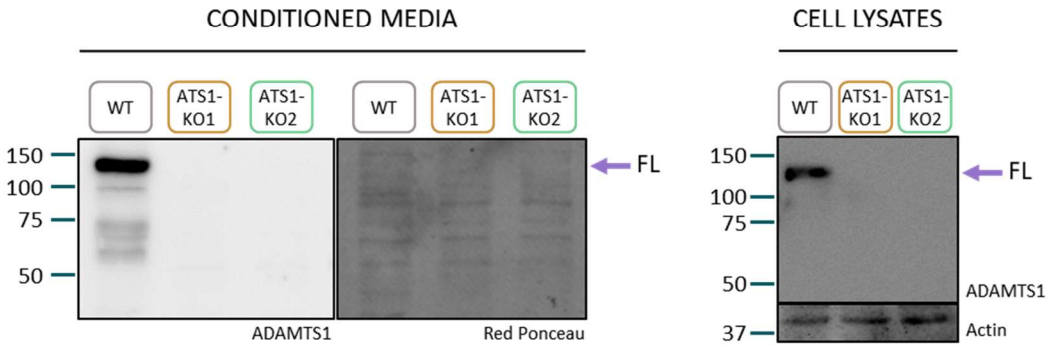

Figure 32. ADAMTS1 inhibition by CRISPR/Cas9.
(**a**) Schematic view of the ADAMTS1 (NM_006988) gene edition in MUM-2B and C8161 cell lines to obtain ADAMTS1-KO cells. Editions in MUM-2B were: ATS1-KO1, an insertion of a cytosine (C) in position 614; ATS1-KO2, a substitution of a guanine-cytosine (GC) for a cytosine-thymine (CT) in positions 612-613. Editions in C8161 were: ATS1-KO3, deletions in positions 613, 626 and 627; ATS1-KO4, deletions in positions 613 and 625. (**b**) Western blot analysis of conditioned media and cell lysates of ADAMTS1 in MUM-2B WT and ADAMTS1-KO cells. Purple arrows point full-length (FL) ADAMTS1. Red Ponceau staining and Actin were used as loading controls for conditioned media and cell lysates, respectively.

Once the ADAMTS1-KO cells were successfully obtained, a first issue was to determine whether *ADAMTS1* inhibition had any consequence on the endothelial-like phenotype of these cells, addressed in the next section.

2.2. Evaluation of the consequences of *ADAMTS1* inhibition over melanoma *in vitro* endothelial-like phenotype

Matrigel assays were used to evaluate the endothelial-like phenotype of MUM-2B ADAMTS1-KO (ATS1-KO) clones. As shown in Figure 33, ATS1-KO cells suffered a change in morphology compared with their WT counterpart, although not preventing them from creating endothelial-like networks. The non-biased WimTube tool (Wimasis, 2016) was used to obtain more details on these phenotypic differences. This is an objective, reproducible, easy to use, fast and automated tool for measuring endothelial-like networks in Matrigel and other matrixes (details at *Materials and Methods* section). Using different cell culture densities, the WimTube evaluation confirmed that *ADAMTS1* inhibition affects *in vitro* endothelial-like phenotype of MUM-2B cells. ADAMTS1-KO cells suffered a decrease in the number of tubes, branching points and loops, which is considered a loss of endothelial-like capacity.

The impairment of the endothelial-like phenotype in ADAMTS1-KO cells may be associated with a change on their endothelial-related gene expression signature. Therefore, gene expression levels of the endothelial-related markers considered in this study (*CDH5*, *ENG*, *EPHA2*, *KDR*, *LAMC2*, *TEK* and *TIE1*) were analyzed by qPCR, now comparing WT and ADAMTS1-KO cells (Figure 34). Remarkably, these analyses revealed a significant downregulation of *CDH5* in ATS1-KO cells, not only in uveal MUM-2B but also in cutaneous C8161 (Figure 34a), associating this inhibition with its recognized contribution for VM (Hendrix et al., 2001; Hess et al., 2006). In addition, the endothelial-related markers *KDR* and *TIE1* were also downregulated when *ADAMTS1* was inhibited in MUM-2B cells (Figure 34b).

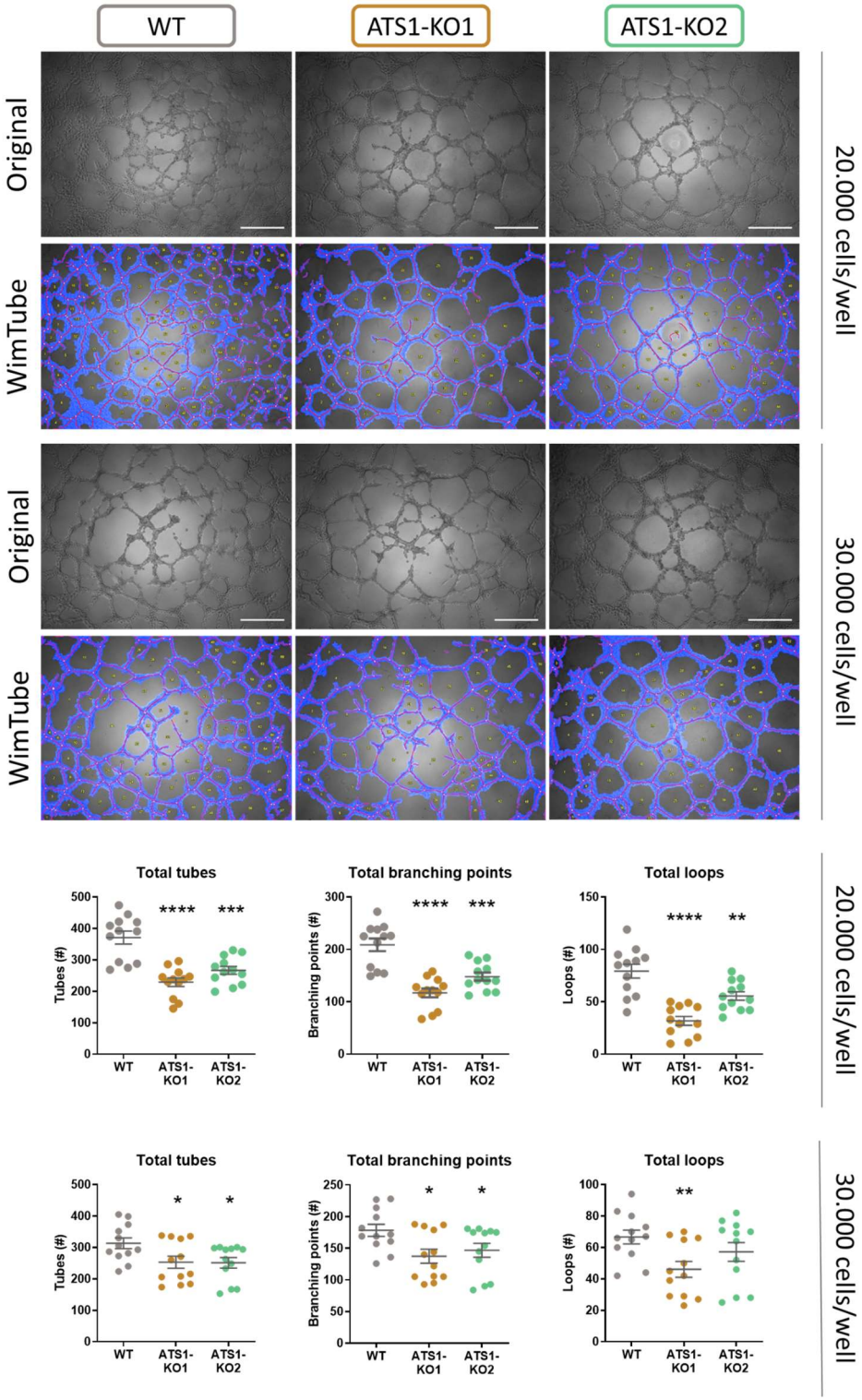

Figure 33. ADAMTS1 inhibition affects in vitro endothelial-like phenotypic properties.

Representative images (original and WimTube filtered) of Matrigel assay for MUM-2B WT and ATS1-KO cells, 24 h after seeding 20.000 or 30.000 cells/well. Scatter plots represent the parameters resulting of WimTube analysis: total tubes, total branching points and total loops (n = 12 for all groups, white scale bar = 500 µm) (****, $p < 0.0001$; ***, $p < 0.001$; **, $p < 0.01$; *, $p < 0.05$. WT cells were used as control for statistical analyses).

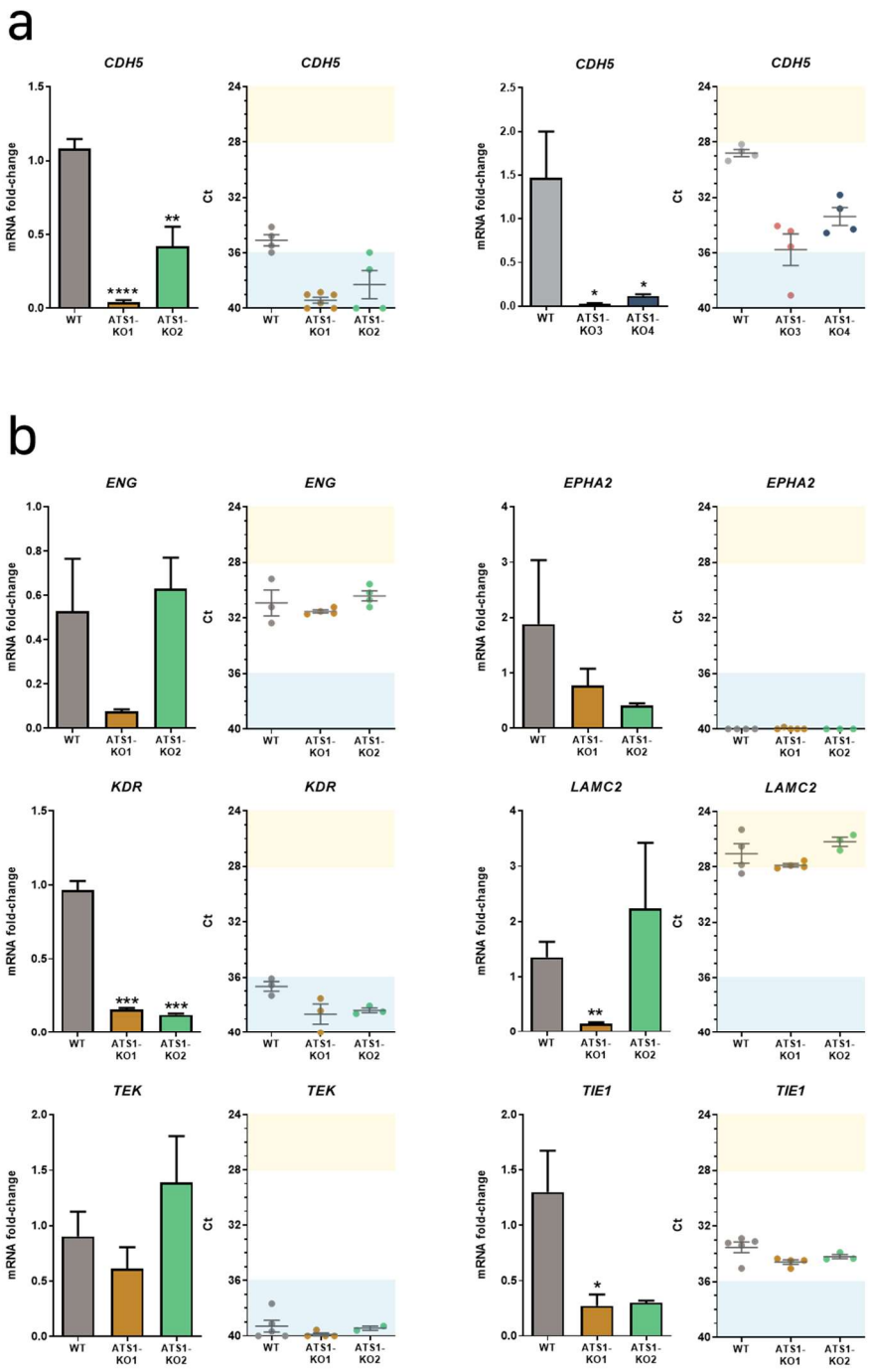

Figure 34. ADAMTS1 inhibition affects endothelial-related gene signature.
*(**a**) Graphs representing mRNA fold-change expression and Ct values of CDH5 in MUM-2B and C8161 cells. (**b**) Graphs representing mRNA fold-change and Ct values of ENG, EPHA2, KDR, LAMC2, TEK and TIE1 in MUM-2B WT and ATS1-KO cells. High and low gene expression is depicted in Ct graphs with yellow and blue backgrounds, respectively (n = 3–5 for MUM-2B WT, n = 3–6 for ATS1-KO1, n = 2–4 for ATS1-KO2, n = 4 for C8161-WT, ATS1-KO3 and ATS1-KO4) (****, p < 0.0001; ***, p < 0.001; **, p < 0.01; *, p < 0.05. WT cells were used as control for statistical analyses).*

Taken together, these results indicated that ADAMTS1 exerts a key contribution to endothelial-like plasticity in melanoma cells, as its inhibition affected *in vitro* endothelial-like phenotype and downregulated endothelial-related genes. In particular, the alteration of *CDH5* expression resulted very interesting for this project, highlighting the relevance of this gene and encouraging its study throughout this work. Once the *in vitro* characterization of the ADAMTS1-KO model was carried out, *in vivo* xenograft studies were the next step to pursue, in order to unveil the role of ADAMTS1 in tumor development.

3. Analysis of ADAMTS1 contribution to *in vivo* development of human uveal melanoma xenografts

The study of human ADAMTS1 in an *in vivo* context was approached by the induction of xenografts in immunodeficient mice. In order to discard any difference in terms of proliferation rate between WT and ADAMTS1-KO cells, previous *in vitro* proliferation assays were performed using xCELLigence platform. These assays were conducted until cells reach a plateau phase, measuring the cell index at different time points and subsequently calculating the cell doubling time. As observed in Figure 35, there were no differences between WT and ADAMTS1-KO cells, concluding that any differences observed in further *in vivo* tumor experiments could not be attributed to a different cell proliferation rate.

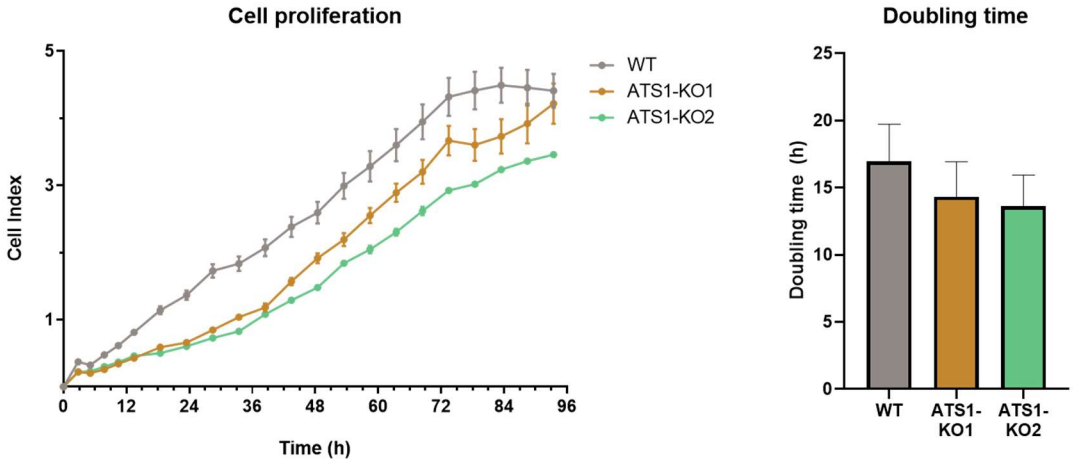

Figure 35. xCELLigence analysis of melanoma cell proliferation.
Graphs representing (a) cell proliferation index and (b) doubling time for MUM-2B WT and ADAMTS1-KO cells. Cell index was measured every 20 minutes but here is represented every 4 sweeps to simplify the graph (WT cells were used as control for statistical analyses)

Prior also to xenograft generation, melanoma cells were modified to express green fluorescent protein (GFP), contributing to an easy and fast identification of human melanoma cells (GFP+) in the murine environment.

3.1. Effect of ADAMTS1 inhibition on tumor growth

In vivo experiments were approached in two different and recognized models: Swiss Nude (SwN) and NOD *scid* gamma (NSG) mice. Since their appearance around 1960s, SwN athymic mice have been widely used for tumor biology studies. In fact this laboratory successfully conducted xenograft experiments with uveal melanoma MUM-2B and MUM-2C cells (Fernández-Rodríguez et al., 2016). Now for this thesis, WT and ADAMTS1-KO MUM-2B cells (ATS1-KO1 and ATS1-KO2) were used for this purpose. Briefly, 1×10^6 cells in 100 µl PBS were injected in the flank of 6-weeks old SwN mice, and tumor growth was monitored every two days until final time point, at day 39 (details at Material and Methods section). Very significantly, all SwN mice injected with WT developed tumors, but none with ADAMTS1-KO cells, corroborated even after sacrifice (Figure 36). This robust result implied a key contribution of ADAMTS1 to tumor growth, since its absence completely blocked tumor development. However, in order to improve the initial tumor engraftment, some modifications were introduced in the xenograft assay.

Nevertheless, the comparison of tumor development by WT and ATS1-KO cells again revealed significant differences in terms of tumor weight, volume and progression (Figure 38b-d).

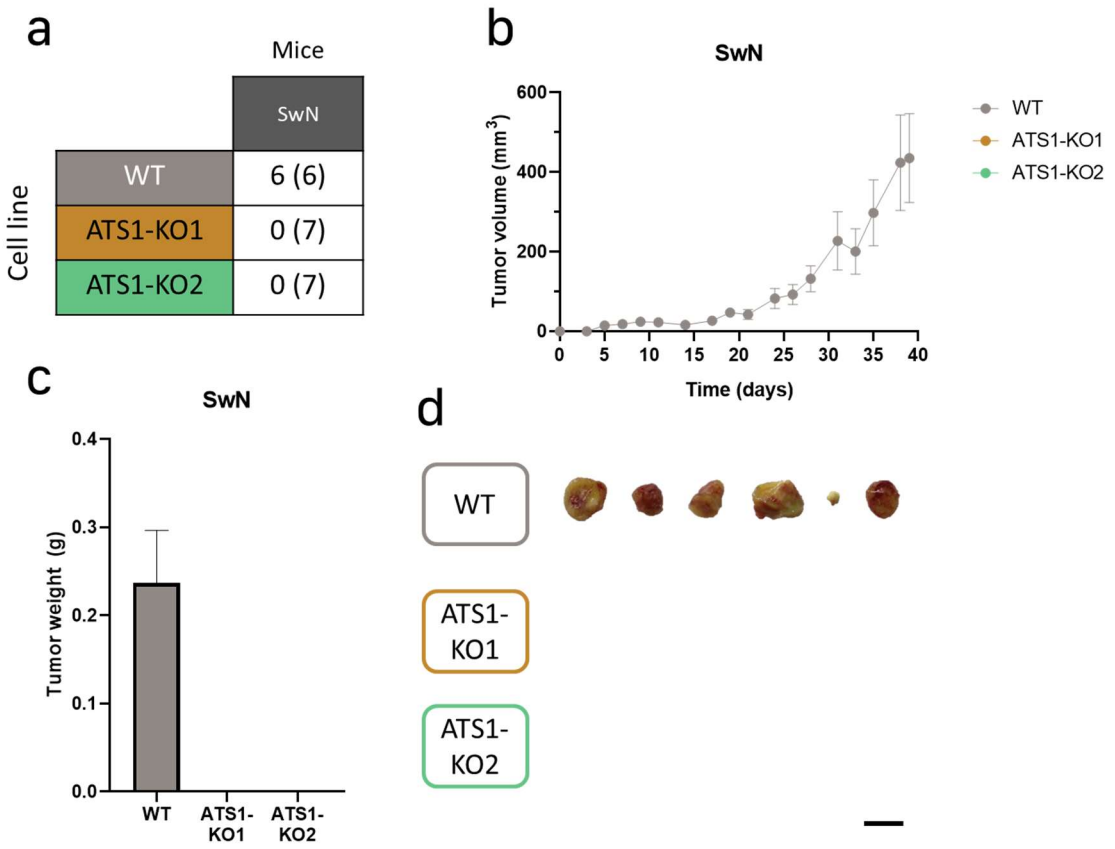

Figure 36. ADAMTS1 inhibition blocks tumorigenesis in SwN mice.
(**a**) Table indicating the number of mice that developed tumors and the total number of injected mice of every experimental group (in parenthesis). (**b**) Graph representing tumor evolution for each experimental group. (**c**) Graph representing final tumor weight of different experimental groups, according to panel (a). (**d**) Pictures of the tumors obtained at the end of the experiment (black scale bar = 1 cm).

These modifications included an increase on the number of injected cells (2×10^6) and the use of Matrigel to support engraftment (in a 1:1 PBS:Matrigel solution) as previously reported (Fridman et al., 1991, 2012). Accordingly, Matrigel gels in contact with mouse body temperature, generating an enriched "plug" that helps initial tumor growth. Under these conditions (named SwN-Matrigel) ADAMTS1-KO cells were able to generate tumors, but not in all animals, and when they did, the overall evaluation of tumor progression of ADAMTS1-KO cells throughout the experiment showed a clear compromise in comparison with WT group (Figure 37).

Still, given the limitations of the results obtained from the two SwN-based approaches, either in terms of quantity of samples, size or reproducibility, NSG mice emerged as a suitable alternative. An increased tumor

engraftment was expected in those mice, since they display a more severe immunodeficiency (Puchalapalli et al., 2016) (Figure 68). Now, NSG mice were injected with 1 × 10^6 cells in 100 µl PBS. Importantly, at the end of the experiment (day 31), all the injected NSG mice developed tumors (Figure 38a). All these data demonstrated the relevance of ADAMTS1 for tumor development, even in different mouse models. However, the actual role of the protease is still uncovered, so further determinations with NSG xenografts were needed. In this regard, the effect of the inhibition of *ADAMTS1* on the tumor vasculature was studied, guided by results obtained previously by this laboratory.

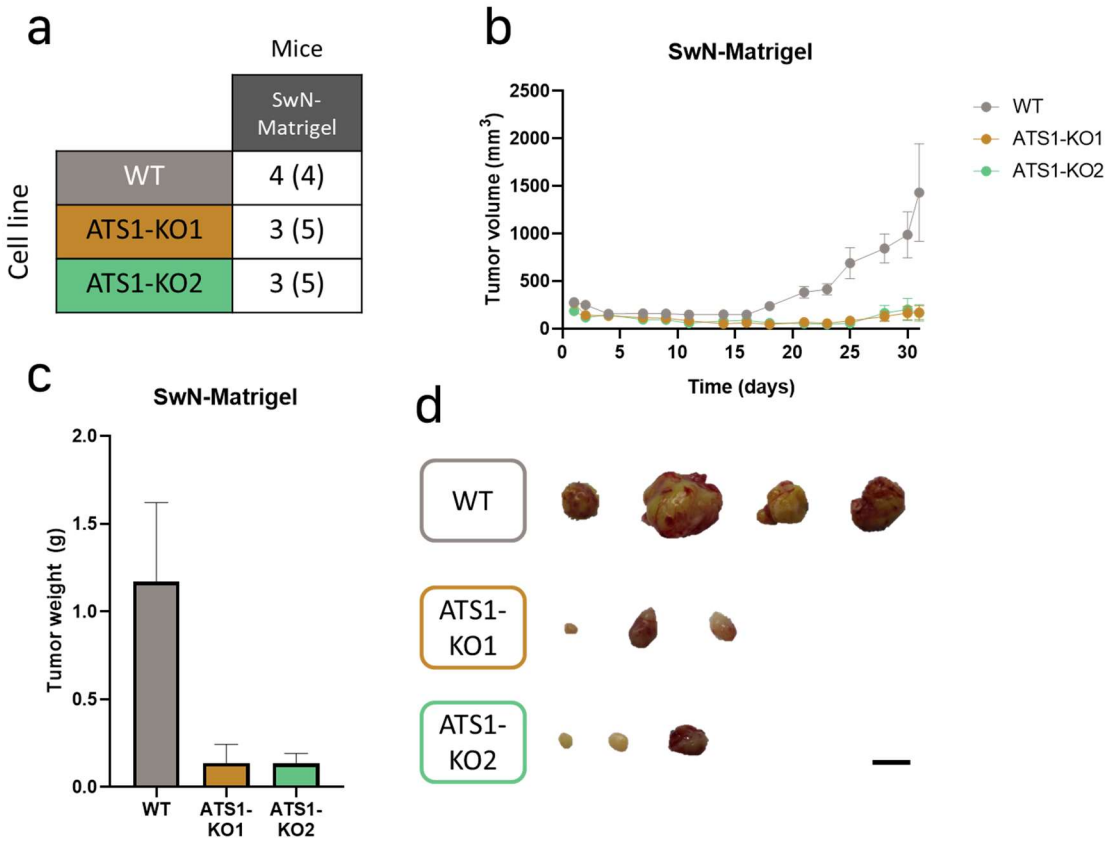

Figure 37. ADAMTS1 inhibition blocks tumorigenesis in SwN-Matrigel mice.
(**a**) Table indicating the number of mice that developed tumors and the total number of injected mice of every experimental group (in parenthesis). (**b**) Graph representing tumor evolution for each experimental group. (**c**) Graph representing final tumor weight of different experimental groups, according to panel (a). (**d**) Pictures of the tumors obtained at the end of the experiment (black scale bar = 1 cm).

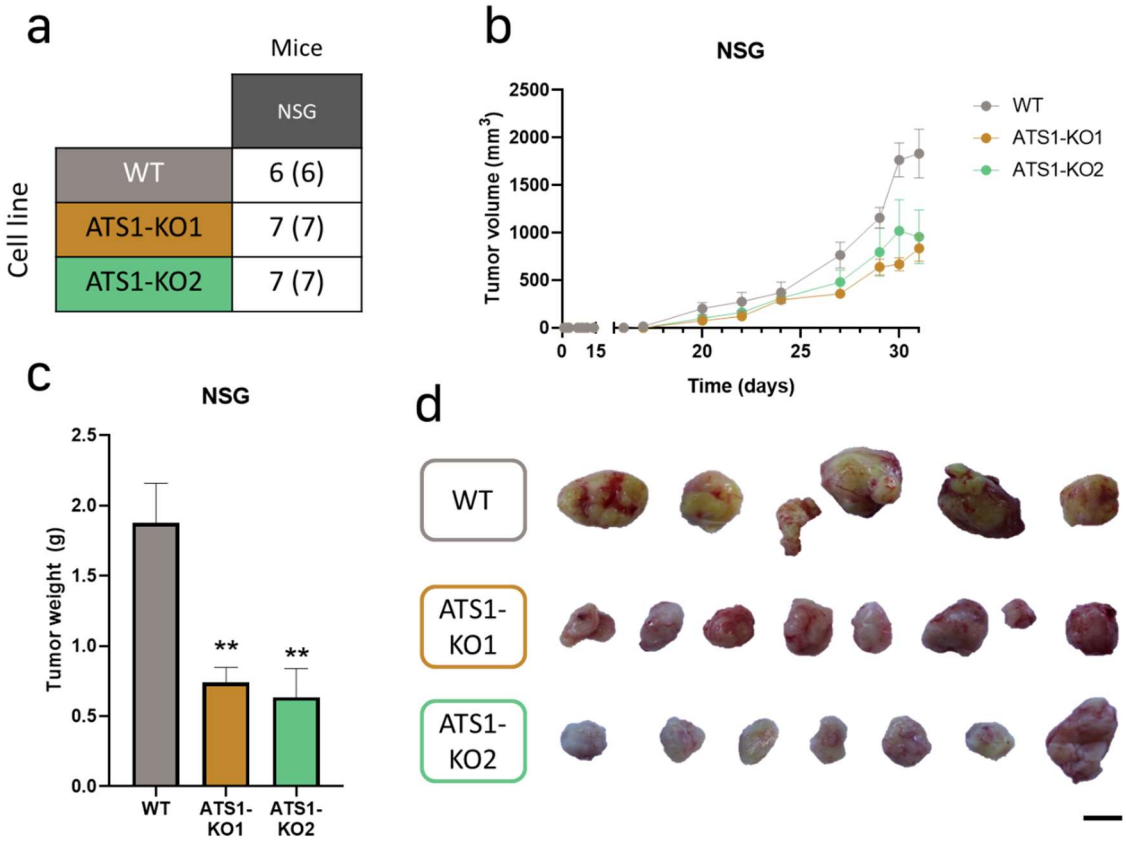

Figure 38. ADAMTS1 inhibition blocks tumorigenesis in NSG mice.
(**a**) Table indicating the number of mice that developed tumors and the total number of injected mice of every experimental group (in parenthesis). (**b**) Graph representing tumor evolution for each experimental group. (**c**) Graph representing final tumor weight of different experimental groups, according to panel (a). (**d**) Pictures of the tumors obtained at the end of the experiment (black scale bar = 1 cm) (**, $p < 0.01$. Tumors generated with WT cells were used as control for statistical analyses).

3.2. Effect of ADAMTS1 inhibition on tumor vasculature

Findings by this laboratory already demonstrated that ADAMTS1 exerts an effect on the tumor vasculature using different mouse models (Fernández-Rodríguez et al., 2016; Rodríguez-Baena et al., 2018a). Accordingly, the vasculature of the new NSG tumors obtained now was analyzed with two different approaches such as flow cytometry and immunofluorescence staining.

Our Flow cytometry analyses used a combination of PECAM1 (platelet endothelial cell adhesion molecule, also named cluster of differentiation 31 or CD31) and GFP expression to detect different cellular types. PECAM1 is an

exclusive endothelial marker, thus it would serve to distinguish endothelial from other cell types. In addition, given the advantage that injected tumor cells expressed GFP, it was possible to differentiate between tumor and the rest of stromal cells. In line with the goals of this work, this combination of PECAM1 and GFP would allow the identification of VM+ cells, which correspond to tumor cells (GFP+) that have acquired the ability to express an endothelial marker such as PECAM1. Using flow cytometry, those VM+ (PECAM1+/GFP+) cells would be easily discriminated from canonic endothelial (PECAM1+/GFP-) and the rest of tumor (PECAM1-/GFP+) cells (Figure 39a). As a first observation, these determinations showed that the proportion of canonic endothelial cells was higher in ADAMTS1-KO samples than in their WT counterparts (Figure 39b), suggesting an increased vascularization. Very interestingly, a population of VM+ cells, although low, could actually be identified with this approach, mainly in WT tumors. Furthermore, the proportion of these PECAM1+/GFP+ cells in ADAMTS1-KO tumors resulted to be significantly lower than in WT samples (Figure 39c), connecting again the contribution of extracellular ADAMTS1 with vasculogenic mimicry phenomenon.

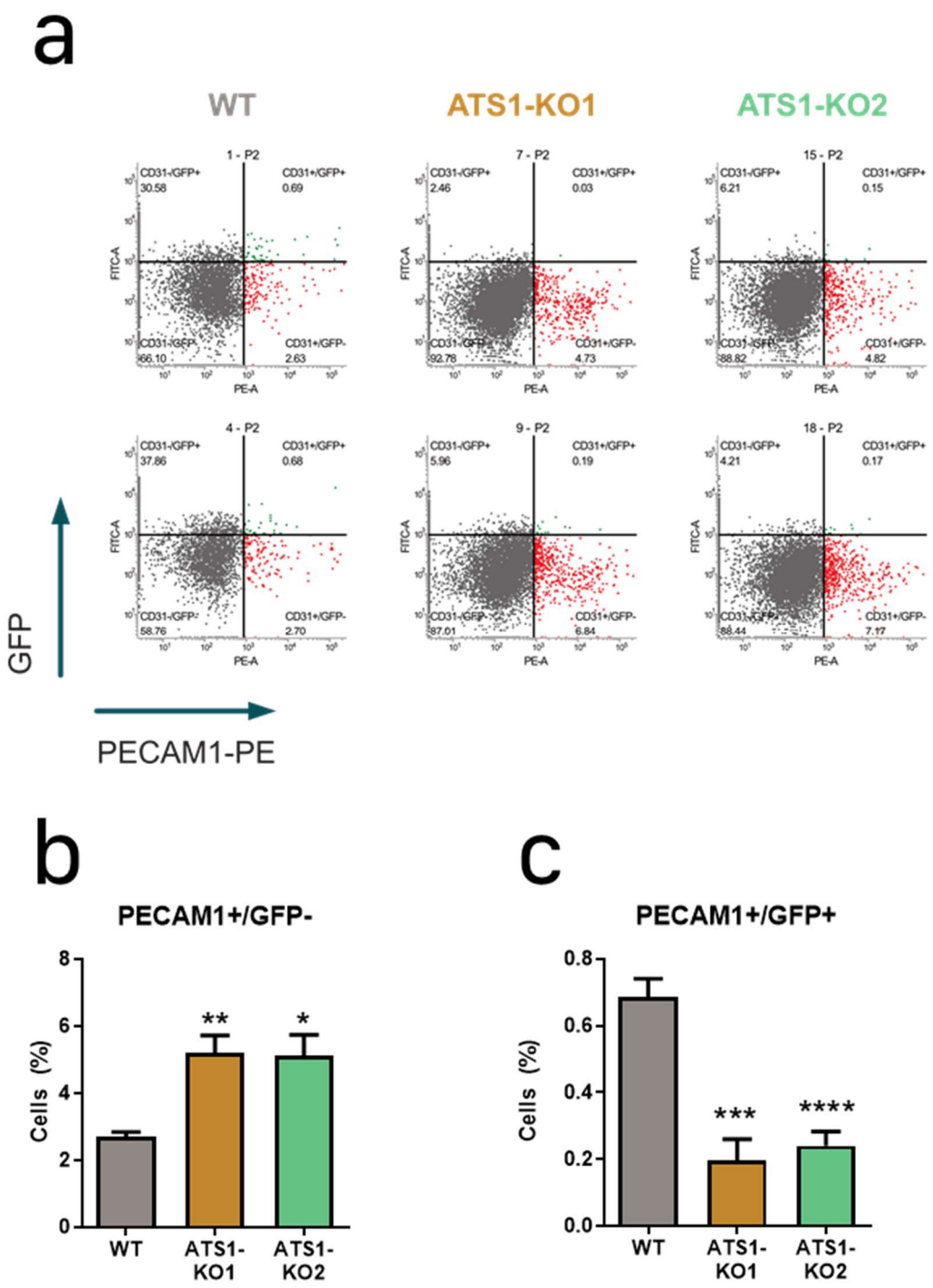

Figure 39. Flow cytometry analysis of tumor vasculature.
(a) Flow cytometry characterization of MUM-2B WT and ADAMTS1-KO NSG xenografts. PECAM1-PE antibody identified canonic endothelial cells and GFP identified human tumor cells. (b-c) Quantification of flow cytometry analyses by experimental groups, according to panel (a) and percentages of cells identified as (b) canonic endothelial cells (PECAM1+/GFP-) and (c) VM+ cells (PECAM1+/GFP+). (****, $p < 0.0001$; ***, $p < 0.001$; **, $p < 0.01$; *, $p < 0.05$. WT xenografts were used as control for statistical analyses).

The approach based on immunofluorescence (IF) to analyze tumor vasculature included endomucin (EMCN) and PECAM1 as vasculature markers. Very similar results were obtained with antibodies for these two molecules, so the results presented here correspond to EMCN determinations, in line with other reports by this laboratory (Fernández-Rodríguez et al., 2016; Martino-Echarri et al., 2013; Rodríguez-Baena et al., 2018a, 2018b). A specific macro for ImageJ software (Schneider et al., 2012) was used to quantify tumor vasculature (details at *Materials and Methods* section). This analysis revealed an increased vessel density in ADAMTS1-KO tumors, but accompanied by a reduction in their perimeter (Figure 40). This apparent compensation resulted in a lack of significant differences in terms of total vessel area between WT and ADAMTS1-KO tumors, in agreement with results obtained by this laboratory in other tumor studies (Fernández-Rodríguez et al., 2016; Martino-Echarri et al., 2013).

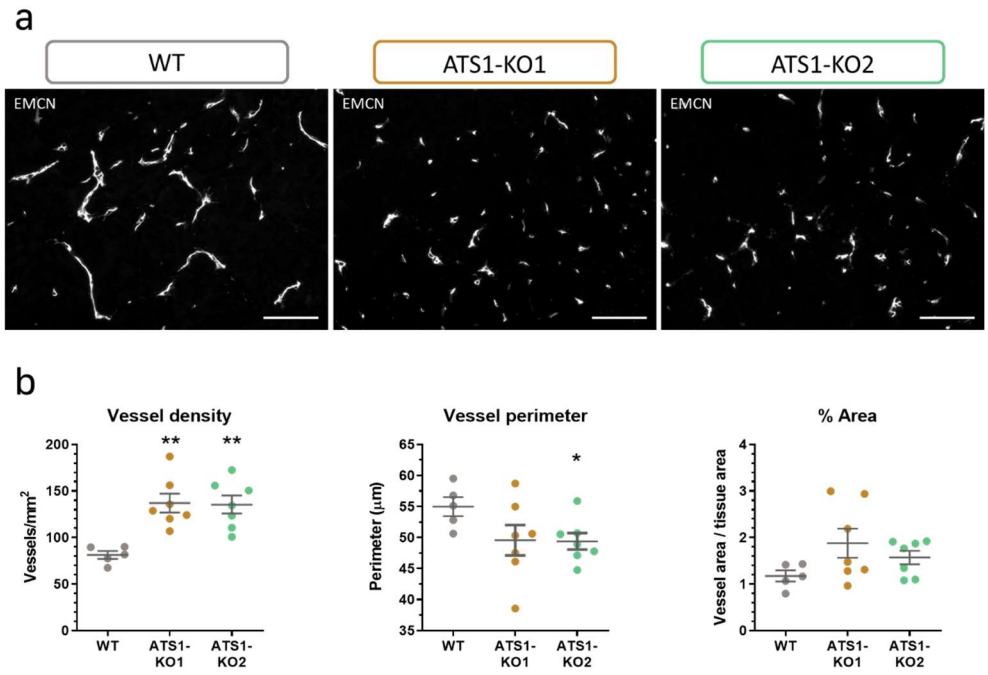

Figure 40. ADAMTS1 inhibition alters tumor vasculature.
(**a**) Representative images of EMCN immunofluorescence analysis of tumor sections from WT and ATS1-KO NSG xenografts (white scale bar = 100 µm); (**b**) Graphs representing tumor vasculature quantification of NSG xenografts: vessel density, vessel perimeter and percentage area (n = 5 for WT; n = 7 for ATS1-KO1 and ATS1-KO2) (**, $p < 0.01$; *, $p < 0.05$. WT xenografts were used as control for statistical analyses).

These later results showed that ADAMTS1 is also involved in the development of the tumor vasculature of NSG xenografts. However, although vasculature alterations were evident in the absence of tumor ADAMTS1, whether they are the reason for the blockade of tumor progression is still questionable. Even despite those alterations, the overall outcome is that ADAMTS1-KO tumors are significantly smaller, so the vasculature may not be the only involved factor.

Taking into account all the consequences that the inhibition of ADAMTS1 implied for xenograft development, as well as the significant changes in gene expression and phenotypic characteristics showed in previous sections of this work, the involvement of ADAMTS1 in stemness-related features was then evaluated. Importantly, these consequent studies were supported by previously work conducted by this laboratory, in which the contribution of ADAMTS1 to tumor plasticity phenomena was demonstrated (Casal et al., 2010).

4. Evaluation of the effect of ADAMTS1 on stemness and plasticity features of melanoma cells

Two different approaches were used to evaluate the relationship between ADAMTS1 and stemness features. In one hand, NSG xenografts were analyzed to corroborate this relationship in an *in vivo* context and, on the other hand, stemness features were determined using *in vitro* melanoma sphere formation assays.

4.1. Determination of *in vivo* stemness and VM features in NSG xenografts

Taking advantage of the distinct origin of tumor (human) and stromal (murine) cells in the generated xenografts, the design of specific qPCR primers allows to distinguish changes in the expression of genes from one origin or the other.

Accordingly, stemness features were studied exclusively in tumor cells analyzing the expression of *NANOG*, *POU5F1*, *PROM1* and *SOX2* stemness genes by qPCR. First, in a WT context, expression in MUM-2B cells *in vitro* were compared with their respective NSG xenografts. Importantly, this analysis revealed an upregulation of *NANOG* and *POUF5F1* in tumors when comparing with the original tumor cells under 2D culture conditions (Figure 41).

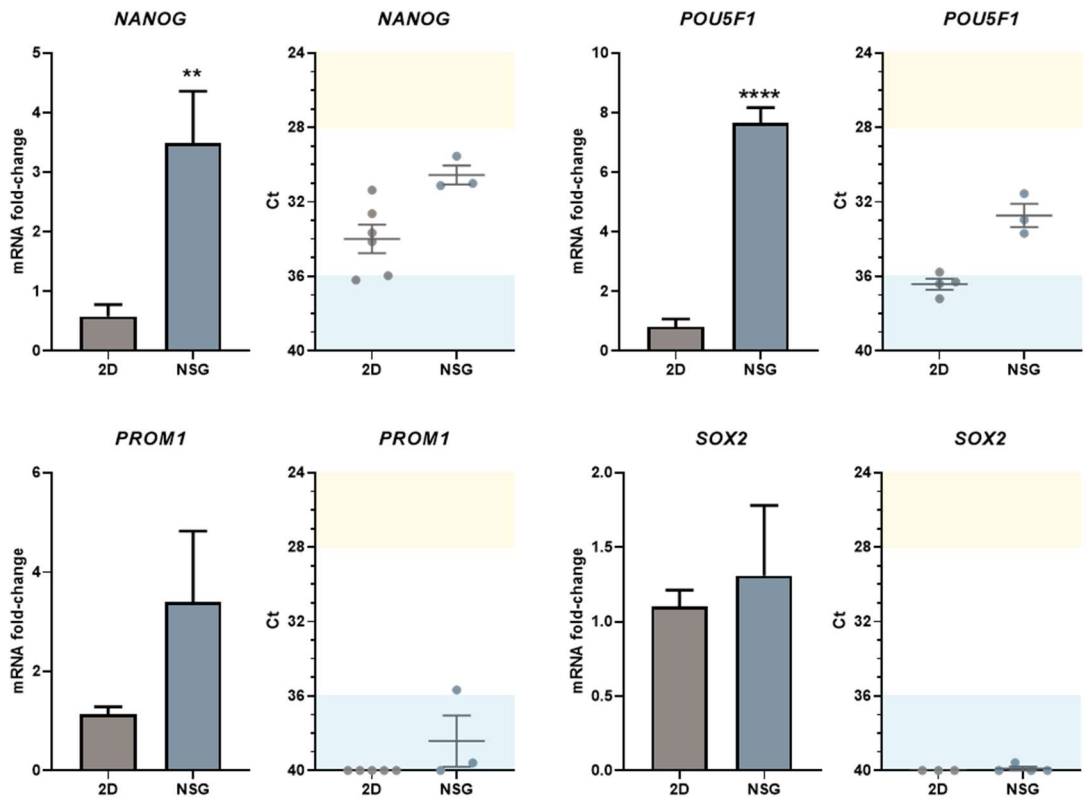

Figure 41. Upregulation of stemness markers of human origin in NSG xenografts. Graphs representing mRNA fold change expression and Ct values of NANOG, POU5F1, PROM1 and SOX2, in MUM-2B WT 2D cultured cells and NSG xenografts. High and low gene expression is depicted in Ct graphs with yellow and blue backgrounds, respectively (n = 3–6 for 2D cells and n = 3–4 for NSG) (****, $p < 0.0001$; **, $p < 0.01$. 2D cultured cells were used as control for statistical analyses).

This *in vivo* upregulation of stemness genes confirmed the high impact of the tumor microenvironment (TME) on promoting stemness. Since TME appeared as a main factor to take under consideration, the expression levels of other genes related with ECM regulation or the endothelial-like phenotype were also evaluated in the NSG model. Interestingly for this study, *ADAMTS1* and *CDH5* also appeared significantly overexpressed in this *in vivo* tumor context (Figure 42), suggesting again their direct link to tumor progression and plasticity phenomena.

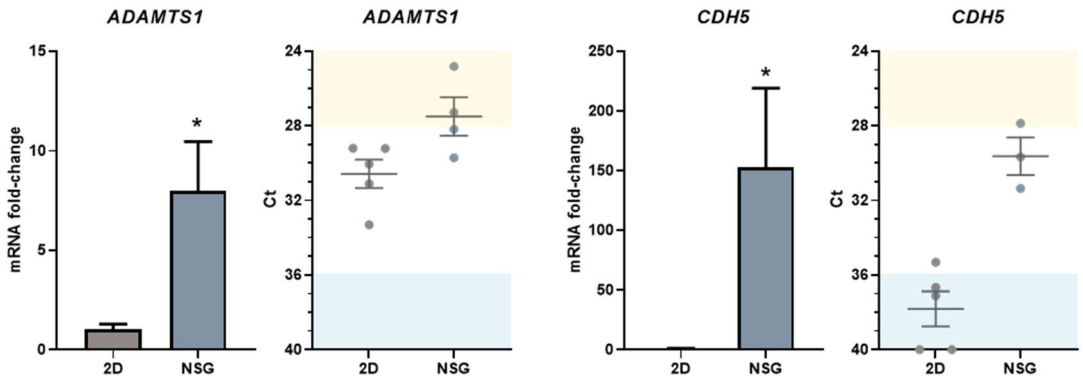

Figure 42. Upregulation of human ADAMTS1 and CDH5 in NSG xenografts.
Graphs representing mRNA fold change expression and Ct values of ADAMTS1 and CDH5, in MUM-2B WT 2D cultured cells and NSG xenografts. High and low gene expression is depicted in Ct graphs with yellow and blue backgrounds, respectively (n = 3–6 for 2D cells and n = 3–4 for NSG) (*, $p < 0.05$. 2D cultured cells were used as control for statistical analyses).

Since these analyses revealed such interesting changes, the comparison between WT and ADAMTS1-KO tumors was then addressed in an attempt to characterize the consequences of ADAMTS1 inhibition. In line with the impaired tumor progression shown in previous section (Figure 38), ADAMTS1-KO tumors showed an overall downregulation of stemness markers compared with WT samples, especially significant for the more abundant *NANOG* and *POU5F1* (Figure 43).

Furthermore, the gene expression of endothelial-related makers was also evaluated comparing WT and ADAMTS1-KO xenografts. Interestingly, ADAMTS1-KO tumors showed a chief reduction of *CDH5* mRNA levels compared with WT samples (Figure 44), in a similar manner that occurred when comparing WT and ADAMTS1-KO cells *in vitro* (Figure 34). Such downregulation of the endothelial gene *CDH5* when the extracellular protease ADAMTS1 is absent gave strength to the *in vitro* analysis showed above, and also proposed *CDH5* as a potential contributor to the impaired tumor vasculature observed in ADAMTS1-KO NSG xenografts (Figure 40). In addition to the reported importance of CDH5 in VM phenomenon (Hendrix et al., 2001; Hess et al., 2006), also cancer stem cells have shown to express *CDH5* in other tumor types such as glioblastoma (Wang et al., 2010). This close relationship between stemness properties and endothelial features,

which is being described in this work, encouraged the enquiry of VM in NSG xenografts.

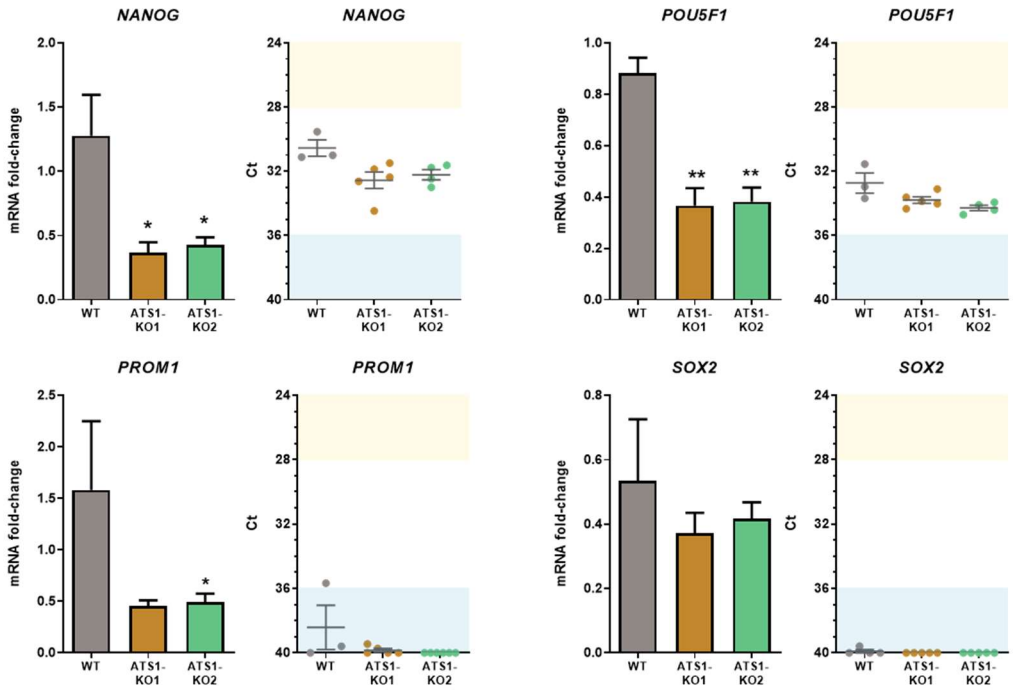

Figure 43. ADAMTS1 inhibition compromises stemness capacities in NSG tumor xenografts.
Graphs representing mRNA fold change expression and Ct values of NANOG, POU5F1, PROM1 and SOX2 in NSG xenografts generated with WT and ADAMTS1-KO cells. High and low gene expression is depicted in Ct graphs with yellow and blue backgrounds, respectively (n = 3 for WT, n = 5 for ATS1-KO1 and n = 4–6 for ATS1-KO2) (**, $p < 0.01$; and *, $p < 0.05$. WT NSG xenografts were used as control for statistical analyses).

This analysis was initiated by determining the presence of CDH5 in histological sections of xenografts. In an attempt to establish whether it exists any kind of relationship between this endothelial-related molecule and the vasculature itself, double staining for CDH5 and EMCN was performed. The analysis of WT NSG tumors allowed the identification of a cell surface pattern for CDH5. It was noticeably associated with tumor cells in the vicinity of EMCN-positive vascular niches, although not colocalizing with endothelial cells (Figure 45). When the same analysis was performed in ADAMTS1-KO tumors, this pattern was more arduous to find, and it was generally less consistent that in WT samples. In addition, when CDH5-

positive staining was detected, it appeared not as close to the vascular niche as occurred with the WT samples.

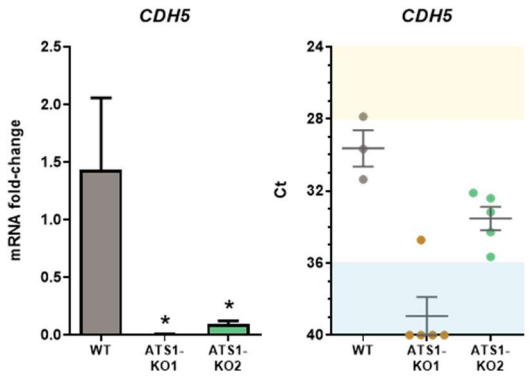

Figure 44. ADAMTS1 inhibition compromises endothelial CDH5 expression on NSG xenografts.
Graphs representing mRNA fold change expression and Ct values of CDH5 in NSG xenografts generated with WT and ATS1-KO cells. High and low gene expression is depicted in Ct graphs with yellow and blue backgrounds, respectively (n = 3 for WT and n = 5 for ATS1-KO1 and ATS1-KO2) (*, $p < 0.05$. WT NSG xenografts were used as control for statistical analyses).

Once that the *in vivo* evaluation of CDH5 corroborated its association with the presence of tumor ADAMTS1, a deeper study of its relationship with stemness features was pursued to support its role as a VM agent. According to the similar behavior shown by *CDH5* and *NANOG* in previous qPCR analyses (Figure 41 and Figure 42), a closer study in tumor sections was performed. Co-staining of these two molecules was not feasible due to methodological limitations, so immunohistochemistry (IHC) analysis in sequential tumor sections was performed (Figure 46). Importantly, IHC determinations not only confirmed previously obtained IF results for CDH5 (Figure 45), but also demonstrated a clearly compromised appearance of NANOG staining in ADAMTS1-KO tumors. Moreover, a spatial coincidence of NANOG and CDH5 expression was detected in WT samples which was very difficult to appreciate in ADAMTS1-KO sections, suggesting again the link between these two molecules (reference to figure again I think).

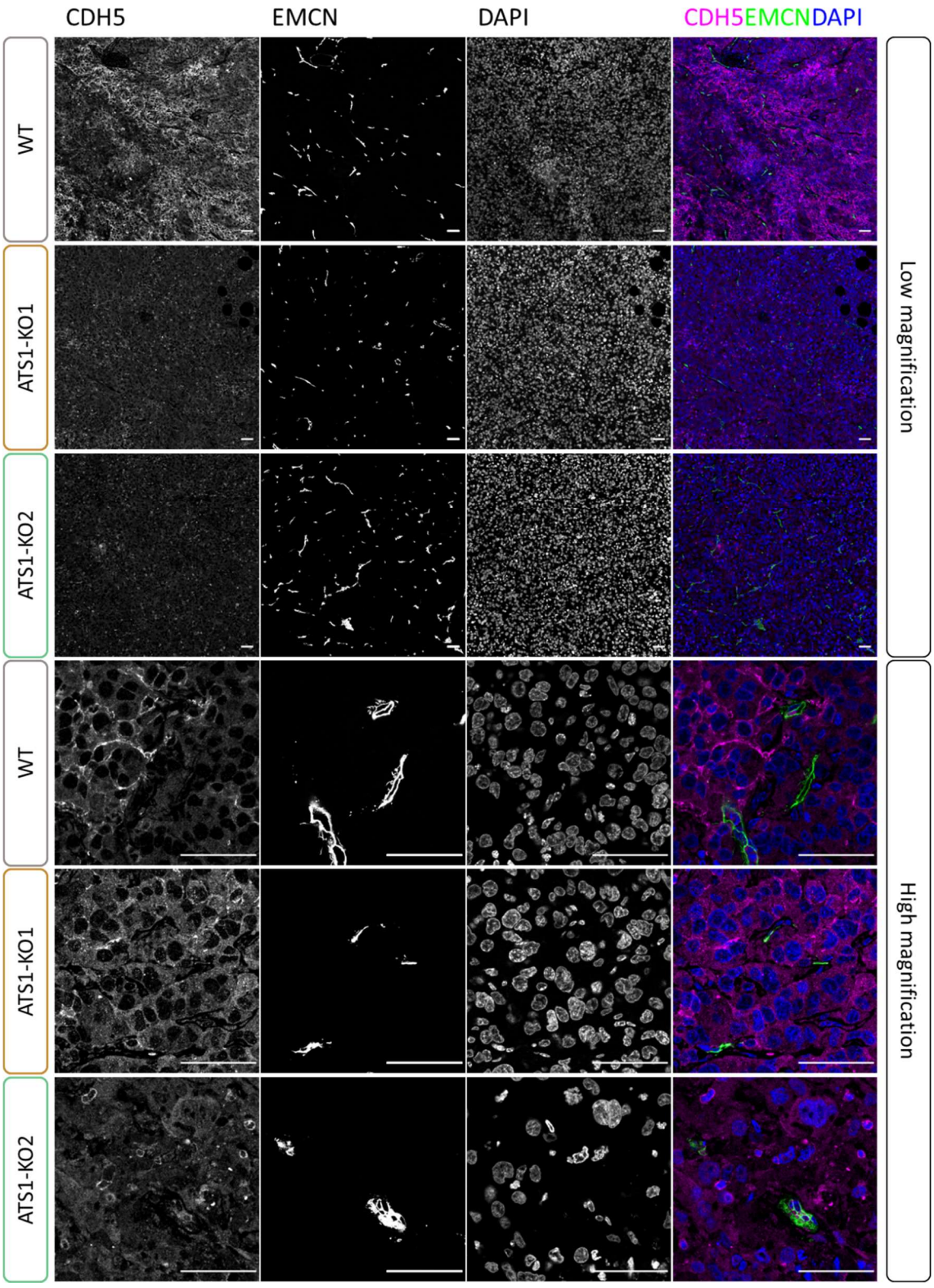

Figure 45. ADAMTS1 inhibition compromises endothelial-like phenotype in tumor xenografts.

Representative images of IF analysis of WT and ADAMTS1-KO NSG xenografts, at low and high magnification. Columns, from left to right: CDH5, EMCN, DAPI and merge (white scale bar = 50 μm).

To complete the analysis of vasculogenic mimicry in NSG xenografts, tumor sections were subjected to periodic acid-Schiff (PAS) staining. Since earliest reports, the identification of vasculogenic mimicry in tumor sections has been associated with PAS-positive loops and networks, which were presumably associated with tumor microcirculation (Maniotis et al., 1999). Now in this work, a double CDH5-PAS immunostaining was conducted to check for spatial coincidences between CDH5 and PAS-positive loops. Certainly, a significant increase of VM+ PAS-positive networks in WT tumors was observed compared with ADAMTS1-KO samples, as well as a better spatial coincidence with CDH5 in WT tumors that were very difficult to detect in ADAMTS1-KO ones (Figure 47). The similar behaviors shown by the CDH5-NANOG and the CDH5-PAS stainings suggested that the absence of ADAMTS1 resulted in a loss of vasculogenic mimicry capacities. In other words, these IHC evaluations revealed that tumors expressing ADAMTS1 showed vasculogenic mimicry features, which together with the fact that

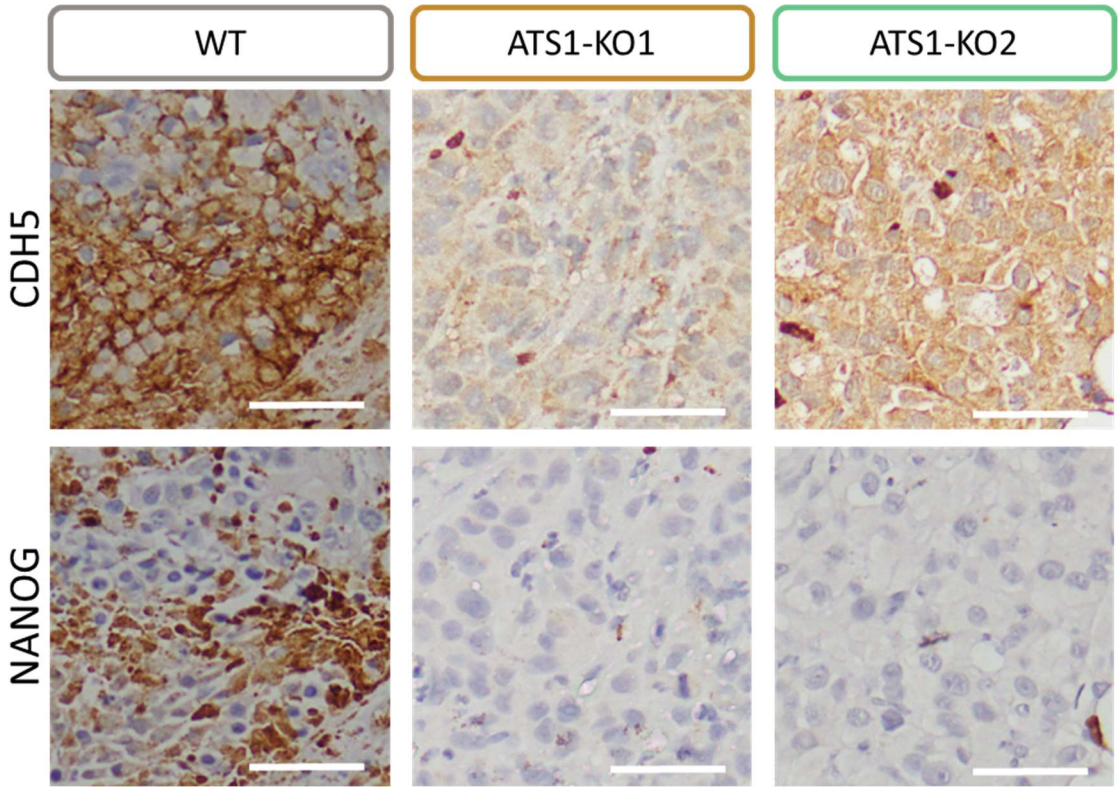

Figure 46. ADAMTS1 inhibition compromises stemness capacities and endothelial-like phenotype in tumor xenografts.
Representative images of IHC staining of CDH5 and NANOG in consecutive sections of WT and ADAMTS1-KO NSG xenografts (white scale bar = 50 µm).

they were significantly bigger than the ADAMTS1-KO ones would corroborate that ADAMTS1 contributes to vasculogenic mimicry and tumor progression in general.

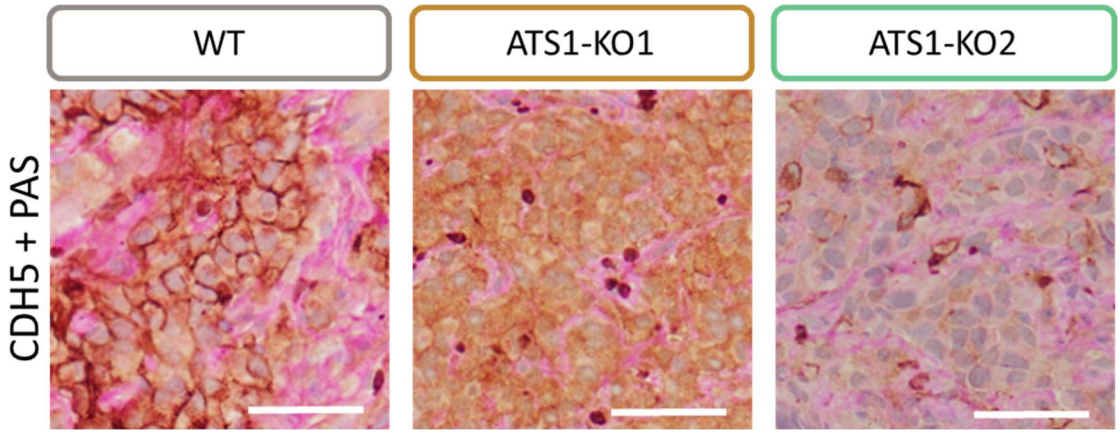

Figure 47. ADAMTS1 inhibition in vivo vasculogenic mimicry in NSG xenografts. Representative images of IHC co-staining of CDH5 (brown) and PAS (pink), in WT and ATS1-KO NSG xenografts (white scale bar = 50 µm).

As a conclusion of this part, the showed results confirmed a close association between stemness, endothelial plasticity and ADAMTS1 that would lead to vasculogenic mimicry events. In an attempt to achieve a deeper study regarding stemness features, *in vitro* tumor sphere assays were performed with the ADAMTS1-inhibited MUM-2B uveal melanoma model.

4.2. Use of melanoma spheres to study *in vitro* stemness properties and the role of ADAMTS1

As previously shown, neither MUM-2B nor the other melanoma cell lines used in this work showed a high expression of CSC markers (Figure 21). However, in an attempt to achieve an induction of stemness properties, melanoma spheres were pursued with MUM-2B cells. Sphere-generation assays are a well-recognized model to evaluate stemness features and CSCs *in vitro* (Perego et al., 2010). In this thesis, melanoma cells were cultured in low-attachment conditions with a specific and supplemented culture medium. If cancer cells succeeded to grow in suspension as spheres, after 21 days they were considered primary spheres. They were collected or, if

necessary, disaggregated and cultured for another 15 days under the same conditions to obtain secondary spheres. Tertiary and successive spheres could be achieved by subsequent disaggregations, but in this study only primary and secondary spheres of MUM-2B cells were considered.

The expression of stemness genes was evaluated by qPCR in MUM-2B spheres, looking for their enrichment attributed to the process of sphere generation. Accordingly, gene expression was compared with 2D cultured cells. qPCR analyses confirmed a significant induction of stemness *NANOG*, *POU5F1* and *PROM1* after the melanoma sphere formation process, in both primary and secondary WT spheres (Figure 48a). Since *ADAMTS1* and *CDH5* have proven their relevance in previous stemness-related experiments, their gene expression was also determined in this melanoma sphere model. Importantly, as occurred with CSC markers, a significant induction of both *ADAMTS1* and *CDH5* in primary and secondary spheres was also detected (Figure 48b), again evoking the involvement of these two molecules in melanoma plasticity phenomena.

These promising results encouraged the evaluation of the sphere formation capacity of ADAMTS1-KO MUM-2B cells. Remarkably, the absence of ADAMTS1 had a dramatic effect, as ADAMTS1-KO cells were completely unable to generate melanoma spheres, neither primary nor secondary (Figure 49). ADAMTS1-KO cells remained on suspension but they were not able to proliferate and therefore they did not generate melanoma spheres.

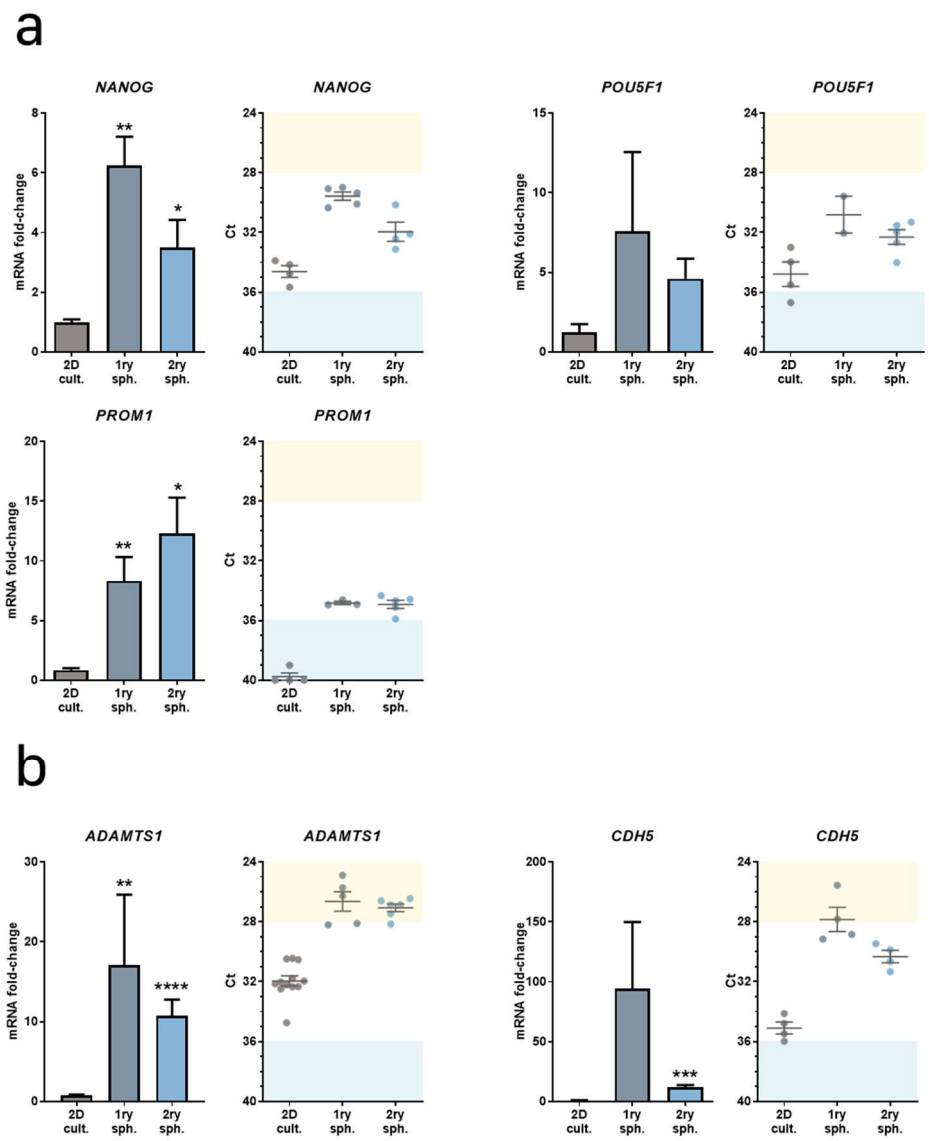

Figure 48. Melanoma spheres generation induces upregulation of stemness genes but also ADAMTS1 and CDH5.

Graphs representing mRNA fold-change expression and Ct values of (a) NANOG, POU5F1, PROM1, and (b) ADAMTS1 and CDH5 in MUM-2B WT 2D culture (2D cult.), primary (1ry sph.) and secondary (2ry sph.) melanoma spheres. High and low gene expression is depicted in Ct graphs with yellow and blue backgrounds, respectively (n = 4 for 2D culture, except for ADAMTS1 which is 12; n = 2–5 for primary spheres, and n = 4–6 for secondary spheres) (****, $p < 0.0001$; ***, $p < 0.001$; **, $p < 0.01$; *, $p < 0.05$. 2D cultured cells were used as control for statistical analyses).

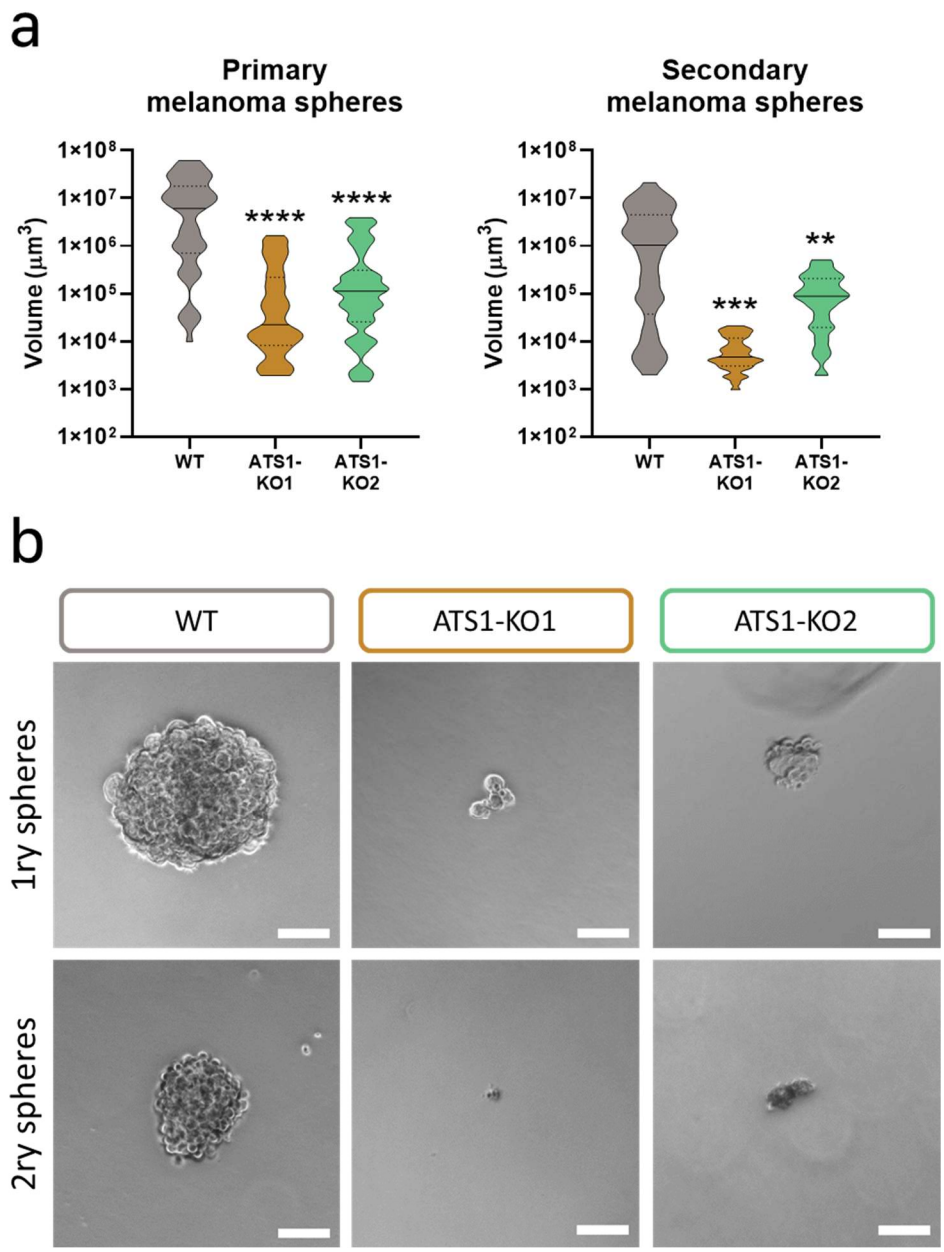

Figure 49. Inhibition of ADAMTS1 compromises melanoma sphere formation.
(**a**) Violin plots representing volume of primary (n = 49 for WT, n = 62 for ATS1-KO1, and n = 58 for ATS1-KO2) and secondary (n = 46 for WT, n = 34 for ATS1-KO1 and n = 21 for ATS1-KO2) melanoma spheres (****, $p < 0.0001$; ***, $p < 0.001$; **, $p < 0.01$. Violin plots indicate the median of every experimental group. WT spheres volume was used as control for statistical analyses). (**b**) Representative images of WT and ATS1-KO primary and secondary melanoma spheres grown in CSC medium (white scale bar = 100 µm).

The strong impairment of ADAMTS1-KO cells to form spheres was not only evident in terms of their volume. Morphologically, these melanoma spheres appeared extremely irregular, far from a spheroid shape. Due to methodological limitations caused by the low amount of RNA obtained from

ADAMTS1-KO spheres, it was not possible to analyze all the markers of interest for this study. However, gene expression levels of *NANOG* and *CDH5* did get analyzed in ADAMTS1-KO primary spheres, encouraged by their alteration shown in previous tumor (Figure 46) and WT sphere (Figure 48) models. Contrary to WT cells, ADAMTS1-KO spheres presented no significant changes in the expression of these genes when comparing with 2D cultured cells (Figure 50). It was noteworthy that the low levels of *CDH5* that ADAMTS1-KO cells displayed in 2D culture were not induced at all in the process of sphere formation, contrary to the observed induction in WT cells.

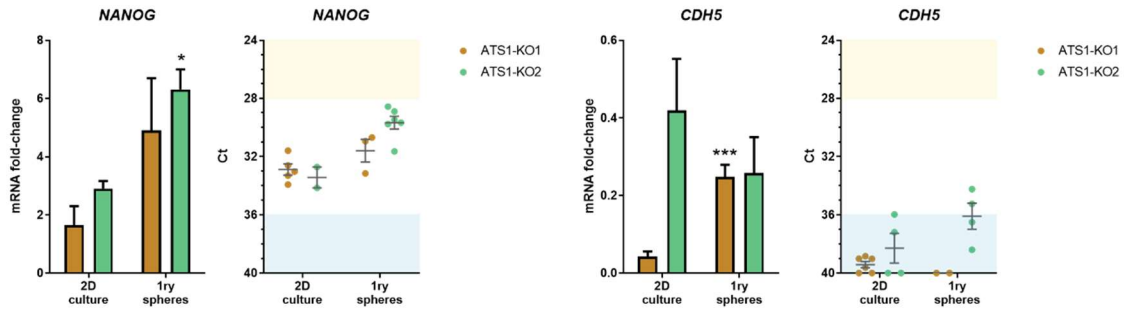

Figure 50. ADAMTS1 inhibition blocks the enrichment of melanoma spheres on stemness and EL markers.
Graphs representing mRNA fold-change expression and Ct values of NANOG and CDH5 in 2D culture (n = 4–6 for ATS1-KO1 and n = 2–4 for ATS1-KO2) and primary melanoma spheres (n = 2 for ATS1-KO1 and n = 4–7 for ATS1-KO2). High and low gene expression is depicted in Ct graphs with yellow and blue backgrounds, respectively (***, $p < 0.001$; *, $p < 0.05$. 2D cultured conditions were used as control for statistical analyses).

All these data demonstrated that ADAMTS1 inhibition also compromises stemness capacities in uveal melanoma MUM-2B cells. However, to reinforce the role of ADAMTS1 in this process, and according to the extracellular nature of the protease, subsequent analyses sought to determine whether secreted ADAMTS1 could affect sphere formation capacity. 24 hours conditioned medium (CM) of MUM-2B cells was first used for this purpose. This medium was identified as ADAMTS1+ CM, according to the fact that MUM-2B cells secrete the protease (details in *Materials and Methods* section and in Figure 67). Very briefly, MUM-2B spheres were grown under two different conditions: with standard CSC medium or ADAMTS1+ CM. Notably, ADAMTS1+ CM enhanced the formation of spheres

for both WT and ADAMTS1-KO cells, even allowing the latter to reach a comparable size to the WT spheres under standard CSC medium conditions (Figure 51). These experiments suggested that secreted ADAMTS1 affects the capacity of sphere formation of MUM-2B cells, not only by recovering it in the ADAMTS1-KO spheres but also by increasing it when ADAMTS1 was already present in MUM-2B WT cells.

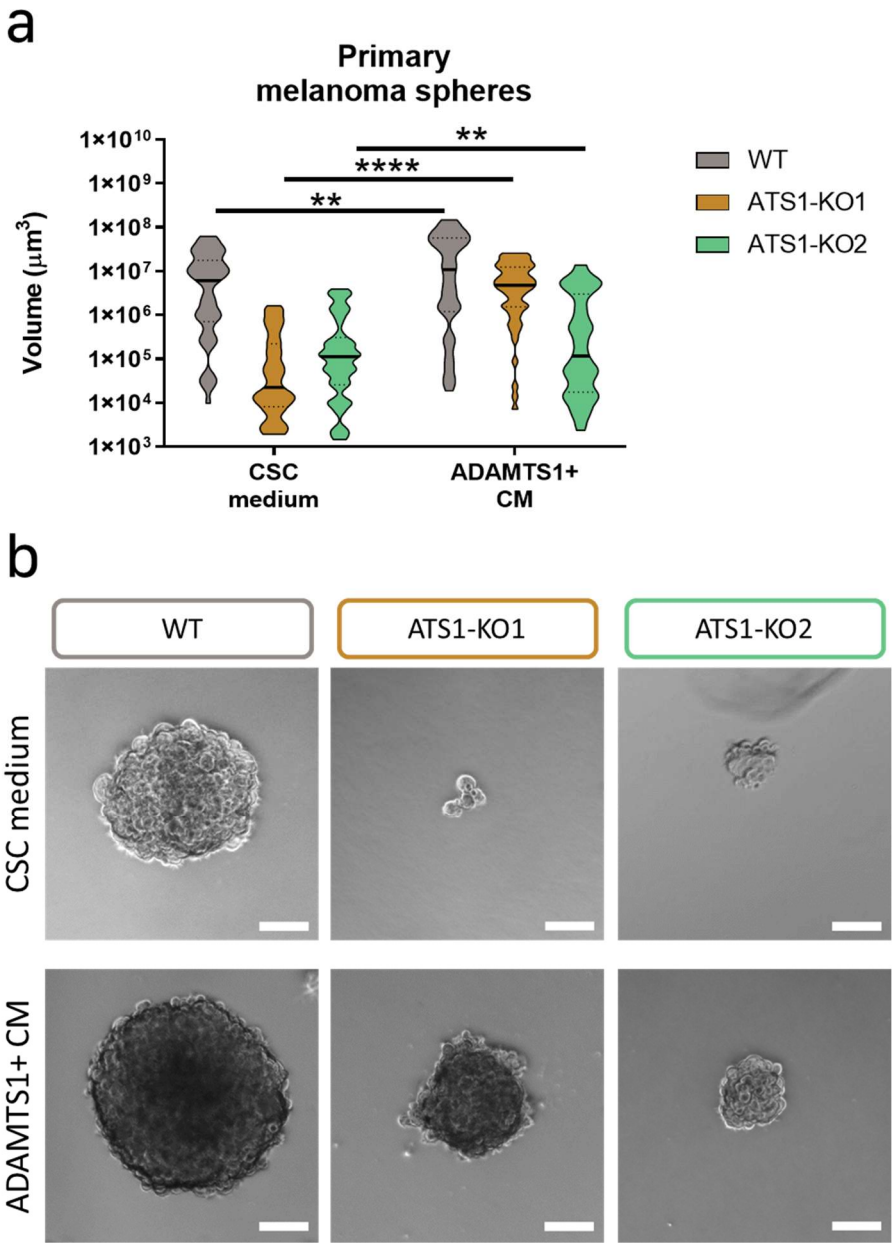

Figure 51. Conditioned medium containing secreted ADAMTS1 improves the sphere formation capacity of ADAMTS1-KO cells.

(**a**) Violin plots representing volume of WT and ADAMTS1-KO primary melanoma spheres grown in CSC medium (n = 49 for WT, n = 62 for ATS1-KO1, and n = 58 for ATS1-KO2) or in ADAMTS1+ CM (n = 44 for WT, n = 48 for ATS1-KO1, and n = 49 for ATS1-KO2) (****, $p < 0.0001$; **, $p < 0.01$. Violin plots indicate the median of every experimental group. CSC medium spheres were used as control

for statistical analyses. (**b**) Representative images of WT and ADAMTS1-KO primary melanoma spheres in CSC and ADAMTS1+ CM media (white scale bar = 100 µm).

These results encouraged the execution of sphere formation experiments using pure recombinant human ADAMTS1 (rhATS1) instead of conditioned medium. CM presents a highly complex nature, composed by a large amount of different proteins secreted by the cells among which ADAMTS1 is only one of them. This fact could mask the actual role of the protease in sphere formation capacity, so the use of rhATS1 would help to determine its specific effect. Importantly, these experiments revealed that rhATS1 in the medium did not affect WT sphere formation but it had a significant effect on the sphere formation capacity of ADAMTS1-KO1 cells (Figure 52). Although their volume did not reach that of the WT cells, the presence of rhATS1 triggered a very significant increase in terms of volume, suggesting that ADAMTS1 is essential for sphere formation of MUM-2B uveal melanoma cells.

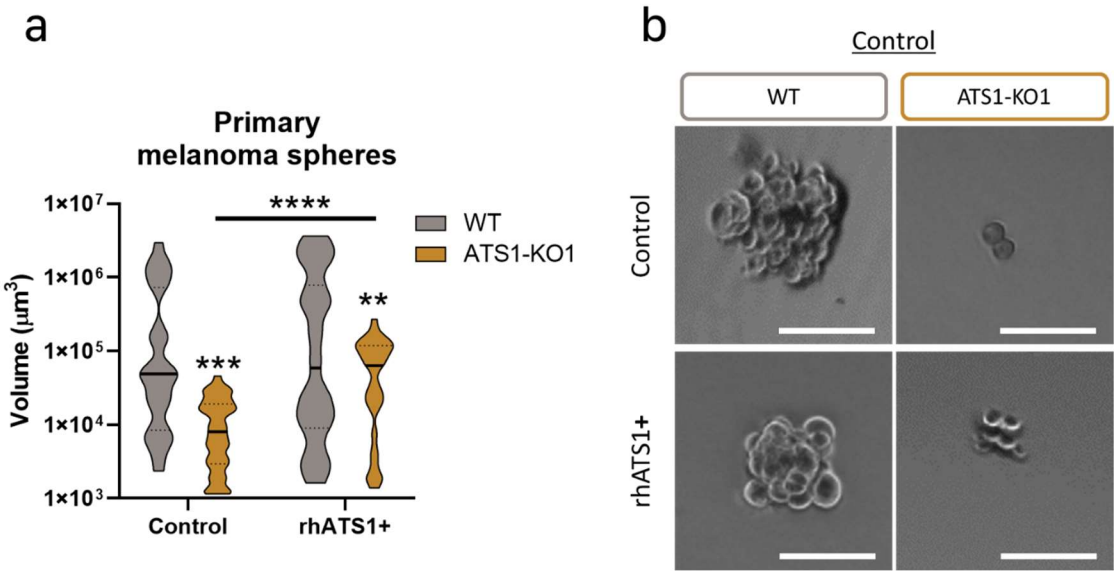

Figure 52. Recombinant human ADAMTS1 recovers the sphere generation capacity of ATS1-KO1 cells.

(**a**) Violin plots representing WT and ATS1-KO1 primary melanoma spheres volume, grown in control CSC (n = 27 for WT, and n = 44 for ATS1-KO1) or rhATS1+ CSC medium (n = 35 for WT, and n = 28 for ATS1-KO1) (****, $p < 0.0001$; ***, $p < 0.001$; **, $p < 0.01$. Violin plots indicate the median of every experimental group. WT spheres volume, except when indicated, was used as control for statistical analyses. (**b**) Representative images of WT and ATS1-KO1 primary melanoma spheres grown in control and rhATS1+ CSC medium (white scale bar = 100 µm).

While these findings with melanoma spheres confirmed the implication of recognized stemness markers, the fact that *ADAMTS1* appeared also induced during the process of melanoma sphere formation and that its inhibition blocked the formation of spheres resulted fully novel and very interesting. Furthermore, the induction of endothelial *CDH5* in melanoma spheres revealed an unexpected link between uveal melanoma stemness features and its putative endothelial-like phenotypic properties. So far, all experiments in this study (both *in vitro* and *in vivo*) have identified ADAMTS1 and CDH5 as important elements to gain tumor stemness and plasticity features, closely related to vasculogenic mimicry.

To endow this basic and experimental research with a translational dimension, available online databases were mined to obtain gene expression and clinical data of human uveal melanoma samples. These data served to conduct several *in silico* analyses detailed in the next section.

5. In silico assessment of the relevance of the endothelial-like plasticity and ADAMTS proteases in human uveal melanoma

Since consistent alterations of endothelial-related and stemness markers modulated by ADAMTS1 were observed and described above, a close study of their contribution in human uveal melanoma was addressed. Considering the infrequent nature of this tumor, the availability of gene expression data in the The Cancer Genome Atlas Uveal Melanoma (TCGA-UVM) Project (Robertson et al., 2017) allowed to pursue such analysis in a relevant number of samples, including prognosis parameters and staging classification. TCGA-UVM project included 80 patients of primary uveal melanoma, with a mean diagnosis age of 61,65 years and a mean disease-specific survival of 26,74 months. These and other interesting data such as disease-specific survival status, clinical stage and mutation count and fraction of the genome altered are represented in Figure 53.

Gene	# of mutated cases	Frequency
GNAQ	40	50,0 %
GNA11	36	45,0 %
SF3B1	18	22,5 %
BAP1	13	16,3 %
EIF1AX	10	12,5 %
SRSF2	3	3,8 %
CYSLTR2	3	3,8 %
APC	2	2,5 %
FAT1	2	2,5 %
GNB1	2	2,5 %

Figure 53. Clinical summary of TCGA-UVM project.
Pie charts representing gender (n = 45 for Male and n = 35 for Female), disease-specific survival status (n = 59 for Alive or dead tumor free and n = 21 for Dead with tumor) and clinical stage (n = 4 for IIA, n = 32 for IIB, n = 27 for IIIA, n = 10 for IIIB, n = 3 for IIIC and n = 4 for IV) of the 80 patients compiled within TCGA-UVM Project. Graphs representing diagnosis age and months of disease-specific survival. Table with information of the top 10 mutated genes on TCGA-UVM project.

5.1. Evaluation of endothelial markers as prognostic factors in human uveal melanoma

A first analysis was related with the involvement of the endothelial-like phenotype. Now, thanks to the Xena Functional Genomics Explorer, developed at University of California Santa Cruz (UCSC) (Goldman et al., 2020), expression data of specific genes could be compared among the 80 patients included in the TCGA-UVM project. Moreover, survival curves can be obtained from each of the analyzed endothelial-related genes. Among them, *CDH5* and *KDR* appeared as significant poor prognosis factors for uveal melanoma (Figure 54), as patients with lower expression achieved a

better survival rate. This clinical data not only confirmed the relevance of *CDH5* in uveal melanoma, already stated by the experimental observations of this study, but also uncovered the contribution of *KDR*, another endothelial gene also involved in vasculogenic mimicry. According to these results, these two endothelial genes may be considered as therapeutic targets in uveal melanoma. Evidently, these data confirmed that tumor vasculature has a critical role on tumor development and patient survival. Furthermore, vasculogenic mimicry, whose causative cancer cells share the expression of *CDH5* and *KDR* with endothelial cells, should be pondered in this poor prognosis scenario and therefore it requires further research.

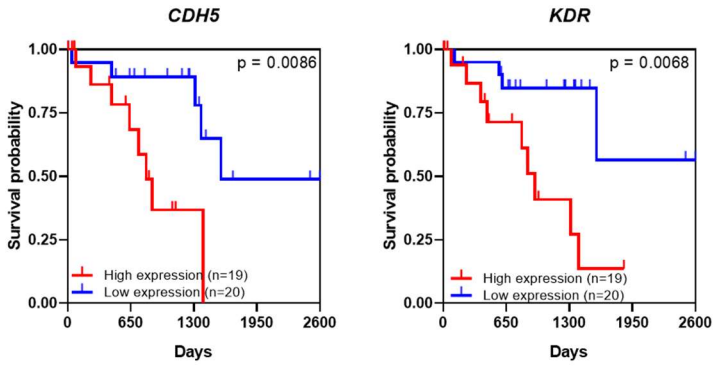

Figure 54. Identification of endothelial-related genes as poor prognosis factors in TCGA Uveal Melanoma Project (TCGA-UVM).
Kaplan–Meier survival curves for low and high gene expression levels of endothelial markers CDH5 and KDR.

The finding of *CDH5* as a poor prognosis factor in uveal melanoma, together with the experimental data obtained in this study, encouraged further *in silico* analyses. Importantly, the identification of genes co-expressed with *CDH5* in UVM cases would uncover its relationship with other processes that might also be related to a worse prognosis in this neoplasia. In this case, cBioPortal platform (Cerami et al., 2012; Gao et al., 2013) allowed to identify those genes whose expression was positively correlated with *CDH5*, revealing a total of 1196 genes significantly co-expressed with *CDH5* (Table 7). As it could be expected, a relevant number of additional endothelial-related genes appeared significantly correlated with *CDH5.* Some of them were also explored in this study (*ENG*, *KDR, TEK* and *TIE1*), but others not (*CD34, FLT4* and *COL4A1*) (Figure 55). In any case, such strong association confirms the

chief relevance of an endothelial-related signature in uveal melanoma, although a deeper comprehension of which cells are contributing with which genes is still demanded to design the best therapies.

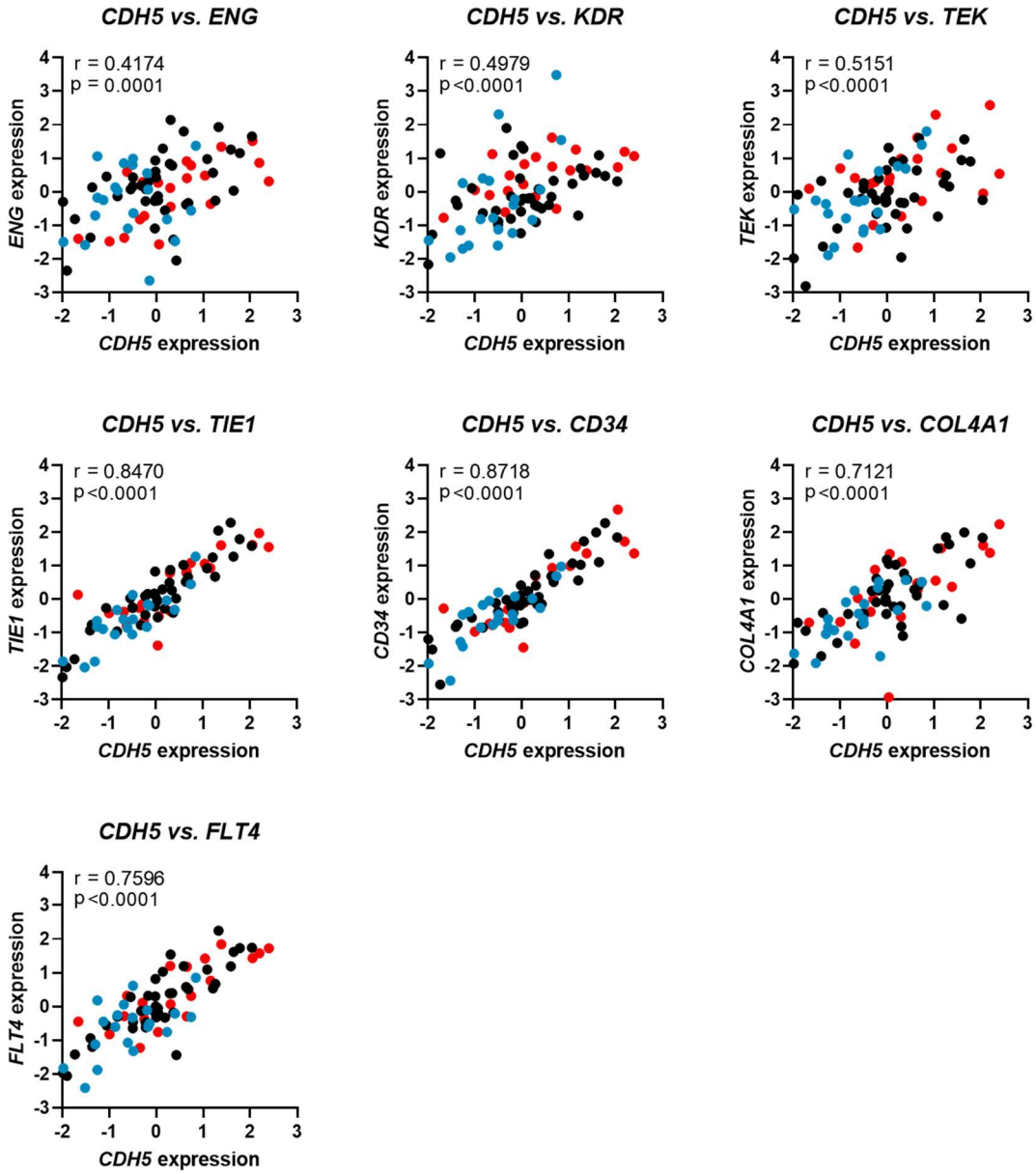

Figure 55. Identification of endothelial-like phenotype related genes that correlate with CDH5 in TCGA-UVM.

Scatter plots representing Spearman correlation analysis between gene expression levels of CDH5 and endothelial-related ENG, KDR, TEK, TIE1, CD34, COL4A1 and FLT4. Overall survival time is depicted with red and blue dots, representing short and long survival time, respectively (r = Spearman correlation coefficient).

Beyond these endothelial-enriched correlations, it was important to know in which biological processes are involved the global gene signature

associated to *CDH5.* For that purpose, GO enrichment analysis was performed using those 1196 genes (Table 7). Importantly, this new GO analysis disclosed a strong relationship between *CDH5* and ECM organization in uveal melanoma patients, supporting the experimental results of this thesis. This relationship with ECM resulted even more significant than with other expected biological processes, such as regulation of angiogenesis (Figure 56 and Table 8).

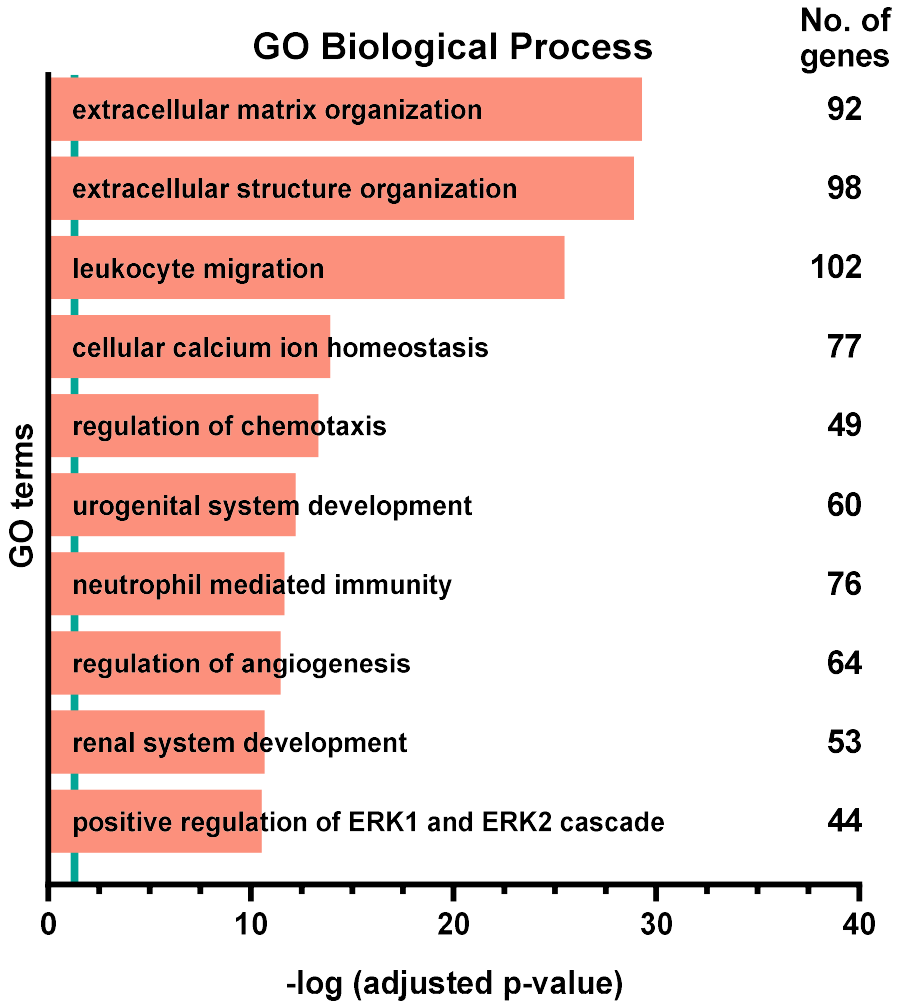

Figure 56. GO enrichment analysis uncovers a correlation between endothelial CDH5 and extracellular matrix remodeling.

Representation of top ten GO Biological Processes after enrichment analysis using genes that positively correlated (q-value < 0.05) with CDH5. Turquoise line determined the limit of significance: -log (0.05). More details in Table 8

5.2. Study of the contribution of ADAMTSs and their substrates to clinical outcome of UVM

The importance of ECM organization for tumor development has been highlighted throughout this study. Indeed, here it has been again underlined by appearing so closely related with endothelial *CDH5* (Figure 56) in the context of UVM, so a closer examination appeared mandatory.

Our exploration of the relationship between endothelial CDH5 and ECM regulation was initiated with the analysis of ADAMTS extracellular proteases in general, and ADAMTS1 in particular, as a main goal of this work. As already introduced, human ADAMTS proteases family consists of 19 members whose role in the ECM remodeling in different diseases has been widely reported. However, their specific action in the uveal melanoma tumor microenvironment has not been addressed yet, with the exception of this current work and some parallel research also developed by this laboratory (Casal et al., 2010; Fernández-Rodríguez et al., 2016) (Peris-Torres et al., 2020a). Returning to the comprehensive analysis of the TCGA-UVM project, the global evaluation of all ADAMTS proteases revealed that three of them were consistently co-expressed with endothelial-related *CDH5*: *ADAMTS4*, *ADAMTS9* and *ADAMTS12* (Figure 57a). Indeed, additional extracellular proteases belonging to the ADAM (*ADAM12*, *ADAM15*, *ADAM19* and *ADAM23*) and MMP (*MMP1*, *MMP9* and *MMP28*) families also appeared correlating with *CDH5* (Table 7). Importantly, the additional evaluation of survival showed that, besides their co-expression with *CDH5*, *ADAMTS4*, *ADAMTS9* and *ADAMTS12* resulted themselves to be poor prognostic factors in uveal melanoma (Figure 57b). The role of these proteases on cancer biology has not yet been widely explored but some promising contributions have been made, as it will be discussed next.

.

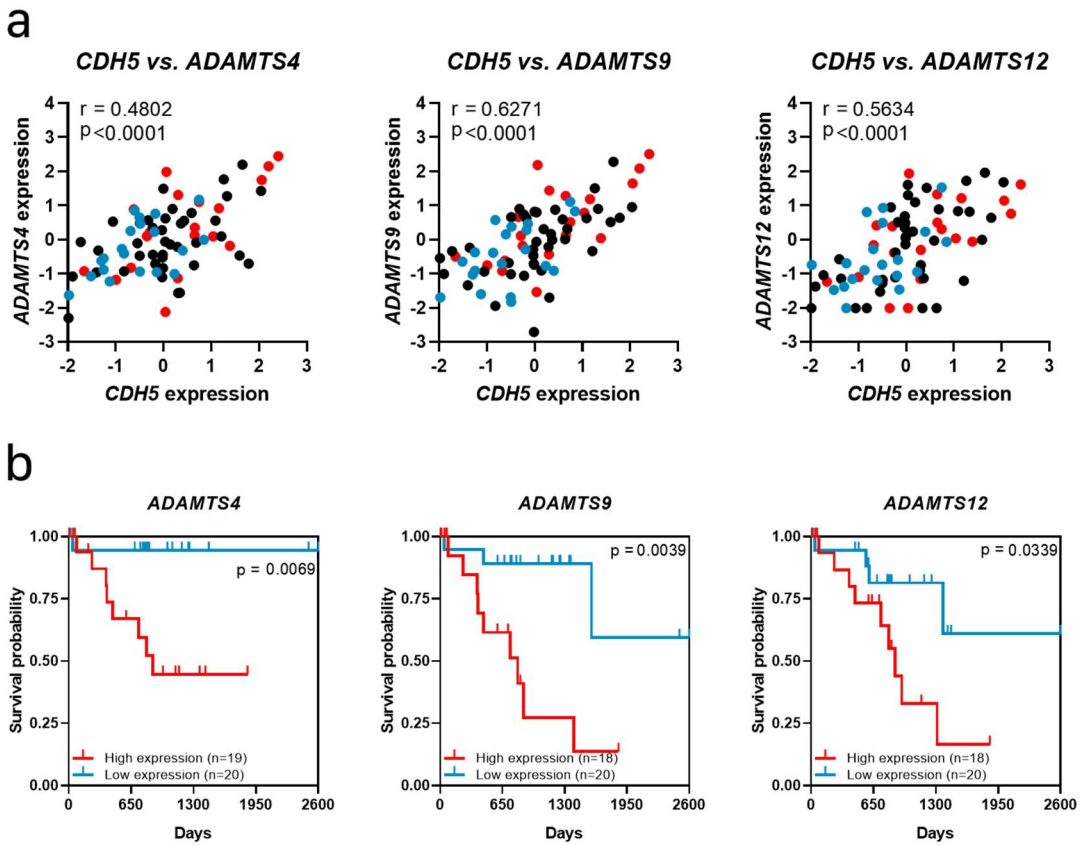

Figure 57. Identification of ADAMTS proteases as poor prognosis factors in UVM. (**a**) Scatter plots representing Spearman correlation analysis between gene expression levels of CDH5 and extracellular proteases ADAMTS4, ADAMTS9 and ADAMTS12. Overall survival time is depicted with red and blue dots, representing short and long survival time, respectively (r = Spearman correlation coefficient). (**b**) Kaplan–Meier survival curves for low and high gene expression levels of extracellular proteases ADAMTS4, ADAMTS9 and ADAMTS12.

These results triggered the evaluation of the remaining members of the ADAMTS family as prognosis factors even though they were not correlated with *CDH5*. Indeed, such analysis also revealed *ADAMTS2*, *ADAMTS5* and *ADAMTS14* as poor prognosis factors for uveal melanoma (Figure 58), thus increasing the number of ADAMTSs that showed this specific behavior.

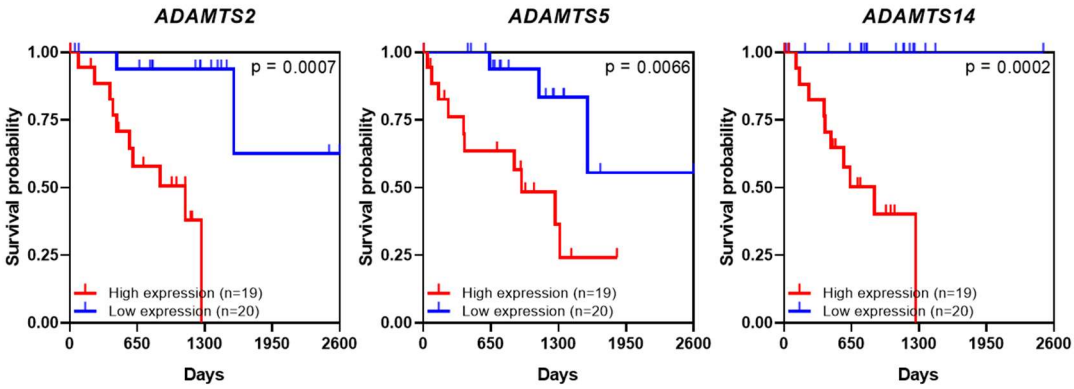

Figure 58. Other ADAMTSs act as poor prognosis factors in UVM.
Kaplan–Meier survival curves for low and high gene expression levels of extracellular proteases ADAMTS2, ADAMTS5 and ADAMTS14.

At first, the fact that ADAMTS1 did not appear throughout this *in silico* analyses resulted disappointing for this study. However, a closer evaluation of the TCGA-UVM project also revealed the lack of data for stemness markers, which relevance in melanoma initiation phases has been widely reported (Fang et al., 2005; Monzani et al., 2007; Santini et al., 2014). In a significant manner, these apparently negative results prompted a shift in the exploration of the TCGA-UVM data towards a new inquiry considering the clinical stage of uveal melanoma as a key factor. If CSC properties are usually related with tumor initiating stages, it is feasible that their effect and expression could be masked and undetectable in analyses employing advance stages of tumor development, such as those generally included in the TCGA. Likewise, since the experimental work of this thesis showed the involvement of ADAMTS1 at initial tumor development steps and its relationship with CSC features, the analysis of the protease in early clinical stages of uveal melanoma might serve to determine its connection with stemness. Accordingly, *ADAMTS1* expression was evaluated among the different uveal melanoma clinical stages using the UCSC Xena platform. In fact, it revealed a very important finding. *ADAMTS1* appeared to be significantly more expressed at the earliest clinical stage (stage IIA) of UVM compared to the subsequent ones (Figure 59). Moreover, this higher expression progressively decreased as the clinical stage progresses, reaching its lowest level at stage IV (Figure 59). Definitely, these new observations strengthen the experimentally obtained results in this study.

They supported the role of ADAMTS1 in the acquisition of an EL-phenotype, the generation and initial growth of xenografts and the sphere formation capacity, all of them processes that would mainly occur at earlier stages of the melanoma development.

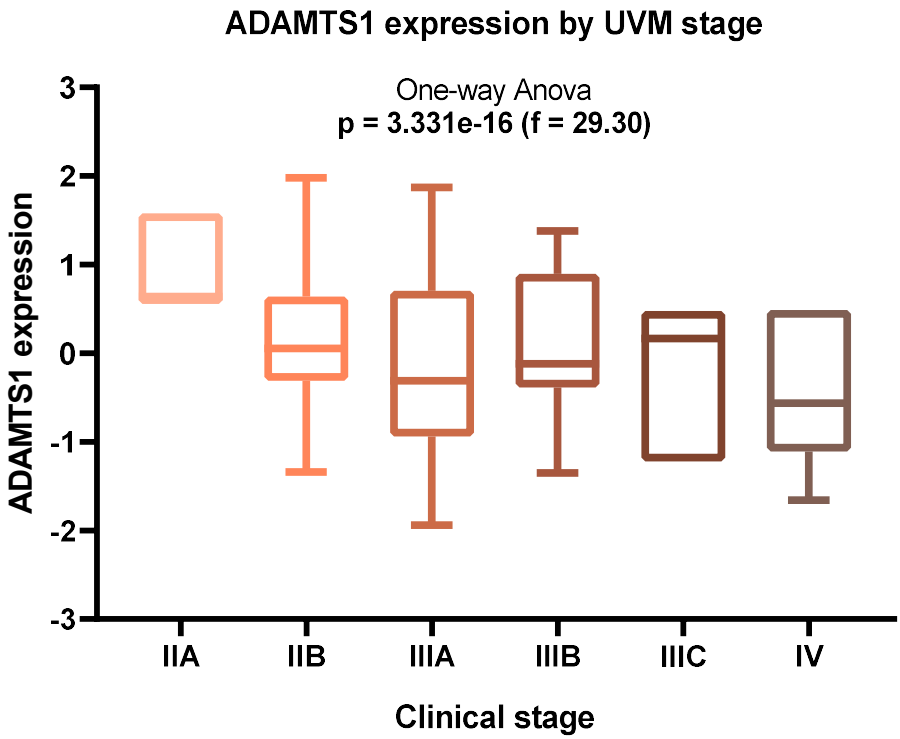

Figure 59. ADAMTS1 is significantly highly expressed in early stages of uveal human melanoma.
Box graph representing ADAMTS1 expression among different clinical stages of human uveal melanoma, from stage IIA to IV (n = 4 for IIA, n = 32 for IIB, n = 27 for IIIA, n = 10 for IIIB, n = 3 for IIIC and n = 4 for IV).

Again, these later analyses remarked the complexity and relevance of ECM elements for tumor development. While ADAMTS1 appeared involved in the initial stages of uveal melanoma, these studies revealed that additional ADAMTSs -phylogenetically close to ADAMTS1- correlated with endothelial CDH5 and were identified as poor prognosis factors at later stages. Furthermore, the analysis of other genes related to the ECM regulation did show motivating results, as those encoding for some ADAMTS1 substrates. Among them, aggrecan (*ACAN*), *IGFBP2*, both nidogens (*NID1* and *NID2*), thrombospondin-1 (*THBS1*) and versican (*VCAN*) appeared co-expressed

with *CDH5* (Figure 60). In addition, all of these substrates except nidogen 2 resulted poor prognosis factors for uveal melanoma (Figure 61).

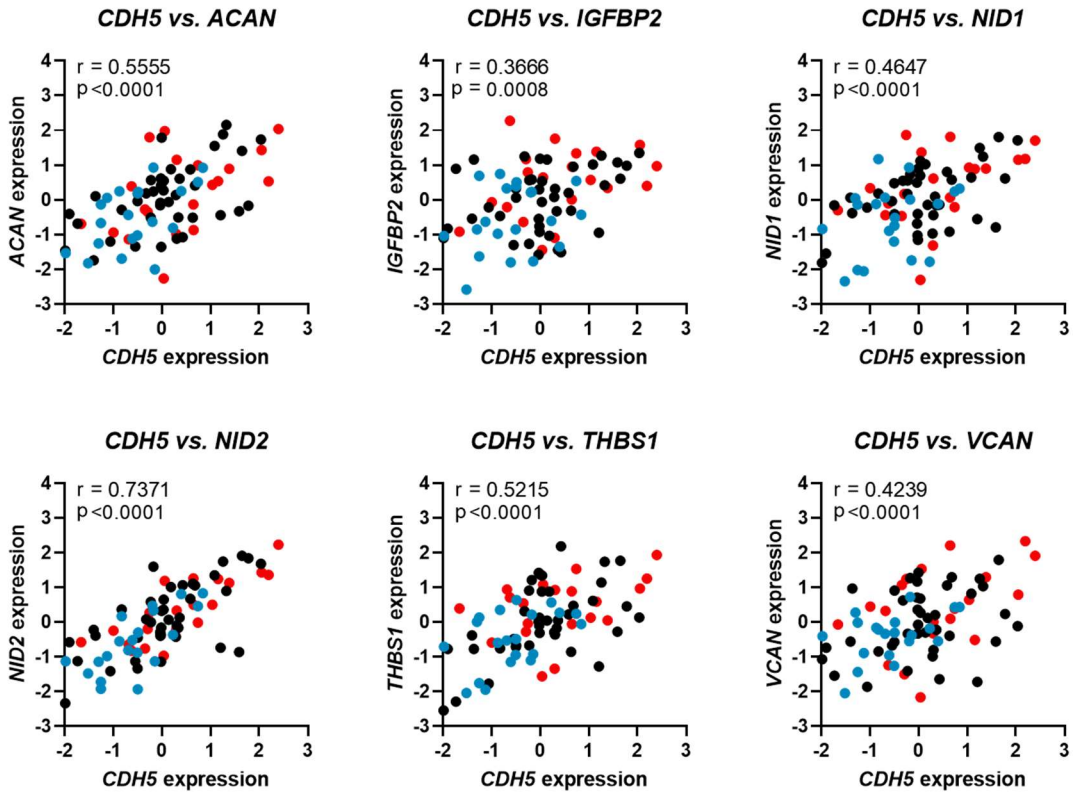

Figure 60. CDH5 is co-expressed with many ADAMTS1 substrates in TCGA-UVM. Scatter plots representing Spearman correlation analysis between gene expression levels of CDH5 and extracellular proteases ACAN, IGFBP2, NID1, NID2, THBS1 and VCAN. Overall survival time is depicted with red and blue dots, representing short and long survival time, respectively (r = Spearman correlation coefficient).

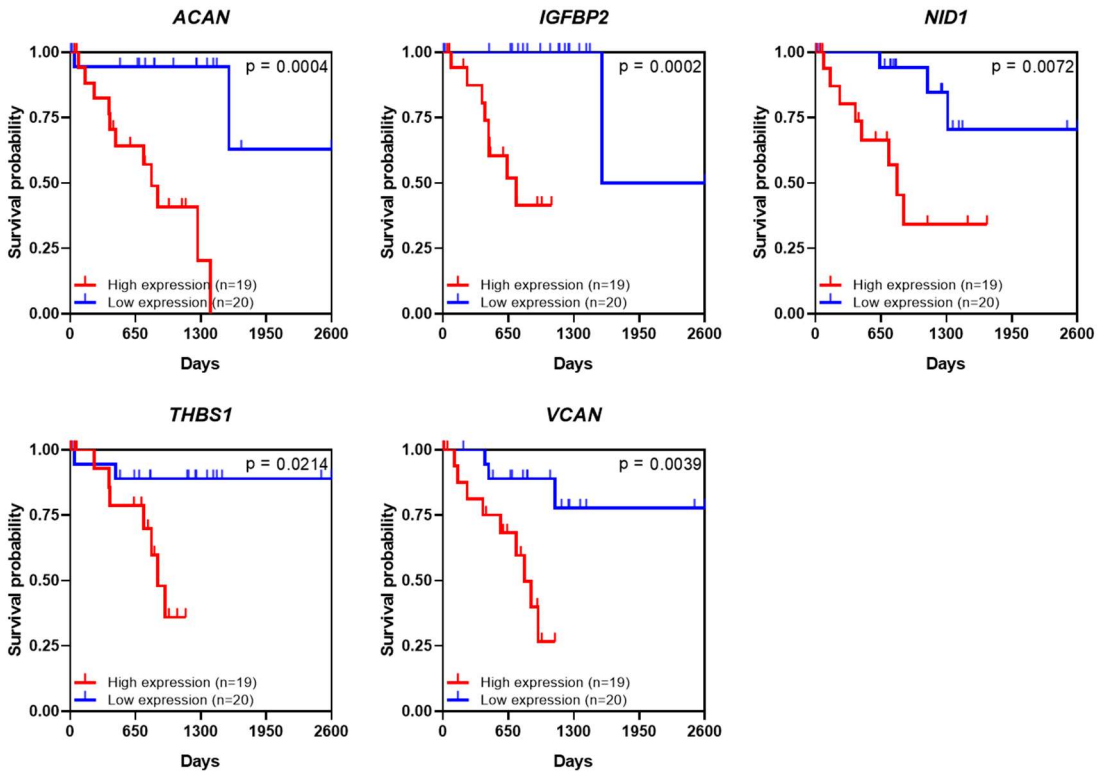

Figure 61. ADAMTS1 substrates are poor prognosis factors in UVM.
Kaplan–Meier survival curves for low and high gene expression levels of ADAMTS1 substrates ACAN, IGFBP2, NID1, THBS1 and VCAN.

Conclusively, if the poor prognosis shown for these substrates is dependent or not of the high levels of *ADAMTS1* at early stages and its decreasing throughout tumor development, it is something that remained unsolved in this study. There is therefore much work to do in this scenario, to closely evaluate the physical interaction between these substrates and their proteases, but also to confirm the clinical value of these signatures at various uveal melanoma stages and the possibilities to target them from a therapeutic perspective.

DISCUSSION

Tumor microenvironment (TME) remodeling is being recognized as a relevant contributor to the complex tumor heterogeneity. To date, although a number of extracellular proteases has been identified as possible therapeutic targets due to their actions during tumor growth, their clinical applications still require much deeper investigations. The main attention of this thesis is focused on the impact of the extracellular protease ADAMTS1 on human uveal melanoma (UVM), and particularly on its effects on cancer plasticity phenomena. However, this work also expands the knowledge on skin cutaneous melanoma, not only in terms of results but also regarding methodology for future research. In general, the results compiled here revealed a new relationship between the extracellular protease ADAMTS1, intrinsic endothelial-like (EL) properties on tumor cells and their enrichment on stemness features. A combination of experimental *in vitro* and *in vivo* approaches, together with the implementation of advanced bioinformatics methodologies using public tumor databases, allowed to unveil the unexplored relevance of ADAMTS1 and other ADAMTS proteases in UVM, which resulted to be strongly correlated with endothelial-specific molecules such as CDH5.

1. Tumor cell lines characterization revealed their genetic and phenotypic heterogeneity

As expected, the initial and comprehensive characterization of human uveal and skin melanoma cell lines approached here confirmed their heterogeneity and, more important, it served as a starting point for subsequent research due to the interesting relationships observed between some of them. The evaluated genes were classified into three different groups attending to their nature, i.e. extracellular matrix (ECM) regulation (*ADAMTS1*, *IGFBP2*, *NID1*, *NID2* and *VCAN*), EL phenotype (*CDH5*, *ENG*, *EPHA2*, *KDR*, *LAMC2*, *TEK* and *TIE1*), and stemness-related (*NANOG*, *POU5F1*, *PROM1* and *SOX2*). Importantly, differences between aggressive UVM MUM-2B and non-aggressive MUM-2C cells were evidenced in the expression of genes related with ECM regulation (Figure 19) and EL-phenotype (Figure 20). Although the differences between these two lines in terms of the EL-phenotype were expected according to previous reports (Maniotis et al., 1999), the finding of differentially expressed genes related to the ECM was novel and resulted very interesting for this thesis. ECM remodeling affects a wide variety of processes, as it will be shown throughout this work. In fact, although this effect has already been described in many tumor contexts (Hanahan and Coussens, 2012), the appearance of differences between these two uveal melanoma cell lines for *ADAMTS1* expression and their substrates implies an even greater relevance of ECM remodeling. At an equivalent level of relevance, uveal MUM-2B and cutaneous C8161 have shown a very similar gene signature (Figure 22), being more evident for relevant genes for this thesis such as *ADAMTS1*, *CDH5* or *LAMC2*. Both MUM-2B and C8161 cells are considered aggressive melanoma cells, but this and other similarities that will be further shown make them appropriate models to study specific processes in two different melanoma subtypes.

These initial studies also revealed significant expression correlations between genes which are involved in ECM remodeling with those related with the acquisition of an EL phenotype. These correlations corroborate the aforementioned relevant effect of ECM, in this case directly involved in the

obtaining of this specific phenotype. In this line, *CDH5* and *LAMC2* shown to be positively correlated in the cell lines considered in this thesis. LAMC2 is not only an element of the ECM but it has also been associated with vasculogenic mimicry, as well as CDH5, so this could be considered a correlation between two EL phenotype-related elements. ECM and EL phenotype were also positively correlated when comparing *EPHA2* and *NID1*. EPHA2 is involved in angiogenesis and related with VM, and NID1 is a main linker of the basement membrane.

In a global manner, the interesting results gathered from the cell characterization encouraged further bioinformatics analyses. The use of the Heuristic Online Phenotype Prediction (HOPP) algorithm, which allows to attribute an invasive or a proliferative phenotype to melanoma cells, revealed a very clear distinction between aggressive MUM-2B and non-aggressive MUM-2C lines, as well as the great similarity between uveal MUM-2B and cutaneous C8161.

As mentioned, HOPP also allows to associate a given gene with a particular invasive or proliferative phenotype. Within the genes of interest for this thesis, we confirmed the classification of *ADAMTS1* towards an invasive phenotype, association that was already experimentally reported by this laboratory (Casal et al., 2010; Peris-Torres et al., 2020a) and others (Ricciardelli et al., 2011). A similar association to invasiveness, confirming experimental data, was detected for *ENG* (Pardali et al., 2011), *EPHA2* (Hess et al., 2001), *KDR* (Maniotis et al., 1999) and *LAMC2* (Seftor et al., 2001). The analysis by HOPP served to confirm the already reported involvements of these genes with the invasive phenotype, relying on the great amount of cellular samples that are included in this *in silico* tool.

Since these studies remarked the relevance of some endothelial-related genes (such as ENG, EPHA2, KDR and LAMC2) and their direct relationship with an invasive phenotype, the evaluation of endothelial-like phenotype of the melanoma cell lines used in this work was strongly supported. Importantly, this evaluation confirmed the association of the obtained results of invasiveness and aggressiveness with the *in vitro* study of

vasculogenic mimicry, so the research looking at the classification of these cell lines suggested further discussions as follows.

2. Melanoma cells exhibit a specific gene signature depending on their endothelial-like phenotype which include ECM-remodeling genes.

The initial characterization of melanoma cell lines reinforced their classification as EL+ or EL- according to their phenotype and behavior in the well-recognized Matrigel assay (Figure 27). The literature has already shown the existence of differential gene signatures among melanoma cell lines with different aggressiveness (Seftor et al., 2002, 2001), but the approach included in this thesis, most of it published at (Peris-Torres et al., 2020a), was grounded in the different gene signature shown by distinct EL phenotypes. Indeed, this work unveiled some new differences in the context of ECM regulation. In this context, *ADAMTS1* showed to be significantly upregulated in EL+ cells (Figure 28), confirming the important contribution of this protease to the acquisition of an EL phenotype (Casal et al., 2010). Furthermore, other genes showed expression differences between EL+ and EL- cells such as VM-involved endothelial ones *CDH5*, *KDR* and *TEK*, which displayed an expression pattern consistent with VM+ aggressive cells (Figure 29). At this point it would be relevant to highlight that these expression analyses were conducted with cells under standard culture settings and not growing in Matrigel, revealing the intrinsic plastic capacities of such cells that showed important basal expression of genes related with the EL phenotype. Indeed, no significant changes were observed on gene expression between different time points of cells growing in Matrigel (data not shown).

Furthermore, another significant observation regards the coincidences between the experimental classification on EL+ and EL- cells and the HOPP-derived on invasive and proliferative phenotypes (Figure 24). In general, EL+ cells presented in this work showed a more invasive phenotype while EL- were predominantly proliferative. Interestingly, the association of EL and aggressive phenotypes was already established since the initial description of vasculogenic mimicry (Maniotis et al., 1999) and further described in other reports (Casal et al., 2010; Harrell et al., 2014; Pardali et al., 2011). Significantly, the work presented in this thesis expanded these observations

and supported the combination of experimental and in silico results to evaluate the capacities of distinct cell lines.

Finally, reinforcing these *in vitro* and *in silico* studies of melanoma cell lines, the bioinformatic analysis of available RNA-Seq data allowed the identification of differentially expressed genes (DEGs) between EL+ versus EL- phenotypes (Figure 30, Table 5). Among these DEGs appeared endothelial *CDH5*, which strongly supported the experimental data of this work at this initial point and served as a precedent for further determinations, as it will be more deeply discussed. In addition, *NID1*, an ADAMTS1 substrate, appeared also significantly upregulated in EL+ cells. Although this thesis is not focused on the relationship of ADAMTS1 with its substrates, some of them have proved to be poor prognosis factors in UVM, including *NID1* (Figure 61), and their relevance will be discussed in subsequent sections. Indeed, a deeper study of the connection between ADAMTS1 and its substrates in cancer, and particularly in UVM, it is a stimulating future perspective drawn from this work.

Nevertheless, contrasting with the experimentally obtained results, it is remarkable that this later *in silico* analysis did not show *ADAMTS1* as a DEG between EL+ and EL- cells. Such finding coincided with the fact that none of the stemness related genes studied in this thesis appeared as consistent DEGs either. Although the possible explanations for these absences are multiple, they may probably be related with the low expression levels that cell lines show of these genes, which could make them undetectable for transcriptomics procedures. Therefore, their study in UVM models at initial stages of tumorigenesis would expose new and significant results that will be discussed later.

Returning to the DEGs between EL+/EL- cells, Gene Ontology (GO) enrichment analysis confirmed the importance of the endothelial component and the ECM in the development of melanomas. As this analysis was conducted with the differentially up-regulated genes in EL+ cells, it was expected the involvement of vascular functions, in this case represented by coagulation and hemostasis. Indeed, the identification of ECM organization processes corroborated some of the main topics of this thesis (Figure 32).

For example, *CDH5* and *NID1* appeared actually involved in these interconnected processes, such as extracellular matrix and structure organization, regulation of epithelial cell differentiation or response to external stimulus (Table 6), encouraging a deeper study of them.

Moreover, the involvement of coagulation pathway genes in EL+ cells supported their role on vasculogenic mimicry and it blood dynamics, as already suggested (Ruf et al., 2003). Hemostasis regulation is driven by the expression of anticoagulant proteins, such as TFPI or THBD, and they have also been related to vasculogenic mimicry. Tumor VM cells may express these factors to ensure blood flow (M. Dunleavey and C. Dudley, 2012). Indeed, *TFPI* has already demonstrated it expression in aggressive VM+ cells, facilitating tumor cell adhesion and migration and affecting metastatic dissemination and/or survival of uveal melanoma (Seftor et al., 2002). It has been also proposed as a facilitator of blood flow through VM channel networks (Ruf et al., 2003) and its expression has reported in glioblastoma stem cells (El Hallani et al., 2010). Regarding THBD, it is associated with tumor angiogenesis (Hsu et al., 2016) and it has been found upregulated in tumor vessels (Lugano et al., 2020). Moreover, native THBD resulted an important determinant of metastasis (Horowitz et al., 2011), although its thrombin-mediated action has been associated with a non-aggressive melanoma phenotype (De Oliveira et al., 2014). Taken together, these data suggested that genes involved in anticoagulation processes deserve a deepen study in relation to the endothelial-like phenotype in melanoma, which could be considered one of the future perspectives of this thesis.

With all these results it seems clear that ADAMTS1 plays an important role in uveal melanoma through its effect on ECM remodeling and with consequences on the acquisition of an endothelial-like phenotype. Still, the crosstalk between endothelium and tumor cells is unsolved. Preliminary results of this laboratory using co-culture Matrigel assays of melanoma cells with HUVECs already suggested a relationship between *ADAMTS1* expression and the endothelial-like phenotype (data not shown). Now in this work, the edition and inhibition of the protease were conducted in UVM cells, which would yield conclusive results to uncover its specific role.

3. *ADAMTS1* edition alters endothelial-like phenotype of melanoma cells

As showed in this thesis, ADAMTS1 gene edition and inhibition by CRISPR/Cas9 technology was achieved in uveal MUM-2B and cutaneous C8161 cell lines. Although promising results were also obtained for cutaneous SK-MEL-103 and SK-MEL-147 cells, their study was too preliminary to be showed here. From a methodological perspective, it is important to highlight the stronger inhibition and reproducible results obtained using CRISPR/Cas9 approach, in contrast with shRNA knockdown technology. The improvement of gene editing tools is constant and this work confirms a better performance of CRISPR/Cas9 methods.

Importantly, the inhibition of *ADAMTS1* in uveal melanoma MUM-2B cells confirmed the disruption of relevant tumorigenic features, deserving a brief discussion. First, Matrigel assays showed that the absence of ADAMTS1 compromised the endothelial-like phenotype of these melanoma cells (Figure 33). Moreover, those deficient cells showed a clear downregulation of endothelial-related genes (Figure 34). Leading such downregulation appeared the recognized endothelial-related markers *CDH5* and *KDR*, two genes which have been also related with vasculogenic mimicry and CSC-like features in several types of cancer including melanoma (Seftor et al., 2001; Yao et al., 2013). Significantly, *CDH5* blockade also occurred in cutaneous melanoma C8161 ADAMTS1-KO cells (Figure 34), suggesting a more global role of ADAMTS1 in melanoma and not specific to the uveal subtype. Regarding *KDR*, its downregulation was also observed in cutaneous C8161 ADAMTS1-KO cells although without statistical significance (data not shown). In addition, not so evident but significant was the reduction of endothelial-related *LAMC2* and *TIE1* when *ADAMTS1* was edited in MUM-2B cells, which indicates that the consequences of this protease editing for the endothelial-related gene signature still need further investigation. All these endothelial-related markers have been involved in aggressive vasculogenic mimicry processes (El Hallani et al., 2010; Hendrix et al., 2003b; Yao et al., 2013), as well as *EPHA2*, whose expression also decreased, although no significant differences were reached, when ADAMTS1 was inhibited in MUM-2B cells.

These findings corroborate the potential relationship that aggressive endothelial-like cells establish with their ECM through extracellular proteases as ADAMTS1. For example, similar relationships have already been described in the literature, such as the cooperative interaction between LAMC2 and MMP2 in aggressive melanoma cells (Seftor et al., 2001), thus further research is needed to unveil how this endothelial-related genes downregulation caused by ADAMTS1 inhibition could suggest a direct connection of ECM remodeling with the acquisition of an EL phenotype.

4. ADAMTS1 inhibition impairs tumor development and vasculature

Notably, the xenograft assays in distinct mouse models showed in this work supported the pro-tumorigenic actions of ADAMTS1 in UVM. Indeed, initial data obtained with SwN mice disclosed a complete halt of tumor growth when using ADAMTS1-KO cells (Figure 36). Despite this dramatic effect of the absence of ADAMTS1 for tumorigenesis, experimental modifications were undertaken in order to challenge these striking finding. For this purpose, tumor engraftment was promoted by injecting cells in a Matrigel solution. Although some ADAMTS1-KO tumors progressed under this new setting, the process was still quite irregular. They continued showing a significant blockade on tumor growth compared with WT tumors, as well as a huge variability among them that prevented an appropriate analysis (Figure 37). This strong impairment on tumor generation was partially overcome by using a third model, the NSG mice. Although the overall development of tumors was improved in this model, the absence of ADAMTS1 still prompted a relevant compromise comparing to WT samples (Figure 38). It is suggestive the fact that ADAMTS1-KO cells showed an improved growth in NSG mice, known to display a stronger immune deficiency. In some way, this finding recalls the recently described immunomodulatory role attributed to this protease (Rodríguez-Baena et al., 2018a). Certainly, these results encouraged deeper studies to unveil the impact of this ECM-modifying enzyme on the immune system, although alternative and adequate models must be considered.

Regarding tumor vasculature, this study keeps showing alterations in ADAMTS1-KO tumors that evokes observations of previous reports. In this current model, the changes in vasculature should be considered more as a compensation, since ADAMTS1-KO tumors displayed more but smaller vessels than their WT counterparts (Figure 40). Indeed, this finding is reminiscent of previous reports by this laboratory despite being conducted in different tumor and mice models. For example, xenografts of ADAMTS1-overexpressing HEK293T cells into Nu/Nu BALB/c mice demonstrated enlarged lumens size and decreased vessel density compared with non-

overexpressing cells (Martino-Echarri et al., 2013). In this case, ADAMTS1 was attributed to provide an anti-tumorigenic effect, since its higher levels resulted in the inhibition of tumor growth. On the other hand, this laboratory reported a pro-tumorigenic role of ADAMTS1 using syngeneic B16F1 melanoma cells in *Adamts1*-deficient C57BL/6 mouse model (Fernández-Rodríguez et al., 2016). In that work, the impaired tumor growth in *Adamts1* KO mice concurred with an increased vascular density but smaller and hypoxic vessels. The differences and similarities between these previous works and that obtained in this thesis, most of it published in (Peris-Torres et al., 2020a), are aligned with the widely described role of ADAMTSs as modulators of vasculature (Rodríguez-Manzaneque et al., 2015).

Finally, relevant data in this thesis suggest the existence of alternative mechanisms of vascularization. Flow cytometry evaluations suggested that the inhibition of ADAMTS1 also affected the cellular composition of tumor vasculature. Interestingly, this technique allowed the identification of a small fraction of endothelial marker PECAM1+ cells which also showed GFP expression, unique of tumor cells. Such cells, PECAM1+/GFP+, could be considered vasculogenic mimicry positive and deserve a deeper study. Furthermore, ADAMTS1-KO tumors showed an overall increased number of PECAM1+/GFP- cells but a decreased ratio of PECAM1+/GFP+ cells (Figure 39), already corroborating the actions of ADAMTS1 in such alternative phenomena as previously described (Peris-Torres et al., 2020a).

5. ADAMTS1 is closely related to stemness features, as well as CDH5, both *in vivo* and *in vitro*

Since the initial evaluation of NSG xenografts showed that ADAMTS1 inhibition affected vasculature development and involved vasculogenic mimicry phenomenon, further experiments were conducted to study its connection with endothelial and stemness parameters. Importantly, comparing MUM-2B cells before and after injection into NSG mice revealed an overall upregulation of stemness genes, leaded by *NANOG* and *POU5F1* in xenografted cells (Figure 41). A parallel upregulation was also observed for *ADAMTS1* and *CDH5* genes (Figure 42), highlighting once again their relationship with stemness features. Indeed, the genetic blockade of the protease in MUM-2B cells provoked a significant downregulation not only of *NANOG* and *POU5F1* stemness markers (Figure 43) but also of endothelial *CDH5* in the resulting tumors (Figure 44).

Following gene expression analyses, NSG xenografts were subjected to immunohistochemistry (IHC) determinations in an attempt to deepen in the aforementioned relationship. These assays not only confirmed a differential expression of CDH5 in ADAMTS1-WT and KO tumors, but also showed a spatial proximity of CDH5+ cells to blood vessels that disappeared in ADAMTS1-KO tumors (Figure 45). Moreover, the analysis of correlative histological sections showed an additional connection between CDH5 and NANOG positive signals, in addition to confirming the results of gene expression analysis that showed a significant halt of their expression when ADAMTS1 is absent. Indeed, CDH5 showed spatial proximity not only with blood vessels and NANOG, but also with periodic acid-schiff (PAS)-positive patterns (Figure 47). PAS-positive patterns are considered indicators of *in vivo* vasculogenic mimicry since its initial description (Maniotis et al., 1999), and here they showed a significant reduction when ADAMTS1 was absent and the aforementioned relationship with CDH5.

These later results remarked the intimate relationship between stemness, plasticity and the acquisition of endothelial-like properties. Indeed, the observed modulatory capacities of ADAMTS1, both *in vitro* and *in vivo*, emphasize the chief contribution of ECM modifying enzymes. Suggestively,

these findings resume the necessity to design new and improved specific inhibitors of matrix metalloproteases to overcome former disappointing results in clinical trials (Coussens et al., 2002). In addition, this study supports a main involvement of CDH5-related pathways, but taking into account its relevant expression in plastic tumor cell populations in addition to its canonical endothelial origin.

These findings are additionally reinforced by tumor sphere assays reported in this work. Importantly, although the development of melanoma spheres from MUM-2B cell line was already reported (Joshi et al., 2016), this thesis presents for the first time their deeper description and characterization (Peris-Torres et al., 2020a). Furthermore, this evaluation showed that MUM-2B-derived spheres displayed a clear upregulation of main stemness markers (Figure 48), together with the newly reported induction of *CDH5* and the protease *ADAMTS1* (**¡Error! No se encuentra el origen de la referencia.**). While CDH5 has been already related with stemness parameters and vasculogenic mimicry events (Castet et al., 2019; Lai et al., 2012; Mao et al., 2013), the data presented here exposed that extracellular proteases such as ADAMTS1 should also been considered when studying the stemness and tumor-initiating capacities. In fact, progression of tumor spheres derived from ADAMTS1-KO cells was clearly compromised (Figure 49), and also there were no significant changes on the expression of key endothelial and stemness genes already mentioned (Figure 50). This finding was strongly supported using ADAMTS1-enriched media, either by CM of melanoma cells (Figure 51) or as exogenous recombinant protein (Figure 52), adding the relevance of the extracellular contribution of this protease. This role of ADAMTS1 during initiating stages of tumorigenesis probably justifies its absence in standard gene expression notations, as previously mentioned in cell lines studies, as well as in human UVM samples like will be further discussed.

6. TCGA database analysis revealed new prognostic elements for human UVM

According to the modest knowledge of UVM, considered a rare type of cancer (Castet et al., 2019), the new findings achieved by this thesis reinforce its suggested plastic nature. Moreover, a comprehensive study of genes of interest in human UVM datasets from TCGA was conducted. In line with the global goals of this thesis and the gained experimental observations, three different groups of genes were assessed, including endothelial-related genes, members of the ADAMTS family of proteases and, finally, a set of ADAMTS1 substrates in an attempt to elucidate the putative mechanisms of action of this and related proteases. A brief discussion follows next.

6.1. *CDH5* and other endothelial VM-related genes are poor prognosis factors in UVM

Among the endothelial-related genes, *CDH5* and *KDR*, deserved special attention. Although throughout this work it is remarked that *CDH5* should be considered a determinant factor for uveal melanoma, the fact that other endothelial-related gene such as *KDR* displayed similar features resulted especially interesting due to their common involvement in vasculogenic mimicry and stemness features (Frank et al., 2011; Yao et al., 2013). Very suggestively, this *in silico* analysis revealed *CDH5* and *KDR* as significant poor prognosis factors in uveal melanoma (Figure 54), which supported the close connection, in this case in patient samples, between an endothelial-like phenotype and a worse clinical outcome.

The fundamental role of CDH5 in uveal melanoma development, confirmed both by the experimental results of this thesis and by the *in silico* analysis of human data, converted this endothelial gene into the central element of subsequent determinations. Consequently, the identification of genes co-expressed with CDH5 in uveal melanoma was conducted, as well as the biological processes in which they are involved. This analysis confirmed a large number of endothelial genes similarly regulated to *CDH5* (Figure 55) but, more significantly, that there is a large proportion of co-expressed genes

involved in ECM organization (Figure 56). This last observation supported the main hypothesis of this study, demonstrating that the ECM remodeling and the endothelial component act together also in patients. In addition, the appearance of *leukocyte migration* GO term in this enrichment analysis deserves a special attention and its investigation would be an interesting future perspective from this thesis. As described elsewhere, ADAMTS1 has been proposed as a modulator of the tumor immune system (Rodríguez-Baena et al., 2018a), with together with its ECM remodeling function could affect leukocyte migration. Moreover, this migration has been demonstrated to be altered in different cancer contexts, affecting tumor development, and CDH5 is also involved in this response.

Following the main objective of this thesis, ECM-related genes that were co-expressed with *CDH5* were analyzed and will be discussed in the following sections.

6.2. ADAMTS proteases also act as poor prognosis factors and ADAMTS1 is crucial for early stages of UVM

Several genes that code for extracellular proteases were found among the subset of ECM-related genes that co-expressed with *CDH5*. Very interestingly for this thesis, ADAMTS proteases *ADAMTS4*, *ADAMTS9* and *ADAMTS12* were included in this group of extracellular proteases. Further analyses on them revealed that they not only were co-expressed genes with CDH5, but also resulted to be poor prognosis factors for uveal melanoma by themselves (Figure 57). These findings definitively implied a key role of these proteases during melanoma progression, which will be briefly discussed now. Since the role of these ADAMTSs in several pathologies has been previously introduced, here it will be discussed exclusively their functions in melanoma or other pathologies specific to the eye. None of these processes has yet involved ADAMTS12, and ADAMTS4 and ADAMTS9 have not yet been reported to be related to human melanoma. Nevertheless, some reports have been conducted in B16F10 murine melanoma models, in which ADAMTS4 and ADAMTS9 have shown different tumorigenic functions depending on their catalytic states. Thereby, while full-length ADAMTS4

promotes melanoma growth and angiogenesis, its isoform containing only the C-terminal ancillary domain suppressed both processes (Rao et al., 2013). On the contrary, ADAMTS9 active isoform demonstrated to exert an anti-angiogenic effect in a proteolytic activity-dependent manner (Koo et al., 2010). Beyond melanoma, ADAMTS9 has been related to human ocular morphogenesis and age-related macular degeneration, a major cause of blindness. It has been found to be involved in the proteolytic modifications of retinal ECM in a dose-dependent manner, as well as in the prevention of corneal opacity and anomaly (Bevitt et al., 2003; Dubail et al., 2016; Whitmore et al., 2013). All these data provided an overview of their potential actions on uveal melanoma, and functional studies are needed to unveil the cause of their appearance as poor prognosis factors in this neoplasia.

Furthermore, additional ADAMTS members, such as *ADAMTS2*, *ADAMTS5* and *ADAMTS14* also resulted poor prognosis factors of UVM, although they were not found co-expressed with *CDH5* (Figure 58). Although the importance of ADAMTSs in uveal melanoma development has been evidenced, further analyses would shed more light on the complex role of extracellular proteases.

Among all ADAMTSs, it was appealing the fact that *ADAMTS1* did not appear co-expressed with *CDH5* in UVM patients neither as a bad prognosis factor, although our experimental results strongly suggested the contrary. However, a deeper analysis of this data collection allowed to reach quite important conclusions. *ADAMTS1* showed its highest expression levels at early stages of uveal melanoma, and decreased as the disease progresses to advanced clinical stages (Figure 59). This behavior resulted very interesting since ADAMTS1 seemed to act in harmony with stemness features, mainly upregulated at early stages of tumor development. Indeed, this hypothesis was supported by experimental results of this thesis, including those revealed from the *in vivo* xenografts generation and from the melanoma sphere formation assays. Furthermore, it is necessary to remark the strong similarity that exists between ADAMTS1 and the rest of members of the ADAMTS family that resulted to be prognostic factors. This great similarity

could make them act as perfectly complementary elements within the highly complex TME scenario, which remains an open field of cancer research.

6.3. ADAMTS1 substrates contribute to a worse clinical outcome of UVM

Definitively, the study of ADAMTSs substrates still remains an open field that requires much research. The modulatory capacity of such substrates has been recognized according to their nature as intrinsic elements of the TME. Suggestively, this work revealed that some ADAMTSs substrates were found among genes co-expressed with CDH5 in UVM, indeed included as ECM related molecules (Table 8). Focusing on ADAMTS1 substrates, the analysis of *ACAN*, *IGFBP2, THBS1*, *NID1*, *NID2* and *VCAN* showed their significant positive correlation with *CDH5* among human uveal melanoma patients (Figure 60). Some of these co-expressions have already been described in other tumor types, such the identification of IGFBP2 as an enhancer of vasculogenic mimicry by activating CDH5 in glioma (Liu et al., 2019) but they have not been described yet for uveal melanoma. The *in silico* analysis conducted in this thesis also proposed for the first time ADAMTS1 substrates as prognosis markers in uveal melanoma. In this line, *ACAN*, *IGFBP2*, *THBS1*, *NID1* and *VCAN* resulted poor prognosis factors in this neoplasia (Figure 61). Among these genes, it is remarkable that *NID1* was identified as an upregulated DEG in EL+ cells in the first part of this work. Interestingly, a pro-tumorigenic role of *NID1* was already reported enhancing the *in vitro* EL phenotype in breast cancer and cutaneous melanoma cell lines and promoting *in vivo* metastasis of these tumors to the lungs (Alečković et al., 2017). In addition, it has shown to be a poor prognosis factor in these two aforementioned cancer types (Alečković et al., 2017), as well as in ovarian cancer promoting EMT-dependent cell migration and invasion (Zhou et al., 2017). On the contrary, an anti-tumorigenic role has also been reported for nidogen 1 in a breast cancer model (Ferraro et al., 2019). All these effects may be orchestrated by the catalytic cleavage of nidogen 1 by extracellular proteases such as ADAMTS1. This laboratory has profoundly contributed to this knowledge, not only by unveiling that

nidogen 1 is one of the ADAMTS1 substrates (Canals et al., 2006), but also by demonstrating that its effect and deposition on tumor vasculature of breast carcinoma directly depend on the proteolytic activity of this protease, which acted in this context as a tumor suppressor factor (Martino-Echarri et al., 2013). Once again, the important connection between ECM remodeling, the endothelial component and tumor development has been highlighted, encouraging future investigations in this line in UVM.

As a conclusive comment, the *in vitro* and *in vivo* findings showed in this work reinforce the robust relationship between the endothelial-like plasticity and stemness features intrinsic to uveal melanoma cases, all orchestrated by ECM-mediated mechanisms. According to the rare nature of this melanoma, these results showing the significant crosstalk between endothelial-related genes, such as *CDH5*, stemness markers and members of the ADAMTS family of extracellular proteases, propose a previously unknown scenario in which their full comprehension would help to define new therapeutic strategies (Figure 62).

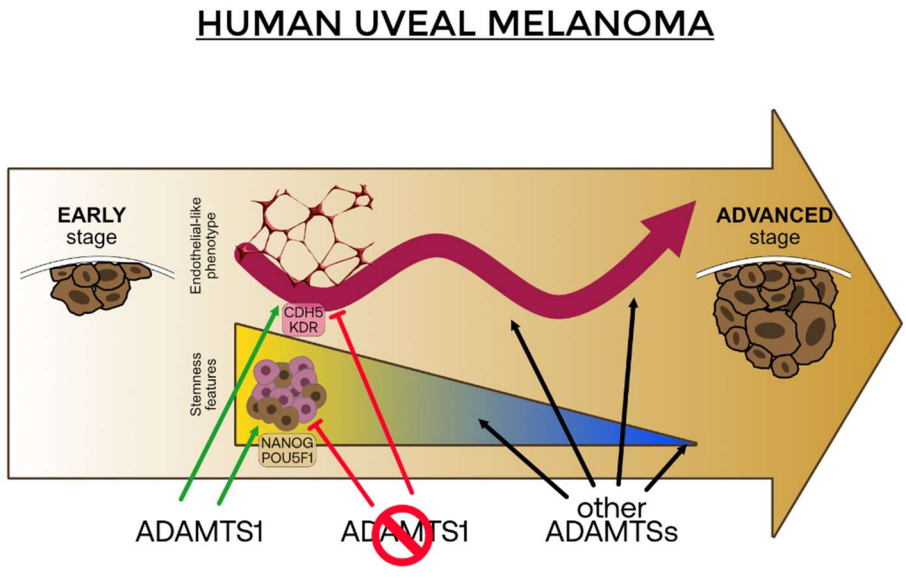

Figure 62. Graphical abstract.
Graphical representation of the work presented in this thesis.

CONCLUSIONS

- The initial characterization of human melanoma cell lines highlighted a huge heterogeneity among them in terms of gene expression. Besides it, promising relationships were obtained between genes of different nature such as ECM remodeling and endothelial-related.

- The classification of the human melanoma cell lines attending to their endothelial-like phenotype allowed the identification of differentially expressed genes according to their EL+ or EL- condition.

- *ADAMTS1* edition alters the endothelial-like phenotype of melanoma cell lines, noted not only by the impairment of vascular-like networks generation-capacity, but also by affecting the expression of genes involved in the acquisition of this phenotype.

- ADAMTS1 is necessary for normal tumor growth and the development of an appropriate tumor vasculature.

- An up-regulation of *ADAMTS1* and *CDH5*, together with stemness markers, was detected in mouse xenografts. ADAMTS1 inhibition provoked a down-regulation of both *CDH5* and stemness genes in such mouse models.

- CDH5 showed to be spatially related to tumor vasculature, NANOG expression and *in vivo* VM patterns, everything in an ADAMTS1-dependent manner.

- *ADAMTS1* and *CDH5* are up-regulated in uveal melanoma spheres, and ADAMTS1 demonstrated an essential role on sphere generation capacity.

- *CDH5* plays a fundamental role on the clinical outcome of TCGA-UVM project patients. It is a poor prognosis factor and it showed to be co-expressed with several endothelial and ECM-remodeling-related genes that also contribute to this worse outcome.

- *ADAMTS4*, *ADAMTS9*, *ADAMTS12*, *ADAMTS2*, *ADAMTS5* and *ADAMTS14* resulted poor prognosis factors for UVM samples of TCGA.

- *ADAMTS1* demonstrated an up-regulation at early stages of UVM that decreased as the diseases progresses, suggesting again its close relationship to stemness features and its role in tumors initiation.

CONCLUSIONES

- La caracterización inicial de las líneas celulares de melanoma puso de manifiesto la enorme heterogeneidad que existe entre ellas en cuanto a la expresión génica. Además, se obtuvieron interesantes relaciones entre genes de diferente naturaleza como la remodelación de la matriz extracelular y los relacionados con el endotelio.

- La clasificación de las líneas celulares de melanoma humano atendiendo a su fenotipo *endothelial-like* permitió la identificación de genes diferencialmente expresados en función de su condición de EL+ o EL-.

- La edición de *ADAMTS1* altera el fenotipo *endothelial-like* de líneas de melanoma, que se observa no sólo por el deterioro en la capacidad de generar estructuras similares a vasculatura sino también por la afectación de la expresión de genes implicados en la adquisición de este fenotipo.

- ADAMTS1 es necesaria para el crecimiento tumoral normal y el desarrollo de una adecuada vasculatura tumoral.

- Se detectó un incremento en la expresión de *ADAMTS1* y *CDH5*, junto a marcadores *stemness*, en los ensayos de xenógrafos. La inhibición de ADAMTS1 provocó una reducción en la expresión tanto de *CDH5* como de marcadores stemness en dichos modelos murinos.

- CDH5 demostró estar relacionada espacialmente con la vasculatura tumoral, la expresión de NANOG y la aparición de patrones VM *in vivo*, siendo dependiente todo de ADAMTS1.

- *ADAMTS1* y *CDH5* están sobre-expresados en esferas de melanoma uveal, y ADAMTS1 ha demostrado un papel esencial en la capacidad de generación de dichas esferas.

- *CDH5* juega un papel fundamental en el resultado clínico de los pacientes del proyecto TCGA-UVM. Se trata de un factor de mal pronóstico, y resultó estar co-expresada con una gran variedad de genes relacionados con la remodelación de la matriz extracelular que también contribuyen con este peor resultado.

- *ADAMTS4*, *ADAMTS9*, *ADAMTS12*, *ADAMTS2*, *ADAMTS5* y *ADAMTS14* son también factores de mal pronóstico en las muestras de melanoma uveal recogidas en el TCGA.
- *ADAMTS1* demostró estar altamente expresada en estadios tempranos del melanoma uveal y su expresión disminuye con el progreso de la enfermedad, sugiriendo de nuevo su relación con las capacidades *stemness* y su papel en la iniciación de tumores.

MATERIALS AND METHODS

1. Cell culture

Two human uveal (UVM) and six skin cutaneous (SKCM) melanoma cell lines were used. UVM cell lines were MUM-2B and MUM-2C. According to the literature, both were cloned from a single hepatic uveal metastasis (Maniotis et al., 1999). However, Maniotis' laboratory revealed that MUM-2C was not derived from the same patient as MUM-2B, but shares origin with the OCM1 cell line, also of UVM (Folberg et al., 2008). In addition, authors concluded in that work that MUM-2B cell line is derived from a primary and not a metastatic UVM, as originally considered (Folberg et al., 2008). Although these findings changed the historically used view of MUM-2B and MUM-2C, it is important to note that the MUM-2B/MUM-2C comparisons are still valid in terms of their aggressive/non aggressive phenotype. SKCM cell lines used in this thesis were A-375, C8161, G-361, SK-MEL-28, SK-MEL-103 and SK-MEL-147. A-375, G-361 and SK-MEL-28 are primary skin cutaneous melanoma cell lines, while C8161, SK-MEL-103 and SK-MEL-147 are derived from SKCM metastasis. Additional characteristics and the most relevant mutations of these cell lines are compiled in Figure 63.

MUM-2B, MUM-2C, and C8161 cell lines were kindly provided by Dr. Arjan W. Griffioen (VU Medical Center, VUmc, Amsterdam); SK-MEL-28, SK-MEL-103, SK-MEL-147 by Dr. Juan A. Recio (Vall d'Hebron Research Institute, VHIR, Barcelona); A-375 and G-361 by Dr. Javier Oliver (Instituto de Parasitología y Biomedicina López Neyra – Consejo Superior de Investigaciones Científicas, IPBLN-CSIC, Granada).

In addition, two non-cancer cell lines were used: human embryonic kidney 293T (HEK293T) cells, kindly provided by Dr. Pablo Menéndez (Instituto de Investigación contra la Leucemia Josep Carreras, IJC, Barcelona), and human umbilical vein endothelial cells (HUVECs), purchased from TCS Cellworks (Buckingham, United Kingdom, code ZHC-2101).

All cell lines were cultured in the appropriate medium supplemented with 10% fetal bovine serum (Gibco, Waltham, MA, USA) and 1% Penicillin-Streptomycin (Pen-Strep) solution (Biowest, Nuaillé, France), under standard conditions (37 °C, 5% CO2 and 95% relative humidity). Specific

growth media were: RPMI 1640 with stable glutamine (Biowest, Nuaillé, France) for MUM-2B, MUM-2C and C8161; High Glucose Dulbecco's Modified Eagle Medium (DMEM) with stable glutamine and sodium pyruvate (Biowest, Nuaillé, France) for A-375, G-361, SK-MEL-28, SK-MEL-103, SK-MEL-147 and HEK293T. HUVECs were cultured in EGM™-2 Endothelial Cell Growth Medium-2 BulletKitTM (CC-3162, Lonza, Basel, Switzerland).

All cell lines were routinely tested for Mycoplasma (Venor®GeM qEP, Minerva Biolabs, Berlin, Germany).

Short tandem repeat (STR) profiling (AmpFLSTR® Identifiler® Plus, Applied Biosystems, Waltham, MA, USA) served to authenticate MUM-2B and A-375 and to characterize SK-MEL-103 cells (Table 3).

MUM-2B	*D8S1179*		*D21S11*		*D7S820*		*CSF1PO*		*D3S1358*		*TH01*		*D13S317*		*D16S539*	
	13	13	30	30	12	12	10	11	16	16	8	9	11	11	8	12
	D2S1338		*D19S433*		*vWA*		*TPOX*		*D18S51*		*AMEL*		*D5S818*		*FGA*	
	24	24	13	14	16	17	11	11	15	15	X	X	11	12	20	21
A-375	*D8S1179*		*D21S11*		*D7S820*		*CSF1PO*		*D3S1358*		*TH01*		*D13S317*		*D16S539*	
	11	14	29	30	9	9	11	12	15	17	8	8	11	14	9	9
	D2S1338		*D19S433*		*vWA*		*TPOX*		*D18S51*		*AMEL*		*D5S818*		*FGA*	
	16	24	13	14	16	17	8	10	12	17	X	X	12	12	23	23
SK-MEL-103	*D8S1179*		*D21S11*		*D7S820*		*CSF1PO*		*D3S1358*		*TH01*		*D13S317*		*D16S539*	
	12	17	30	31	9	11	10	12	17	18	6	9	9	9	12	13
	D2S1338		*D19S433*		*vWA*		*TPOX*		*D18S51*		*AMEL*		*D5S818*		*FGA*	
	20	24	13	14	17	18	9	12	13	13	X	X	10	13	21	24

Table 3. STR profiling of MUM-2B, A-375 and SK-MEL-103 melanoma cell lines.
Number of repetitions of every of the 16 markers evaluated to determine de short tandem repeat (STR) profile of each cell line.

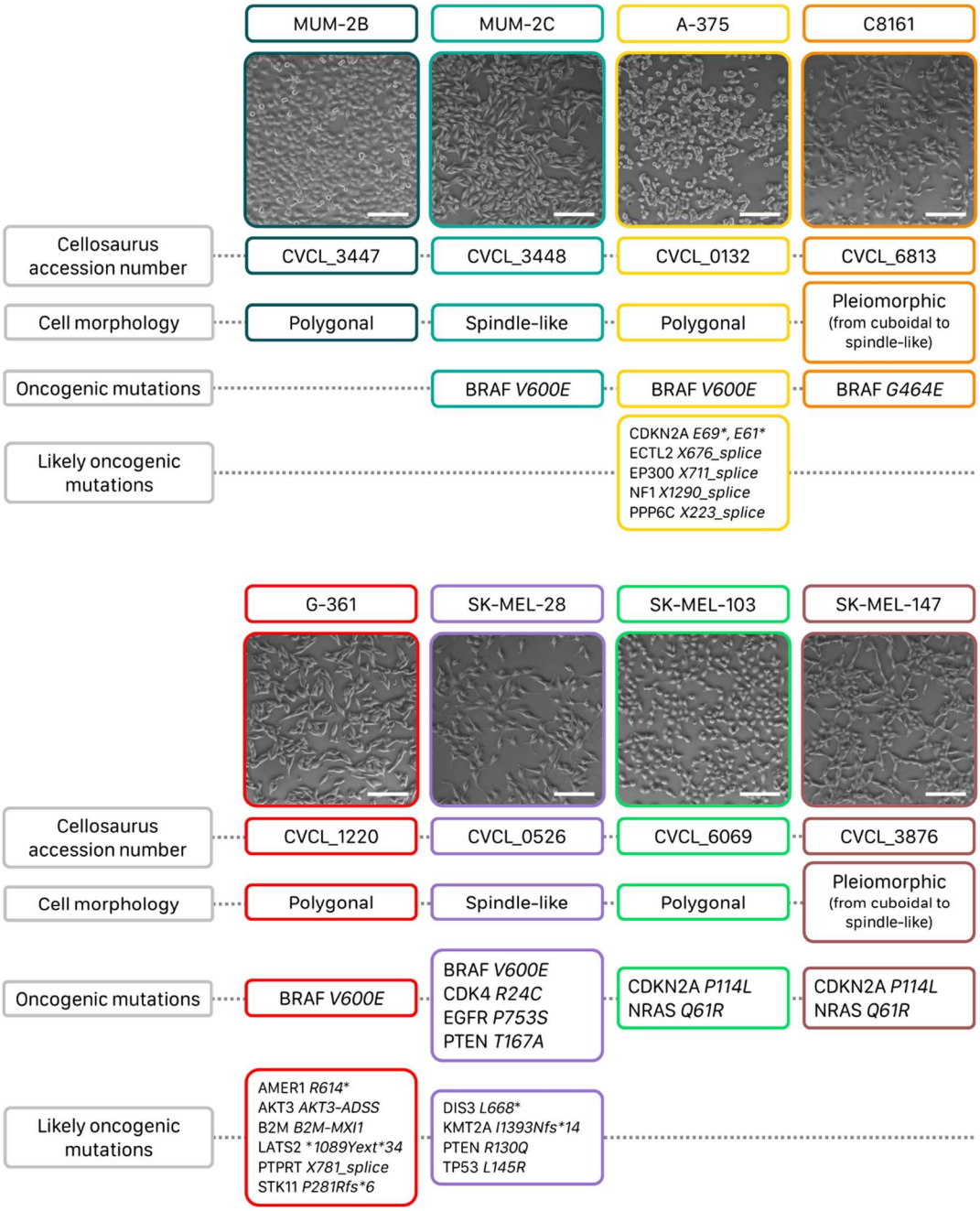

Figure 63. General information and mutations of melanoma cell lines.
Name, aspect, Cellosaurus accession number, cell morphology and mutations (oncogenic and likely oncogenic) of the eight human melanoma cell lines included in this thesis (white scale bar = 200 µm).

2. Lentiviral cancer cell infection

Lentiviral particles were used for the generation of ADAMTS1-KO cells and the overexpression of green fluorescent protein (GFP). HEK293T cells were transfected to generate lentiviral particles with a DNA-$CaCl_2$ mixture (20 µg of the plasmid of interest, 15 µg of psPAX2 packaging vector, 6 µg of pVSV-G

envelope vector and 62 µl of 2 M $CaCl_2$) in 2x HBS solution (0,28 M NaCl; 10,19 mM KCl; 1,41 mM Na_2HPO_4-anhydrous; 0,43 M HEPES and 11,10 mM glucose dissolved in ultrafiltrated water, pH 7,05). Medium must be changed 9-14 h after transfection, and after additional 48 h it could be used for infection.

Cancer cells were infected maintaining the quantity of lentiviral-containing medium as low as possible to maximize transduction efficiency. The replacement with fresh medium was made 15-20 h after infection.

3. Generation of ADAMTS1-knockout cells

The CRISPR/Cas9 system allows to target a specific gene and disrupts it by generating a double strand break (DSB) at a specific point, triggering the error-prone mechanisms of DNA repair, such as non-homologous end joining (NHEJ) process. This mechanism generates unintentional insertions or deletions (INDELs), which can produce frame shifts and stop codons that cause the functional knockout of the gene (Figure 64). CRISPR/Cas9 gene editing technology is currently suffering a lot of modifications leading to more specific editing mechanisms. This is the case of the use of homologous recombination (HR) repairing mechanism to introduce a specific sequence in the gene; or the use of dCas9 (modified version of Cas9 without endonuclease activity) to activate or repress gene expression, among others.

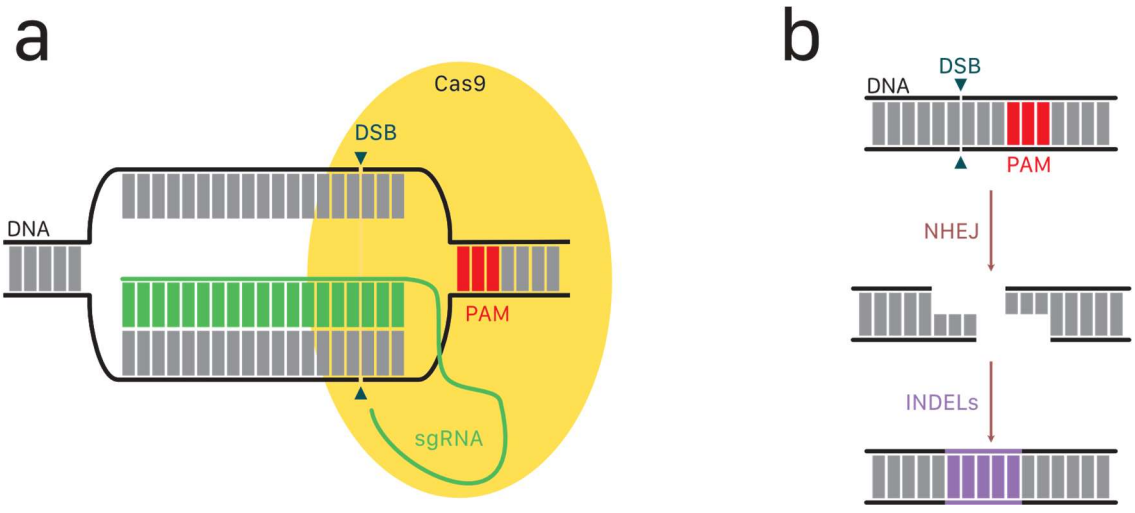

Figure 64. Schematic representation of gene editing by CRISPR/Cas9.
a) General process of gene editing by CRISPR/Cas9, where it can be seen the double strand break (DSB) site, the PAM sequence and the single-guide RNA (sgRNA). b) Scheme of the gene edition

taking advantage of the non-homologous end joining mechanism of DNA repair, which create INDELs that disrupt the target gene. Modified from The CRISPR page at CNB (http://wwwuser.cnb.csic.es/~montoliu/CRISPR/#1).

Here, the generation of ADAMTS1-KO cells was carried out with the all-in-one lentivirus-based CRISPR/Cas9 system (Sigma-Aldrich) (Figure 65a), which allow an efficient delivery and chromosomal integration of CRISPR components, combined with a greater facility to edit genes even in cells that are difficult to transfect. The complete protocol is described in (Peris-Torres et al., 2020b) and is schematically illustrated in Figure 65b. MUM-2B and C8161 cell lines were infected with lentiviral particles previously generated in HEK293T cells, obtaining two clonal populations for each cell line (named ATS1-KO1 and ATS1-KO2 for MUM-2B, and ATS1-KO3 and ATS1-KO4 for C8161). The all-in-one vector provided both puro and GFP elements to monitor and select effectively edited cells. However, edited cells failed expressing GFP, so monitoring and selection of clones were done based on their acquired resistance to puromycin (0,25 µg/ml). ADAMTS1-KO cells were obtained after two weeks of selection, and single cell cloning isolation and expansion processes. Clones were subjected to Sanger DNA sequencing and Western Blot to confirm gene edition and inhibition, respectively.

4. Sanger DNA sequencing

Genomic DNA was isolated from cells, quantified, and subjected to PCR to amplify the region of *ADAMTS1* containing the CRISPR/Cas9 guide RNA (primers sequences in Table 9). After electrophoresis and purification, Sanger DNA sequencing was performed in an Applied Biosystems® 3130 (4-capillary) Genetic Analyzer. Sequences analysis was achieved with SeqScape™ Software (Catalog Number 4474978, Applied Biosystems) as already described (Peris-Torres et al., 2020b).

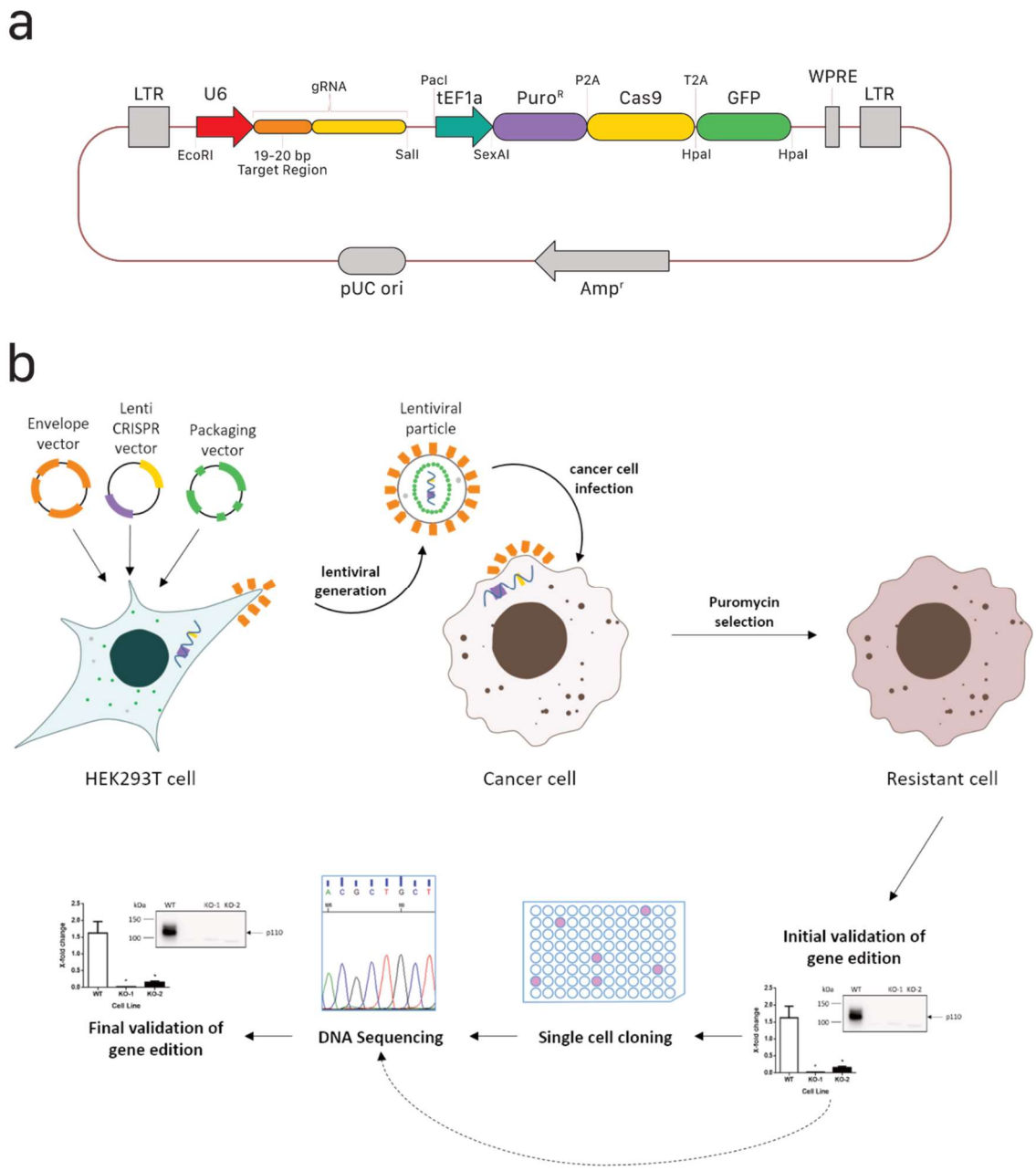

Figure 65. CRISPR/Cas9 protocol highlights.
a) Scheme map of the all-in-one lenti-CRISPR vector. b) Scheme of the ADAMTS1-KO cells generation protocol by CRISPR/Cas9.

5. Western Blot analysis

Total protein was obtained from 24 h CM of melanoma cell cultures and concentrated with StrataClean resin (Agilent Technologies) as described (Canals et al., 2006). Proteins were resolved by SDS-PAGE (Box 4), and transferred to polyvinylidene difluoride (PVDF) membranes (BioRad). Precision Plus Protein™ All Blue Prestained Protein Standards were used to

identify molecular weight. Membranes were blocked with 5 % low-fat milk in 1 x PBS-0,05 Tween, and incubated with a sheep anti-human ADAMTS1 (AF5867, R&D Systems, 1:500 dilution) antibody. After incubation with the appropriate anti-sheep HRP-conjugated secondary antibody (HAF016, R&D Systems, 1:1000 dilution), signal was detected with the Amersham ECL Prime Western Blotting Detection Reagent (GE Healthcare Life Sciences) in an ImageQuant LAS4000 (GE Healthcare Life Sciences).

Box 4. SDS-PAGE gels preparation

Stacking (4% acrylamide) and resolving (10% acrylamide) gels for SDS-PAGE were supplemented with 1:100 ammonium persulfate (APS, A3678-25G, Sigma-Aldrich) and 1:1000 N,N,N',N'-Tetramethyl-ethylenediamine (TEMED, 35930.02, SERVA).

	STACKING GEL	RESOLVING GEL
Molecular grade H_2O (ml)	357	98,8
Tris 1M ph = 8,8 (ml)	83	49,2
Acrylamide 40 % (ml)	46,8	55
SDS 10 % (ml)	5	2

6. Generation of GFP+ cells

The generation of MUM-2B GFP+ cells was achieved with the pHR'SINcPPT-SE lentiviral vector containing a SFFV-EGFP element (Demaison et al., 2002), kindly provided by Francisco Martin's Laboratory (GENyO, Granada, Spain). Lentiviral particles containing this GFP-expressing vector were generated as described above and served to infect both WT and ADAMTS1-KO cells. GFP+ cells were separated 48 h after the infection with a BD FACSAria cell sorter (BD Biosciences, San Jose, CA, USA), and they were monitored for two weeks to verify that GFP expression was preserved.

7. *In vitro* 3D Matrigel-based assay

Matrigel is a solubilized basement membrane preparation extracted from the Engelbreth-Holm-Swarm (EHS) mouse sarcoma with high content of ECM proteins such as laminin, collagen IV, heparan sulfate proteoglycans, nidogen and growth factors (Corning Incorporated, Corning, NY, USA, https://www.corning.com/[...]/matrigel-matrix.html). 35 µl/well of Matrigel

were dispensed in a 96-well plate kept on ice to avoid gelling. After Matrigel gelling by incubation at 37 °C during 30 minutes, 100 µl of serum-free medium were added to each well. Finally, 100 µl of serum-free medium containing 20.000 or 30.000 cells were added. Follow-up was performed by taking pictures at various time points (0.5, 3, 8 and 24 hours) with an Axio Vert microscope, Zeiss (A-Plan 5x/0.12 objective). When appropriate, 24 h pictures were subjected to WimTube analysis (Wimasis, https://www.wimasis.com/en/WimTube) as indicated (Peris-Torres et al., 2020a). WimTube generates an output comma-separated values (CSV) sheet file for every image, containing the following measured parameters and statistics: area covered by the cells, number and length of tubes, number of branching points, and number, area and perimeters of loops (Figure 66).

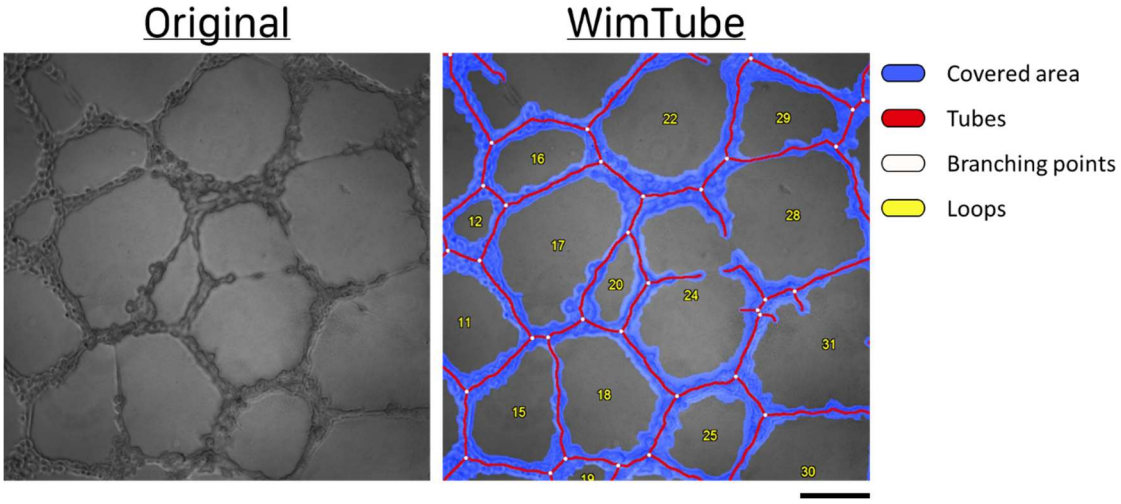

Figure 66. Parameters measured by WimTube.
Original and WimTube output images of a Matrigel assay. The non-biased WimTube tool measures the area that is covered by the cells (blue) and the length and number of cell tubes (red), and it also counts the number of branching points (white dots) and loops (numbers in yellow) (black scale bar = 200 µm).

8. xCELLigence cell proliferation assay

Cell proliferation assays were carried out in a xCELLigence RTCA DP instrument (ACEA Biosciences, San Diego, CA, USA) using E-plates. E-plates have a set of gold microelectrodes fused to their bottom surface needed for the application of the electrical potential on which xCELLigence platform is based. When cells adhered to the surface of the E-plate, they would impede the electron flow between these electrodes in a cell number-, size- and

shape-dependent manner. Based on this principle, xCELLigence platform records impedance values and report them via an unitless parameter called cell index (CI), allowing the conduction of real-time cell adhesion and proliferation experiments. CI is obtained with the following formula:

$$Cell\ index = \frac{impedance\ at\ time\ point\ n - impedance\ in\ the\ absence\ of\ cells}{nominal\ impedance}$$

To improve cell adhesion, E-plates were pre-coated with a 1:30 dilution of Matrigel in culture medium containing 5 % of FBS and incubated at 37 °C during 1 hour. After washing the wells, 100 µl of culture medium were added for each plate for background calibrating. Then, 5×10^3 cells were added in each well in additional 100 µl of culture medium. Cell index was measured every 20 minutes for 35 - 40 sweeps (considered adhesion time) and then every hour for 155 - 160 sweeps (proliferation time). Subsequent analysis with RTCA Software (ACEA Biosciences, San Diego (CA), USA) allowed to determine the doubling time for each cell line included in the experiment.

9. Melanoma sphere formation assay

For melanoma sphere formation experiments, 5×10^3 cells/ml were seeded in non-adherent bacterial plates containing 8 ml of culture medium. This medium was renewed weekly by low speed centrifugation (5 minutes, 129 relative centrifugal force [RCF]) and melanoma spheres were plated back. Primary spheres were obtained after 21 days following these conditions. To generate secondary spheres, primary spheres were disaggregated through a 29G needle and seeded again at a density of 5×10^3 cells/ml in 60 mm suspension culture dishes (Corning) containing 3 ml of culture medium. Secondary spheres were obtained after 15 days under these conditions, which included a medium renewal after the initial 7 days as described above.

Different culture media were used in these assays. Standard cancer stem cell (CSC) medium was DMEM-F12 without L-Glutamine nor HEPES (Biowest) supplemented with 1 % Pen-Strep (Biowest), B-27™ (40 ml/l, 17504-044,

ThermoFisher Scientific), human fibroblast growth factor (FGF-2, 0,01 µg/ml, 130-093-838, Miltenyi Biotec) and human epidermal growth factor (EGF, 0,02 µg/ml, 130-093-825, Miltenyi Biotec). For assays using conditioned medium (CM) from MUM-2B cells (named ADAMTS1+ CM), cells were seeded in adherent plates until they reach a 70 % of confluence, then medium was removed and cells were washed several times to eliminate any remaining FBS. After that, DMEM-F12 with Pen-Strep was added to cells and let them secrete ADAMTS1+ CM for 24 hours. After this time, medium was collected, centrifuged 5 minutes at 11.000 RCF to remove cell debris, supplemented with B-27, FGF-2 and EGF as described above, and added to growing spheres (schematic view of the protocol in Figure 67). For assays using recombinant human ADAMTS1 (rhATS1, 2197-AD, R&D), spheres were grown in 6-well ultralow attachment plates (Corning), containing 3 ml of CSC medium supplemented with 1 µg/ml rhATS1 (Figure 67).

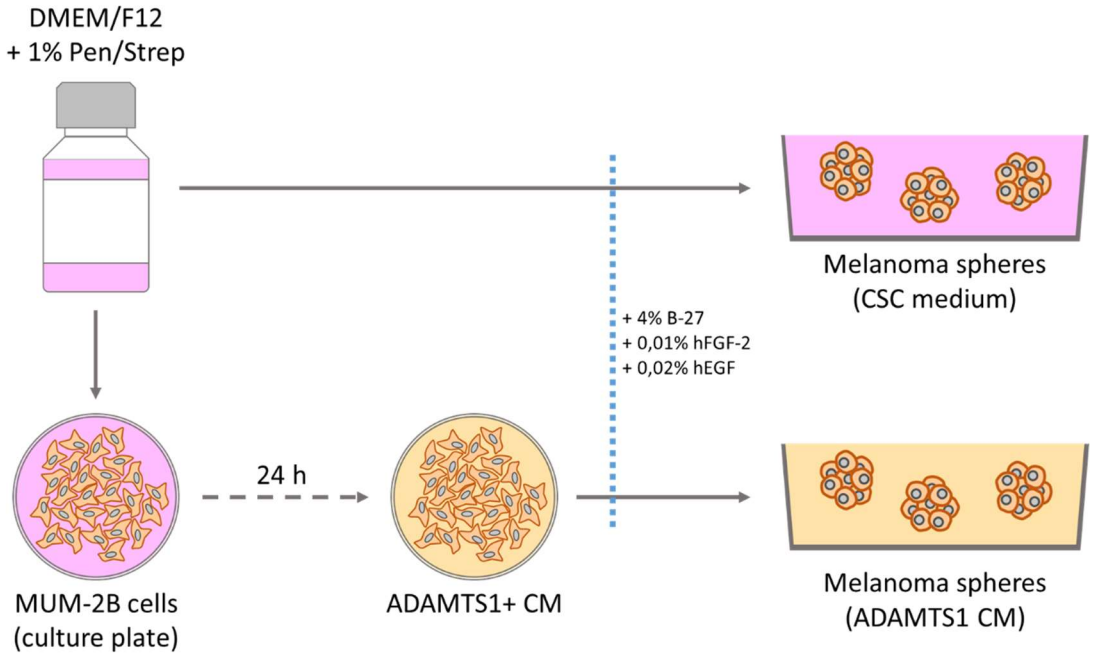

Figure 67. Schematic view of the followed protocol to obtain melanoma spheres in ADAMTS1+ CM.

Images of melanoma spheres were captured with an Axio Vert microscope (Zeiss, A-Plan 5x/0.12 objective), and evaluated with Carl Zeiss ZEN 2.3 SP1 (black) software. To calculate spheres volume, length and width of single

spheres were measured with the Line tool of this software. The following equation was applied:

$$sphere\ volume = \frac{\pi \times length \times width^2}{6}$$

10. Tumor xenograft assays

Due to the human origin of the melanoma cells used in this study, xenografts were generated in immunodeficient mice. Two different mouse strains were used: Swiss Nude (SwN) and NOD *scid* gamma (NSG).

Swiss Nude mice

This outbred athymic and albino strain surged in 1962 at the Ruchill Hospital in Glasgow (UK). Since then, it has been widely used in tumor biology and xenograft research, as the lack of thymus and therefore of T cells allow human cells growth within the mice (Figure 68). In addition to classical xenografts experiments, tumor cells were also injected in a Matrigel solution, helping initial tumor engraftment and growth by creating a scaffold. This use has been widely reported in tumor studies (Fridman et al., 1991, 2012).

NSG mice

NOD *scid* gamma (NSG) mice are one of the most highly immunodeficient models, so they are also a very successful option for xenografts studies. This inbred strain was created at The Jackson Laboratory and it combines features of the NOD/ShiLtJ background (conferring a number of deficiencies in innate immunity), the severe combined immune deficiency mutation (scid) and an IL2 receptor gamma chain deficiency which disables cytokine signaling. As a result, NSG mice lack mature T cells, B cells, functional NK cells, and they are also deficient in cytokine signaling (Figure 68). NSG mice were used in this study in order to achieve better *in vivo* results that the obtained with the SwN model, since the differences in terms of immune

capabilities between both models would represent a crucial factor for tumor development.

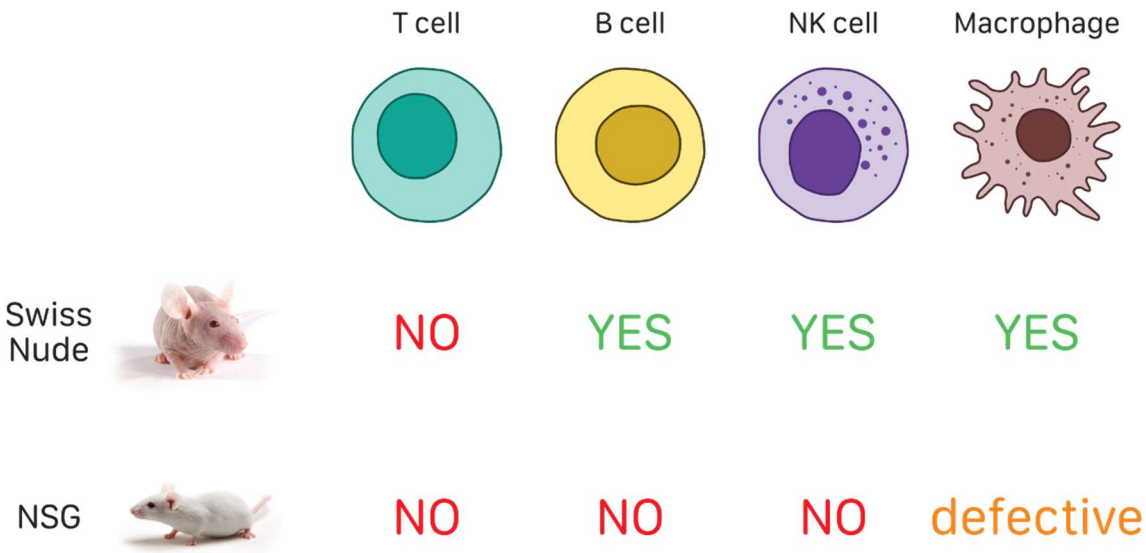

Figure 68. Immune cell differences between Swiss Nude and NSG mouse models.

For this study, 1×10^6 cells in 100 µl PBS were subcutaneously injected in the flanks of 6-weeks old female SwN and NSG mice (Charles River Laboratories). When using Matrigel as scaffold, 2×10^6 cells in a 150 µl PBS:Matrigel dilution (1:1) were subcutaneously injected in the flank of 16-weeks old SwN mice. For all cases, animal weight and tumor progression (measured with a digital caliper) were monitored every two days after cell injection until final time point, when they were sacrificed and tumors were dissected for further analyses. Tumor volume was calculated with the following formulas, as described (Rodríguez-Baena et al., 2018a):

$$in\ progress\ volume = \frac{\pi \times length \times width^2}{6}$$

$$final\ tumor\ volume = \frac{\pi \times length \times width \times height}{6}$$

11. Ethical approvals

All animals used in this thesis were housed at Centro de Investigación Biomédica – Universidad de Granada (CIBM-UGR) animal facility. They were handled and euthanized according to ethical and institutional guidelines established by the Approved Ethical Committee 152-CEEA-OH-2016.

12. Flow cytometry assays

Tumor pieces obtained from NSG xenografts were subjected to flow cytometry analysis. Tumors were extracted and maintained in 1 ml of cold RPMI medium. Then, samples were mechanically disaggregated with sharp scissors on a plate until they reached a pâté-like consistency, and incubated in 0.1% type I collagenase (17100017, Gibco, Waltham, MA, USA) in PBS for 1 hour in a 37 °C water bath including shakes every 10 minutes. Homogenates were passed through a syringe with a 19,5G needle 3-4 times and then through a 70 µm cell strainer. Cell suspension was centrifuged 5 minutes at 300 RCF. After removing the supernatant, cells were resuspended and incubated 4 minutes at room temperature (RT) in 5 ml of Ammonium-Chloride-Potassium (ACK) buffer pH 7,2 to remove red blood cells. After an additional centrifugation of 10 minutes at 300 RCF, cells were resuspended in 5-10 ml of PBS and counted. 2×10^5 tumor cells were resuspended in 1 ml of PBS, centrifuged 5 minutes at 300 RCF, and incubated 5 minutes on ice in 50 µl of FACS buffer (2 % FBS in PBS), containing 1:100 7-Amino-actinomycin D (7-AAD) to identify dead cells and 1:100 FcR Blocking Reagent (130-092-575, Miltenyi Biotec) to increase the specificity of further antibody labelling. The conjugated-primary antibody solution was then added and incubated for 25 minutes on ice. Labeled cells were centrifuged 5 minutes at 300 RCF and resuspended in FACS buffer for definitive flow cytometry, performed in a FACSverse Flow Cytometer (BD Biosciences, San Jose, CA, USA). Data were analyzed with BD FACSuite software.

The antibody used in this study was a rat anti mouse PECAM1-PE conjugated one (102408, Biolegend, San Diego, CA, USA).

13. Immunofluorescence and immunohistochemistry assays

Paraffin-embedded sections of tumor xenografts were first deparaffinized at 65 °C during a 30 minutes incubation or until paraffin melted. Rehydration protocol included the following washes under gentle shaking: xylene substitute (x3), 100% EtOH (x2), 95% EtOH (x1), 70% EtOH (x1), PBS (x1) and ddH_2O (x1). Antigen retrieval was performed by slide immersion in Tris-HCl 0,5 M pH=10 solution and 10 minutes boiling. After cooling, tumor sections were washed twice in PBS 0,5 % tween (PBS-T) during 5 minutes and incubated with a blocking solution (3% BSA, 1% secondary antibody host serum in PBS-T) during 1 h at RT. Then, after two additional washes of 5 minutes with PBS-T, sections were incubated in a solution of 1% BSA and 1% secondary antibody host serum in PBS-T at 4 °C overnight, containing the appropriate concentration of the primary antibody. The following day, after three washes with PBS-T during 5 minutes, sections were incubated in a solution of 1% BSA and 1% secondary antibody host serum in PBS-T containing the appropriate concentration of secondary antibody during 1 hour at RT. After that and additional three washes of 5 minutes with PBS-T, sections were ready to be mounted for microscopy evaluation.

For IF analyses, rat anti-mouse EMCN (V.7C7, SC-65495, SCBT) and rabbit anti-human CDH5 (160840, Cayman Chemical) antibodies were used. Alexa Fluor 488 donkey anti-rat (A21208, ThermoFisher Scientific) and Alexa Fluor 647 goat anti-rabbit (A-21245, ThermoFisher Scientific) secondary antibodies were used to detect EMCN and CDH5, respectively. 4′,6-diamidino-2-phenylindole (DAPI, D8417, Sigma-Aldrich) solution was used for nuclear counterstain, and antifade Mowiol (81381, Sigma-Aldrich)-DABCO (D27802, Sigma-Aldrich) mixture was used as mounting medium. Confocal images were captured with a LSM 710 Axio Observer microscope (Zeiss, Plan-Apochromat 63x/1.4 Oil DIC M27 objective).

For IHC analyses, an additional blocking step was carried out just after antigen retrieval with Peroxidase Blocking Solution (S2023, Dako) during 20 minutes at RT. Rabbit anti-human CDH5 (160840, Cayman Chemical) and rabbit anti-human NANOG (4903, Cell Signaling Technology) antibodies

were used. Dako Envision™ + System-HRP (DAB) (K4010, Dako) was used as secondary antibody. NANOG staining required a permeabilization step, which was performed with a 0,4 % dilution of Triton X-100 (93426, Sigma-Aldrich) in PBS during 5 minutes at RT. Dako Mayer's Hematoxylin (S3309, Dako) was used for nuclear counterstain. After dehydrating slides with 70% EtOH (x1), 95% EtOH (x1), 100% EtOH (x2) and xylene substitute (x3); they were mounted with Dibutylphthalate Polystyrene Xylene (D.P.X.), 317616, Sigma-Aldrich). IHC images were captured with a BX43 microscope (Olympus, Plan-Achromat 20x/0.4 objective).

For periodic acid-Schiff (PAS) staining, some steps were added to the general process of immunostaining. Slides were immersed in periodic acid solution (3951, Sigma-Aldrich) during 35 minutes and in Schiff's reagent (3952016, Sigma-Aldrich) during 1 h, both at RT. Final counterstaining was done with hematoxylin.

14. Vasculature characterization

For the morphometric analysis of the vasculature, images of tumor paraffin sections previously subjected to IF for vascular EMCN were captured (Axio Imager A.1 microscope, Zeiss, EC Plan-Neofluar 10x/0.30 Ph 1 objective, AxioCam MR R3) and converted to 8-bits. Images from complete tumor sections were analyzed with ImageJ software as described (Fernández-Rodríguez et al., 2016). At the beginning of the analyses, a threshold was established to differentiate between blood vessels and image background, and it was maintained for all the experimental replicates. The particle size, which is the minimum size that the software would consider to be a blood vessel, also needed to be established in order to avoid false positives. Once such parameters were established, ImageJ software estimated the area, perimeter, number and density of the blood vessels.

15. RNA isolation and quantitative PCR

RNA from cells and tumors was extracted with NucleoSpin® RNA kit (Macherey-Nagel), quality tested in an agarose gel, and reverse transcribed with iScript™ cDNA Synthesis Kit (Bio-Rad). Cells were cultured under standard conditions until they reach an 80 % of confluence before RNA isolation was undertaken, and tumor samples were disrupted until a cell suspension was obtained. qPCR reactions were performed with Fast SYBR™ Green Master Mix (Applied Biosystems), using 7900HT Fast Real-Time PCR (Applied Biosystems) and QuantStudio 6 Flex Real-Time PCR (Applied Biosystems) platforms. mRNA fold-change was calculated with the 2^(-ΔΔCt) method, using *ACTB*, *B2M* and *RNA18S1* as housekeeping genes (primer sequences in Table 9), depending on the sample origin and the platform. Cycle threshold (Ct) values were also shown as an absolute quantification of mRNA levels.

16. Collection of gene expression and clinical data from public databases

The *in silico* analyses included in this thesis were conducted with heterogeneous data from distinct public databases.

Gene expression data of cell lines were obtained from The National Center for Biotechnology Information (NCBI) Gene Expression Omnibus (GEO) (Barrett et al., 2013). This database was mined to find optimal datasets of melanoma cell lines and human umbilical vein endothelial cells (HUVECs), which would be used in subsequent Heuristic Online Phenotype Prediction (HOPP) or differentially expressed genes (DEG) identification analyses (

Table 4).

Gene expression and clinical data of uveal melanoma patients were obtained from Genomic Data Commons (GDC) The Cancer Genome Atlas (TCGA) Uveal Melanoma Project (TCGA-UVM) (Grossman et al., 2016; Robertson et al., 2017). TCGA data were analyzed using the following platforms: University of California Santa Cruz (UCSC) Xena Functional Genomics Explorer (Goldman et al., 2020) and cBioPortal (Cerami et al., 2012; Gao et al., 2013).

17. *In silico* analyses

Several *in silico* analyses were conducted in this thesis as follows.

HOPP analysis compares the gene expression of a given sample with two standard gene signatures (composed by the same 97 genes or 134 probesets) whose expression is significantly different between proliferative and invasive melanoma cells. This comparison results in a prediction of the phenotype of a given sample and gives it a Pearson product-moment correlation coefficient with proliferative and invasive gene signatures. These coefficients allow the representation of predicted phenotypes for different cell lines. This thesis includes HOPP analysess of 27 melanoma samples from 17 different RNA-Seq datasets (GEO accession numbers in

Table 4). HOPP platform also allows the comparison of the expression level of a certain gene between all the proliferative and all the invasive cell lines included in the database.

For DEG identification between EL+ and EL- cells and subsequent Gene Ontology (GO) enrichment analysis, GEO mining yielded a total of 31 samples from 12 different datasets (

Table 4**¡Error! No se encuentra el origen de la referencia.**), analyzed with the help of GENYO's Bioinformatics Unit. RNA-Seq expression data were downloaded, probe identifiers were annotated with gene symbols and median gene expression values were calculated for duplicated genes and rank normalized to allow sample comparisons from different technologies. Linear models implemented in limma R package (Ritchie et al., 2015) allowed to analyze differential gene expression between groups of cell lines. Differentially expressed genes were selected by false discovery rate (FDR) < 0.05. GO enrichment analyses were conducted with a combination of clusterProfiler (Yu et al., 2012) and REViGO (Supek et al., 2011) softwares. While clusterProfiler was used to evaluate representative enriched biological processes and select GO terms showing an adjusted p-value < 0.05, REViGO helped in data interpretation by applying a clustering algorithm to remove redundant GO terms and summarize the others. REViGO analysis parameters were adjusted as follows: medium (0.7) allowed similarity, p-values as numbers associated to GO categories, whole UniProt (default) database and SimRel semantic similarity measure.

The analyses of TCGA data of human uveal melanoma samples included the following. Kaplan Meier survival curves were obtained by comparing data hosted on UCSC Xena platform from patients with low (quartile 1 [Q1]) and high (above quartile 3 [Q3]) gene expression levels. Pearson correlation analyses were conducted with the list of co-expressed genes that identified by cBioPortal platform (Cerami et al., 2012; Gao et al., 2013), and comparing normalized gene expression levels from Xena platform. GO enrichment analysis of co-expressed genes were conducted as previously described with cell lines data. Clinical data of TCGA-UVM project hosted in UCSC Xena platform served to evaluate *ADAMTS1* expression among the different uveal melanoma clinical stages. In this case, data presented here are a direct output obtained from this platform, which included a one-way ANOVA among the normalized *ADAMTS1* expression levels of the different uveal melanoma clinical stages.

18. Statistical analysis

Statistical analyses were made with GraphPad Prism 8 (GraphPad software Inc.). Except when indicated, graphs represent *mean ± SEM*, and unpaired t tests were performed to compare means of two experimental groups. Robust regression and outlier removal (ROUT) method was applied to identify outliers when necessary, using a maximum desired FDR (Q) of 1 %. For qPCR analysis, values of ΔΔCt out of *mean ± SD* were considered as outliers, as well as values of Ct that were lower than *Q1 − 1,5 × IQR* (interquartile range) or greater than *Q3 + 1,5 × IQR*.

APPENDIX: TABLES

Table 4. Identification of cell lines for in silico analyses.

GEO accession numbers (and their corresponding data set) of the cell lines included in this work. Their use in either HOPP or DEG identification analyses is also indicated. When necessary, HOPP correlation coefficients for proliferative (Pro) or invasive (Inv) phenotypes are also included.

			Used in		HOPP coefficients	
Data set	**Sample**	**Cell line**	**HOPP?**	**DEG?**	**Pro (r)**	**Inv (r)**
GSE44295	GSM1082564	MUM-2B	YES	-	-0,0583	0,257
GSE71161	GSM1828669	MUM-2B	-	YES		
	GSM2399832	MUM-2B	-	YES		
	GSM2399833	MUM-2B	-	YES		
GSE93666	GSM2460242	MUM-2C	-	YES		
GSE28846	GSM714350	MUM-2C	YES	YES	0,8882	-0,0145
GSE10916	GSM276771	A-375	YES	-	-0,1137	0,5311
GSE111766	GSM3039510	A-375	-	YES		
	GSM3039516	A-375	-	YES		
	GSM3039517	A-375	-	YES		
	GSM3039518	A-375	-	YES		
GSE11812	GSM298627	A-375	YES	-	0,505	0,1853
GSE13487	GSM339978	A-375	YES	-	-0,0937	0,2483
	GSM339980	A-375	YES	-	-0,0837	0,2156
GSE1845	GSM29663	A-375	YES	-	-0,1379	0,7073
GSE22301	GSM555121	A-375	YES	-	0,377	0,3719
GSE57083	GSM1374382	A-375	YES	-	-0,182	0,479
GSE64985	GSM206443	A-375	YES	-	-0,1475	0,5599
GSE68453	GSM1671962	A-375	-	YES		
	GSM1671987	A-375	-	YES		
	GSM1672062	A-375	-	YES		
	GSM1672102	A-375	-	YES		
	GSM1672119	A-375	-	YES		
	GSM1672135	A-375	-	YES		
GSE28846	GSM714351	C8161	YES	YES	-0,136	0,4948
GSE11812	GSM298629	C8161	YES	YES	-0,152	0,5077
GSE9118	GSM230905	C8161	YES	YES	-0,1472	0,4201
GSE10843	GSM274684	G-361	YES	YES	0,621	-0,011
GSE122907	GSM3487966	G-361	-	YES		
GSE28846	GSM887016	G-361	-	YES		
GSE57083	GSM1374482	G-361	YES	-	0,657	-0,027
GSE8332	GSM206469	G-361	YES	YES	0,8638	-0,0491
GSE56309	GSM1358831	HUVECS	-	YES		
	GSM1358832	HUVECS	-	YES		
	GSM1358833	HUVECS	-	YES		
GSE10086	GSM254953	SK-MEL-28	YES	-	0,924	0,015
GSE10916	GSM276739	SK-MEL-28	YES	-	0,9283	-0,0525
GSE1845	GSM29666	SK-MEL-28	YES	-	0,9002	-0,0446
GSE20051	GSM501260	SK-MEL-28	YES	-	0,9387	-0,0911
GSE32474	GSM803669	SK-MEL-28	YES	-	0,6659	-0,1076
	GSM803727	SK-MEL-28	YES	-	0,6642	-0,1159
GSE6833	GSM157169	SK-MEL-28	YES	-	0,7818	-0,0104
GSE68453	GSM1671969	SK-MEL-28	-	YES		
GSE7127	GSM171012	SK-MEL-28	YES	-	0,8951	0,0011
GSE8332	GSM206543	SK-MEL-28	YES	-	0,9471	-0,0818
GSE68453	GSM1671986	SK-MEL-28	-	YES		
	GSM1672056	SK-MEL-28	-	YES		
GSE111766	GSM3039513	SK-MEL-103	-	YES		
GSE22301	GSM555127	SK-MEL-103	YES	YES	0,0669	0,816
	GSM555128	SK-MEL-147	YES	YES	0,3073	0,5428

Table 5. Differentially expressed genes between EL+ and EL- cells.
Differential gene expression analysis revealed a total of 467 differentially expressed genes (DEGs) with an adjusted p-value < 0,05 between EL+ and EL- cells: 47 upregulated (upper panel) and 420 downregulated (bottom panel). Corresponding fold change (LogFC) for every gene is indicated in brackets.

UP-REGULATED GENES IN EL+ CELLS			
AADAC (4482,2)	*ANXA3* (9464,4)	*ARMCX1* (8901,2)	*ARMCX2* (10540,3)
ARNTL2 (4304,6)	*ATP8B1* (4941,3)	*B3GALNT1* (6284,9)	*BASP1* (5322,6)
CDH5 (7181)	*CLGN* (5271,2)	*DNAJA4* (7573,4)	*DYSF* (3660,2)
EFEMP1 (5777,1)	*EPAS1* (5753,6)	*FGF5* (3422,4)	*FILIP1L* (4881,6)
FOXF1 (4613,8)	*FSTL1* (5986,1)	*FUT4* (5576,3)	*G0S2* (5444,6)
GJA1 (6892,1)	*HCLS1* (5717,4)	*HYI* (3652,6)	*ICAM2* (5570,5)
IFI27 (7712,2)	*IGFBP1* (5829,1)	*IL6* (3657,6)	*LAPTM5* (5486,9)
LOX (9601,4)	*MICAL2* (5224,7)	*MYL9* (5542,8)	*NID1* (3672,6)
PAX6 (4268)	*PDPN* (4910)	*PIGZ* (4985,4)	*PLEK2* (4140,6)
PPP1R13L (4743,6)	*PRSS3* (5729,6)	*RHOD* (4566,6)	*SERPINB2* (4481,2)
SERPINE1 (5414,7)	*SRGN* (4450,6)	*STXBP2* (5340,8)	*TFPI* (4235,4)
THBD (4701,5)	*TNFRSF10D* (5389,9)	*UCHL1* (10513)	

DOWN-REGULATED GENES IN EL+ CELLS			
ABCC2 (-7166,1)	*ABCF2* (-3433,6)	*ACACA* (-3991,6)	*ACADSB* (-3737)
ACPP (-4443,7)	*ACTR3B* (-3149,1)	*ADD3* (-3845,7)	*ADORA2B* (-5143,5)
ADSL (-2958,3)	*ALDH5A1* (-3515,8)	*ALDOC* (-4555,1)	*ALKBH4* (-3197,2)
ANGPT1 (-4984,4)	*ANP32C* (-4332,8)	*AP1S1* (-3682,2)	*APOC1* (-4388,6)
ARHGAP12 (-2560)	*ARNT2* (-7455,9)	*ART3* (-6539,9)	*ATP6V0A4* (-5423,1)
ATPAF2 (-3176,8)	*B3GAT1* (-4073,7)	*B4GALT6* (-3455,6)	*BAIAP2L2* (-6169,9)
BARX1 (-4870)	*BCL9* (-3944,6)	*BMP8B* (-4230,2)	*BPNT1* (-4413,3)
BRCA1 (-3561,4)	*BYSL* (-4485,3)	*C1orf109* (-2770,2)	*C1orf56* (-2824,3)
C4BPA (-3379,4)	*C9orf116* (-3462)	*CACNA1D* (-3088,1)	*CARD9* (-4426,8)
CASC1 (-2857,4)	*CASQ1* (-3163,4)	*CBLL1* (-4092,2)	*CBX2* (-3503,4)
CBX4 (-3646)	*CCDC121* (-3451)	*CCNE1* (-3301,3)	*CD247* (-3449)
CD96 (-9024,6)	*CDC25A* (-4365)	*CDH12* (-6270,3)	*CDH19* (-5991,2)
CDK5 (-4613,5)	*CDKAL1* (-4005,9)	*CELSR3* (-5055)	*CEP164* (-3992,4)
CEP290 (-4631,8)	*CFD* (-5703,3)	*CGREF1* (-4700,9)	*CHGB* (-5120,4)
CHL1 (-6282,4)	*CHM* (-4145,5)	*CHRNA5* (-4052,5)	*CHSY1* (-3322,3)
CKB (-5070)	*CLPX* (-3300,9)	*COBL* (-6228,4)	*COCH* (-5957,7)
COL9A3 (-8035,7)	*COQ9* (-3878,3)	*CORO2A* (-2779,5)	*CPN1* (-4926,7)
CPT2 (-3776)	*CRIPT* (-3270,2)	*CRLF3* (-3733,6)	*CSPG4* (-6105,9)
CSPG5 (-2875,4)	*CTRL* (-3818,8)	*CYB5A* (-3792,3)	*CYP27B1* (-4710,1)
CYP2E1 (-3311,7)	*DAAM2* (-4513)	*DARS2* (-3628,8)	*DDX47* (-2605,9)
DFFB (-3876,1)	*DHRS2* (-5759,4)	*DHX35* (-2943,3)	*DHX9* (-3764)
DLL3 (-5052,9)	*DMBT1* (-3290,8)	*DNAJC12* (-4888,6)	*DUS4L* (-3489)
DUSP2 (-3660,7)	*EDEM1* (-3197,2)	*EEA1* (-5241,7)	*EEF1A2* (-4289,2)
EFNB3 (-3359,1)	*EGR3* (-5402,2)	*EHBP1* (-3730,1)	*ELK1* (-3925,2)
ELK4 (-3144,7)	*EMG1* (-3847)	*EMILIN1* (-5811,1)	*EML4* (-3607)
EN2 (-6951,6)	*ENTPD7* (-2871,5)	*EPHA3* (-6759,3)	*ERBB3* (-5454,2)
ERCC4 (-3714,3)	*ERF* (-3008,4)	*ETV3* (-4489,3)	*ETV4* (-4000)

EXOSC5 (-3276,9)	*EYA1* (-4776,8)	*EYA4* (-5829,6)	*EZH2* (-3897,5)
F12 (-3902,1)	*FABP6* (-5666,1)	*FCGR2B* (-3029,7)	*FLG* (-4435,4)
FLRT3 (-4576)	*FOXD3* (-4199)	*FRAT2* (-3104)	*FRMPD4* (-3634,9)
FSD1 (-4197,1)	*FZD3* (-3825,1)	*FZD9* (-4391,3)	*GABRB3* (-5869,9)
GAL (-6889,8)	*GALNT3* (-5031,3)	*GATAD1* (-3185,5)	*GDF11* (-4650,7)
GLI2 (-4393,6)	*GNE* (-3770,4)	*GNG4* (-7040,9)	*GNGT1* (-4338,6)
GPD1L (-3615,3)	*GPR19* (-3637,5)	*GPR3* (-4033,8)	*GPR37* (-6370)
GRM8 (-5803,5)	*GRTP1* (-3709)	*GSPT2* (-5460,9)	*GSTM4* (-4517,5)
GTF2A1 (-5194,3)	*GTPBP10* (-4561,8)	*GTPBP3* (-2360,5)	*GUF1* (-3086,9)
GYPC (-6221,6)	*HAPLN1* (-7071,7)	*HBE1* (-9791,3)	*HEATR1* (-3174,8)
HEY2 (-5018,6)	*HIP1* (-4290,2)	*HIPK2* (-3921,8)	*HOMER1* (-3867,5)
HOMER2 (-4470)	*HOXA4* (-3802,1)	*HOXC4* (-3730,7)	*HOXD13* (-6485,8)
HPCAL4 (-4703,1)	*HR* (-4041,1)	*HS3ST3A1* (-8476,4)	*HSDL2* (-3226,2)
HTR7 (-3617,1)	*ICK* (-4397)	*IFI30* (-4777,9)	*IGSF3* (-3746)
IL11 (-4805)	*IL27RA* (-4430,7)	*IL6R* (-4511,2)	*IMPA2* (-3995)
ING3 (-3804,5)	*IRX5* (-5092,8)	*ISG20L2* (-2954,5)	*ITGA4* (-6351,9)
ITGA7 (-4988,1)	*JAG1* (-3258,8)	*JAKMIP2* (-5047,3)	*KCNK5* (-3471,5)
KIAA0895 (-3704,3)	*KIF1A* (-5232,5)	*KIF3B* (-3509)	*KIF5C* (-4646,9)
KLF5 (-3083,6)	*KRIT1* (-3852,4)	*KYNU* (-6622,9)	*LCMT2* (-5637,4)
LDHC (-5438,6)	*LEF1* (-6604,1)	*LETM1* (-3151,3)	*LHX1* (-4138,4)
LPL (-4447,2)	*LRRTM2* (-3136,8)	*LY6E* (-3221,9)	*MAGEA1* (-7477,4)
MAGEA10 (-5814,5)	*MAGEA11* (-4843,3)	*MAGEA4* (-7486,2)	*MAGEB2* (-5333,3)
MAGEC2 (-9546,4)	*MAP2K6* (-3848,8)	*MAPRE3* (-4611,8)	*MARK2* (-3617,9)
MCF2L (-3415,8)	*ME2* (-3122,8)	*MFAP2* (-4164)	*MOCOS* (-5662,5)
MPI (-3391,3)	*MPL* (-3517,7)	*MPP6* (-3095,8)	*MRPL9* (-2546)
MRPS31 (-3313,7)	*MTAP* (-7098,4)	*MTMR4* (-2939,6)	*MUC1* (-3258,2)
MX2 (-5816,8)	*MXD1* (-3902,2)	*MXRA5* (-3087,5)	*MYH14* (-4024,6)
NAB2 (-3494,9)	*NAP1L3* (-4540,2)	*NCAM2* (-5556)	*NCAPG2* (-3857,9)
NDN (-6621,1)	*NEFH* (-4729,7)	*NEFL* (-6992,7)	*NFE2* (-4221,9)
NGDN (-3616,4)	*NIPSNAP1* (-3001,1)	*NIT2* (-2961)	*NKX2*-2 (-5451,5)
NKX2-5 (-7766,3)	*NLGN4X* (-5773,6)	*NMB* (-3026,9)	*NOLC1* (-3460,1)
NPAS1 (-4482,1)	*NPL* (-4530,4)	*NR4A2* (-4423)	*NSUN5* (-4042,2)
NTHL1 (-3361,6)	*NUP160* (-4163,4)	*OGDHL* (-4954,5)	*OSGEPL1* (-3340,6)
PACSIN3 (-4937,1)	*PAFAH2* (-5018,9)	*PAGE1* (-3193,8)	*PAK6* (-4577,2)
PARN (-3042,5)	*PAX9* (-3737,5)	*PAXIP1* (-3208,4)	*PCDHB6* (-4444,8)
PCDHB8 (-5067,6)	*PCOLCE* (-3841,9)	*PCOLCE2* (-4635,5)	*PCYOX1* (-4455,2)
PDE3A (-4453,7)	*PDGFRB* (-4241,1)	*PDK3* (-3953)	*PDK4* (-8129)
PDZD8 (-3320,5)	*PEX1* (-4582,8)	*PFKFB4* (-6908,7)	*PI15* (-5956,9)
PIGA (-5134,9)	*PIGH* (-3855,4)	*PIM2* (-3547,4)	*PLA2G7* (-5298,6)
PLTP (-5109,9)	*PMM2* (-3208,8)	*PMPCB* (-3273,5)	*POLG2* (-2547,2)
POLR3D (-3427,2)	*POLR3K* (-3074,2)	*POR* (-3610,6)	*POU2F1* (-3855,8)
POU3F2 (-5026,6)	*PPAT* (-3229,4)	*PPFIA1* (-3786,4)	*PPFIA4* (-3763,7)
PPM1E (-5758,8)	*PPME1* (-3181,4)	*PRAME* (-8839,9)	*PRKAB2* (-2796,5)
PRKCD (-4225,5)	*PRKCZ* (-5270,5)	*PRRX1* (-6235)	*PSME4* (-3170,4)
PTN (-2830,4)	*PTPN13* (-3655,1)	*PTPN3* (-3575)	*PTPRZ1* (-6225,7)
PUS7 (-3356,8)	*RAB17* (-5878,6)	*RAB26* (-4362,9)	*RAB36* (-4379,4)
RAMP1 (-8257,5)	*RAPGEFL1* (-4074,9)	*RBBP5* (-2929,1)	*RBM28* (-3708,8)

REEP1 (-3924,5)	*REEP2* (-4238,2)	*RFC3* (-3726,4)	*RFX3* (-3558,7)
RGS16 (-4720,8)	*RIPK4* (-5301,3)	*RNF125* (-6989,1)	*RNMT* (-3602,6)
RPGR (-3297,2)	*RPP25* (-5396,4)	*RSAD1* (-3200,2)	*RUNX3* (-4264,6)
RXRG (-6244,1)	*SAGE1* (-8678,9)	*SARM1* (-5437)	*SATB2* (-3339,1)
SCARB1 (-4869,4)	*SCARB2* (-3924,8)	*SDAD1* (-3077,5)	*SEC14L4* (-4837,2)
SEC23IP (-2951,5)	*SEMA3B* (-5332,2)	*SETBP1* (-3708,2)	*SETD6* (-5287,5)
SKP2 (-5164,3)	*SLC16A4* (-4930)	*SLC1A3* (-4173,7)	*SLC24A3* (-7213,2)
SLC25A13 (-3974,2)	*SLC25A15* (-3601,1)	*SLC25A20* (-2946,7)	*SLC25A40* (-3123,4)
SLC26A2 (-3594,5)	*SLC27A3* (-5281,6)	*SLC27A5* (-5220,9)	*SLC29A2* (-6512,2)
SLC39A6 (-3165,5)	*SLC6A15* (-6427,2)	*SLCO3A1* (-3777,9)	*SMG1* (-3681,9)
SNTB1 (-5909,1)	*SNX10* (-6204,6)	*SNX27* (-3532,2)	*SOCS3* (-3100,7)
SOX10 (-7067,9)	*SOX11* (-5937,8)	*SOX2* (-5059,8)	*SOX5* (-5785,2)
SP4 (-4790,5)	*SPATA6* (-4412,8)	*SSX3* (-5232)	*SSX5* (-3875,7)
ST3GAL4 (-3976,1)	*ST8SIA5* (-4068,2)	*STK32B* (-5723,1)	*STRN* (-3455,8)
SV2A (-4792)	*SVEP1* (-3709,5)	*SYN3* (-3344,9)	*TAF1* (-3354,1)
TAF1A (-4121,6)	*TAGLN3* (-6177,9)	*TBX2* (-5798)	*TCN1* (-4464,2)
TESC (-8034,9)	*TFAP2B* (-5480,9)	*TFCP2* (-5997,2)	*TGFA* (-6189,1)
TIMP3 (-6397,6)	*TIPRL* (-3553,6)	*TMCO1* (-3673,3)	*TNNT2* (-3408)
TNPO3 (-3215,3)	*TPTE* (-5920,6)	*TRIM2* (-4780,2)	*TRIM58* (-4012,2)
TRIM9 (-5761,7)	*TRIT1* (-3183,7)	*TRPV4* (-3450,9)	*TRRAP* (-3369,1)
TSEN2 (-3254,7)	*TUBB2B* (-4845,4)	*TYRO3* (-3188)	*UCHL5* (-2846,4)
UNC13A (-3566,9)	*USP21* (-2791,7)	*UST* (-3927,9)	*UTP14A* (-3181,1)
VGF (-6894,6)	*VIPR1* (-4224)	*VPS72* (-2869,1)	*VSNL1* (-3276,2)
WASL (-4659,3)	*WDR73* (-3490,5)	*WNT10B* (-5206,8)	*WWTR1* (-3228,4)
XPO4 (-3407,5)	*XYLT1* (-5895,5)	*ZDHHC11* (-3768,5)	*ZDHHC17* (-3015,7)
ZFP37 (-3852,8)	*ZFX* (-3336,2)	*ZMYM5* (-3320,8)	*ZNF200* (-3340,8)
ZNF217 (-3733,9)	*ZNF234* (-3705,1)	*ZNF254* (-3492)	*ZNF257* (-4113,5)
ZNF26 (-2702,5)	*ZNF407* (-3765,9)	*ZNF426* (-4564)	*ZNF43* (-4297,2)
ZNF493 (-3501,4)	*ZNF536* (-4150,4)	*ZNF556* (-7044,8)	*ZNF562* (-3811,6)
ZNF573 (-4591,1)	*ZNF589* (-3085,9)	*ZNF614* (-3971,5)	*ZNF675* (-4936,7)
ZNF682 (-5875,9)	*ZNF696* (-4468,7)	*ZNF701* (-3805,9)	*ZNF91* (-4953,5)

Table 6. GO enrichment analysis of DEGs up-regulated in EL+ cells.
GO term ID, description, adjusted p-value and involved genes of the top 19 most significantly enriched GO Biological Processes associated with the DEGs from EL+ cells.

GO term ID	Description	Adj. p-value	Genes ID			
GO:0061041	regulation of wound healing	4,42E-04	*GJA1*	*PDPN*	*SERPINB2*	*SERPINE1*
			TFPI	*THBD*		
GO:0050818	regulation of coagulation	4,42E-04	*PDPN*	*SERPINB2*	*SERPINE1*	*TFPI*
			THBD			
GO:1900046	regulation of hemostasis	4,42E-04	*PDPN*	*SERPINB2*	*SERPINE1*	*TFPI*
			THBD			
GO:0030198	extracellular matrix organization	1,94E-03	*FOXF1*	*ICAM2*	*IL6*	*LOX*
			NID1	*PDPN*	*SERPINE1*	
GO:0050817	coagulation	1,94E-03	*IL6*	*MYL9*	*PDPN*	*SERPINB2*

			SERPINE1	*TFPI*	*THBD*	
GO:0032102	negative regulation of response to external stimulus	2,03E-03	*CDH5*	*FOXF1*	*GJA1*	*SERPINB2*
			SERPINE1	*TFPI*	*THBD*	
GO:0050878	regulation of body fluid levels	2,44E-03	*GJA1*	*IL6*	*MYL9*	*PDPN*
			SERPINB2	*SERPINE1*	*TFPI*	*THBD*
GO:0043062	extracellular structure organization	3,13E-03	*FOXF1*	*ICAM2*	*IL6*	*LOX*
			NID1	*PDPN*	*SERPINE1*	
GO:0048568	embryonic organ development	4,51E-03	*EFEMP1*	*EPAS1*	*FOXF1*	*GJA1*
			MICAL2	*PAX6*	*PPP1R13L*	
GO:0060541	respiratory system development	7,30E-03	*BASP1*	*EPAS1*	*FOXF1*	*LOX*
			PDPN			
GO:0010810	regulation of cell-substrate adhesion	8,47E-03	*FOXF1*	*NID1*	*PDPN*	*RHOD*
			SERPINE1			
GO:0048747	muscle fiber development	1,70E-02	*DYSF*	*LOX*	*UCHL1*	
GO:0030858	positive regulation of epithelial cell differentiation	2,74E-02	*CDH5*	*PAX6*	*SERPINE1*	
GO:0032496	response to lipopolysaccharide	3,33E-02	*GJA1*	*IL6*	*SERPINE1*	*TFPI*
			THBD			
GO:0030324	lung development	3,37E-02	*EPAS1*	*FOXF1*	*LOX*	*PDPN*
GO:0031016	pancreas development	3,63E-02	*FOXF1*	*IL6*	*PAX6*	
GO:0023019	signal transduction involved in regulation of gene expression	3,80E-02	*FGF5*	*PAX6*		
GO:0031589	cell-substrate adhesion	4,14E-02	*FOXF1*	*NID1*	*PDPN*	*RHOD*
			SERPINE1			
GO:0031099	regeneration	4,52E-02	*ANXA3*	*DYSF*	*GJA1*	*IGFBP1*

Table 7. Co-expressed genes with CDH5.
List of 1196 genes from TCGA-UVM project that showed a significant positive correlation (co-expression) with CDH5. Spearman r coefficient of their relation with CDH5 is indicated in brackets. Data obtained from cBioPortal database.

Genes ID (Spearman r)			
A4GALT (0,64)	AACS (0,33)	ABCA4 (0,4)	ABCA7 (0,33)
ABCB6 (0,36)	ABCB8 (0,36)	ABCB9 (0,34)	ABCC1 (0,38)
ABCC3 (0,44)	ABCC9 (0,41)	ABCG4 (0,39)	ABI3 (0,49)
ABLIM3 (0,42)	ACAN (0,57)	ACAP1 (0,38)	ACE (0,67)
ACKR1 (0,53)	ACO1 (0,33)	ACOT8 (0,42)	ACOX3 (0,33)
ACTA2 (0,34)	ACTG2 (0,37)	ACVRL1 (0,37)	ADA2 (0,35)
ADAM12 (0,36)	ADAM15 (0,43)	ADAM19 (0,51)	ADAM23 (0,33)
ADAMTS12 (0,57)	ADAMTS18 (0,35)	ADAMTS4 (0,49)	ADAMTS9 (0,65)
ADAMTSL1 (0,54)	ADAMTSL3 (0,34)	ADAP2 (0,41)	ADCY2 (0,39)
ADCY4 (0,75)	ADGRB2 (0,38)	ADGRE1 (0,33)	ADGRF5 (0,43)
ADGRL2 (0,56)	ADGRL3 (0,36)	ADGRL4 (0,36)	ADIRF (0,34)

ADORA1 (0,35)	ADRA1B (0,57)	ADRA2B (0,39)	AFAP1L2 (0,42)
AGAP2 (0,37)	AGPAT4 (0,32)	AIF1 (0,42)	AIFM2 (0,37)
AKR1C3 (0,37)	ALDH16A1 (0,37)	ALDH4A1 (0,34)	ALOX15B (0,34)
ALPK3 (0,46)	ANGPT2 (0,39)	ANGPTL4 (0,33)	ANK1 (0,38)
ANKRD35 (0,34)	ANO1 (0,72)	ANO7 (0,34)	ANPEP (0,53)
AOAH (0,36)	AOC3 (0,49)	AP2A1 (0,33)	AP2S1 (0,35)
APBB1IP (0,41)	APLN (0,46)	APLNR (0,82)	APLP1 (0,34)
APOBR (0,48)	APOL1 (0,41)	APOL3 (0,48)	APOL4 (0,34)
AQP1 (0,67)	AQP3 (0,42)	ARC (0,34)	ARF3 (0,34)
ARHGAP30 (0,4)	ARHGAP6 (0,36)	ARHGEF15 (0,85)	ARL4C (0,32)
ARMC9 (0,37)	ARMH3 (0,36)	ARPC2 (0,34)	ARSA (0,33)
ASGR1 (0,35)	ASGR2 (0,34)	ASIC1 (0,34)	ATOX1 (0,34)
ATP1A2 (0,5)	ATP6V0B (0,37)	ATP6V0D2 (0,41)	B4GALNT1 (0,37)
B4GALT1 (0,45)	B9D2 (0,33)	BAALC (0,51)	BASP1 (0,33)
BATF (0,42)	BATF3 (0,34)	BCAT1 (0,34)	BCL11B (0,33)
BCL3 (0,39)	BCL6B (0,85)	BGN (0,45)	BHLHE22 (0,37)
BIN2 (0,4)	BMP2 (0,48)	BMP7 (0,36)	BORCS8 (0,32)
BRI3BP (0,39)	BRINP2 (0,36)	C10ORF105 (0,47)	C16ORF54 (0,34)
C19ORF38 (0,35)	C1ORF116 (0,39)	C1ORF162 (0,35)	C1QA (0,43)
C1QB (0,43)	C1QC (0,44)	C1QTNF2 (0,47)	C2CD4B (0,58)
C3AR1 (0,37)	C4A (0,35)	C4ORF48 (0,35)	C5AR1 (0,4)
C9ORF50 (0,34)	CA12 (0,45)	CA14 (0,33)	CABP1 (0,43)
CACNA1C (0,49)	CALHM2 (0,36)	CALHM5 (0,57)	CAMK1G (0,34)
CAPG (0,42)	CAPN11 (0,32)	CARNS1 (0,34)	CASC10 (0,55)
CASP10 (0,44)	CASQ2 (0,5)	CBFA2T3 (0,36)	CCDC134 (0,32)
CCDC184 (0,43)	CCL13 (0,34)	CCL14 (0,64)	CCL22 (0,41)
CCL26 (0,44)	CCL3 (0,32)	CCL4 (0,37)	CCL4L1 (0,36)
CCL5 (0,39)	CCL8 (0,36)	CCM2L (0,75)	CCN1 (0,49)
CCN2 (0,52)	CCNJL (0,39)	CCR1 (0,38)	CCR5 (0,33)
CCR7 (0,45)	CCRL2 (0,48)	CD14 (0,43)	CD163 (0,39)
CD163L1 (0,36)	CD180 (0,46)	CD2 (0,37)	CD209 (0,38)
CD247 (0,45)	CD248 (0,35)	CD276 (0,4)	CD300A (0,38)
CD300C (0,42)	CD300LF (0,37)	CD34 (0,9)	CD36 (0,47)
CD37 (0,39)	CD3D (0,4)	CD3E (0,42)	CD5 (0,45)
CD52 (0,45)	CD53 (0,39)	CD6 (0,32)	CD7 (0,4)
CD74 (0,42)	CD86 (0,34)	CD8A (0,39)	CD8B (0,36)
CD93 (0,78)	CD96 (0,39)	CDA (0,45)	CDC25B (0,34)
CDC42EP2 (0,42)	CDCP1 (0,36)	CDH11 (0,35)	CDH13 (0,64)
CDH23 (0,55)	CDH6 (0,55)	CDHR1 (0,34)	CDK16 (0,39)
CDK5 (0,34)	CDK5R2 (0,36)	CDK5RAP1 (0,33)	CDK9 (0,37)
CDR2L (0,44)	CEACAM21 (0,33)	CEBPA (0,35)	CES1 (0,36)
CFI (0,42)	CFP (0,41)	CHAC1 (0,36)	CHI3L1 (0,42)
CHI3L2 (0,35)	CHN1 (0,35)	CHPF2 (0,38)	CHRD (0,53)
CHRNA1 (0,33)	CHRNA3 (0,32)	CHST1 (0,72)	CHST13 (0,39)
CHST15 (0,69)	CHST2 (0,4)	CHST7 (0,64)	CHTF18 (0,35)
CIB1 (0,35)	CIITA (0,4)	CKAP4 (0,43)	CLDN11 (0,35)
CLDN5 (0,72)	CLEC10A (0,35)	CLEC14A (0,84)	CLEC1A (0,44)

CLEC3B (0,52)	CLEC4G (0,34)	CLIP3 (0,34)	CLPB (0,34)
CMKLR1 (0,36)	CNNM2 (0,41)	CNTN2 (0,33)	COL12A1 (0,45)
COL14A1 (0,53)	COL15A1 (0,61)	COL18A1 (0,37)	COL1A1 (0,52)
COL26A1 (0,35)	COL3A1 (0,49)	COL4A1 (0,73)	COL4A2 (0,71)
COL5A1 (0,61)	COL5A2 (0,47)	COL5A3 (0,53)	COL6A1 (0,34)
COL6A2 (0,36)	COL6A3 (0,65)	COL8A1 (0,33)	COL9A2 (0,34)
COQ4 (0,35)	CORO1A (0,45)	COTL1 (0,4)	COX4I2 (0,6)
COX7A1 (0,35)	CPNE5 (0,39)	CPT1C (0,4)	CPXM1 (0,32)
CPZ (0,33)	CRAT (0,34)	CREB3 (0,39)	CREB3L1 (0,39)
CRIP1 (0,35)	CRISPLD2 (0,41)	CRYBG1 (0,36)	CSF1R (0,37)
CSF2RB (0,34)	CSF3R (0,37)	CSRP2 (0,39)	CST7 (0,44)
CTSA (0,36)	CTSW (0,41)	CXCL10 (0,34)	CXCL12 (0,46)
CXCR1 (0,33)	CXCR2 (0,33)	CXCR3 (0,4)	CYP2S1 (0,52)
CYTH4 (0,42)	CYTIP (0,44)	CYTOR (0,4)	CYYR1 (0,55)
DACT1 (0,4)	DAP (0,37)	DAPP1 (0,34)	DCANP1 (0,36)
DCLK3 (0,46)	DCSTAMP (0,33)	DDAH1 (0,51)	DDX39A (0,34)
DGCR6 (0,36)	DGKQ (0,33)	DGLUCY (0,39)	DHRS3 (0,48)
DHRS9 (0,35)	DIPK2B (0,86)	DKK1 (0,33)	DKK3 (0,43)
DLL4 (0,39)	DLST (0,35)	DLX5 (0,51)	DLX6 (0,36)
DNASE1L3 (0,43)	DOK1 (0,38)	DOK2 (0,38)	DOLK (0,39)
DOLPP1 (0,37)	DPP4 (0,33)	DPYS (0,33)	DPYSL3 (0,4)
DTX1 (0,37)	DUSP14 (0,35)	DUSP5 (0,38)	DYSF (0,52)
EBF2 (0,4)	ECE1 (0,55)	ECM1 (0,33)	ECM2 (0,33)
ECRG4 (0,41)	ECSCR (0,79)	EDNRA (0,35)	EEPD1 (0,5)
EFHD2 (0,45)	EFNA3 (0,38)	EFNB2 (0,63)	EGFLAM (0,57)
EGLN2 (0,34)	EIF4E2 (0,33)	ELMO1 (0,43)	ELN (0,52)
EMX2 (0,37)	EMX2OS (0,35)	EN2 (0,34)	ENG (0,42)
EPAS1 (0,44)	EPB41L1 (0,33)	EPHA4 (0,38)	EPHB2 (0,52)
ERG (0,47)	ERICH4 (0,34)	ESAM (0,88)	EXOC3L1 (0,68)
EXOC3L2 (0,51)	EYA1 (0,34)	F2R (0,34)	F2RL3 (0,58)
FABP3 (0,37)	FAM107A (0,44)	FAM110A (0,38)	FAM110D (0,59)
FAM124B (0,67)	FAM131B (0,44)	FAM162B (0,5)	FAM163A (0,38)
FAM225A (0,33)	FAM225B (0,35)	FAM43A (0,35)	FAM43B (0,43)
FAM83B (0,32)	FASLG (0,35)	FATE1 (0,39)	FBLN2 (0,44)
FBLN5 (0,34)	FBXO10 (0,4)	FCER1G (0,43)	FCN1 (0,48)
FCN3 (0,4)	FCRL3 (0,35)	FDPS (0,48)	FGD2 (0,35)
FGD3 (0,38)	FGR (0,43)	FILIP1 (0,34)	FILIP1L (0,46)
FKBP1A (0,38)	FLI1 (0,42)	FLOT2 (0,36)	FLT1 (0,45)
FLT3 (0,33)	FLT4 (0,77)	FLVCR2 (0,42)	FN1 (0,55)
FOLR2 (0,4)	FOXC1 (0,47)	FOXC2 (0,43)	FOXD1 (0,37)
FOXF1 (0,45)	FOXG1 (0,38)	FOXI2 (0,34)	FOXL1 (0,58)
FOXL2 (0,45)	FOXL2NB (0,35)	FOXRED1 (0,35)	FOXS1 (0,5)
FPR1 (0,32)	FPR3 (0,45)	FRZB (0,56)	FST (0,44)
FSTL4 (0,34)	FTH1 (0,33)	FTL (0,34)	FUT7 (0,43)
FZD8 (0,36)	G0S2 (0,38)	G6PC3 (0,33)	GABRG3 (0,35)
GALNT10 (0,36)	GALNT15 (0,53)	GALNT16 (0,41)	GALNT5 (0,37)
GAS2L1 (0,34)	GASK1B (0,41)	GATA2 (0,6)	GATA3 (0,35)

GATA5 (0,37)	GATA6 (0,47)	GBA (0,4)	GBAP1 (0,39)
GBP4 (0,36)	GBX2 (0,32)	GDF3 (0,47)	GDPGP1 (0,35)
GEM (0,35)	GFRA2 (0,49)	GGCX (0,33)	GGT5 (0,49)
GGTLC2 (0,35)	GIMAP1 (0,52)	GIMAP4 (0,46)	GIMAP5 (0,42)
GIMAP6 (0,52)	GIMAP8 (0,58)	GIPC2 (0,36)	GJA4 (0,8)
GJA5 (0,61)	GJD3 (0,65)	GLA (0,36)	GLI1 (0,34)
GLI2 (0,38)	GLIPR2 (0,34)	GLIS2 (0,38)	GMFG (0,51)
GMIP (0,33)	GMPPA (0,33)	GNA14 (0,37)	GNA15 (0,39)
GNGT2 (0,39)	GNLY (0,41)	GPBAR1 (0,43)	GPC4 (0,41)
GPIHBP1 (0,57)	GPR162 (0,36)	GPR20 (0,36)	GPR37L1 (0,33)
GPR4 (0,59)	GPR55 (0,36)	GRAP (0,43)	GRAP2 (0,38)
GRIN2D (0,43)	GRK5 (0,45)	GRM8 (0,38)	GSN (0,33)
GSTM5 (0,41)	GUCY1A1 (0,38)	GUCY1B1 (0,41)	GUSB (0,36)
GYS1 (0,32)	GZMB (0,42)	GZMH (0,39)	GZMK (0,33)
H19 (0,37)	HAGH (0,34)	HAVCR2 (0,39)	HBA1 (0,4)
HBA2 (0,37)	HBB (0,42)	HCK (0,35)	HCLS1 (0,45)
HCST (0,33)	HDAC3 (0,35)	HDGF (0,34)	HECW1 (0,41)
HECW2 (0,53)	HEG1 (0,63)	HEPH (0,55)	HES5 (0,36)
HEXA (0,35)	HEY2 (0,47)	HEYL (0,44)	HGD (0,32)
HIC1 (0,5)	HID1 (0,4)	HIGD1B (0,45)	HK1 (0,41)
HK3 (0,38)	HKDC1 (0,34)	HLA-DMB (0,37)	HLA-DOA (0,36)
HLA-DPA1 (0,39)	HLA-DPB1 (0,34)	HLA-DQA1 (0,35)	HLA-DQA2 (0,38)
HLA-DQB1 (0,39)	HLA-DQB2 (0,33)	HLA-DRA (0,39)	HLA-DRB1 (0,42)
HLA-DRB5 (0,39)	HLA-DRB6 (0,37)	HM13 (0,38)	HMOX1 (0,46)
HMX1 (0,33)	HOXA13 (0,34)	HOXB2 (0,33)	HOXB5 (0,34)
HOXC13 (0,4)	HOXC4 (0,42)	HOXC5 (0,42)	HOXC6 (0,33)
HRC (0,73)	HRCT1 (0,35)	HRH1 (0,48)	HS3ST1 (0,41)
HS3ST2 (0,36)	HSD11B2 (0,35)	HSPA12B (0,66)	HTRA1 (0,35)
HTRA3 (0,37)	ICAM2 (0,4)	ICOSLG (0,34)	ID1 (0,58)
ID3 (0,64)	IDUA (0,36)	IGFBP2 (0,38)	IGFBP4 (0,65)
IGFLR1 (0,33)	IKZF1 (0,45)	IL15RA (0,42)	IL1B (0,4)
IL1RN (0,36)	IL21R (0,42)	IL22RA1 (0,33)	IL2RB (0,44)
IL2RG (0,44)	IL32 (0,52)	IL3RA (0,34)	IL4I1 (0,34)
IL6 (0,37)	INA (0,33)	INHBB (0,6)	INMT (0,5)
INPP5D (0,44)	INPPL1 (0,37)	IRAK1 (0,38)	IRF1 (0,36)
IRF5 (0,38)	IRF8 (0,34)	IRX1 (0,41)	ISG15 (0,35)
ISLR2 (0,42)	ISOC2 (0,38)	ITGA1 (0,35)	ITGA10 (0,39)
ITGA11 (0,42)	ITGA5 (0,57)	ITGA7 (0,57)	ITGAL (0,45)
ITGAX (0,34)	ITGB2 (0,42)	ITGB3 (0,43)	ITK (0,36)
ITPKA (0,44)	JAG2 (0,33)	JAM2 (0,53)	JAML (0,35)
JCAD (0,54)	JDP2 (0,39)	KANK4 (0,37)	KCNH1 (0,33)
KCNJ5 (0,39)	KCNJ8 (0,52)	KCNK6 (0,39)	KCNMB1 (0,51)
KCNN3 (0,4)	KCP (0,34)	KCTD17 (0,35)	KDELR3 (0,35)
KDR (0,47)	KIF19 (0,46)	KIR2DL1 (0,34)	KIR2DL3 (0,46)
KLF2 (0,48)	KLRB1 (0,38)	KRT18 (0,35)	LAG3 (0,38)
LAIR1 (0,41)	LAMB1 (0,4)	LAMB3 (0,36)	LAMC1 (0,35)
LAMTOR2 (0,41)	LAPTM5 (0,44)	LAT2 (0,36)	LCK (0,45)

LCP1 (0,43)	LCP2 (0,46)	LEF1 (0,43)	LEFTY2 (0,36)
LETM1 (0,47)	LFNG (0,46)	LGALS1 (0,32)	LGALS9 (0,37)
LGI2 (0,4)	LGMN (0,41)	LHB (0,36)	LHFPL6 (0,45)
LHX6 (0,33)	LILRA1 (0,37)	LILRA3 (0,36)	LILRA4 (0,34)
LILRA5 (0,42)	LILRA6 (0,34)	LILRB2 (0,44)	LILRB4 (0,35)
LILRB5 (0,35)	LIMS3 (0,43)	LINC02381 (0,38)	LMAN2 (0,32)
LMO2 (0,55)	LMOD1 (0,4)	LOC341056 (0,38)	LOC606724 (0,36)
LONRF3 (0,32)	LOXL2 (0,76)	LPCAT1 (0,34)	LRG1 (0,5)
LRIT2 (0,34)	LRP1 (0,33)	LRP8 (0,36)	LRRC17 (0,39)
LRRC20 (0,35)	LRRC25 (0,45)	LRRC32 (0,6)	LRRC4 (0,33)
LRRC55 (0,41)	LRRN2 (0,42)	LRSAM1 (0,37)	LSP1 (0,38)
LSP1P5 (0,34)	LST1 (0,46)	LTB (0,42)	LTBR (0,33)
LTF (0,52)	LY6H (0,56)	LY86 (0,42)	LY9 (0,37)
LYPD1 (0,44)	LYZ (0,37)	MAB21L2 (0,33)	MAGED1 (0,36)
MALL (0,43)	MAOB (0,41)	MAP1A (0,39)	MAP1B (0,44)
MARCH4 (0,52)	MARS (0,35)	MARVELD3 (0,38)	MCHR1 (0,33)
MECOM (0,52)	MED18 (0,35)	MEDAG (0,46)	METRNL (0,33)
METTL7B (0,47)	MFNG (0,57)	MFSD10 (0,35)	MFSD2A (0,37)
MGAT3 (0,44)	MGLL (0,47)	MICAL2 (0,59)	MILR1 (0,36)
MLC1 (0,34)	MMP1 (0,47)	MMP28 (0,52)	MMP9 (0,47)
MMRN2 (0,79)	MN1 (0,44)	MORN3 (0,38)	MPEG1 (0,37)
MPP2 (0,34)	MPV17L2 (0,4)	MPZL2 (0,45)	MRC2 (0,38)
MRO (0,39)	MROH1 (0,34)	MRPS11 (0,39)	MRVI1 (0,53)
MS4A4A (0,36)	MSRB3 (0,35)	MSX1 (0,47)	MTCL1 (0,34)
MTG1 (0,33)	MX2 (0,34)	MXRA5 (0,55)	MXRA8 (0,36)
MYCN (0,49)	MYCT1 (0,56)	MYF6 (0,32)	MYH11 (0,5)
MYL4 (0,5)	MYL6 (0,33)	MYLK (0,34)	MYO1F (0,41)
MYO1G (0,36)	MYOCD (0,38)	MYOM3 (0,43)	NAA60 (0,33)
NAAA (0,33)	NACC1 (0,33)	NACC2 (0,33)	NAGK (0,35)
NCDN (0,33)	NCF1 (0,45)	NCF1B (0,33)	NCF2 (0,41)
NCF4 (0,39)	NCKAP1L (0,41)	NCLN (0,34)	NCS1 (0,45)
NDRG4 (0,33)	NDST1 (0,4)	NDUFA4L2 (0,54)	NEURL1B (0,6)
NFAM1 (0,43)	NFASC (0,42)	NFE2 (0,34)	NGF (0,44)
NGFR (0,44)	NID1 (0,49)	NID2 (0,74)	NINJ2 (0,45)
NKG7 (0,45)	NLRP1 (0,44)	NMNAT2 (0,46)	NNMT (0,45)
NOS2 (0,37)	NOS3 (0,57)	NOTCH3 (0,65)	NOTCH4 (0,51)
NOVA2 (0,72)	NPAS1 (0,4)	NPNT (0,44)	NPR1 (0,78)
NPR3 (0,48)	NR2E1 (0,34)	NR2F1 (0,34)	NR5A2 (0,38)
NRARP (0,41)	NREP (0,36)	NRGN (0,37)	NRP1 (0,59)
NRSN2 (0,36)	NTMT1 (0,35)	NTN1 (0,37)	NTNG2 (0,43)
NTRK3 (0,4)	NUAK1 (0,43)	NUAK2 (0,47)	NUDT16L1 (0,33)
NUMBL (0,34)	OAF (0,35)	OAS2 (0,35)	OIT3 (0,55)
OLFML1 (0,56)	OLFML2B (0,52)	OLFML3 (0,34)	OPCML (0,36)
OR51E1 (0,51)	ORAI2 (0,44)	ORMDL2 (0,36)	OSCAR (0,44)
OSR2 (0,41)	P2RX1 (0,43)	P2RX4 (0,34)	P2RY6 (0,42)
P2RY8 (0,54)	P3H1 (0,43)	P3H2 (0,39)	P4HA2 (0,36)
PADI3 (0,38)	PAEP (0,36)	PANX2 (0,32)	PARVG (0,41)

PCARE (0,34)	PCDH1 (0,51)	PCDH12 (0,8)	PCDH17 (0,46)
PCED1B (0,37)	PCOLCE (0,43)	PCSK5 (0,55)	PDCD1 (0,4)
PDE1A (0,38)	PDE2A (0,83)	PDGFB (0,35)	PDGFRB (0,75)
PDLIM4 (0,45)	PEAK3 (0,4)	PEAR1 (0,46)	PECAM1 (0,69)
PGF (0,52)	PGM5 (0,61)	PGP (0,42)	PGR (0,38)
PHOSPHO1 (0,38)	PIGT (0,37)	PIK3C2B (0,41)	PIK3CD-AS1 (0,34)
PIK3R3 (0,41)	PIK3R5 (0,33)	PIK3R6 (0,39)	PITX1 (0,42)
PKD1L1 (0,36)	PLA2G7 (0,38)	PLAC9 (0,41)	PLAU (0,54)
PLAUR (0,38)	PLBD2 (0,39)	PLCE1 (0,52)	PLEK (0,37)
PLEKHB1 (0,35)	PLEKHG2 (0,38)	PLEKHG6 (0,37)	PLEKHO1 (0,36)
PLVAP (0,69)	PLXDC1 (0,59)	PLXNA4 (0,34)	PMEPA1 (0,55)
PNKP (0,41)	PODNL1 (0,36)	PODXL (0,5)	POMT1 (0,38)
POR (0,48)	PPIC (0,42)	PPIF (0,37)	PPP1R14A (0,45)
PRDM1 (0,45)	PRDM16 (0,47)	PRDM16-DT (0,36)	PRDM8 (0,38)
PREB (0,35)	PREX1 (0,33)	PRF1 (0,49)	PRND (0,68)
PROCR (0,39)	PRR5L (0,33)	PRRX1 (0,38)	PRSS35 (0,36)
PRSS36 (0,34)	PSAP (0,41)	PSMC4 (0,35)	PTGDR (0,33)
PTGER2 (0,33)	PTGER3 (0,34)	PTGIR (0,6)	PTN (0,33)
PTPN5 (0,32)	PTPN6 (0,42)	PTPN7 (0,44)	PTPRCAP (0,33)
PTPRD (0,33)	PTPRE (0,45)	PTX3 (0,35)	PURG (0,34)
PWP2 (0,38)	PXDN (0,43)	PYGM (0,39)	QPCTL (0,36)
QPRT (0,37)	RAB15 (0,38)	RAB31 (0,34)	RAB4B (0,39)
RAB5IF (0,4)	RABIF (0,32)	RAI2 (0,35)	RAMP3 (0,48)
RAP1GAP (0,37)	RASAL3 (0,47)	RASGRF2 (0,37)	RASGRP2 (0,42)
RASL11A (0,42)	RASL11B (0,36)	RASL12 (0,63)	RASSF5 (0,35)
RCAN2 (0,43)	RCSD1 (0,45)	REM1 (0,62)	RET (0,35)
RFTN1 (0,56)	RGL1 (0,42)	RGN (0,4)	RGS16 (0,42)
RGS5 (0,41)	RHBDD2 (0,41)	RHBDD3 (0,36)	RHBDL2 (0,43)
RHOB (0,43)	RIMS1 (0,36)	RNASE6 (0,42)	RNPEPL1 (0,34)
ROBO4 (0,79)	ROGDI (0,41)	ROR2 (0,4)	RPS6KA2 (0,36)
RRAD (0,5)	RTN1 (0,34)	RTN4R (0,36)	RUNX1 (0,43)
RUNX2 (0,36)	S100A4 (0,4)	S100A8 (0,39)	S100A9 (0,47)
S1PR1 (0,69)	S1PR3 (0,36)	S1PR4 (0,5)	S1PR5 (0,59)
SAMD14 (0,36)	SASH3 (0,43)	SCHIP1 (0,41)	SCN4B (0,42)
SCNN1B (0,34)	SCRG1 (0,39)	SDF4 (0,33)	SDK2 (0,34)
SDS (0,45)	SEC14L2 (0,33)	SECTM1 (0,34)	SEL1L3 (0,37)
SELE (0,33)	SELENOW (0,42)	SELL (0,42)	SELPLG (0,44)
SEMA3F (0,71)	SEMA3G (0,54)	SEMA5B (0,59)	SEMA6B (0,67)
SEPTIN5 (0,39)	SERPINA1 (0,38)	SERPINA3 (0,38)	SERPINE1 (0,42)
SETBP1 (0,43)	SEZ6 (0,34)	SFTA1P (0,33)	SFXN5 (0,37)
SH2D1B (0,46)	SH2D3C (0,69)	SHC1 (0,35)	SHISA2 (0,37)
SHISA9 (0,36)	SHKBP1 (0,38)	SHPK (0,36)	SIGLEC1 (0,38)
SIGLEC10 (0,37)	SIGLEC11 (0,32)	SIGLEC12 (0,41)	SIGLEC5 (0,44)
SIGLEC7 (0,43)	SIGLEC9 (0,42)	SIGMAR1 (0,35)	SIL1 (0,4)
SIRPB2 (0,34)	SIT1 (0,4)	SIX1 (0,48)	SIX2 (0,48)
SKAP1 (0,36)	SKIDA1 (0,34)	SKIV2L (0,41)	SLA (0,36)
SLA2 (0,39)	SLAMF6 (0,36)	SLAMF8 (0,37)	SLC16A8 (0,34)

SLC19A1 (0,34)	SLC22A18 (0,32)	SLC27A4 (0,42)	SLC29A4 (0,41)
SLC35F6 (0,39)	SLC36A1 (0,33)	SLC38A3 (0,43)	SLC39A1 (0,33)
SLC43A2 (0,35)	SLC44A2 (0,43)	SLC45A1 (0,45)	SLC46A3 (0,43)
SLC47A1 (0,34)	SLC4A8 (0,4)	SLC50A1 (0,44)	SLC5A6 (0,35)
SLC6A9 (0,33)	SLC8A1 (0,36)	SLC8B1 (0,35)	SLCO2A1 (0,62)
SLCO2B1 (0,4)	SLCO3A1 (0,44)	SLIT3 (0,59)	SMOC2 (0,47)
SMTN (0,42)	SNAI1 (0,52)	SNCAIP (0,41)	SNCG (0,54)
SNPH (0,39)	SOCS2 (0,43)	SOCS3 (0,41)	SOX17 (0,68)
SOX18 (0,68)	SOX7 (0,33)	SP5 (0,39)	SP6 (0,47)
SPAAR (0,41)	SPARC (0,54)	SPARCL1 (0,38)	SPHK1 (0,41)
SPHK2 (0,33)	SPI1 (0,42)	SPN (0,46)	SPNS2 (0,59)
SPOCK2 (0,37)	SPON1 (0,33)	SRA1 (0,34)	SRC (0,33)
SRL (0,48)	SRRM4 (0,32)	ST8SIA1 (0,37)	STAB1 (0,42)
STARD8 (0,51)	STC2 (0,46)	STEAP3 (0,36)	STEAP4 (0,35)
STON2 (0,36)	STRA6 (0,34)	STX4 (0,39)	SULF1 (0,38)
SULF2 (0,37)	SURF4 (0,37)	SUSD2 (0,34)	SVEP1 (0,38)
SYNDIG1 (0,33)	SYNPO2 (0,4)	SYT12 (0,36)	SYTL4 (0,34)
SYTL5 (0,41)	TACSTD2 (0,51)	TAGLN (0,56)	TAL1 (0,55)
TAOK2 (0,37)	TARS2 (0,37)	TBC1D10A (0,39)	TBC1D10C (0,41)
TBC1D2 (0,33)	TBX15 (0,42)	TBX21 (0,37)	TBX3 (0,35)
TBXAS1 (0,41)	TCF4 (0,42)	TCIM (0,42)	TCIRG1 (0,37)
TEAD4 (0,32)	TEK (0,51)	TENM4 (0,33)	TESPA1 (0,45)
TEX261 (0,33)	TGFA (0,33)	TGFB1 (0,37)	TGFB2 (0,37)
TGM2 (0,49)	THAP8 (0,38)	THBD (0,33)	THBS1 (0,57)
THSD1 (0,45)	THY1 (0,68)	TIE1 (0,89)	TIFAB (0,37)
TIGIT (0,33)	TIMELESS (0,33)	TIMP1 (0,34)	TIMP4 (0,36)
TINAGL1 (0,76)	TM4SF1 (0,57)	TM4SF18 (0,52)	TMEM119 (0,42)
TMEM130 (0,41)	TMEM132E (0,5)	TMEM155 (0,33)	TMEM158 (0,44)
TMEM163 (0,41)	TMEM176A (0,36)	TMEM176B (0,33)	TMEM184B (0,38)
TMEM200A (0,4)	TMEM214 (0,38)	TMEM233 (0,47)	TMEM255B (0,47)
TMEM273 (0,37)	TMEM37 (0,49)	TMEM52 (0,37)	TMEM88 (0,4)
TMEM8A (0,36)	TMSB4XP8 (0,36)	TMUB1 (0,37)	TNC (0,49)
TNFAIP2 (0,35)	TNFAIP8L1 (0,45)	TNFAIP8L2 (0,43)	TNFAIP8L3 (0,33)
TNFRSF11B (0,4)	TNFRSF1A (0,39)	TNFRSF1B (0,43)	TNFRSF21 (0,35)
TNFRSF4 (0,33)	TNFRSF8 (0,37)	TNFSF10 (0,33)	TOX2 (0,46)
TP53I11 (0,53)	TP53INP2 (0,33)	TPO (0,33)	TPPP3 (0,63)
TPST2 (0,34)	TRAM2 (0,36)	TRIL (0,44)	TRIM32 (0,35)
TRPC4 (0,42)	TRPC6 (0,35)	TRPM2 (0,39)	TRPM4 (0,35)
TRPV4 (0,39)	TSC22D3 (0,37)	TSPAN17 (0,48)	TSPAN18 (0,72)
TSPAN2 (0,41)	TSPAN5 (0,37)	TTC39A (0,38)	TTI1 (0,46)
TTYH3 (0,37)	TUBA1B (0,33)	TUBA8 (0,39)	TUBB2B (0,42)
TUBB3 (0,32)	TWIST1 (0,37)	TYMP (0,38)	TYROBP (0,43)
U2AF2 (0,37)	UBA1 (0,4)	UBTD1 (0,39)	UCP2 (0,47)
UNC5A (0,48)	UNC5B (0,48)	USHBP1 (0,76)	VARS2 (0,37)
VASH1 (0,55)	VAT1L (0,34)	VAV1 (0,38)	VAX1 (0,33)
VCAM1 (0,38)	VCAN (0,46)	VCP (0,43)	VIPR1 (0,36)
VOPP1 (0,35)	VSIG4 (0,33)	VSIR (0,59)	VSTM4 (0,46)

VTN (0,33)	VWA1 (0,34)	VWF (0,69)	WAS (0,4)
WDR62 (0,4)	WFS1 (0,42)	WNK2 (0,37)	WNT5B (0,33)
XCL2 (0,33)	YIF1A (0,36)	YIF1B (0,39)	ZAP70 (0,37)
ZBTB7B (0,36)	ZBTB7C (0,37)	ZDHHC12 (0,41)	ZFHX4 (0,34)
ZFP36 (0,33)	ZFPM2 (0,42)	ZHX3 (0,35)	ZNF366 (0,58)
ZNF385A (0,39)	ZNF467 (0,52)	ZNF576 (0,42)	ZNF683 (0,42)

Table 8. GO enrichment analysis of genes that co-express with CDH5.
GO term ID, description, adjusted p-value and involved genes of the top 10 most significantly enriched GO Biological Processes associated with positively correlated genes with CDH5 expression.

GO:0030198 - extracellular matrix organization					**Adj. p-value = 5,02E-30**	
ACAN	*ADAM12*	*ADAM15*	*ADAM19*	*ADAMTS4*	*ADAMTS9*	*B4GALT1*
BGN	*CCN1*	*CCN2*	*COL12A1*	*COL14A1*	*COL15A1*	*COL18A1*
COL3A1	*COL4A1*	*COL4A2*	*COL5A1*	*COL5A2*	*COL5A3*	*COL6A1*
COL6A3	*COL8A1*	*COL9A2*	*CREB3L1*	*CRISPLD2*	*DPP4*	*ECM2*
ELN	*ENG*	*FBLN2*	*FBLN5*	*FN1*	*FOXC1*	*FOXC2*
HTRA1	*ICAM2*	*IL6*	*ITGA1*	*ITGA10*	*ITGA11*	*ITGA5*
ITGAL	*ITGAX*	*ITGB2*	*ITGB3*	*JAM2*	*KDR*	*LAMB1*
LAMC1	*LCP1*	*LOXL2*	*LRP1*	*MMP1*	*MMP28*	*MMP9*
NID1	*NID2*	*NPNT*	*NR2E1*	*PDGFB*	*PECAM1*	*POMT1*
PXDN	*SERPINE1*	*SMOC2*	*SPARC*	*SPOCK2*	*SULF1*	*SULF2*
TGFB2	*THBS1*	*TIMP1*	*TNC*	*TNFRSF11B*	*TNFRSF1A*	*TNFRSF1B*
VCAN	*VTN*	*VWA1*	*VWF*			

GO:0043062 - extracellular structure organization					**Adj. p-value = 1,25E-29**	
ABCA7	*ACAN*	*ADAM12*	*ADAM15*	*ADAM19*	*ADAMTS4*	*ADAMTS9*
BCL3	*BGN*	*BMP7*	*CCN1*	*CCN2*	*CD34*	*CD36*
COL14A1	*COL15A1*	*COL18A1*	*COL1A1*	*COL3A1*	*COL4A1*	*COL4A2*
COL5A2	*COL5A3*	*COL6A1*	*COL6A2*	*COL6A3*	*COL8A1*	*COL9A2*
CRISPLD2	*DPP4*	*ECM2*	*EGFLAM*	*ELN*	*ENG*	*FBLN2*
FN1	*FOXC1*	*FOXC2*	*FOXF1*	*GPIHBP1*	*HTRA1*	*ICAM2*
ITGA1	*ITGA10*	*ITGA11*	*ITGA5*	*ITGA7*	*ITGAL*	*ITGAX*
ITGB3	*JAM2*	*KDR*	*LAMB1*	*LAMB3*	*LAMC1*	*LCP1*
LRP1	*MMP1*	*MMP28*	*MMP9*	*MYH11*	*NID1*	*NID2*
NR2E1	*PDGFB*	*PECAM1*	*PLA2G7*	*POMT1*	*PTX3*	*PXDN*
SMOC2	*SPARC*	*SPOCK2*	*SULF1*	*SULF2*	*TGFB1*	*TGFB2*
TIMP1	*TNC*	*TNFRSF11B*	*TNFRSF1A*	*TNFRSF1B*	*VCAM1*	*VCAN*
VWA1	*VWF*					

GO:0050900 - leukocyte migration					**Adj. p-value = 3,33E-26**	
ADORA1	*AIF1*	*ANGPT2*	*B4GALT1*	*C3AR1*	*C5AR1*	*CCL13*
CCL14	*CCL22*	*CCL26*	*CCL3*	*CCL4*	*CCL4L1*	*CCL5*
CCL8	*CCR1*	*CCR5*	*CCR7*	*CD2*	*CD300A*	*CD34*

CD74	*CMKLR1*	*COL1A1*	*CORO1A*	*CREB3*	*CSF3R*	*CXCL10*
CXCL12	*CXCR1*	*CXCR2*	*CXCR3*	*DOK2*	*DYSF*	*ECM1*
ESAM	*FCER1G*	*FLT1*	*FN1*	*FUT7*	*GATA3*	*HCK*
HMOX1	*HRH1*	*IL1B*	*IL1RN*	*IL6*	*INPP5D*	*ITGA1*
ITGA5	*ITGAL*	*ITGAX*	*ITGB2*	*ITGB3*	*JAM2*	*JAML*
LCK	*LGALS9*	*LGMN*	*MMP1*	*MMP28*	*MYO1G*	*NCKAP1L*
P2RX4	*PDGFB*	*PECAM1*	*PGF*	*PLA2G7*	*PLVAP*	*PREX1*
PTN	*PTPN6*	*RET*	*ROR2*	*S100A8*	*S100A9*	*S1PR1*
SELE	*SELL*	*SELPLG*	*SERPINE1*	*SHC1*	*SLAMF8*	*SLC16A8*
SLC8B1	*SPN*	*SPNS2*	*SRC*	*TBX21*	*TEK*	*TGFB1*
TGFB2	*THBD*	*THBS1*	*THY1*	*TRPM2*	*TRPM4*	*TRPV4*
VAV1	*VCAM1*	*XCL2*	*ZAP70*			

GO:0006874 - cellular calcium ion homeostasis					**Adj. p-value = 1,20E-14**	
ADORA1	*ADRA1B*	*APLNR*	*ATP1A2*	*C3AR1*	*C5AR1*	*CACNA1C*
CASQ2	*CCL13*	*CCL14*	*CCL3*	*CCL5*	*CCL8*	*CCR1*
CCR5	*CCR7*	*CCRL2*	*CD36*	*CD52*	*CDH23*	*CDK5*
CMKLR1	*CORO1A*	*CXCL10*	*CXCL12*	*CXCR1*	*CXCR2*	*CXCR3*
EDNRA	*F2R*	*F2RL3*	*FASLG*	*FATE1*	*FKBP1A*	*FPR1*
FPR3	*GATA2*	*GNA15*	*GPR20*	*GPR4*	*GPR55*	*GRIN2D*
HRC	*KCTD17*	*LCK*	*LETM1*	*LRP1*	*MCHR1*	*NCS1*
P2RX1	*P2RX4*	*P2RY6*	*P2RY8*	*PLCE1*	*PTGDR*	*PTGER2*
PTGER3	*PTGIR*	*PTPN6*	*RAMP3*	*RGN*	*S1PR1*	*S1PR3*
S1PR4	*SLC8A1*	*SLC8B1*	*STC2*	*TCIRG1*	*TGFB1*	*TGM2*
THY1	*TRPC4*	*TRPC6*	*TRPM2*	*TRPM4*	*TRPV4*	*WFS1*

GO:0050920 - regulation of chemotaxis					**Adj. p-value = 4,66E-14**	
AIF1	*ANGPT2*	*C3AR1*	*C5AR1*	*CCL26*	*CCL3*	*CCL4*
CCL5	*CCR1*	*CCR7*	*CD74*	*CDH13*	*CMKLR1*	*CREB3*
CXCL10	*CXCL12*	*CXCR2*	*DYSF*	*EFNB2*	*IL6*	*KDR*
LGALS9	*LGMN*	*MMP28*	*NCKAP1L*	*NRP1*	*NTRK3*	*P2RX4*
GFB	*PDGFRB*	*PGF*	*PLA2G7*	*PLXNA4*	*PTN*	*S1PR1*
SEMA3F	*SEMA3G*	*SEMA5B*	*SEMA6B*	*SERPINE1*	*SLAMF8*	*SLC8B1*
SMOC2	*STX4*	*TGFB1*	*THBS1*	*TRPV4*	*TUBB2B*	*XCL2*

GO:0001655 - urogenital system development					**Adj. p-value = 6,06E-13**	
ACE	*ACTA2*	*ALOX15B*	*ANGPT2*	*BASP1*	*BMP2*	*BMP7*
CD34	*COL4A1*	*CRIP1*	*CXCR2*	*EFNB2*	*EMX2*	*EPHA4*
EPHB2	*EYA1*	*FOXC1*	*FOXC2*	*FOXD1*	*FOXF1*	*GATA2*
GATA3	*GLI1*	*GLI2*	*GLIS2*	*GPR4*	*HES5*	*HEYL*
ID3	*IRX1*	*MAGED1*	*MMP9*	*MYOCD*	*NID1*	*NOTCH3*
NPNT	*NRP1*	*OSR2*	*PCSK5*	*PDGFB*	*PDGFRB*	*PECAM1*
PGF	*PLCE1*	*PODXL*	*PSAP*	*RET*	*RGN*	*SIX1*
SIX2	*SOX17*	*STRA6*	*SULF1*	*SULF2*	*TACSTD2*	*TEK*

TGFB1	*TGFB2*	*TNC*	*WFS1*			

GO:0002446 - neutrophil mediated immunity					**Adj. p-value = 2,22E-12**	
ACE	*ADA2*	*ANPEP*	*ARSA*	*B4GALT1*	*BIN2*	*C3AR1*
C5AR1	*CD14*	*CD300A*	*CD36*	*CD53*	*CD93*	*CDA*
CFP	*CHI3L1*	*CKAP4*	*COTL1*	*CRISPLD2*	*CTSA*	*CXCR1*
CXCR2	*DNASE1L3*	*FCER1G*	*FCN1*	*FGR*	*FPR1*	*FTH1*
FTL	*GLA*	*GMFG*	*GSN*	*GUSB*	*HBB*	*HK3*
IL6	*ITGAL*	*ITGAX*	*ITGB2*	*LAIR1*	*LAMTOR2*	*LILRA3*
LILRB2	*LPCAT1*	*LRG1*	*LTF*	*LYZ*	*MMP9*	*NCKAP1L*
NFAM1	*NFASC*	*OSCAR*	*P2RX1*	*PECAM1*	*PLAU*	*PLAUR*
PSAP	*PTPN6*	*PTX3*	*RAB31*	*RAB4B*	*S100A8*	*S100A9*
SELL	*SERPINA1*	*SERPINA3*	*SIGLEC5*	*SIGLEC9*	*SLC44A2*	*SURF4*
TBC1D10C	*TCIRG1*	*TNFRSF1B*	*TRPM2*	*TYROBP*	*VCP*	

GO:0045765 - regulation of angiogenesis					**Adj. p-value = 3,43E-12**	
ACVRL1	*ADAM12*	*ADAMTS9*	*ADGRB2*	*ANGPT2*	*ANGPTL4*	*APLNR*
AQP1	*C3AR1*	*C5AR1*	*CD34*	*CHI3L1*	*CIB1*	*COL4A2*
CREB3L1	*CXCL10*	*CXCR2*	*DDAH1*	*DLL4*	*ECM1*	*ECSCR*
EFNA3	*ENG*	*FASLG*	*FLT1*	*FOXC1*	*FOXC2*	*GATA2*
GATA6	*GPR4*	*HMOX1*	*ID1*	*IL1B*	*IL6*	*ITGA5*
ITGAX	*ITGB2*	*JCAD*	*KDR*	*KLF2*	*LRG1*	*MMRN2*
NGFR	*NOS3*	*NPR1*	*NR2E1*	*NRP1*	*PGF*	*PIK3R6*
PTN	*RHOB*	*RUNX1*	*SERPINE1*	*SMOC2*	*SPARC*	*SPHK1*
STAB1	*SULF1*	*TEK*	*TGFB2*	*THBS1*	*TIE1*	*TWIST1*
VASH1						

GO:0072001 - renal system development					**Adj. p-value = 2,05E-11**	
ACE	*ACTA2*	*ANGPT2*	*BASP1*	*BMP2*	*BMP7*	*CD34*
COL4A1	*CXCR2*	*EFNB2*	*EMX2*	*EPHA4*	*EYA1*	*FOXC1*
FOXC2	*FOXD1*	*FOXF1*	*GATA3*	*GLI2*	*GLIS2*	*GPR4*
HES5	*HEYL*	*ID3*	*IRX1*	*MAGED1*	*MMP9*	*MYOCD*
NID1	*NOTCH3*	*NPNT*	*NRP1*	*OSR2*	*PCSK5*	*PDGFB*
PDGFRB	*PECAM1*	*PGF*	*PLCE1*	*PODXL*	*RET*	*RGN*
SIX1	*SIX2*	*SOX17*	*STRA6*	*SULF1*	*SULF2*	*TACSTD2*
TEK	*TGFB1*	*TGFB2*	*WFS1*			

GO:0070374 - positive regulation of ERK1 and ERK2 cascade					**Adj. p-value = 2,85E-11**	
ABCA7	*BMP2*	*C5AR1*	*CCL13*	*CCL14*	*CCL22*	*CCL26*
CCL3	*CCL4*	*CCL4L1*	*CCL5*	*CCL8*	*CCN2*	*CCR1*
CCR7	*CD36*	*CD74*	*CHI3L1*	*CIB1*	*CSF1R*	*F2R*
FLT1	*FLT3*	*FLT4*	*GLIPR2*	*GPR55*	*HAVCR2*	*KDR*
LGALS9	*LRP1*	*NDRG4*	*NPNT*	*NRP1*	*P2RY6*	*PDGFB*

PDGFRB	*RAMP3*	*SHC1*	*SRC*	*TEK*	*TGFB1*	*TNFAIP8L3*
TRPV4	*XCL2*					

Table 9. Sequences of the primers used for every gene of interest.
Primers were used for Sanger DNA sequencing or qPCR. HUGO Gene Nomenclature Committee (HGNC) ID is also indicated, as well as the specific role that each primers pair played in this work.

ECHNIQUE	GENE ID	HGNC ID	SENSE	SEQUENCE (5′-3′)	ROLE IN THIS WORK
Sanger	*ADAMTS1*	HGNC:217	Fwd	CTGCTACGAGCGGTGTCTC	ECM REMODELING
			Rv	GTGCCGGAGTAGAAGCAGTG	
qPCR	*ADAMTS1*	HGNC:217	Fwd	CCCACAGGAACTGGAAGCATA	
			Rv	CCACTGCCGTGGAATTCTG	
	IGFBP2	HGNC:5471	Fwd	CAACCTCAAACAGTGCAAGATG	
			Rv	CTGCTGCTATTGTAGAAGAGAT	
	NID1	HGNC:7821	Fwd	ACGCAGTCTACGTCACCACAAA	
			Rv	GCGACTGCACCGAATGTTG	
	NI2	HGNC:13389	Fwd	GCGCTTACGAGGAGGTCAAG	
			Rv	ACCCATCAGATGCCAAAACTG	
	VCAN	HGNC:2464	Fwd	AGGTGGTCTACTTGGGGTGA	
			Rv	TGGTTGTAGCCTCTTTAGGTTT	
	CDH5	HGNC:1764	Fwd	TGGTCACTCTGCAAGACATCAA	ENDOTHELIAL-LIKE PHENOTYPE
			Rv	TCCTCAACAAACAGAGAGCCCACA	
	ENG	HGNC:3349	Fwd	AACATGCAGATCTGGACCACTGGA	
			Rv	TTGAGGTGTGTCTGGGAGCTTGAA	
	EPHA2	HGNC:3386	Fwd	TCGGACCGAGAGCGAGAA	
			Rv	AGCAGTACCACTTCCTTGCC	
	KDR	HGNC:6307	Fwd	CCACTGGTATTGGCAGTTGGA	
			Rv	CACAAGGGTATGGGTTTGTCACT	
	LAMC2	HGNC:6493	Fwd	GTGGCTCCTGCCAAATTTCT	
			Rv	ACATCATGGGCAGATGGGTG	
	TEK	HGNC:11724	Fwd	TGTGGAGTCAGCTTGCTCCTTTCT	
			Rv	AGAGGCAATGCAGGTGAGAGATGT	
	TIE1	HGNC:11809	Fwd	TGGCTTCTCATGTGGGCCG	
			Rv	GGGTGCGCACGATACGG	
	NANOG	HGNC:20857	Fwd	CCCAAAGGCAAACAACCCACTTCT	STEMNESS FEATURES
			Rv	AGCTGGGTGGAAGAGAACACAGTT	
	POU5F1	HGNC:9221	Fwd	CGAGAAGGATGTGGTCCGAG	
			Rv	TGTGCATAGTCGCTGCTTGA	
	PROM1	HGNC:9454	Fwd	AACAGCACCTTGAAGAGCTTGCAC	
			Rv	ACCAAGCACAGAGGGTCATTGAGA	
	SOX2	HGNC:11195	Fwd	GAGAGTGTTTGCAAAAGGGGG	
			Rv	CGCCGCCGATGATTGTTATTA	
	ACTB	HGNC:132	Fwd	GATGGCCACGGCTGCTT	HOUSEKEEPING GENES
			Rv	AGGACTCCATGCCCAGGAA	
	B2B	HGNC:914	Fwd	GGACTGGTCTTTCTATCTCTTGT	
			Rv	TCTCGATCCCACTTAACTATCTTG	
	RNA18S1	HGNC:44278	Fwd	CACGGACAGGATTGACAGATT	
			Rv	GCCAGAGTCTCGTTCGTTATC	

BIBLIOGRAPHY

Afshar, A.R., Damato, B.E., Stewart, J.M., Zablotska, L.B., Roy, R., Olshen, A.B., Joseph, N.M., and Bastian, B.C. (2019). Next-generation sequencing of uveal melanoma for detection of genetic alterations predicting metastasis. Transl. Vis. Sci. Technol. *8*.

Alberts, B., Johnson, A., Lewis, J., Raff, M., Roberts, K., and Walter, P. (2002). The Extracellular Matrix of Animals.

Alečković, M., Wei, Y., LeRoy, G., Sidoli, S., Liu, D.D., Garcia, B.A., and Kang, Y. (2017). Identification of Nidogen 1 as a lung metastasis protein through secretome analysis. Genes Dev. *31*, 1439–1455.

Alessandrino, F., Smith, D.A., Tirumani, S.H., and Ramaiya, N.H. (2019). Cancer genome landscape: a radiologist's guide to cancer genome medicine with imaging correlates. Insights Imaging *10*, 111.

Apte, S.S. (2004). A disintegrin-like and metalloprotease (reprolysin type) with thrombospondin type 1 motifs: The ADAMTS family. Int. J. Biochem. Cell Biol. *36*, 981–985.

Arozarena, I., and Wellbrock, C. (2019). Phenotype plasticity as enabler of melanoma progression and therapy resistance. Nat. Rev. Cancer *19*, 377–391.

Asahara, T., and Kawamoto, A. (2004). Endothelial progenitor cells for postnatal vasculogenesis. Am. J. Physiol. - Cell Physiol. *287*, C572–C579.

Asano, K., Nelson, C.M., Nandadasa, S., Aramaki-Hattori, N., Lindner, D.J., Alban, T., Inagaki, J., Ohtsuki, T., Oohashi, T., Apte, S.S., et al. (2017). Stromal Versican Regulates Tumor Growth by Promoting Angiogenesis. Sci. Rep. *7*, 17225.

Ashlin, T.G., Kwan, A.P.L., and Ramji, D.P. (2013). Regulation of ADAMTS-1, -4 and -5 expression in human macrophages: Differential regulation by key cytokines implicated in atherosclerosis and novel synergism between TL1A and IL-17. Cytokine *64*, 234–242.

Barrett, T., Wilhite, S.E., Ledoux, P., Evangelista, C., Kim, I.F., Tomashevsky, M., Marshall, K.A., Phillippy, K.H., Sherman, P.M., Holko, M., et al. (2013). NCBI GEO: archive for functional genomics data sets--update. Nucleic Acids Res. *41*, D991-5.

Benton, G., Arnaoutova, I., George, J., Kleinman, H.K., and Koblinski, J. (2014). Matrigel: From discovery and ECM mimicry to assays and models for cancer research. Adv. Drug Deliv. Rev. *79*, 3–18.

Bevitt, D.J., Mohamed, J., Catterall, J.B., Li, Z., Arris, C.E., Hiscott, P., Sheridan, C., Langton, K.P., Barker, M.D., Clarke, M.P., et al. (2003). Expression of ADAMTS metalloproteinases in the retinal pigment epithelium derived cell line ARPE-19: Transcriptional regulation by TNFα. Biochim. Biophys. Acta - Gene Struct. Expr. *1626*, 83–91.

Binder, M.J., McCoombe, S., Williams, E.D., McCulloch, D.R., and Ward, A.C. (2020). ADAMTS-15 has a tumor suppressor role in prostate cancer.

Biomolecules *10*, 682.

Blum, E.S., Yang, J., Komatsubara, K.M., and Carvajal, R.D. (2016). Clinical Management of Uveal and Conjunctival Melanoma. Oncology (Williston Park). *30*, 29–32, 34–43, 48.

Bonnans, C., Chou, J., and Werb, Z. (2014). Remodelling the extracellular matrix in development and disease. Nat. Rev. Mol. Cell Biol. *15*, 786–801.

Bradshaw, A., Wickremsekera, A., Tan, S.T., Peng, L., Davis, P.F., and Itinteang, T. (2016). Cancer Stem Cell Hierarchy in Glioblastoma Multiforme. Front. Surg. *3*, 21.

Brown, Y., Hua, S., and Tanwar, P.S. (2019). Extracellular matrix-mediated regulation of cancer stem cells and chemoresistance. Int. J. Biochem. Cell Biol. *109*, 90–104.

Cai, X., Jia, Y., Mei, J., and Tang, R. (2004). Tumor blood vessels formation in osteosarcoma: vasculogenesis mimicry. Chin. Med. J. (Engl). *117*, 94–98.

Cal, S., and López-Otín, C. (2015). ADAMTS proteases and cancer (Elsevier B.V.).

Canals, F., Colomé, N., Ferrer, C., Plaza-Calonge, M. del C., and Rodríguez-Manzaneque, J.C. (2006). Identification of substrates of the extracellular protease ADAMTS1 by DIGE proteomic analysis. Proteomics *6*, S28–S35.

Carmeliet, P., and Jain, R.K. (2011). Molecular mechanisms and clinical applications of angiogenesis. Nature *473*, 298–307.

Casal, C., Torres-Collado, A.X., Plaza-Calonge, M.D.C., Martino-Echarri, E., Ramón Y Cajal, S., Rojo, F., Griffioen, A.W., and Rodríguez-Manzaneque, J.C. (2010). ADAMTS1 contributes to the acquisition of an endothelial-like phenotype in plastic tumor cells. Cancer Res. *70*, 4676–4686.

Castet, F., Garcia-Mulero, S., Sanz-Pamplona, R., Cuellar, A., Casanovas, O., Caminal, J., and Piulats, J. (2019). Uveal Melanoma, Angiogenesis and Immunotherapy, Is There Any Hope? Cancers (Basel). *11*, 834.

Cerami, E., Gao, J., Dogrusoz, U., Gross, B.E., Sumer, S.O., Aksoy, B.A., Jacobsen, A., Byrne, C.J., Heuer, M.L., Larsson, E., et al. (2012). The cBio cancer genomics portal: an open platform for exploring multidimensional cancer genomics data. Cancer Discov. *2*, 401–404.

Chattopadhyay, C., Kim, D.W., Gombos, D.S., Oba, J., Qin, Y., Williams, M.D., Esmaeli, B., Grimm, E.A., Wargo, J.A., Woodman, S.E., et al. (2016). Uveal melanoma: From diagnosis to treatment and the science in between. Cancer *122*, 2299–2312.

Chen, L., Tang, J., Feng, Y., Li, S., Xiang, Q., He, X., Ren, G., Peng, W., and Xiang, T. (2017). ADAMTS9 is Silenced by Epigenetic Disruption in Colorectal Cancer and Inhibits Cell Growth and Metastasis by Regulating Akt/p53 Signaling. Cell. Physiol. Biochem. *44*, 1370–1380.

Chen, X., Ai, Z., Rasmussen, M., Bajcsy, P., Auvil, L., Welge, M., Leach, L.,

Vangveeravong, S., Maniotis, A.J., and Folberg, R. (2003). Three-dimensional reconstruction of extravascular matrix patterns and blood vessels in human uveal melanoma tissue: Techniques and preliminary findings. Investig. Ophthalmol. Vis. Sci. *44*, 2834–2840.

Chen, Y.S., Wu, M.J., Huang, C.Y., Lin, S.C., Chuang, T.H., Yu, C.C., and Lo, J.F. (2011). CD133/Src axis mediates tumor initiating property and epithelial-mesenchymal transition of head and neck cancer. PLoS One *6*, e28053.

Choi, J.E., Kim, D.S., Kim, E.J., Chae, M.H., Cha, S.I., Kim, C.H., Jheon, S., Jung, T.H., and Park, J.Y. (2008). Aberrant methylation of ADAMTS1 in non-small cell lung cancer. Cancer Genet. Cytogenet. *187*, 80–84.

Collins-Racie, L.A., Flannery, C.R., Zeng, W., Corcoran, C., Annis-Freeman, B., Agostino, M.J., Arai, M., DiBlasio-Smith, E., Dorner, A.J., Georgiadis, K.E., et al. (2004). ADAMTS-8 exhibits aggrecanase activity and is expressed in human articular cartilage. Matrix Biol. *23*, 219–230.

Cooke, V.G., LeBleu, V.S., Keskin, D., Khan, Z., O'Connell, J.T., Teng, Y., Duncan, M.B., Xie, L., Maeda, G., Vong, S., et al. (2012). Pericyte depletion results in hypoxia-associated epithelial-to-mesenchymal transition and metastasis mediated by met signaling pathway. Cancer Cell *21*, 66–81.

Coussens, L.M., Fingleton, B., and Matrisian, L.M. (2002). Matrix metalloproteinase inhibitors and cancer: trials and tribulations. Science *295*, 2387–2392.

Crawford, Y., and Ferrara, N. (2009). VEGF inhibition: Insights from preclinical and clinical studies. Cell Tissue Res. *335*, 261–269.

Demaison, C., Parsley, K., Brouns, G., Scherr, M., Battmer, K., Kinnon, C., Grez, M., and Thrasher, A.J. (2002). High-level transduction and gene expression in hematopoietic repopulating cells using a human imunodeficiency virus type 1-based lentiviral vector containing an internal spleen focus forming virus promoter. Hum. Gene Ther. *13*, 803–813.

Demircan, K., Yonezawa, T., Takigawa, T., Topcu, V., Erdogan, S., Ucar, F., Armutcu, F., Yigitoglu, M.R., Ninomiya, Y., and Hirohata, S. (2013). ADAMTS1, ADAMTS5, ADAMTS9 and aggrecanase-generated proteoglycan fragments are induced following spinal cord injury in mouse. Neurosci. Lett. *544*, 25–30.

Demou, Z.N., and Hendrix, M.J.C. (2008). Microgenomics profile the endogenous angiogenic phenotype in subpopulations of aggressive melanoma. J. Cell. Biochem. *105*, 562–573.

Djirackor, L., Kalirai, H., Coupland, S.E., and Petrovski, G. (2019). CD166high uveal melanoma cells represent a subpopulation with enhanced migratory capacity. Investig. Ophthalmol. Vis. Sci. *60*, 2696–2704.

Dobrzanski, P., Hunter, K., Jones-Bolin, S., Chang, H., Robinson, C., Pritchard, S., Zhao, H., and Ruggeri, B. (2004). Antiangiogenic and Antitumor Efficacy of EphA2 Receptor Antagonist. Cancer Res. *64*, 910–919.

Döme, B., Hendrix, M.J.C., Paku, S., Tóvári, J., and Tímár, J. (2007). Alternative vascularization mechanisms in cancer: Pathology and therapeutic implications. Am. J. Pathol. *170*, 1–15.

Dubail, J., Vasudevan, D., Wang, L.W., Earp, S.E., Jenkins, M.W., Haltiwanger, R.S., and Apte, S.S. (2016). Impaired ADAMTS9 secretion: A potential mechanism for eye defects in Peters Plus Syndrome. Sci. Rep. *6*, 1–15.

Dunn, J.R., Reed, J.E., Du Plessis, D.G., Shaw, E.J., Reeves, P., Gee, A.L., Warnke, P., and Walker, C. (2006). Expression of ADAMTS-8, a secreted protease with antiangiogenic properties, is downregulated in brain tumours. Br. J. Cancer *94*, 1186–1193.

Esselens, C., Malapeira, J., Colomé, N., Casal, C., Rodríguez-Manzaneque, J.C., Canals, F., and Arribas, J. (2010). The cleavage of semaphorin 3C induced by ADAMTS1 promotes cell migration. J. Biol. Chem. *285*, 2463–2473.

Fang, D., Nguyen, T.K., Leishear, K., Finko, R., Kulp, A.N., Hotz, S., Van Belle, P.A., Xu, X., Elder, D.E., and Herlyn, M. (2005). A tumorigenic subpopulation with stem cell properties in melanomas. Cancer Res. *65*, 9328–9337.

Fernández-Rodríguez, R., Rodríguez-Baena, F.J., Martino-Echarri, E., Peris-Torres, C., Del Carmen Plaza-Calonge, M., Rodríguez-Manzaneque, J.C., Plaza-Calonge, M. del C., Rodríguez-Manzaneque, J.C., Javier Rodríguez-Baena, F., Del Carmen Plaza-Calonge, M., et al. (2016). Stroma-derived but not tumor ADAMTS1 is a main driver of tumor growth and metastasis. Oncotarget *7*, 34507–34519.

Ferraro, D.A., Patella, F., Zanivan, S., Donato, C., Aceto, N., Giannotta, M., Dejana, E., Diepenbruck, M., Christofori, G., and Buess, M. (2019). Endothelial cell-derived nidogen-1 inhibits migration of SK-BR-3 breast cancer cells. BMC Cancer *19*, 312.

Filou, S., Stylianou, M., Triantaphyllidou, I.E., Papadas, T., Mastronikolis, N.S., Goumas, P.D., Papachristou, D.J., Ravazoula, P., Skandalis, S.S., and Vynios, D.H. (2013). Expression and distribution of aggrecanases in human larynx: ADAMTS-5/aggrecanase-2 is the main aggrecanase in laryngeal carcinoma. Biochimie *95*, 725–734.

Folberg, R., and Maniotis, A.J. (2004). Vasculogenic mimicry. APMIS *112*, 508–525.

Folberg, R., Kadkol, S.S., Frenkel, S., Valyi-Nagy, K., Jager, M.J., Pe'er, J., and Maniotis, A.J. (2008). Authenticating cell lines in ophthalmic research laboratories. Invest. Ophthalmol. Vis. Sci. *49*, 4697–4701.

Fontanil, T., Mohamedi, Y., Cobo, T., Cal, S., and Obaya, Á.J. (2019). Novel associations within the tumor microenvironment: Fibulins meet ADAMTSs. Front. Oncol. *9*, 796.

Francescone, R., Scully, S., Bentley, B., Yan, W., Taylor, S.L., Oh, D., Moral, L., and Shao, R. (2012). Glioblastoma-derived tumor cells induce vasculogenic mimicry through Flk-1 protein activation. J. Biol. Chem. *287*, 24821–24831.

Frank, N.Y., Schatton, T., Kim, S., Zhan, Q., Wilson, B.J., Ma, J., Saab, K.R., Osherov, V., Widlund, H.R., Gasser, M., et al. (2011). VEGFR-1 expressed by malignant melanoma-initiating cells is required for tumor growth. Cancer Res. *71*, 1474–1485.

Frenkel, S., Barzel, I., Levy, J., Lin, A.Y., Bartsch, D.-U., Majumdar, D., Folberg, R., and Pe'er, J. (2008). Demonstrating circulation in vasculogenic mimicry patterns of uveal melanoma by confocal indocyanine green angiography. Eye *22*, 948–952.

Fridman, R., Kibbey, M.C., Royce, L.S., Zain, M., Sweeney, T.M., Jicha, D.L., Yannelli, J.R., Martin, G.R., and Kleinman, H.K. (1991). Enhanced tumor growth of both primary and established human and murine tumor cells in athymic mice after coinjection with matrigel. J. Natl. Cancer Inst. *83*, 769–774.

Fridman, R., Benton, G., Aranoutova, I., Kleinman, H.K., and Bonfil, R.D. (2012). Increased initiation and growth of tumor cell lines, cancer stem cells and biopsy material in mice using basement membrane matrix protein (Cultrex or Matrigel) co-injection. Nat. Protoc. *7*, 1138–1144.

Fu, Y., Nagy, J.A., Brown, L.F., Shih, S.C., Johnson, P.Y., Chan, C.K., Dvorak, H.F., and Wight, T.N. (2011). Proteolytic cleavage of versican and involvement of ADAMTS-1 in VEGF-A/VPF-induced pathological angiogenesis. J. Histochem. Cytochem. *59*, 463–473.

Gao, J., Aksoy, B.A., Dogrusoz, U., Dresdner, G., Gross, B., Sumer, S.O., Sun, Y., Jacobsen, A., Sinha, R., Larsson, E., et al. (2013). Integrative analysis of complex cancer genomics and clinical profiles using the cBioPortal. Sci. Signal. *6*, pl1.

Garza Treviño, E.N., González, P.D., Valencia Salgado, C.I., and Martinez Garza, A. (2019). Effects of pericytes and colon cancer stem cells in the tumor microenvironment. Cancer Cell Int. *19*, 1–12.

Goldman, M.J., Craft, B., Hastie, M., Repečka, K., McDade, F., Kamath, A., Banerjee, A., Luo, Y., Rogers, D., Brooks, A.N., et al. (2020). Visualizing and interpreting cancer genomics data via the Xena platform. Nat. Biotechnol. *38*, 675–678.

Gomis-Rüth, F.X. (2003). Structural aspects of the metzincin clan of metalloendopeptidases. Appl. Biochem. Biotechnol. - Part B Mol. Biotechnol. *24*, 157–202.

Gougos, A., and Letarte, M. (1990). Primary structure of endoglin, an RGD-containing glycoprotein of human endothelial cells. J. Biol. Chem. *265*, 8361–8364.

Grossman, R.L., Heath, A.P., Ferretti, V., Varmus, H.E., Lowy, D.R., Kibbe, W.A., and Staudt, L.M. (2016). Toward a Shared Vision for Cancer Genomic Data. N. Engl. J. Med. *375*, 1109–1112.

Grzywa, T.M., Paskal, W., and Włodarski, P.K. (2017). Intratumor and Intertumor Heterogeneity in Melanoma. Transl. Oncol. *10*, 956–975.

Gueye, N.A., Mead, T.J., Koch, C.D., Biscotti, C. V., Falcone, T., and Apte, S.S. (2017). Versican proteolysis by ADAMTS proteases and its influence on sex steroid receptor expression in uterine leiomyoma. J. Clin. Endocrinol. Metab. *102*, 1631–1641.

Gustavsson, H., Wang, W., Jennbacken, K., Welén, K., and Damber, J.E. (2009). ADAMTS1, a putative anti-angiogenic factor, is decreased in human prostate cancer. BJU Int. *104*, 1786–1790.

Gustavsson, H., Tešan, T., Jennbacken, K., Kuno, K., Damber, J.E., and Welén, K. (2010). ADAMTS1 alters blood vessel morphology and TSP1 levels in LNCaP and LNCaP-19 prostate tumors. BMC Cancer *10*, 288.

Halaban, R., and Neufeld, G. (1993). Human melanoma cells but not normal melanocytes express vascular endothelial growth factor receptors. Biochem. Biophys. Res. Commun. *190*, 702–709.

El Hallani, S., Boisselier, B., Peglion, F., Rousseau, A., Colin, C., Idbaih, A., Marie, Y., Mokhtari, K., Thomas, J.L., Eichmann, A., et al. (2010). A new alternative mechanism in glioblastoma vascularization: Tubular vasculogenic mimicry. Brain *133*, 973–982.

Hanahan, D., and Coussens, L.M. (2012). Accessories to the Crime: Functions of Cells Recruited to the Tumor Microenvironment. Cancer Cell *21*, 309–322.

Hanahan, D., and Folkman, J. (1996). Patterns and emerging mechanisms of the angiogenic switch during tumorigenesis. Cell *86*, 353–364.

Hanahan, D., and Weinberg, R.A. (2000). The hallmarks of cancer. Cell *100*, 57–70.

Hanahan, D., and Weinberg, R.A. (2011). Hallmarks of Cancer: The Next Generation. Cell *144*, 646–674.

Haraguchi, N., Ohara, N., Koseki, J., Takahashi, H., Nishimura, J., Hata, T., Mizushima, T., Yamamoto, H., Ishii, H., Doki, Y., et al. (2017). High expression of ADAMTS5 is a potent marker for lymphatic invasion and lymph node metastasis in colorectal cancer. Mol. Clin. Oncol. *6*, 130–134.

Harbour, J.W. (2014). A prognostic test to predict the risk of metastasis in uveal melanoma based on a 15-gene expression profile. Methods Mol. Biol. *1102*, 427–440.

Harrell, J.C., Pfefferle, A.D., Zalles, N., Prat, A., Fan, C., Khramtsov, A., Olopade, O.I., Troester, M.A., Dudley, A.C., and Perou, C.M. (2014). Endothelial-like properties of claudin-low breast cancer cells promote

tumor vascular permeability and metastasis. Clin. Exp. Metastasis *31*, 33–45.

Hayashi, Y., Caboni, L., Das, D., Yumoto, F., Clayton, T., Deller, M.C., Nguyen, P., Farr, C.L., Chiu, H.J., Miller, M.D., et al. (2015). Structure-based discovery of NANOG variant with enhanced properties to promote self-renewal and reprogramming of pluripotent stem cells. Proc. Natl. Acad. Sci. U. S. A. *112*, 4666–4671.

Hendrix, M.J.C., Seftor, E.A., Meltzer, P.S., Gardner, L.M.G., Hess, A.R., Kirschmann, D.A., Schatteman, G.C., and Seftor, R.E.B. (2001). Expression and functional significance of VE-cadherin in aggressive human melanoma cells: Role in vasculogenic mimicry. Proc. Natl. Acad. Sci. *98*, 8018–8023.

Hendrix, M.J.C., Seftor, E.A., Hess, A.R., and Seftor, R.E.B. (2003a). Vasculogenic mimicry and tumour-cell plasticity: lessons from melanoma. Nat. Rev. Cancer *3*, 411–421.

Hendrix, M.J.C., Seftor, E.A., Kirschmann, D.A., Quaranta, V., and Seftor, R.E.B. (2003b). Remodeling of the microenvironment by aggressive melanoma tumor cells. In Annals of the New York Academy of Sciences, (John Wiley & Sons, Ltd), pp. 151–161.

Hendrix, M.J.C., Seftor, E.A., Hess, A.R., and Seftor, R.E.B. (2003c). Molecular plasticity of human melanoma cells. Oncogene *22*, 3070–3075.

Hess, A.R., Seftor, E.A., Gardner, L.M.G., Carles-Kinch, K., Schneider, G.B., Seftor, R.E.B., Kinch, M.S., and Hendrix, M.J.C. (2001). Molecular regulation of tumor cell vasculogenic mimicry by tyrosine phosphorylation: Role of epithelial cell kinase (eck/epha2). Cancer Res. *61*, 3250–3255.

Hess, A.R., Seftor, E.A., Gruman, L.M., Kinch, M.S., Seftor, R.E.B., and Hendrix, M.J.C. (2006). VE-cadherin regulates EphA2 in aggressive melanoma cells through a novel signaling pathway: Implications for vasculogenic mimicry. Cancer Biol. Ther. *5*, 228–233.

Hillebrand, L.E., and Reinheckel, T. (2019). Impact of proteolysis on cancer stem cell functions. Biochimie *166*, 214–222.

Holash, J., Maisonpierre, P.C., Compton, D., Boland, P., Alexander, C.R., Zagzag, D., Yancopoulos, G.D., and Wiegand, S.J. (1999). Vessel cooption, regression, and growth in tumors mediated by angiopoietins and VEGF. Science (80-.). *284*, 1994–1998.

Horowitz, N.A., Blevins, E.A., Miller, W.M., Perry, A.R., Talmage, K.E., Mullins, E.S., Flick, M.J., Queiroz, K.C.S., Shi, K., Spek, C.A., et al. (2011). Thrombomodulin is a determinant of metastasis through a mechanism linked to the thrombin binding domain but not the lectin-like domain. Blood *118*, 2889–2895.

Hsu, Y.P., Staton, C.A., Cross, N., and Buttle, D.J. (2012). Anti-angiogenic properties of ADAMTS-4 in vitro. Int. J. Exp. Pathol. *93*, 70–77.

Hsu, Y.Y., Shi, G.Y., Wang, K.C., Ma, C.Y., Cheng, T.L., and Wu, H.L. (2016).

Thrombomodulin promotes focal adhesion kinase activation and contributes to angiogenesis by binding to fibronectin. Oncotarget *7*, 68122–68139.

Huang, J., Sun, Y., Chen, H., Liao, Y., Li, S., Chen, C., and Yang, Z. (2019). ADAMTS5 acts as a tumor suppressor by inhibiting migration, invasion and angiogenesis in human gastric cancer. Gastric Cancer *22*, 287–301.

Hynes, R.O., and Naba, A. (2012). Overview of the matrisome-An inventory of extracellular matrix constituents and functions. Cold Spring Harb. Perspect. Biol. *4*, a004903.

Iida, H., Suzuki, M., Goitsuka, R., and Ueno, H. (2012). Hypoxia induces CD133 expression in human lung cancer cells by up-regulation of OCT3/4 and SOX2. Int. J. Oncol. *40*, 71–79.

Iruela-Arispe, M.L., Lombardo, M., Krutzsch, H.C., Lawler, J., and Roberts, D.D. (1999). Inhibition of angiogenesis by thrombospondin-1 is mediated by 2 independent regions within the type 1 repeats. Circulation *100*, 1423–1431.

Jain, R.K. (2005). Normalization of tumor vasculature: An emerging concept in antiangiogenic therapy. Science (80-.). *307*, 58–62.

Jain, R.K., and Carmeliet, P. (2012). SnapShot: Tumor Angiogenesis. Cell *149*, 1408-1408.e1.

Joshi, P., Kooshki, M., Aldrich, W., Varghai, D., Zborowski, M., Singh, A.D., and Triozzi, P.L. (2016). Expression of natural killer cell regulatory microRNA by uveal melanoma cancer stem cells. Clin. Exp. Metastasis *33*, 829–838.

Junttila, M.R., and De Sauvage, F.J. (2013). Influence of tumour micro-environment heterogeneity on therapeutic response. Nature *501*, 346–354.

Kalirai, H., Damato, B.E., and Coupland, S.E. (2011). Uveal melanoma cell lines contain stem-like cells that self-renew, produce differentiated progeny, and survive chemotherapy. Investig. Ophthalmol. Vis. Sci. *52*, 8458–8466.

Kelwick, R., Desanlis, I., Wheeler, G.N., and Edwards, D.R. (2015a). The ADAMTS (A Disintegrin and Metalloproteinase with Thrombospondin motifs) family. Genome Biol. *16*, 113.

Kelwick, R., Wagstaff, L., Decock, J., Roghi, C., Cooley, L.S., Robinson, S.D., Arnold, H., Gavrilović, J., Jaworski, D.M., Yamamoto, K., et al. (2015b). Metalloproteinase-dependent and -independent processes contribute to inhibition of breast cancer cell migration, angiogenesis and liver metastasis by a disintegrin and metalloproteinase with thrombospondin motifs-15. Int. J. Cancer *136*, E14–E26.

van Kempen, L.C.L., de Visser, K.E., and Coussens, L.M. (2006). Inflammation, proteases and cancer. Eur. J. Cancer *42*, 728–734.

Kern, C.B., Wessels, A., McGarity, J., Dixon, L.J., Alston, E., Argraves, W.S.,

Geeting, D., Nelson, C.M., Menick, D.R., and Apte, S.S. (2010). Reduced versican cleavage due to Adamts9 haploinsufficiency is associated with cardiac and aortic anomalies. Matrix Biol. *29*, 304–316.

Kirschmann, D.A., Seftor, E.A., Hardy, K.M., Seftor, R.E.B., and Hendrix, M.J.C. (2012). Molecular pathways: Vasculogenic mimicry in tumor cells: Diagnostic and therapeutic implications. Clin. Cancer Res. *18*, 2726–2732.

Koo, B.-H., Coe, D.M., Dixon, L.J., Somerville, R.P.T., Nelson, C.M., Wang, L.W., Young, M.E., Lindner, D.J., and Apte, S.S. (2010). ADAMTS9 is a cell-autonomously acting, anti-angiogenic metalloprotease expressed by microvascular endothelial cells. Am. J. Pathol. *176*, 1494–1504.

Kumar, S., Sharghi-Namini, S., Rao, N., and Ge, R. (2012). ADAMTS5 functions as an anti-angiogenic and anti-tumorigenic protein independent of its proteoglycanase activity. Am. J. Pathol. *181*, 1056–1068.

Kuno, K. (2013). ADAMTS1. In Handbook of Proteolytic Enzymes, (Academic Press), pp. 1156–1161.

Kuno, K., Kanada, N., Nakashima, E., Fujiki, F., Ichimura, F., and Matsushima, K. (1997). Molecular Cloning of a Gene Encoding a New Type of Metalloproteinase-disintegrin Family Protein with Thrombospondin Motifs as an Inflammation Associated Gene. J. Biol. Chem. *272*, 556–562.

Kurz, H., Burri, P.H., and Djonov, V.G. (2003). Angiogenesis and vascular remodeling by intussusception: From form to function. News Physiol. Sci. *18*, 65–70.

Lai, C.Y., Schwartz, B.E., and Hsu, M.Y. (2012). CD133+ melanoma subpopulations contribute to perivascular niche morphogenesis and tumorigenicity through vasculogenic mimicry. Cancer Res. *72*, 5111–5118.

Lapidot, T., Sirard, C., Vormoor, J., Murdoch, B., Hoang, T., Caceres-Cortes, J., Minden, M., Paterson, B., Caligiuri, M.A., and Dick, J.E. (1994). A cell initiating human acute myeloid leukaemia after transplantation into SCID mice. Nature *367*, 645–648.

Lee, N. V, Sato, M., Annis, D.S., Loo, J.A., Wu, L., Mosher, D.F., and Iruela-Arispe, M.L. (2006). ADAMTS1 mediates the release of antiangiogenic polypeptides from TSP1 and 2. EMBO J. *25*, 5270–5283.

Lee, Y.-J., Koch, M., Karl, D., Torres-Collado, A.X., Fernando, N.T., Rothrock, C., Kuruppu, D., Ryeom, S., Iruela-Arispe, M.L., and Yoon, S.S. (2010). Variable inhibition of thrombospondin 1 against liver and lung metastases through differential activation of metalloproteinase ADAMTS1. Cancer Res. *70*, 948–956.

Lemarchant, S., Dunghana, H., Pomeshchik, Y., Leinonen, H., Kolosowska, N., Korhonen, P., Kanninen, K.M., García-Berrocoso, T., Montaner, J., Malm, T., et al. (2016). Anti-inflammatory effects of ADAMTS-4 in a mouse model of ischemic stroke. Glia *64*, 1492–1507.

Lenos, K.J., Miedema, D.M., Lodestijn, S.C., Nijman, L.E., van den Bosch, T.,

Romero Ros, X., Lourenço, F.C., Lecca, M.C., van der Heijden, M., van Neerven, S.M., et al. (2018). Stem cell functionality is microenvironmentally defined during tumour expansion and therapy response in colon cancer. Nat. Cell Biol. *20*, 1193–1202.

Lima, M.A., Dos Santos, L., Turri, J.A., Nonogaki, S., Buim, M., Lima, J.F., De Jesus Viana Pinheiro, J., Bueno De Toledo Osório, C.A., Soares, F.A., and Freitas, V.M. (2016). Prognostic value of ADAMTS proteases and their substrates in epithelial ovarian cancer. Pathobiology *83*, 316–326.

Lind, T., Birch, M.A., and McKie, N. (2006). Purification of an insect derived recombinant human ADAMTS-1 reveals novel gelatin (type I collagen) degrading activities. Mol. Cell. Biochem. *281*, 95–102.

Liou, G.Y. (2019). CD133 as a regulator of cancer metastasis through the cancer stem cells. Int. J. Biochem. Cell Biol. *106*, 1–7.

Liu, T.J., Sun, B.C., Zhao, X.L., Zhao, X.M., Sun, T., Gu, Q., Yao, Z., Dong, X.Y., Zhao, N., and Liu, N. (2013). CD133 + cells with cancer stem cell characteristics associates with vasculogenic mimicry in triple-negative breast cancer. Oncogene *32*, 544–553.

Liu, Y., Li, F., Yang, Y.T., Xu, X.D., Chen, J.S., Chen, T.L., Chen, H.J., Zhu, Y.B., Lin, J.Y., Li, Y., et al. (2019). IGFBP2 promotes vasculogenic mimicry formation via regulating CD144 and MMP2 expression in glioma. Oncogene *38*, 1815–1831.

Liu, Y.J., Xu, Y., and Yu, Q. (2006). Full-length ADAMTS-1 and the ADAMTS-1 fragments display pro- and antimetastatic activity, respectively. Oncogene *25*, 2452–2467.

Lo, P.H.Y., Lung, H.L., Cheung, A.K.L., Apte, S.S., Chan, K.W., Kwong, F.M., Ko, J.M.Y., Cheng, Y., Law, S., Srivastava, G., et al. (2010). Extracellular Protease ADAMTS9 Suppresses Esophageal and Nasopharyngeal Carcinoma Tumor Formation by Inhibiting Angiogenesis. Cancer Res. *70*, 5567–5576.

Lu, P., Weaver, V.M., and Werb, Z. (2012). The extracellular matrix: a dynamic niche in cancer progression. J. Cell Biol. *196*, 395–406.

Lugano, R., Ramachandran, M., and Dimberg, A. (2020). Tumor angiogenesis: causes, consequences, challenges and opportunities. Cell. Mol. Life Sci. *77*, 1745–1770.

Luo, Q., Wang, J., Zhao, W., Peng, Z., Liu, X., Li, B., Zhang, H., Shan, B., Zhang, C., and Duan, C. (2020). Vasculogenic mimicry in carcinogenesis and clinical applications. J. Hematol. Oncol. *13*, 19.

Luque, A., Carpizo, D.R., and Iruela-Arispe, M.L. (2003). ADAMTS1/METH1 inhibits endothelial cell proliferation by direct binding and sequestration of VEGF165. J. Biol. Chem. *278*, 23656–23665.

M. Dunleavey, J., and C. Dudley, A. (2012). Vascular Mimicry: Concepts and Implications for Anti-Angiogenic Therapy. Curr. Angiogenesise *1*, 133–138.

Mabeta, P. (2020). Paradigms of vascularization in melanoma: Clinical significance and potential for therapeutic targeting. Biomed. Pharmacother. *127*, 110135.

Malemud, C.J. (2019). Inhibition of MMPs and ADAM/ADAMTS. Biochem. Pharmacol. *165*, 33–40.

Maniotis, A.J., Folberg, R., Hess, A., Seftor, E.A., Gardner, L.M., Pe'er, J., Trent, J.M., Meltzer, P.S., and Hendrix, M.J. (1999). Vascular channel formation by human melanoma cells in vivo and in vitro: vasculogenic mimicry. Am. J. Pathol. *155*, 739–752.

Mao, X.G., Xue, X.Y., Wang, L., Zhang, X., Yan, M., Tu, Y.Y., Lin, W., Jiang, X.F., Ren, H.G., Zhang, W., et al. (2013). CDH5 is specifically activated in glioblastoma stemlike cells and contributes to vasculogenic mimicry induced by hypoxia. Neuro. Oncol. *15*, 865–879.

Martino-Echarri, E., Fernández-Rodríguez, R., Rodríguez-Baena, F.J., Barrientos-Durán, A., Torres-Collado, A.X., Del Carmen Plaza-Calonge, M., Amador-Cubero, S., Cortés, J., Reynolds, L.E., Hodivala-Dilke, K.M., et al. (2013). Contribution of ADAMTS1 as a tumor suppressor gene in human breast carcinoma. Linking its tumor inhibitory properties to its proteolytic activity on nidogen-1 and nidogen-2. Int. J. Cancer *133*, 2315–2324.

Martino-Echarri, E., Fernández-Rodríguez, R., Bech-Serra, J.J., Plaza-Calonge, M. del C., Vidal, N., Casal, C., Colomé, N., Seoane, J., Canals, F., and Rodríguez-Manzaneque, J.C. (2014). Relevance of IGFBP2 proteolysis in glioma and contribution of the extracellular protease ADAMTS1. Oncotarget *5*, 4295–4304.

Marusyk, A., and Polyak, K. (2010). Tumor heterogeneity: Causes and consequences. Biochim. Biophys. Acta - Rev. Cancer *1805*, 105–117.

Masiero, M., Simões, F.C., Han, H.D., Snell, C., Peterkin, T., Bridges, E., Mangala, L.S., Wu, S.Y.Y., Pradeep, S., Li, D., et al. (2013). A core human primary tumor angiogenesis signature identifies the endothelial orphan receptor ELTD1 as a key regulator of angiogenesis. Cancer Cell *24*, 229–241.

Masui, T., Hosotani, R., Tsuji, S., Miyamoto, Y., Yasuda, S., Ida, J., Nakajima, S., Kawaguchi, M., Kobayashi, H., Koizumi, M., et al. (2001). Expression of METH-1 and METH-2 in Pancreatic Cancer. Clin. Cancer Res. *7*, 3437–3443.

Matthews, R.T., Gary, S.C., Zerillo, C., Pratta, M., Solomon, K., Arner, E.C., and Hockfield, S. (2000). Brain-enriched hyaluronan binding (BEHAB)/brevican cleavage in a glioma cell line is mediated by a disintegrin and metalloproteinase with thrombospondin motifs (ADAMTS) family member. J. Biol. Chem. *275*, 22695–22703.

McDonald, D.M., Munn, L., and Jain, R.K. (2000). Vasculogenic mimicry: How convincing, how novel, and how significant? Am. J. Pathol. *156*, 383–388.

Medina, R.J., Barber, C.L., Sabatier, F., Dignat-George, F., Melero-Martin,

J.M., Khosrotehrani, K., Ohneda, O., Randi, A.M., Chan, J.K.Y., Yamaguchi, T., et al. (2017). Endothelial progenitors: A consensus statement on nomenclature. Stem Cells Transl. Med. *6*, 1316–1320.

Miguel, R.F., Pollak, A., and Lubec, G. (2005). Metalloproteinase ADAMTS-1 but not ADAMTS-5 is manifold overexpressed in neurodegenerative disorders as Down syndrome, Alzheimer's and Pick's disease. Mol. Brain Res. *133*, 1–5.

Miraglia, S., Godfrey, W., Yin, A.H., Atkins, K., Warnke, R., Holden, J.T., Bray, R.A., Waller, E.K., and Buck, D.W. (1997). A novel five-transmembrane hematopoietic stem cell antigen: Isolation, characterization, and molecular cloning. Blood *90*, 5013–5021.

Mohamedi, Y., Fontanil, T., Cobo, T., Cal, S., and Obaya, A.J. (2020). New insights into adamts metalloproteases in the central nervous system. Biomolecules *10*, 403.

Monzani, E., Facchetti, F., Galmozzi, E., Corsini, E., Benetti, A., Cavazzin, C., Gritti, A., Piccinini, A., Porro, D., Santinami, M., et al. (2007). Melanoma contains CD133 and ABCG2 positive cells with enhanced tumourigenic potential. Eur. J. Cancer *43*, 935–946.

Mushtaq, M.U., Papadas, A., Pagenkopf, A., Flietner, E., Morrow, Z., Chaudhary, S.G., and Asimakopoulos, F. (2018). Tumor matrix remodeling and novel immunotherapies: The promise of matrix-derived immune biomarkers. J. Immunother. Cancer *6*, 65.

Nakada, M., Miyamori, H., Kita, D., Takahashi, T., Yamashita, J., Sato, H., Miura, R., Yamaguchi, Y., and Okada, Y. (2005). Human glioblastomas overexpress ADAMTS-5 that degrades brevican. Acta Neuropathol. *110*, 239–246.

Nakamura, K., Hirohata, S., Murakami, T., Miyoshi, T., Demircan, K., Oohashi, T., Ogawa, H., Koten, K., Toeda, K., Kusachi, S., et al. (2004). Dynamic induction of ADAMTS1 gene in the early phase of acute myocardial infarction. J. Biochem. *136*, 439–446.

Nomura, A., Banerjee, S., Chugh, R., Dudeja, V., Yamamoto, M., Vickers, S.M., and Saluja, A.K. (2015). CD133 initiates tumors, induces epithelial-mesenchymal transition and increases metastasis in pancreatic cancer. Oncotarget *6*, 8313–8322.

Obika, M., Ogawa, H., Takahashi, K., Li, J., Hatipoglu, O.F., Cilek, M.Z., Miyoshi, T., Inagaki, J., Ohtsuki, T., Kusachi, S., et al. (2012). Tumor growth inhibitory effect of ADAMTS1 is accompanied by the inhibition of tumor angiogenesis. Cancer Sci. *103*, 1889–1897.

De Oliveira, A.D.S., Yang, L., Echevarria-Lima, J., Monteiro, R.Q., and Rezaie, A.R. (2014). Thrombomodulin modulates cell migration in human melanoma cell lines. Melanoma Res. *24*, 11–19.

Onken, M.D., Worley, L.A., Ehlers, J.P., and Harbour, J.W. (2004). Gene

expression profiling in uveal melanoma reveals two molecular classes and predicts metastatic death. Cancer Res. *64*, 7205–7209.

Pardali, E., van der Schaft, D.W.J., Wiercinska, E., Gorter, a, Hogendoorn, P.C.W., Griffioen, A.W., and ten Dijke, P. (2011). Critical role of endoglin in tumor cell plasticity of Ewing sarcoma and melanoma. Oncogene *30*, 334–345.

Peichev, M., Naiyer, A.J., Pereira, D., Zhu, Z., Lane, W.J., Williams, M., Oz, M.C., Hicklin, D.J., Witte, L., Moore, M.A.S., et al. (2000). Expression of VEGFR-2 and AC133 by circulating human CD34+ cells identifies a population of functional endothelial precursors. Blood *95*, 952–958.

Perego, M., Tortoreto, M., Tragni, G., Mariani, L., Deho, P., Carbone, A., Santinami, M., Patuzzo, R., Mina, P. Della, Villa, A., et al. (2010). Heterogeneous phenotype of human melanoma cells with in vitro and in vivo features of tumor-initiating cells. J. Invest. Dermatol. *130*, 1877–1886.

Peris-Torres, C., Plaza-Calonge, M.D.C., López-Domínguez, R., Domínguez-García, S., Barrientos-Durán, A., Carmona-Sáez, P., and Rodríguez-Manzaneque, J.C. (2020a). Extracellular protease adamts1 is required at early stages of human uveal melanoma development by inducing stemness and endothelial-like features on tumor cells. Cancers (Basel). *12*, 1–20.

Peris-Torres, C., Serrano, O., Plaza-Calonge, M. del C., and Rodríguez-Manzaneque, J.C. (2020b). Inhibition of ADAMTS1 Expression by Lentiviral CRISPR/Cas9 Gene Editing Technology. In Methods in Molecular Biology, (New York, NY: Humana Press Inc.), pp. 13–24.

Pickup, M.W., Mouw, J.K., and Weaver, V.M. (2014). The extracellular matrix modulates the hallmarks of cancer. EMBO Rep. *15*, 1243–1253.

Poltavets, V., Kochetkova, M., Pitson, S.M., and Samuel, M.S. (2018). The role of the extracellular matrix and its molecular and cellular regulators in cancer cell plasticity. Front. Oncol. *8*, 431.

Polyak, K., Haviv, I., and Campbell, I.G. (2009). Co-evolution of tumor cells and their microenvironment. Trends Genet. *25*, 30–38.

Puchalapalli, M., Zeng, X., Mu, L., Anderson, A., Hix Glickman, L., Zhang, M., Sayyad, M.R., Mosticone Wangensteen, S., Clevenger, C. V, and Koblinski, J.E. (2016). NSG Mice Provide a Better Spontaneous Model of Breast Cancer Metastasis than Athymic (Nude) Mice. PLoS One *11*, e0163521.

Quesada-Gómez, J.M., Santiago-Mora, R., Navarro-Valverde, C., Dorado, G., and Casado-Díaz, A. (2015). Stimulation of in-vitro angiogenesis by low concentrations of risedronate is mitigated by 1,25-dihydroxyvitamin D3 or 24,25-dihydroxyvitamin D3. J. Steroid Biochem. Mol. Biol. *148*, 214–218.

Rao, N., Ke, Z., Liu, H., Ho, C.-J.J., Kumar, S., Xiang, W., Zhu, Y., and Ge, R. (2013). ADAMTS4 and its proteolytic fragments differentially affect melanoma growth and angiogenesis in mice. Int. J. Cancer *133*, 294–306.

Ren, P., Zhang, L., Xu, G., Palmero, L.C., Albini, P.T., Coselli, J.S., Shen, Y.H., and Lemaire, S.A. (2013). ADAMTS-1 and ADAMTS-4 levels are elevated in thoracic aortic aneurysms and dissections. Ann. Thorac. Surg. *95*, 570–577.

Reya, T., Morrison, S.J., Clarke, M.F., and Weissman, I.L. (2001). Stem cells, cancer, and cancer stem cells. Nature *414*, 105–111.

Reynolds, L.E., Watson, A.R., Baker, M., Jones, T.A., D'Amico, G., Robinson, S.D., Joffre, C., Garrido-Urbani, S., Rodriguez-Manzaneque, J.C., Martino-Echarri, E., et al. (2010). Tumour angiogenesis is reduced in the Tc1 mouse model of Down's syndrome. Nature *465*, 813–817.

Ribatti, D., Nico, B., Floris, C., Mangieri, D., Piras, F., Ennas, M.G., Vacca, A., and Sirigu, P. (2005). Microvascular density, vascularendothelial growth factor immunoreactivity in tumor cells, vessel diameter and intussusceptive microvascular growth in primary melanoma. Oncol. Rep. *14*, 81–84.

Ricci-Vitiani, L., Pallini, R., Biffoni, M., Todaro, M., Invernici, G., Cenci, T., Maira, G., Parati, E.A., Stassi, G., Larocca, L.M., et al. (2010). Tumour vascularization via endothelial differentiation of glioblastoma stem-like cells. Nature *468*, 824–830.

Ricciardelli, C., Frewin, K.M.M., Tan, I.D.A.D.A., Williams, E.D.D., Opeskin, K., Pritchard, M. a. a., Ingman, W.V. V., and Russell, D.L.L. (2011). The ADAMTS1 protease gene is required for mammary tumor growth and metastasis. Am. J. Pathol. *179*, 3075–3085.

Risau, W., and Flamme, I. (1995). Vasculogenesis. Annu. Rev. Cell Dev. Biol. *11*, 73–91.

Ritchie, M.E., Phipson, B., Wu, D., Hu, Y., Law, C.W., Shi, W., and Smyth, G.K. (2015). limma powers differential expression analyses for RNA-sequencing and microarray studies. Nucleic Acids Res. *43*, e47.

Robertson, A.G., Shih, J., Yau, C., Gibb, E.A., Oba, J., Mungall, K.L., Hess, J.M., Uzunangelov, V., Walter, V., Danilova, L., et al. (2017). Integrative Analysis Identifies Four Molecular and Clinical Subsets in Uveal Melanoma. Cancer Cell *32*, 204-220.e15.

Rodríguez-Baena, F.J., Redondo-García, S., Peris-Torres, C., Martino-Echarri, E., Fernández-Rodríguez, R., Plaza-Calonge, M. del C., Anderson, P., and Rodríguez-Manzaneque, J.C. (2018a). ADAMTS1 protease is required for a balanced immune cell repertoire and tumour inflammatory response. Sci. Rep. *8*, 13103.

Rodríguez-Baena, F.J., Redondo-García, S., Plaza-Calonge, M. del C., Fernández-Rodríguez, R., and Rodríguez-Manzaneque, J.C. (2018b). Evaluation of tumor vasculature using a syngeneic tumor model in wild-type and genetically modified mice. In Methods in Molecular Biology, pp. 179–192.

Rodríguez-Manzaneque, J.C., Milchanowski, A.B., Dufour, E.K., Leduc, R.,

and Iruela-Arispe, M.L. (2000). Characterization of METH-1/ADAMTS1 processing reveals two distinct active forms. J. Biol. Chem. *275*, 33471–33479.

Rodríguez-Manzaneque, J.C., Westling, J., Thai, S.N.M., Luque, A., Knauper, V., Murphy, G., Sandy, J.D., and Iruela-Arispe, M.L. (2002). ADAMTS1 cleaves aggrecan at multiple sites and is differentially inhibited by metalloproteinase inhibitorsq. Biochem. Biophys. Res. Commun. *293*, 501–508.

Rodríguez-Manzaneque, J.C., Carpizo, D., Plaza-Calonge, M. del C., Torres-Collado, A.X., Thai, S.N.-M., Simons, M., Horowitz, A., and Iruela-Arispe, M.L. (2009). Cleavage of syndecan-4 by ADAMTS1 provokes defects in adhesion. Int. J. Biochem. Cell Biol. *41*, 800–810.

Rodríguez-Manzaneque, J.C., Fernández-Rodríguez, R., Rodríguez-Baena, F.J., and Iruela-Arispe, M.L. (2015). ADAMTS proteases in vascular biology. Matrix Biol. *44-46C*, 38–45.

Romagnani, P., Annunziato, F., Liotta, F., Lazzeri, E., Mazzinghi, B., Frosali, F., Cosmi, L., Maggi, L., Lasagni, L., Scheffold, A., et al. (2005). CD14+CD34low cells with stem cell phenotypic and functional features are the major source of circulating endothelial progenitors. Circ. Res. *97*, 314–322.

Rossi, G.R., Trindade, E.S., and Souza-Fonseca-Guimaraes, F. (2020). Tumor Microenvironment-Associated Extracellular Matrix Components Regulate NK Cell Function. Front. Immunol. *11*, 73.

Royer-Bertrand, B., Torsello, M., Rimoldi, D., El Zaoui, I., Cisarova, K., Pescini-Gobert, R., Raynaud, F., Zografos, L., Schalenbourg, A., Speiser, D., et al. (2016). Comprehensive Genetic Landscape of Uveal Melanoma by Whole-Genome Sequencing. Am. J. Hum. Genet. *99*, 1190–1198.

Ruf, W., Seftor, E.A., Petrovan, R.J., Weiss, R.M., Gruman, L.M., Margaryan, N. V., Seftor, R.E.B., Miyagi, Y., and Hendrix, M.J.C. (2003). Differential role of tissue factor pathway inhibitors 1 and 2 in melanoma vasculogenic mimicry. Cancer Res. *63*, 5381–5389.

Rybak, S.M., Sanovich, E., Hollingshead, M.G., Borgel, S.D., Newton, D.L., Melillo, G., Kong, D., Kaur, G., and Sausville, E.A. (2003). "Vasocrine" formation of tumor cell-lined vascular spaces: Implications for rational design of antiangiogenic therapies. Cancer Res. *63*, 2812–2819.

Saigusa, S., Tanaka, K., Toiyama, Y., Yokoe, T., Okugawa, Y., Ioue, Y., Miki, C., and Kusunoki, M. (2009). Correlation of CD133, OCT4, and SOX2 in rectal cancer and their association with distant recurrence after chemoradiotherapy. Ann. Surg. Oncol. *16*, 3488–3498.

Sandy, J.D., Westling, J., Kenagy, R.D., Iruela-Arispe, M.L., Verscharen, C., Rodriguez-Mazaneque, J.C., Zimmermann, D.R., Lemire, J.M., Fischer, J.W., Wight, T.N., et al. (2001). Versican V1 Proteolysis in Human Aorta in Vivo Occurs at the Glu 441-Ala442 Bond, a Site That Is Cleaved by Recombinant

ADAMTS-1 and ADAMTS-4. J. Biol. Chem. *276*, 13372–13378.

Santini, R., Pietrobono, S., Pandolfi, S., Montagnani, V., D'Amico, M., Penachioni, J.Y., Vinci, M.C., Borgognoni, L., and Stecca, B. (2014). SOX2 regulates self-renewal and tumorigenicity of human melanoma-initiating cells. Oncogene 1–12.

van der Schaft, D.W.J., Seftor, R.E.B., Seftor, E.A., Hess, A.R., Gruman, L.M., Kirschmann, D.A., Yokoyama, Y., Griffioen, A.W., and Hendrix, M.J.C. (2004). Effects of angiogenesis inhibitors on vascular network formation by human endothelial and melanoma cells. J. Natl. Cancer Inst. *96*, 1473–1477.

van Schaijik, B., Davis, P.F., Wickremesekera, A.C., Tan, S.T., and Itinteang, T. (2018). Subcellular localisation of the stem cell markers OCT4, SOX2, NANOG, KLF4 and c-MYC in cancer: a review. J. Clin. Pathol. *71*, 88–91.

Schneider, C.A., Rasband, W.S., and Eliceiri, K.W. (2012). NIH Image to ImageJ: 25 years of image analysis. Nat. Methods *9*, 671–675.

Seegar, T.C.M., Eller, B., Tzvetkova-Robev, D., Kolev, M. V., Henderson, S.C., Nikolov, D.B., and Barton, W.A. (2010). Tie1-Tie2 Interactions Mediate Functional Differences between Angiopoietin Ligands. Mol. Cell *37*, 643–655.

Seftor, E.A., Meltzer, P.S., Kirschmann, D.A., Pe'er, J., Maniotis, A.J., Trent, J.M., Folberg, R., and Hendrix, M.J.C. (2002). Molecular determinants of human uveal melanoma invasion and metastasis. Clin. Exp. Metastasis *19*, 233–246.

Seftor, R.E.B., Seftor, E.A., Koshikawa, N., Meltzer, P.S., Gardner, L.M.G., Bilban, M., Stetler-Stevenson, W.G., Quaranta, V., and Hendrix, M.J.C. (2001). Cooperative interactions of laminin 5 γ2 chain, matrix metalloproteinase-2, and membrane type-1-matrix/metalloproteinase are required for mimicry of embryonic vasculogenesis by aggressive melanoma. Cancer Res. *61*, 6322–6327.

Shain, A.H., Bagger, M.M., Yu, R., Chang, D., Liu, S., Vemula, S., Weier, J.F., Wadt, K., Heegaard, S., Bastian, B.C., et al. (2019). The genetic evolution of metastatic uveal melanoma. Nat. Genet. *51*, 1123–1130.

Shang, X.Q., Liu, K.L., Li, Q., Lao, Y.Q., Li, N.S., and Wu, J. (2020). ADAMTS4 is upregulated in colorectal cancer and could be a useful prognostic indicator of colorectal cancer. Rev. Assoc. Med. Bras. *66*, 42–47.

Sharma, N., Seftor, R.E.B., Seftor, E.A., Gruman, L.M., Heidger, P.M., Cohen, M.B., Lubaroff, D.M., and Hendrix, M.J.C. (2002). Prostatic tumor cell plasticity involves cooperative interactions of distinct phenotypic subpopulations: Role in vasculogenic mimicry. Prostate *50*, 189–201.

Shirakawa, K., Kobayashi, H., Heike, Y., Kawamoto, S., Brechbiel, M.W., Kasumi, F., Iwanaga, T., Konishi, F., Terada, M., and Wakasugi, H. (2002). Hemodynamics in vasculogenic mimicry and angiogenesis of inflammatory breast cancer xenograft. Cancer Res. *62*, 560–566.

Smith, S.J., Tilly, H., Ward, J.H., Macarthur, D.C., Lowe, J., Coyle, B., and Grundy, R.G. (2012). CD105 (Endoglin) exerts prognostic effects via its role in the microvascular niche of paediatric high grade glioma. Acta Neuropathol. *124*, 99–110.

Smith, S.J., Ward, J.H., Tan, C., Grundy, R.G., and Rahman, R. (2015). Endothelial-like malignant glioma cells in dynamic three dimensional culture identifies a role for VEGF and FGFR in a tumor-derived angiogenic response. Oncotarget *6*, 22191–22205.

Somerville, R.P.T., Longpre, J.M., Jungers, K.A., Engle, J.M., Ross, M., Evanko, S., Wight, T.N., Leduc, R., and Aptell, S.S. (2003). Characterization of ADAMTS-9 and ADAMTS-20 as a distinct ADAMTS subfamily related to Caenorhabditis elegans GON-1. J. Biol. Chem. *278*, 9503–9513.

Song, W.S., Yang, Y.P., Huang, C.S., Lu, K.H., Liu, W.H., Wu, W.W., Lee, Y.Y., Lo, W.L., Lee, S.D., Chen, Y.W., et al. (2016). Sox2, a stemness gene, regulates tumor-initiating and drug-resistant properties in CD133-positive glioblastoma stem cells. J. Chinese Med. Assoc. *79*, 538–545.

Sood, A.K., Seftor, E.A., Fletcher, M.S., Gardner, L.M.G., Heidger, P.M., Buller, R.E., Seftor, R.E.B., and Hendrix, M.J.C. (2001). Molecular determinants of ovarian cancer plasticity. Am. J. Pathol. *158*, 1279–1288.

Sood, A.K., Fletcher, M.S., and Hendrix, M.J.C. (2002). The Embryonic-Like Properties of Aggressive Human Tumor Cells. J. Soc. Gynecol. Investig. *9*, 2–9.

Sorokin, L. (2010). The impact of the extracellular matrix on inflammation. Nat. Rev. Immunol. *10*, 712–723.

Su, S.C., Mendoza, E.A., Kwak, H. Il, and Bayless, K.J. (2008). Molecular profile of endothelial invasion of three-dimensional collagen matrices: Insights into angiogenic sprout induction in wound healing. Am. J. Physiol. - Cell Physiol. *295*, C1215–C1229.

Supek, F., Bošnjak, M., Škunca, N., and Šmuc, T. (2011). REVIGO Summarizes and Visualizes Long Lists of Gene Ontology Terms. PLoS One *6*, e21800.

Takahashi, K., and Yamanaka, S. (2006). Induction of Pluripotent Stem Cells from Mouse Embryonic and Adult Fibroblast Cultures by Defined Factors. Cell *126*, 663–676.

Thankamony, A.P., Saxena, K., Murali, R., Jolly, M.K., and Nair, R. (2020). Cancer Stem Cell Plasticity – A Deadly Deal. Front. Mol. Biosci. *7*, 79.

Thies, A., Mangold, U., Moll, I., and Schumacher, U. (2001). PAS-positive loops and networks as a prognostic indicator in cutaneous malignant melanoma. J. Pathol. *195*, 537–542.

Thill, M., Berna, M.J., Grierson, R., Reinhart, I., Voelkel, T., Piechaczek, C., Galambos, P., Jager, M.J., Richard, G., Lange, C., et al. (2011). Expression of CD133 and other putative stem cell markers in uveal melanoma. Melanoma

Res. *21*, 405–416.

Thornton, S., Coupland, S.E., Olohan, L., Sibbring, J.S., Kenny, J.G., Hertz-Fowler, C., Liu, X., Haldenby, S., Heimann, H., Hussain, R., et al. (2020). Targeted next-generation sequencing of 117 routine clinical samples provides further insights into the molecular landscape of uveal melanoma. Cancers (Basel). *12*, 1039.

Tolsma, S.S., Volpert, O. V, Good, D.J., Frazier, W.A., Polverini, P.J., and Bouck, N. (1993). Peptides derived from two separate domains of the matrix protein thrombospondin-1 have anti-angiogenic activity. J. Cell Biol. *122*, 497–511.

Torres-Collado, A.X., Kisiel, W., Iruela-Arispe, M.L., and Rodríguez-Manzaneque, J.C. (2006). ADAMTS1 interacts with, cleaves, and modifies the extracellular location of the matrix inhibitor tissue factor pathway inhibitor-2. J. Biol. Chem. *281*, 17827–17837.

Vailhé, B., Vittet, D., and Feige, J.J. (2001). In vitro models of vasculogenesis and angiogenesis. Lab. Investig. *81*, 439–452.

Valdivia, A., Mingo, G., Aldana, V., Pinto, M.P., Ramirez, M., Retamal, C., Gonzalez, A., Nualart, F., Corvalan, A.H., and Owen, G.I. (2019). Fact or Fiction, It Is Time for a Verdict on Vasculogenic Mimicry? Front. Oncol. *9*, 680.

Vazquez, F., Hastings, G., Ortega, M. -a., Lane, T.F., Oikemus, S., Lombardo, M., and Iruela-Arispe, M.L. (1999). METH-1, a Human Ortholog of ADAMTS-1, and METH-2 Are Members of a New Family of Proteins with Angio-inhibitory Activity. J. Biol. Chem. *274*, 23349–23357.

Viallard, C., and Larrivée, B. (2017). Tumor angiogenesis and vascular normalization: alternative therapeutic targets. Angiogenesis *20*, 409–426.

Vitale, I., Manic, G., Coussens, L.M., Kroemer, G., and Galluzzi, L. (2019). Macrophages and Metabolism in the Tumor Microenvironment. Cell Metab. *30*, 36–50.

Vogelstein, B., Papadopoulos, N., Velculescu, V.E., Zhou, S., Diaz, L.A., and Kinzler, K.W. (2013). Cancer genome landscapes. Science (80-.). *340*, 1546–1558.

Vong, S., and Kalluri, R. (2011). The Role of Stromal Myofibroblast and Extracellular Matrix in Tumor Angiogenesis. Genes and Cancer *2*, 1139–1145.

Wågsäter, D., Björk, H., Zhu, C., Björkegren, J., Valen, G., Hamsten, A., and Eriksson, P. (2008). ADAMTS-4 and -8 are inflammatory regulated enzymes expressed in macrophage-rich areas of human atherosclerotic plaques. Atherosclerosis *196*, 514–522.

Walker, C., Mojares, E., and Del Río Hernández, A. (2018). Role of extracellular matrix in development and cancer progression. Int. J. Mol. Sci. *19*.

Wang, R., Chadalavada, K., Wilshire, J., Kowalik, U., Hovinga, K.E., Geber, A., Fligelman, B., Leversha, M., Brennan, C., and Tabar, V. (2010). Glioblastoma stem-like cells give rise to tumour endothelium. Nature *468*, 829–835.

Warso, M.A., Maniotis, A.J., Chen, X., Majumdar, D., Patel, M.K., Shilkaitis, A., Das Gupta, T.K., and Folberg, R. (2001). Prognostic significance of periodic acid-schiff-positive patterns in primary cutaneous melanoma. Clin. Cancer Res. *7*, 473–477.

Wen, Y., Lin, Y., Chu, C., Yang, Y., Yang, S., Liu, Y., Hsiao, M., Lee, W., and Chien, M. (2020). Melatonin-triggered post-transcriptional and post-translational modifications of ADAMTS1 coordinately retard tumorigenesis and metastasis of renal cell carcinoma. J. Pineal Res. *May 14*.

Whitmore, S.S., Braun, T.A., Skeie, J.M., Haas, C.M., Sohn, E.H., Stone, E.M., Scheetz, T.E., and Mullins, R.F. (2013). Altered gene expression in dry age-related macular degeneration suggests early loss of choroidal endothelial cells. Mol. Vis. *19*, 2274–2297.

Widmer, D.S., Cheng, P.F., Eichhoff, O.M., Belloni, B.C., Zipser, M.C., Schlegel, N.C., Javelaud, D., Dummer, R., and Hoek, K.S. (2012). Systematic classification of melanoma cells by phenotype-specific gene expression mapping. Pigment Cell Melanoma Res. *25*, 343–353.

Wimasis (2016). WimTube: Tube Formation Assay Image Analysis Solution. Release 4.0. Available from: https://www.wimasis.com/en/products/13/WimTube.

Wu, T., and Dai, Y. (2017). Tumor microenvironment and therapeutic response. Cancer Lett. *387*, 61–68.

Wu, H.B., Yang, S., Weng, H.Y., Chen, Q., Zhao, X.L., Fu, W.J., Niu, Q., Ping, Y.F., Wang, J.M., Zhang, X., et al. (2017). Autophagy-induced KDR/VEGFR-2 activation promotes the formation of vasculogenic mimicry by glioma stem cells. Autophagy *13*, 1528–1542.

Xu, Z., Yu, Y., and Duh, E.J. (2006). Vascular endothelial growth factor upregulates expression of ADAMTS1 in endothelial cells through protein kinase C signaling. Investig. Ophthalmol. Vis. Sci. *47*, 4059–4066.

Yang, L., Shi, P., Zhao, G., Xu, J., Peng, W., Zhang, J., Zhang, G., Wang, X., Dong, Z., Chen, F., et al. (2020). Targeting cancer stem cell pathways for cancer therapy. Signal Transduct. Target. Ther. *5*, 8.

Yao, X., Ping, Y., Liu, Y., Chen, K., Yoshimura, T., Liu, M., Gong, W., Chen, C., Niu, Q., Guo, D., et al. (2013). Vascular endothelial growth factor receptor 2 (VEGFR-2) plays a key role in vasculogenic mimicry formation, neovascularization and tumor initiation by Glioma stem-like cells. PLoS One *8*, e57188.

Yao, X. hong, Ping, Y. fang, and Bian, X. wu (2011). Contribution of cancer stem cells to tumor vasculogenic mimicry. Protein Cell *2*, 266–272.

Yu, G., Wang, L.G., Han, Y., and He, Q.Y. (2012). ClusterProfiler: An R package for comparing biological themes among gene clusters. Omi. A J. Integr. Biol. *16*, 284–287.

Zhou, Y., Zhu, Y., Fan, X., Zhang, C., Wang, Y., Zhang, L., Zhang, H., Wen, T., Zhang, K., Huo, X., et al. (2017). NID1, a new regulator of EMT required for metastasis and chemoresistance of ovarian cancer cells. Oncotarget *8*, 33110–33121.

ADDITIONAL INFORMATION

1. Original publication that supports this thesis

Part of the work developed in this thesis is supported by the following original publication:

Peris-Torres, C.; Plaza-Calonge, M.C.; López-Domínguez, R.; Domínguez-García, S.; Barrientos-Durán, A.; Carmona-Sáez, P.; Rodríguez-Manzaneque, J.C. Extracellular Protease ADAMTS1 Is Required at Early Stages of Human Uveal Melanoma Development by Inducing Stemness and Endothelial-Like Features on Tumor Cells. *Cancers* **2020**, *12*, 801.

Cancers is a MDPI Open Access journal, which therefore means that "*No special permission is required to reuse all or part of article published by MDPI, including figures and tables. For articles published under an open access Creative Common CC BY license, any part of the article may be reused without permission provided that the original article is clearly cited. Reuse of an article does not imply endorsement by the authors or MDPI*" (https://www.mdpi.com/openaccess).

For that reason, this publication is attached to the thesis as it was originally published.

cancers

MDPI

Article

Extracellular Protease ADAMTS1 Is Required at Early Stages of Human Uveal Melanoma Development by Inducing Stemness and Endothelial-Like Features on Tumor Cells

Carlos Peris-Torres [1], María del Carmen Plaza-Calonge [1], Raúl López-Domínguez [1], Silvia Domínguez-García [1], Antonio Barrientos-Durán [1], Pedro Carmona-Sáez [1,2] and Juan Carlos Rodríguez-Manzaneque [1,*]

[1] GENYO. Centre for Genomics and Oncological Research: Pfizer/Universidad de Granada/Junta de Andalucía, 114, 18016 Granada, Spain
[2] Department of Statistics and Operational Research, University of Granada, 18071 Granada, Spain
* Correspondence: juancarlos.rodriguez@genyo.es; Tel.: +0034-958-715500 (ext. 118)

Received: 5 February 2020; Accepted: 24 March 2020; Published: 27 March 2020

Abstract: Extracellular matrix remodeling within the tumor microenvironment has been recognized as a relevant dynamic framework during tumor growth. However, research on proteases that trigger this remodeling keeps revealing a wide range of actions including both pro- and anti-tumorigenic. The extracellular protease *ADAMTS1* exemplifies this dual role. In this work, we first confirmed a positive correlation of *ADAMTS1* with endothelial-like phenotype of human melanoma cells together with the finding of associated signatures, including key genes such as endothelial *CDH5*. Using a CRISPR-Cas9 approach, we observed that the inhibition of *ADAMTS1* in an aggressive uveal melanoma model compromised its endothelial-like properties, and more importantly, caused a robust blockade on the progression of tumor xenografts. Although vasculature emerged affected in *ADAMTS1*-deficient tumors, the most relevant action implied the downregulation of endothelial *CDH5* in tumor cells, in association with stemness markers. Indeed, melanoma sphere assays also revealed a deficient commitment to form spheres in the absence of *ADAMTS1*, directly correlating with stemness markers and, remarkably, also with CDH5. Finally, taking advantage of advanced bioinformatics tools and available public data of uveal melanomas, we disclosed new prognosis factors, including endothelial elements and ADAMTS proteases. Our findings support the key role of ADAMTS proteases for uveal melanoma development since earlier stages, modulating the complex crosstalk between extracellular matrix and the induction of stemness and endothelial-like features. To our knowledge, this is the first report that supports the development of therapeutic targets on the extracellular matrix to overcome uveal melanoma.

Keywords: ADAMTS; cancer stem cell; endothelial-like phenotype; extracellular matrix; vasculogenic mimicry

1. Introduction

The tumor microenvironment (TME) has been highlighted as a key player during tumor development, providing specific signals that support cell invasion, proliferation and phenotypic plasticity [1]. TME is extremely dynamic, involving all its cellular and extracellular constituents, and its full understanding still requires a multilayered research to identify new targets and biomarkers [2]. On the extracellular side, the actions of a variety of proteases contributed to such dynamism by the alteration of multiple pathways with impact during all stages of neoplasias. In fact, proteolytic activity

has been widely acknowledged in different tumor types [3]. Among these proteases, studies on ADAMTS1, first member of the ADAMTS (A Disintegrin And Metalloprotease with ThromboSpondin motifs) family [4], underlined its tumor suppressive [5,6] but also its protumorigenic properties [7–9], including its key contribution for the acquisition of an endothelial-like (EL) phenotype [10] or its competences to modulate the immune response [11]. Likewise, similar attributes have been reported to further ADAMTS members [12], recognizing the necessary commitment to know better the nature of ADAMTS-mediated actions that concern the modulation of phenotypic properties of cancer cells.

The influence of extracellular matrix (ECM) remodeling on plasticity and stemness capacities of cancer cells is still an open query. For example, the study of vasculogenic mimicry (VM) [13] revealed an alternative mechanism of neovascularization where tumor cells revert to a stem-like state, favoring the acquisition of an EL phenotype [14]. Although few reports have described the contribution of metalloproteases cooperating with ECM factors during this phenomenon [15], ECM remodeling needs to be thoroughly considered, as physical and chemical properties affect cancer plasticity [16]. VM was firstly reported on melanoma cases but many questions remain regarding the relationship between stemness, cancer plasticity and EL phenotype. We now add new insights about the contribution of ECM regulatory molecules in a human uveal melanoma (UVM) setting. Very significantly, although UVM is classified as a rare cancer, it is very aggressive with up to 50% of the patients developing metastasis [17]. Indeed, UVM plasticity has been previously uncovered including the relevant regulation of microenvironment-related pathways [18].

Here, we first demonstrated an in vitro EL phenotype for various melanoma cell lines that correlated with *ADAMTS1* expression, and we also unveiled common gene signatures with endothelial lineages. Moreover, the inhibition of *ADAMTS1* affected in vitro EL attributes and, more importantly, caused a major halt of tumor progression in mice with alterations in vascular and endothelial parameters. We also observed a significant compromise of stemness features in tumor cells, emphasized by our melanoma sphere assays. Finally, taking advantage of advanced bioinformatics tools and available TCGA data on UVM, we disclosed new prognosis elements that sustained our experimental data. To our knowledge, this is the first study reporting the activity of an extracellular protease on the development of UVM by the induction of stemness and endothelial-like features, and it prompts the development of new strategies to fight this fatal malignancy.

2. Results

2.1. ADAMTS1 Expression Correlates with An Endothelial-Like Phenotype of Melanoma Cells

We used the well-established Matrigel assay [19] to characterize the endothelial-like (EL) phenotype of melanoma cells. While MUM-2B, SK-MEL-28, SK-MEL-103, SK-MEL-147 and C8161 generated clear endothelial-like networks in Matrigel, MUM-2C, A-375 and G-361 formed cell clusters (Figure 1a). Accordingly, we classified these lines as EL+ and EL− cell lines, respectively. We evaluated *ADAMTS1* gene expression in all cell lines (Figure 1b and Figure S1a), observing that its expression was significantly higher in EL+ cell lines compared with EL− ones (Figure 1c).

Taking into account the public availability of gene expression data of these cell lines, we executed an in silico comparison of their gene signatures including also human umbilical vein endothelial cells (HUVECs) to ponder their EL related phenotype (Figure 1d and Table S2). We obtained 467 genes with a significantly different expression between EL+ (including HUVECs) and EL− cells: 47 upregulated and 420 downregulated (Figure 1d and Table S3a). Interestingly, within the upregulated group we found relevant endothelial-related genes (e.g., *CDH5* [VE-cadherin], *TFPI* and *THBD*), which were also linked with ECM remodeling (e.g., *NID1*) in our models. Indeed, GO enrichment analysis revealed a prevalence of pathways strongly related with vascular functionality, such as regulation of coagulation, hemostasis, wound healing and ECM organization (Figure 1e and Table S3b), including some of the genes mentioned above. Overall, these results encourage additional studies of the EL phenotype of our melanoma cells and the contribution of ADAMTS1.

Cancers **2020**, *12*, 801

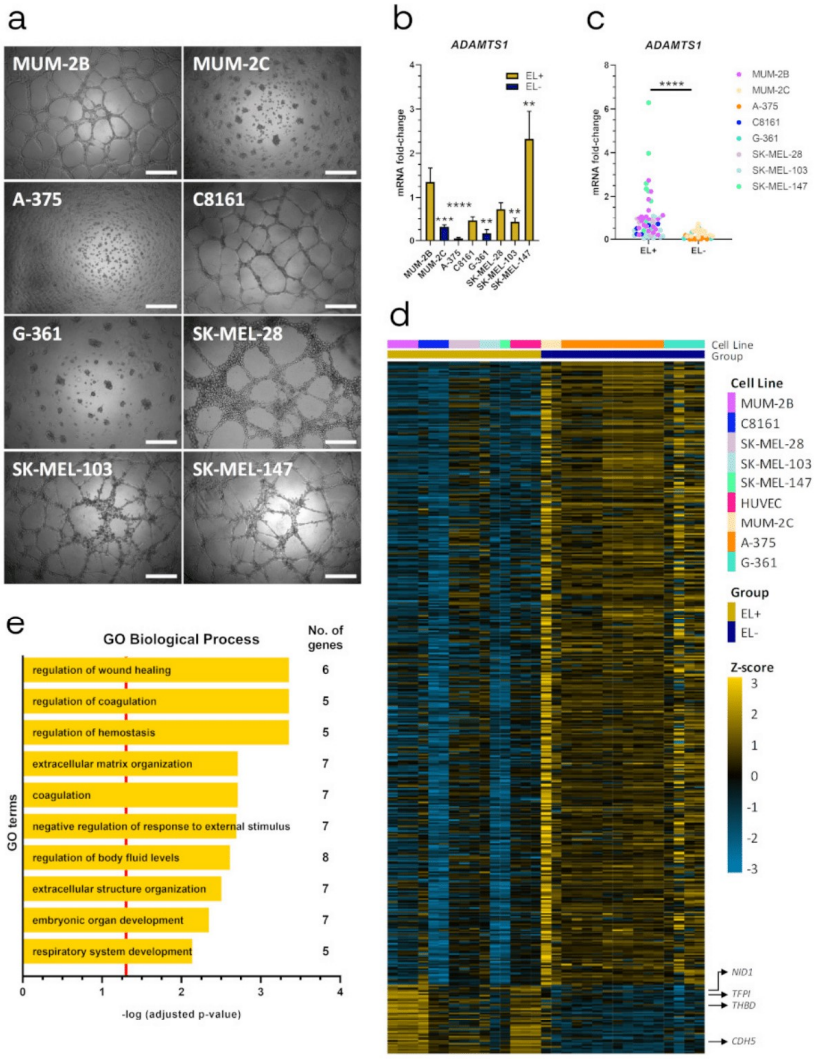

Figure 1. Endothelial-like properties of melanoma cells and correlation with ADAMTS1 expression. (**a**) Representative images of 3D Matrigel-based assay of human melanoma cell lines, 24 h after seeding. 20,000 cells/well were cultured for MUM-2B, SK-MEL-147, C8161, MUM-2C and SK-MEL-103; and 30,000 cells/well for SK-MEL-28, G-361 and A-375 (white scale bar = 500 μm); (**b**) Graph representing

mRNA fold change expression of *ADAMTS1* in human melanoma cell lines. Values are relative to MUM-2B (n = 21 for MUM-2B, n = 17 for MUM-2C, n = 11 for A-375, n = 5 for C8161 and SK-MEL-28, n = 6 for G-361, n = 15 for SK-MEL-103 and n = 9 for SK-MEL-147). EL+ and EL− phenotypes are indicated; (**c**) Graph representing mRNA fold change expression of *ADAMTS1* in human melanoma cell lines, according to their EL+ or EL− phenotype (values are based in same data that Figure 1C); (**d**) Heatmap showing differential gene expression between EL+ (including HUVECs) and EL− cell lines. Only significant differently expressed genes are depicted (47 upregulated and 420 downregulated, FDR < 0.05). Gene Expression Omnibus (GEO) ID samples are listed and color coded in Table S2; (**e**) Representation of top ten GO Biological Processes after enrichment analysis using significantly upregulated genes in EL+ cells. Red line determined the limit of significance: -log (0.05). (****, $p < 0.0001$; ***, $p < 0.001$; and **, $p < 0.01$).

2.2. ADAMTS1 Inhibition Affects In Vitro Endothelial-Like Phenotypic Properties and Endothelial-Related Signature

We evaluated if the inhibition of ADAMTS1 altered EL+ phenotypic plasticity in uveal MUM-2B cells, using CRISPR-Cas9 technology. Once confirmed ADAMTS1 edition and inhibition in two different MUM-2B clones by Sanger sequencing (Figure S1b) and Western blot (Figure 2a and Figure S1c), we studied their EL phenotype performing in vitro Matrigel assays (Figure 2b). We evaluated the resulting structures with the non-biased WimTube tool. Using different cell culture densities, we confirmed that ADAMTS1 inhibition diminished the number of tubes, branching points and loops (Figure 2b and Figure S1d).

Following these findings, we then wondered if the impairment of the EL phenotype in MUM-2B ADAMTS1-knock out (ATS1-KO) cells was also reflected on their endothelial-related signature. We compared the expression levels of recognized endothelial-related genes that are relevant for the VM phenomenon: CDH5 (also found in our global analysis showed above), *ENG*, *EPHA2*, *KDR* (*VEGFR2*), *LAMC2*, *TEK* and *TIE1* [20,21]. Remarkably, these analyses revealed a significant downregulation of *CDH5*, *KDR* and *TIE1* in MUM-2B ATS1-KO cells (Figure 2c and Figure S1e). We approached a similar study with EL+ C8161 cells, also confirming a significant downregulation of *CDH5* in their respective C8161 ATS1-KO (Figure 2d and Figure S1f). These results indicated that ADAMTS1 exerts a key contribution to EL plasticity in melanoma cells, as its inhibition affected in vitro EL phenotype and downregulated endothelial-related genes, particularly *CDH5*, again highlighting the relevance of this gene.

Next, we approached an in vivo tumor model to shed light on the role of ADAMTS1 in UVM plasticity and tumorigenesis.

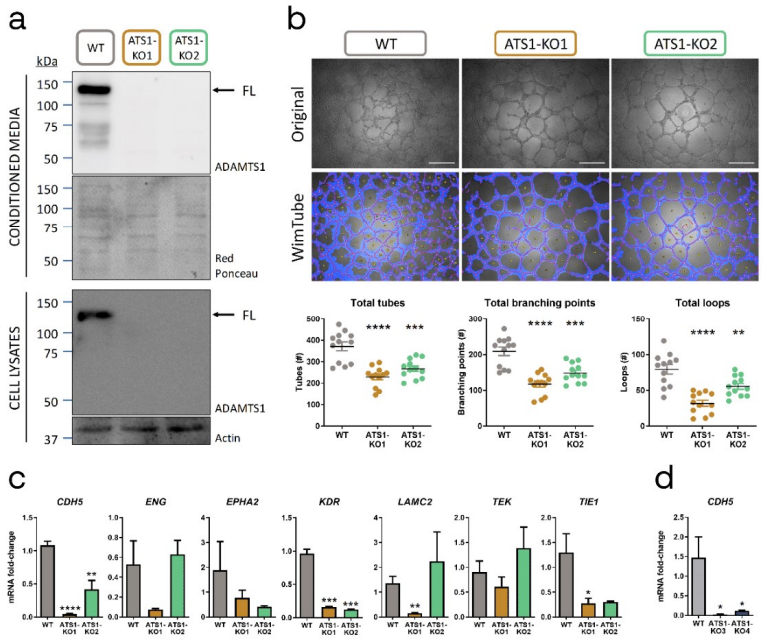

Figure 2. ADAMTS1 inhibition affects in vitro endothelial-like phenotypic properties and endothelial-related signature. (**a**) Western blot analysis of conditioned media and cell lysates of ADAMTS1 in MUM-2B WT and ATS1-KO cells. Black arrows point full-length (FL) ADAMTS1. Red Ponceau staining and Actin were used as loading controls for conditioned media and cell lysates, respectively (uncut blots including a densitometry analysis are shown in Figure S1c); (**b**) Representative images (original and WimTube filtered) of Matrigel assay for MUM-2B WT and ATS1-KO cells, 24 h after seeding 20,000 cells/well. Scatter plots represent the parameters resulting of WimTube analysis: total tubes, total branching points and total loops (n = 12 for all groups, white scale bar = 500 µm); (**c**) Graphs representing mRNA fold change expression of *CDH5*, *ENG*, *EPHA2*, *KDR*, *LAMC2*, *TEK* and *TIE1* in MUM-2B WT and ATS1-KO cells (n = 3–5 for WT, n = 3–6 for ATS1-KO1 and n = 2–4 for ATS1-KO2); (**d**) Graph representing mRNA fold change expression of *CDH5* in C8161 WT and ATS1-KO cells (n = 4 for all groups). (****, $p < 0.0001$; ***, $p < 0.001$; **, $p < 0.01$; and *, $p < 0.05$. WT cells were used as control for statistical analyses).

2.3. ADAMTS1 Inhibition Affects In Vivo Tumor Progression and Vasculature

According to previous reports with MUM-2B cells [9], we first executed xenograft studies using Swiss Nude (SwN) mice. Very significantly, all SwN mice injected with WT but none with ATS1-KO cells developed tumors, corroborated even after sacrifice (Figure 3a,b and d). Although this robust result already implied a key contribution of ADAMTS1, we applied the following conditions to confirm it. We injected cells in a 1:1 PBS:Matrigel solution (SwN-Matrigel), reported to support initial cell engraftment and subsequent tumor progression [22]. Under these conditions, ATS1-KO cells, although inducing some tumors, still displayed lower efficiency than WT cells (Figure 3a). Indeed, progression of ATS1-KO-derived tumors was clearly compromised in comparison with WT group (Figure 3b,d).

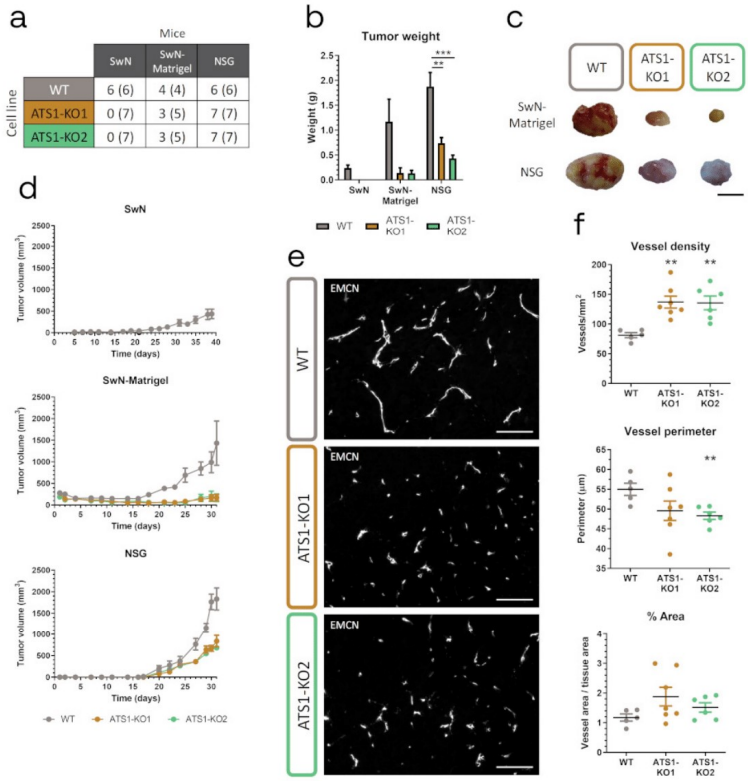

Figure 3. *ADAMTS1* inhibition blocks tumorigenesis and alters tumor vasculature. (**a**) Table indicating the number of mice that developed tumors and the total number of injected mice of every experimental group (in parenthesis); (**b**) Graph representing final tumor weight of different experimental groups, according to panel A; (**c**) Representative pictures of tumors from SwN-Matrigel and NSG groups (black scale bar = 1 cm); (**d**) Graphs representing tumor evolution for each experimental group. (**e**) Representative images of EMCN immunofluorescence analysis of tumor sections from WT and ATS1-KO NSG xenografts (white scale bar = 100 µm); (**f**) Graphs representing tumor vasculature quantification of NSG xenografts: vessel density, vessel perimeter and percentage area ($n = 5$ for WT; $n = 7$ for ATS1-KO1; $n = 6$ for ATS1-KO2). (***, $p < 0.001$ and **, $p < 0.01$. Tumors generated with WT cells were used as control for statistical analyses).

Given the major blockade of tumor growth when ADAMTS1 was inhibited in these two models, we were unable to get relevant biopsies of some experimental groups. Therefore, we pursued tumor progression on NOD *scid* gamma (NSG) mice, expecting an increased tumor engraftment according to the strongest failure of their immune system [23]. Certainly, now all the injected NSG mice developed tumors (Figure 3a). However, again in accordance with previous results, the comparison of tumor development by WT and ATS1-KO cells in NSG mice revealed significant differences in terms of tumor weight and volume (Figure 3b,d).

All these data confirmed the relevance of ADAMTS1 for tumor development. Since previous findings already remarked its effect on the vasculature [9,11,24], we analyzed it in our NSG samples.

Endomucin (EMCN) IF revealed an increased vessel density but a reduction in perimeter in tumors derived from ATS1-KO cells (Figure 3e,f), resulting in a lack of significant differences in terms of total vessel area between WT and ATS1-KO tumors (Figure 3f), as previously described in other tumor studies [6,9].

At this point, although vasculature displayed alterations, the blockade of tumor progression when ADAMTS1 was inhibited is still unsolved. In line with the recognized plasticity of melanoma cells and the putative role of ADAMTS1 in such phenomena [10], we decided to evaluate stemness-related features in our tumors.

2.4. ADAMTS1 Inhibition Compromises Tumor Stemness and Plasticity Features

Taking advantage of the distinct origin of tumor (human) and stromal (murine) cells in our xenografts, we approached the evaluation of stemness genes *NANOG*, *POU5F1* (*OCT4*), *PROM1* (*CD133*) and *SOX2*, from the tumor origin. Importantly, the analysis of WT tumors revealed a significant upregulation of *NANOG* and *POUF5F1* when compared with the original tumor cells under 2D culture conditions (Figure 4a and Figure S2a), confirming the high impact of the tumor microenvironment on promoting stemness. Interestingly, *ADAMTS1* and *CDH5* also appeared significantly induced in the tumor context (Figure 4b,c, Figure S2b,c), suggesting again their direct link during tumor progression.

In line with the impaired progression, ATS1-KO tumors showed an overall downregulation of stemness markers compared with WT samples, especially significant for the more abundant *NANOG* and *POU5F1* (Figure 4d and Figure S2d). Moreover, in the same way that we observed a significant alteration of endothelial genes in ATS1-KO cultured cells (Figure 2c), now ATS1-KO tumors showed a chief reduction in *CDH5* mRNA levels compared with WT samples (Figure 4e, and Figure S2e). The contribution of CDH5 in the VM phenomenon has already been reported [25–27], so we were interested in visualizing human CDH5 in our tumor histological sections by IF. The analysis of WT tumors allowed the identification of a cell surface pattern for CDH5, noticeably associated with tumor cells in the vicinity of EMCN-positive vascular niches (Figure 4f). Furthermore, this pattern was more arduous to find in ATS1-KO tumors, and it was generally less consistent that in WT samples. Therefore, according to the similar behavior of *CDH5* and *NANOG* in our melanoma culture model, we evaluated their relationship in tumor sections. As the co-staining was not feasible, we performed IHC in sequential tumor sections (Figure 4g). In addition to the clearly compromised NANOG positive staining in ATS1-KO tumors, we detected a spatial coincidence of NANOG and CDH5 expression in WT samples that was difficult to appreciate in ATS1-KO sections. Finally, we performed double CDH5-PAS immunostaining to check a similar spatial coincidence between endothelial-related CDH5 and PAS-positive patterns, widely used as identifier of VM [13]. Certainly we observed such concurrence much better in WT than in ATS1-KO tumors, as well as a significant increase in VM+ patterns in WT tumors (Figure 4h).

All these results suggested a close association between stemness and plasticity features that would lead to VM events, so we evaluated such parameters back in tumor cells.

Cancers **2020**, *12*, 801

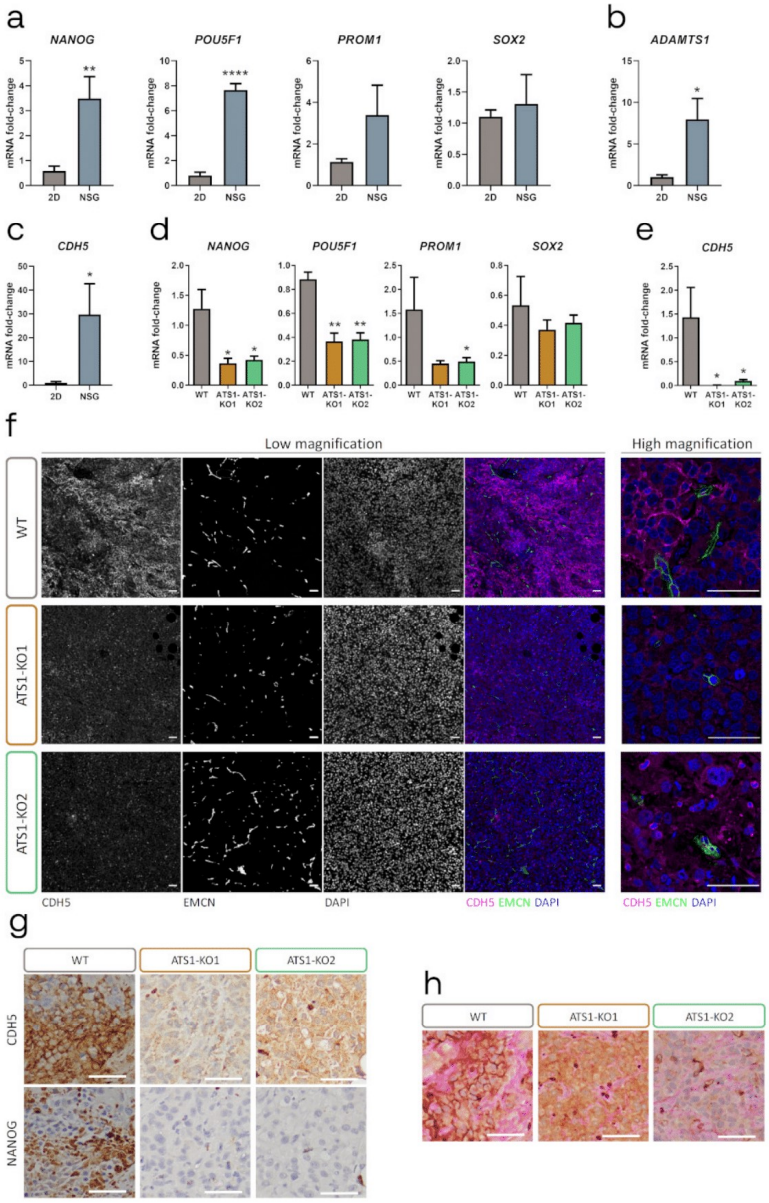

Figure 4. ADAMTS1 inhibition compromises the stemness capacities and endothelial-like phenotype in tumor xenografts. (**a–c**) Graphs representing mRNA fold change expression of *NANOG*, *POU5F1*, *PROM1* and *SOX2* (**a**), ADAMTS1 (**b**) and *CDH5* (**c**), in MUM-2B WT 2D cultured cells and NSG

xenografts (n = 4–6 for cells and n = 3–4 for NSG); (**d-e**) Graphs representing mRNA fold change expression of *NANOG, POU5F1, PROM1* and *SOX2* (**d**), and *CDH5* (**e**) in NSG xenografts generated with WT and ATS1-KO cells (n = 3 for WT, n = 5 for ATS1-KO1 and n = 4–6 for ATS1-KO2); (**f**) Representative images of IF analysis of WT and ATS1-KO NSG xenografts, at low and high magnification. For low magnification, columns from left to right: CDH5, EMCN, DAPI and merge; (**g**) Representative images of IHC staining of CDH5 and NANOG in consecutive sections of WT and ATS1-KO NSG xenografts; (**h**) Representative images of IHC co-staining of CDH5 and PAS, in WT and ATS1-KO NSG xenografts. (****, $p < 0.0001$; **, $p < 0.01$; and *, $p < 0.05$. White scale bar = 50 μm).

2.5. ADAMTS1 Inhibition Compromises In Vitro Stemness Capacities

Although stemness features have been attributed to melanoma, our evaluation of stemness genes (*NANOG*, *POU5F1*, *PROM1* and *SOX2*), revealed a very low expression among the tested cells on 2D culture. In agreement with the recognized induction of stemness properties, we approached the melanoma sphere formation assay with MUM-2B cells. Furthermore, we evaluated the expression levels of stemness genes in this material, as well as *ADAMTS1* and *CDH5*, according to their relevance suggested by our previous results. First, we confirmed a significant induction of stemness *NANOG*, *POU5F1* and *PROM1* in the melanoma sphere formation process, in both primary and secondary WT spheres (Figure 5a and Figure S3a). Importantly, we detected a significant induction of both *ADAMTS1* and *CDH5*, implying again a role for these molecules in melanoma plasticity. With these premises, we generated melanoma spheres with ATS1-KO cells. Remarkably, the absence of ADAMTS1 had a dramatic effect by compromising the formation of both primary and secondary spheres (Figure 5b,c and Figure S3b).

Given the strong impairment of ATS1-KO cells to form spheres, we evaluated gene expression levels of *NANOG* and *CDH5* in their primary spheres, according to their alteration in our tumor model. Contrary to WT cells (Figure 5a), ATS1-KO spheres presented no significant changes in the expression of these genes when comparing with 2D cultures (Figure 5d and Figure S3c). It was noteworthy that the low levels of *CDH5* that ATS1-KO cells displayed in 2D culture were not induced at all in the process of sphere formation, as occurred with WT cells.

All these data demonstrated that ADAMTS1 inhibition also compromises stemness capacities in MUM-2B UVM cells. According to the extracellular nature of ADAMTS1, we then evaluated if medium containing this secreted protease could affect the sphere formation ability. First, we used CM of MUM-2B cells (identified as ADAMTS1+ CM) (scheme in Figure 5e). Notably, this medium enhanced the formation of spheres in both WT and ATS1-KO cells. Indeed, the size and number of spheres of ATS1-KO cells with ADAMTS1+ CM was comparable to that of WT cells with normal CSC medium (Figure 5f,g), suggesting that secreted ADAMTS1 have a positive effect on the recovery of stemness capacities of MUM-2B cells. Second, according to the complex nature of the CM, we performed the sphere assay using CSC medium with and without pure recombinant human ADAMTS1 (rhATS1). Now this experiment revealed that rhATS1 in the medium did not affect WT sphere formation, but it had a significant effect on the sphere formation of ATS1-KO1 cells, although still not reaching WT properties (Figure 5h,i).

While our findings with melanoma spheres confirmed the implication of recognized stemness markers, we were positively surprised that *ADAMTS1* also appeared to be induced during the process and, indeed, that its inhibition blocked the formation of spheres. Furthermore, the induction of endothelial *CDH5* in melanoma spheres revealed an unexpected link between melanoma stemness features and its putative endothelial-like phenotypic properties, supporting the results obtained with our tumor models.

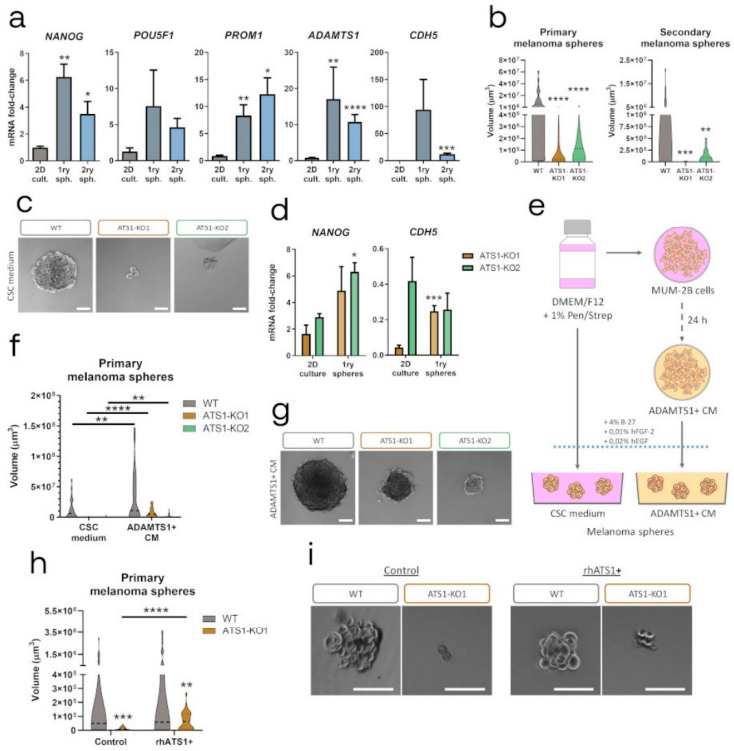

Figure 5. Inhibition of ADAMTS1 compromises melanoma sphere formation. (**a**) Graphs representing mRNA fold-change expression of *NANOG*, *POU5F1*, *PROM1*, *ADAMTS1* and *CDH5* in MUM-2B WT 2D culture, primary and secondary melanoma spheres (n = 4 for 2D culture, except for *ADAMTS1* which is 12; n = 2–5 for primary spheres, and n = 4–6 for secondary spheres). 2D cultured cells were used as control for statistical analyses; (**b**) Violin plots representing volume of primary (n = 49 for WT, n = 62 for ATS1-KO1, and n = 58 for ATS1-KO2) and secondary (n = 46 for WT, n = 34 for ATS1-KO1 and n = 21 for ATS1-KO2) melanoma spheres. WT spheres volume was used as control for statistical analyses; (**c**) Representative images of WT and ATS1-KO primary melanoma spheres grown in CSC medium; (**d**) Graphs representing mRNA fold-change expression of *NANOG* and *CDH5* in 2D culture (n = 4–6 for ATS1-KO1 and n = 2–4 for ATS1-KO2) and primary melanoma spheres (n = 2 for ATS1-KO1 and n = 4–7 for ATS1-KO2). 2D cultured conditions were used as control for statistical analyses; (**e**) Schematic protocol for melanoma spheres formation, using CSC medium and ADAMTS1+ CM; (**f**) Violin plots representing volume of WT and ATS1-KO primary melanoma spheres grown in CSC medium (n = 49 for WT, n = 62 for ATS1-KO1, and n = 58 for ATS1-KO2) or in ADAMTS1+ CM (n = 44 for WT, n = 48 for ATS1-KO1, and n = 49 for ATS1-KO2); (**g**) Representative images of WT and ATS1-KO primary melanoma spheres in ADAMTS1+ CM; (**h**) Violin plots representing WT and ATS1-KO1 primary melanoma spheres, grown in control CSC (n = 27 for WT, and n = 44 for ATS1-KO1) or rhATS1+ CSC medium (n = 35 for WT, and n = 28 for ATS1-KO1); (**i**) Representative images of WT and ATS1-KO1 primary melanoma spheres grown in control and rhATS1+ CSC medium. (****, $p < 0.0001$; ***, $p < 0.001$; **, $p < 0.01$; *, $p < 0.05$. Violin plots indicate the median of every experimental group. White scale bar = 100 µm).

2.6. Relevance of Endothelial-Like Plasticity in Human Uveal Melanoma

Consistent with the alterations of EL-related and stemness markers described above, all of them modulated by ADAMTS1, we approached a close study of their contribution in human UVM. Considering the infrequent nature of this tumor, the public availability of gene expression data in the TCGA-UVM Project [28] allowed us to pursue such analyses in a relevant number of samples, including prognosis parameters and staging classification. First, using the UCSC Xena platform, we found that endothelial-related *CDH5* and *KDR* appeared as significant poor prognosis factors (Figure 6a), in full agreement with our experimental observations. Furthermore, the evaluation of co-expressing genes across these cohorts of patients revealed a higher and significant correlation of *CDH5* with additional endothelial-related genes like *CD34*, *TIE1*, *FLT4*, *KDR* and *COL4A1* (Figure 6b and Figure S4), confirming the strong association of endothelial-related signature in this neoplasia. According to the chief role of CDH5, we then approached a GO-enrichment analysis using the list of significantly positive correlated genes with *CDH5* (Table S4a, 1196 genes). This exploration revealed key features such as ECM organization and the regulation of angiogenesis (Figure 6c and Table S4b), highlighting the close and significant relationship between endothelium and matrix remodeling.

Then, taking into consideration the modulatory role that extracellular proteases exert on tumor plasticity, we approached a whole evaluation of all members of the ADAMTS family of proteases, noticing the strong similarity that exists among them at the structural and functional levels. In agreement with the study of stemness markers, we did not find *ADAMTS1* correlating with survival in UVM patients, which was probably related with their role in initiating stages. Indeed, when we analyzed *ADAMTS1* expression data considering different stages of tumor progression, we observed a clear tendency for *ADAMTS1* to be more expressed at early phases (identified here with stage IIA) and decreases with higher grades (Figure 6d). This higher expression at initial stages of UVM would support our experimental data, as we observed a link between ADAMTS1 and stemness features, closely related with tumor initiation and early UVM progression. Furthermore, it resulted quite appealing the fact that up to six related family members displayed significant values as poor prognosis factors for UVM, including the closer *ADAMTS4*, *ADAMTS5* and *ADAMTS9*, but also others like *ADAMTS12*, *ADAMTS2* or *ADAMTS14* (Figure 6e). Going back to ADAMTSs actions and *CDH5* induction, we observed positive significant correlations between some of these proteases and *CDH5* (Figure 6f), supporting the robust association between endothelial-like plasticity and ADAMTSs activity favoring UVM progression.

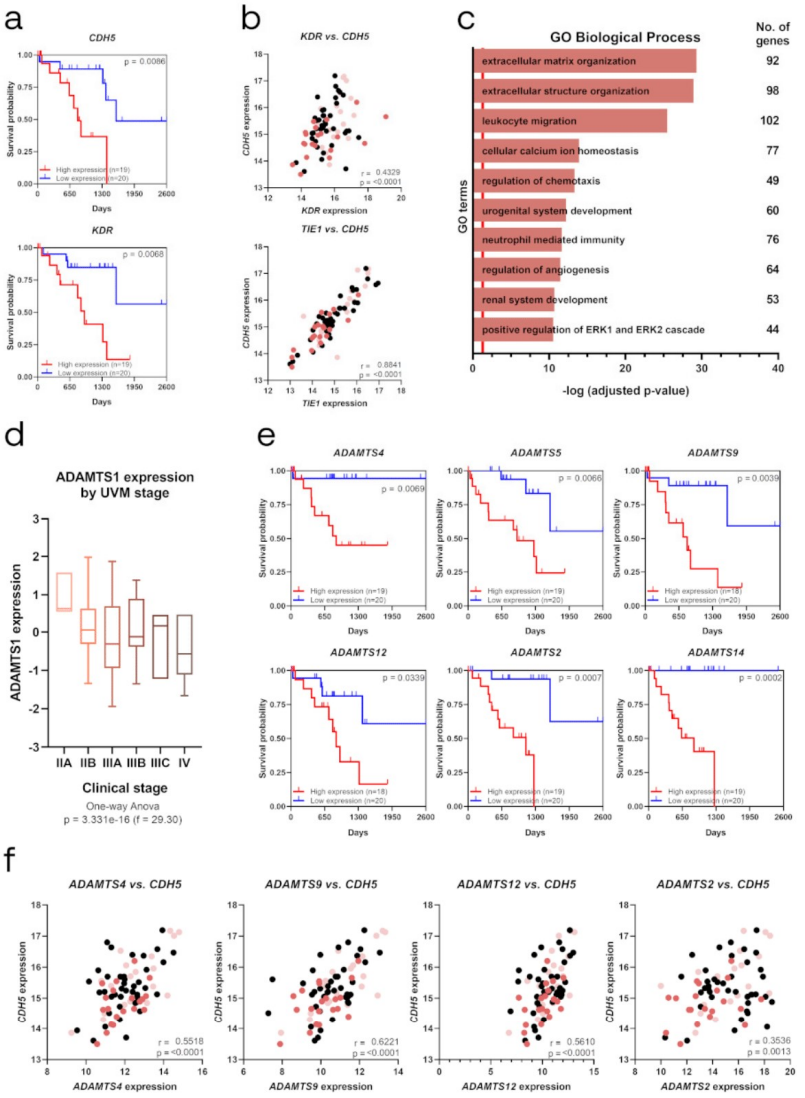

Figure 6. Identification of EL and ECM molecules as poor prognosis factors in TCGA Uveal Melanoma Project (TCGA-UVM). (**a**) Kaplan–Meier survival curves for low and high gene expression levels of EL markers *CDH5* and *KDR*; (**b**) Scatter plot representing Pearson correlation analysis between gene expression levels of *CDH5* and endothelial-related *KDR* and *TIE1*; (**c**) Representation of top ten GO Biological Processes after enrichment analysis using genes that positively correlated (q-value < 0.05) with *CDH5*. Red line determined the limit of significance: -log (0.05); (**d**) Box graph representing *ADAMTS1* expression among different clinical stages of human uveal melanoma, from stage IIA to IV

(n = 4 for IIA, n = 32 for IIB, n = 27 for IIIA, n = 10 for IIIB, n = 3 for IIIC and n = 4 for IV); (**e**) Kaplan–Meier survival curves for low and high gene expression levels of extracellular proteases *ADAMTS4, ADAMTS5, ADAMTS9, ADAMTS12, ADAMTS2* and *ADAMTS14*; (**f**) Scatter plot representing Pearson correlation analysis between gene expression levels of *CDH5* and extracellular proteases *ADAMTS4*, *ADAMTS9*, *ADAMTS12* and *ADAMTS2*. (Survival probability is depicted in correlation analysis plots (panels B and F) with light and dark red dots, representing low and high survival probability, respectively. r = Pearson correlation coefficient).

3. Discussion

Tumor microenvironment (TME) remodeling is being recognized as a relevant contributor to complex tumor heterogeneity, and one to be researched for a better understanding. To date, although a number of extracellular proteases have been identified as possible therapeutic targets due to their actions during tumor growth, their clinical use still requires much deeper investigation. In this work, we first focused our attention on the impact of the extracellular protease ADAMTS1 on human uveal melanoma (UVM), and particularly on its effects on cancer plasticity phenomena, revealing a new relationship between intrinsic endothelial-like (EL) properties on tumor cells and their enrichment on stemness features. A combination of experimental in vitro and in vivo approaches, together with the use of bioinformatics methodologies on public tumor databases, allowed us to unveil the unexplored relevance of endothelial-specific molecules, such as CDH5, strongly correlating with ADAMTS proteases.

Our initial and comprehensive characterization of human uveal and skin melanoma cell lines confirmed their heterogeneity but, more importantly, it supported their classification as EL+ or EL−. Although based on experimental phenotypic properties, our bioinformatics approach using available datasets of melanoma cell lines showed a clear connection with vascular functions as coagulation and hemostasis. This approach also highlighted the contribution of endothelial *CDH5* as a key gene supporting our own data. While the literature has already shown the existence of differential gene signatures among melanoma cell lines with different aggressiveness [15,29], our methodology discriminated according to their behavior in the recognized Matrigel assay. In addition, we detected *ADAMTS1* to be significantly upregulated in EL+ cells. The absence of *ADAMTS1* in our in silico results, as also occurred with stemness related molecules, is probably linked with their low expression levels, making them undetectable for microarray procedures.

Focusing on UVM, we succeeded in inhibiting ADAMTS1 in MUM-2B cells, and our subsequent studies confirmed the disruption of relevant tumorigenic features. First, our Matrigel assays to evaluate the EL phenotype showed that ATS1-KO cells were compromised in comparison with WT cells. Moreover, we detected in these deficient cells a clear downregulation of EL markers, already associated with VM and its aggressive phenotype in melanoma [15,27,30]. Notably, the performance of xenograft assays in distinct mouse models supported the pro-tumorigenic effects of ADAMTS1 in UVM, revealed mainly by the significant blockade of tumor development when ADAMTS1 was inhibited. Indeed, our data with SwN mice disclosed a complete halt using ATS1-KO cells, which was partially overcome using an NSG model. Importantly, the immune system of NSG mice displays a stronger defect than SwN, so the distinct ability of ATS1-KO cells to initiate tumor progression in these two models could be related with an immunomodulatory role already attributed to ADAMTS1 [11]. Certainly, these results encourage further studies to unveil the impact of this ECM-modifying enzyme on the immune system, although distinct models must be considered.

Regarding the tumor vasculature, in agreement with previous reports [6,9], this current study also showed evocative alterations although the overall vasculature appeared normalized. These observations are aligned with the widely described role of some ADAMTSs as modulators of vasculature [24]. Nonetheless, additional actions of ADAMTS1 contribute to tumor development, at least in this setting. Very importantly, we were able to match alterations of endothelial and stemness parameters. To our

knowledge, this is the first time where a tumor displayed a clear correlation between the acquisition of endothelial-like features and an intrinsic stemness signature, indeed correlating with the disruption of tumorigenic properties. Our studies revealed an overall increase in stemness genes in tumors in comparison to the original 2D cultures. Furthermore, we also found the EL marker *CDH5* to be similarly regulated. This intimate relationship between stemness, plasticity and the acquisition of EL properties, both in vitro and in vivo, with everything modulated by the protease ADAMTS1, emphasizes the chief contribution of ECM modifying enzymes. Suggestively, these results encourage the design of new and improved specific inhibitors of matrix metalloproteases to overcome former disappointing results in clinical trials [31]. Indeed, our results support a main involvement of CDH5-related pathways, but not strictly from endothelial origins as originally hypothesized, according to their relevant expression in plastic tumor cell populations.

Our assays involving the formation of tumor spheres also reinforced our findings. Although the development of melanoma spheres from the MUM-2B cell line was already reported [32], to our knowledge, this is the first work including a deeper description and characterization of the resulting spheres. WT cells showed a clear upregulation of main stemness markers, together with the newly reported induction of *CDH5* and the protease *ADAMTS1*. While CDH5 has been already related with stemness parameters [17,33,34] as a causal factor of vasculogenic mimicry events, our data exposed that extracellular proteases such as ADAMTS1 should also been considered when studying the stemness capacities or the aggressiveness of a tumor. In the case of ATS1-KO spheres, not only were they unable to generate optimal spheres, but also, there were no significant changes to the expression of our genes of interest. Importantly, our experiments using ADAMTS1-enriched media (secreted in the CM of melanoma cells or as exogenous recombinant protein) supported the extracellular contribution of this protease as a key factor for tumor initiation and growth, indeed corroborated by our in vivo approaches. This role of ADAMTS1 during initiating stages of tumorigenesis possibly justifies its absence in standard gene expression notations as we mentioned in our studies in cell lines and also in human UVM samples.

According to the modest knowledge of UVM, considered a rare type of cancer with an estimated incidence of 4.9–5.2 cases per million in the United States and a rate of 2–8 cases per million in Europe [17], our new findings give strength to its recognized plastic nature. With the intention to advance the fight against this type of melanoma, we conducted a deep study of genes of interest in human UVM datasets from TCGA. Suggestively, we found that the endothelial-related genes *CDH5* and *KDR* appeared as significant poor prognosis factors in these neoplasias. Although the fact that *CDH5* should be considered a poor prognosis gene is supported all along this work, we find it especially interesting that other EL genes displayed similar features. Indeed, these genes were formerly related with VM and stemness features [30,35], and our own experiments confirm such involvement.

Very importantly, the evaluation of *ADAMTS1* in this tumor collection allowed us to observe its higher expression levels at early phases of this malignant tumor, and then appeared downregulated as the disease progressed to advanced stages, in harmony with our results on stemness features. Indeed, it resulted quite appealing the fact that such positive association did occur with high expression of other ADAMTS proteases (*ADAMTS2*, *ADAMTS4*, *ADAMTS5*, *ADAMTS9*, *ADAMTS12* and *ADAMTS14*) that definitively implied a key role of these proteases during melanoma progression. We need to remark on the strong similarity among these members, perfectly complementary within the highly complex scenario of the TME.

Our in vitro and in vivo findings expose a complex communication between the endothelial phenotype, stemness features and ECM regulation, contributing to the final fate of the tumor. More specifically, the requirement of *ADAMTS*1 for tumor progression in our mouse models, its relationship with stemness and endothelial plasticity features, and its higher expression at earlier stages of UVM, all support the role of *ADAMTS1* as a pro-tumorigenic factor for this rare type of tumor. Lastly, this association suggests the participation of key molecules at the cell-matrix and

cell-cell boundary connecting the proteolytic action of ADAMTS proteases with transmembrane and intracellular pathways, which full comprehension would help to define new therapeutic strategies.

4. Materials and Methods

4.1. Cell Culture and Generation of ADAMTS1-Knockout Cells

Uveal melanoma MUM-2B and MUM-2C, and skin melanoma C8161 cell lines were kindly provided by Dr. Arjan W. Griffioen (VUmc, Amsterdam, The Netherlands); skin melanoma SK-MEL-28, SK-MEL-103, SK-MEL-147 by Dr. Juan A. Recio (VHIR, Barcelona, Spain); A-375 and G-361 by Dr. Javier Oliver (IPBLN-CSIC, Granada, Spain); and HEK293T by Dr. Pablo Menéndez (IJC, Barcelona, Spain). All cell lines were cultured in the appropriate medium supplemented with 10% fetal bovine serum (Gibco) and 1% Penicillin/Streptomycin solution (Biowest, Nuaillé, France), under standard conditions (37 °C, 5% CO_2 and 95% relative humidity). Specific media were: RPMI 1640 with stable glutamine (Biowest, Nuaillé, France) for MUM-2B, MUM-2C and C8161; High Glucose Dulbecco's Modified Eagle Medium (DMEM) with stable glutamine and sodium pyruvate (Biowest, Nuaillé, France) for A-375, G-361, SK-MEL-28, SK-MEL-103, SK-MEL-147 and HEK293T. All cell lines were routinely tested for *Mycoplasma* (Venor®GeM qEP, Minerva Biolabs, Berlin, Germany). MUM-2B cell line was authenticated by STR Profiling (AmpFLSTR® Identifiler® Plus, Applied Biosystems, Waltham, MA, USA).

The generation of ATS1-KO cells with lentivirus-based CRISPR-Cas9 system has been described [36]. Two clonal populations were obtained from MUM-2B cell line (named ATS1-KO1 and ATS1-KO2) and other two from C8161 (named ATS1-KO3 and ATS1-KO4), after two weeks of selection (0.25 µg/mL Puromycin), and single cell cloning isolation and expansion processes. They were subjected to Sanger DNA sequencing (primer sequences in Table S1) and Western blot analysis to confirm gene edition and inhibition, respectively.

4.2. In Vitro 3D Matrigel-Based Assay

35 µL/well of Matrigel (Corning, Corning, NY, USA) were dispensed in a 96-well plate kept on ice to avoid gelling. After Matrigel gelling, 100 µL of serum-free medium were added to each well. Finally, 100 µL of serum-free medium containing cells (20,000–30,000 cells) were added. Follow-up was performed taking pictures at various time points (Axio Vert microscope, A-Plan 5x/0.12 objective, Zeiss, Oberkochen, Germany). If appropriate, 24 h pictures were subjected to WimTube analysis (Wimasis, Córdoba, Spain) as indicated [37].

4.3. Tumor Xenograft Assays

Female Swiss Nude (SwN) and NOD *scid* gamma (NSG) mice were purchased from Charles River Laboratories and housed at CIBM-UGR animal facility according to institutional guidelines (Approved Ethical Committee #152-CEEA-OH-2016). For xenograft generation, 1×10^6 cells in 100 µL PBS were subcutaneously injected in the flank of 6-weeks old mice. When using Matrigel as scaffold, 2×10^6 cells in a 150 µL PBS:Matrigel dilution (1:1) were subcutaneously injected in the flank of 16-weeks old SwN mice. Animals were monitored every two days after cell injection until final time point, when they were sacrificed and tumors were dissected for further analyses. Tumor volume was calculated as: *in progress tumor volume* = $(\pi \times length \times width^2)/6$, and *final tumor volume* = $(\pi \times length \times width \times height)/6$) [11].

4.4. Vasculature Characterization and Immunohistochemistry

For the morphometric analysis of vasculature, tumor paraffin sections were subjected to immunofluorescence (IF) with a rat anti-mouse EMCN (endomucin) antibody (V.7C7, SC-65495, SCBT) and Alexa Fluor 488 donkey anti-rat secondary antibody (A21208, ThermoFisher Scientific, Waltham, MA, USA). IF images were captured (Axio Imager A.1 microscope, EC Plan-Neofluar

10x/0.30 Ph 1 objective, AxioCam MR R3, Zeiss, Oberkochen, Germany) and converted to binary for further analysis as indicated [9]. CDH5 and NANOG were detected with rabbit anti-human CDH5 (160840, Cayman Chemical, Ann Arbor, MI, USA) or NANOG (4903, Cell Signaling Technology, Danvers, MA, USA) antibodies, respectively. Alexa Fluor 647 goat anti-rabbit (A-21245, ThermoFisher Scientific, Waltham, MA, USA), and Dako Envision™ + System-HRP (DAB) (K4010, Agilent Technologies, Santa Clara, CA, USA) were used as secondary antibodies. Antigen retrieval was performed by slide immersion in Tris-HCl 0.5 M pH = 10 solution and 10 min boiling. DAPI (D8417, Sigma-Aldrich, St. Louis, MO, USA) solution and Dako Mayer's Hematoxylin (S3309, Agilent Technologies, Santa Clara, CA, USA) were used for nuclear counterstain in IF and IHC, respectively. Antifade Mowiol (81381, Sigma-Aldrich, St. Louis, MO, USA)-DABCO (D27802, Sigma-Aldrich, St. Louis, MO, USA, St. Louis, MO, USA) mixture and D.P.X. (317616, Sigma-Aldrich) were used as mounting media for IF and IHC, respectively. PAS staining was performed with Periodic acid solution (3951, Sigma-Aldrich, St. Louis, MO, USA) and Schiff's reagent (3952016, Sigma-Aldrich). Confocal images were captured with a LSM 710 Axio Observer (Plan-Apochromat 63x/1.4 Oil DIC M27 objective, Zeiss, Oberkochen, Germany). IHC images were captured with a BX43 microscope (Plan-Achromat 20x/0.4 objective, Olympus, Tokyo, Japan).

4.5. Melanoma Sphere Formation Assay

5000 cells/mL were seeded in non-adherent bacterial plates with CSC medium (DMEM-F12 without L-Glutamine nor Hepes (Biowest, Nuaillé, France) supplemented with 1% Penicillin/Streptomycin (Biowest, Nuaillé, France), B-27™ (40 mL/L, ThermoFisher Scientific, Waltham, MA, USA), human FGF-2 (0.01 µg/mL, Miltenyi Biotec, Bergisch Gladbach, Germany) and human EGF (0.02 µg/mL, Miltenyi Biotec, Bergisch Gladbach, Germany). Medium was renewed weekly by low speed centrifugation (5 min, 800 rpm) until primary spheres were obtained after 3 weeks. To generate secondary spheres, primary spheres were disaggregated through a 29G needle and seeded again at a density of 5000 cells/mL in 60 mm suspension culture dishes (Corning, Corning, NY, USA). For assays using recombinant human ADAMTS1 (rhATS1, 2197-AD, R&D), spheres were grown in 6-well ultralow attachment plates (Corning, Corning, NY, USA), using CSC medium supplemented with 1 µg/mL rhATS1. For assays using conditioned medium (CM), fresh medium was collected from 24 h cultured MUM-2B cells and supplemented with B-27, FGF-2 and EGF as described above. Images were captured with an Axio Vert microscope (A-Plan 5x/0.12 objective, Zeiss, Oberkochen, Germany), and evaluated with Carl Zeiss ZEN 2.3 SP1 (black) software (Oberkochen, Germany). Sphere volume was calculated as: $sphere\ volume = (\pi \times length \times width^2)/6$.

4.6. RNA Isolation and Quantitative RT-PCR

RNA was extracted with NucleoSpin®RNA kit (Macherey-Nagel, Duren, Germany) and reverse transcribed with iScript™ cDNA Synthesis Kit (Bio-Rad, Hercules, CA, USA). qPCR reactions were performed with Fast SYBR™ Green Master Mix (Applied Biosystems, Waltham, MA, USA), using 7900HT Fast Real-Time PCR (Applied Biosystems, Waltham, MA, USA) and QuantStudio 6 Flex Real-Time PCR (Applied Biosystems, Waltham, MA, USA) platforms. *ACTB*, *B2M* and *RNA18S1* were used as housekeeping genes, depending on the sample origin and the platform (primer sequences in Table S1).

4.7. Western Blot Analysis

Secreted proteins were obtained from CM of melanoma cells cultured over 24 h in the absence of serum, and concentrated with StrataClean resin (Agilent Technologies, Santa Clara, CA, USA) [38]. Total protein from cell lysates was extracted with RIPA buffer (containing 10 µg/mL aprotinin, 1 mM PMSF and 100 µM leupeptin) and quantified with Pierce BCA Protein Assay Kit (ThermoFisher, Waltham, MA, USA) in an Infinite 200 PRO NanoQuant (Tecan, Männedorf, Switzerland) absorbance reader. All samples (CM from cells cultured in a 100 mm dish, and 30 µg of cell lysate) were resolved

by SDS-PAGE and transferred to PVDF membranes (Bio-Rad, Hercules, CA, USA). Membranes were stained with a Red Ponceau solution to visualize loaded proteins. Then, membranes were blocked with 5% low-fat milk and incubated with sheep anti-human ADAMTS1 (AF5867, R&D Systems, Minneapolis, MN, USA) and monoclonal mouse anti-Actin (sc-8432, Santa Cruz Biotechnology, Dallas, TX, USA) antibodies. After incubation with HRP-conjugated secondary antibodies (HAF016, R&D Systems, Minneapolis, MN, USA), signal was detected with the ECL Prime Western Blotting Detection Reagent (GE Healthcare Life Sciences, Marlborough, MA, USA) in an ImageQuant LAS4000 (GE Healthcare Life Sciences, Marlborough, MA, USA).

4.8. Bioinformatic Analyses of Cell Lines Datasets and Melanoma Patients

NCBI Gene Expression Omnibus [39] was mined to find optimal datasets of melanoma cell lines used in this study plus human umbilical vein endothelial cells (HUVECs), yielding a total of 31 samples from 13 different datasets (Table S2). Gene expression data were downloaded, probe identifiers were annotated with gene symbols and median gene expression values were calculated for duplicated genes and rank normalized to allow sample comparisons from different technologies. Linear models implemented in limma R package [40] allowed us to analyze differential gene expression between groups of cell lines. Genes were selected by false discovery rate (FDR) < 0.05. A combination of clusterProfiler [41] and REViGO [42] were used to evaluate representative enriched GO biological processes, selecting GO terms showing an adjusted p-value < 0.05.

Genomic Data Commons TCGA Uveal Melanoma Project (TCGA-UVM) [28,43] and UCSC Xena platform [44] were used to obtain survival and gene expression data from patients. Kaplan–Meier curves were obtained comparing patients with low (quartile 1 [Q1]) and high (above quartile 3 [Q3]) gene expression levels. Pearson correlation analyses were performed using the list of genes that positively correlate with *CDH5* using cBioPortal platform [45,46], and comparing normalized gene expression levels from Xena platform. Gene expression data were shown as Fragments Per Kilobase of transcript per Million mapped reads upper quartile (FPKM-UQ).

4.9. Statistical Analysis

Statistical analyses were made with GraphPad Prism 8 (GraphPad software Inc., San Diego, CA, USA). Except when indicated, graphs represent *mean* ± *SEM*, and unpaired t tests were performed to compare means of two experimental groups. Robust regression and Outlier removal (ROUT) method was applied to identify outliers when necessary. For qPCR analysis, values of ΔΔCt out of *mean* ± *SD* were considered as outliers, as well as values of Ct that were lower than $Q1 - 1.5 \times IQR$ (interquartile range) or greater than $Q3 + 1.5 \times IQR$.

5. Conclusions

In this work, we find that the inhibition of the extracellular protease ADAMTS1 alters the endothelial-like properties of uveal melanoma cells in vitro and affects tumor vasculature in vivo. Indeed, our experiments show that ADAMTS1 is also relevant to the stemness capacities of such tumor cells in both in vitro and in vitro approaches, with strong consequences for tumor growth. The inhibition of this protease reveals a new link between stemness and endothelial-like features of uveal melanoma cells, and the evaluation of gene expression data of human samples shows its relevance at early stages, also implying the contribution of further ADAMTS members during more advance stages.

Supplementary Materials: The following are available online at http://www.mdpi.com/2072-6694/12/4/801/s1, Figure S1: ADAMTS1 expression in human melanoma cell lines and effect of its edition on in vitro EL phenotypic properties; Figure S2: ADAMTS1 inhibition compromises the expression of stemness and EL related genes in tumor xenografts; Figure S3: ADAMTS1 inhibition compromises formation of secondary melanoma spheres; Figure S4: Positive correlation of additional endothelial genes with CDH5; Table S1: Sequences of used primers for genes of interest; Table S2: Public gene expression datasets; Table S3A-B: Differently-expressed genes between

EL+ and EL− cells and GO enrichment analysis of upregulated genes in EL+ cells; Table S4A-B: Genes positively correlated with CDH5 and GO enrichment analysis.

Author Contributions: C.P.-T., M.d.C.P.-C., S.D.-G. and A.B.-D. performed experiments with cells; C.P.-T., A.B.-D. and M.d.C.P.-C. performed experiments with mice; R.L.-D., P.C.-S. and C.P.-T. performed bioinformatics analyses; C.P.-T. and J.C.R.-M. conceived all figures; C.P.-T. and J.C.R.-M. conceived and designed the experiments and studies, and they wrote the manuscript; J.C.R.-M. supervised the study. All authors have read and agreed to the published version of the manuscript.

Funding: This research was supported by Ministerio de Economía y Competitividad and Instituto de Salud Carlos III from Spain, co-financed by FEDER (PI16/00345 to JCRM) and from Consejería de Salud de la Junta de Andalucía (OH-0028-2018, PE-0225-2018).

Acknowledgments: We would like to thank members of JCRM's laboratory and GENYO's support units for helping with animal handling, technical assistance, and further discussion. The results published here are in part based upon data generated by the TCGA Research Network (www.cancer.gov/tcga). This manuscript will be part of CPT PhD Thesis belonging to the Doctorate Program on Biomedicine, UGR, Spain.

Conflicts of Interest: The authors declare no conflict of interest.

References

1. Arozarena, I.; Wellbrock, C. Phenotype plasticity as enabler of melanoma progression and therapy resistance. *Nat. Rev. Cancer* **2019**, *19*, 377–391. [CrossRef] [PubMed]
2. Mushtaq, M.U.; Papadas, A.; Pagenkopf, A.; Flietner, E.; Morrow, Z.; Chaudhary, S.G.; Asimakopoulos, F. Tumor matrix remodeling and novel immunotherapies: The promise of matrix-derived immune biomarkers. *J. Immunother. Cancer* **2018**, *6*, 65. [CrossRef] [PubMed]
3. Hillebrand, L.E.; Reinheckel, T. Impact of proteolysis on cancer stem cell functions. *Biochimie* **2019**, *166*, 214–222. [CrossRef] [PubMed]
4. Kuno, K.; Kanada, N.; Nakashima, E.; Fujiki, F.; Ichimura, F.; Matsushima, K. Molecular cloning of a gene encoding a new type of metalloproteinase-disintegrin family protein with thrombospondin motifs as an inflammation associated gene. *J. Biol. Chem.* **1997**, *272*, 556–562. [CrossRef] [PubMed]
5. Reynolds, L.E.; Watson, A.R.; Baker, M.; Jones, T.A.; D'Amico, G.; Robinson, S.D.; Joffre, C.; Garrido-Urbani, S.; Rodriguez-Manzaneque, J.C.; Martino-Echarri, E.; et al. Tumour angiogenesis is reduced in the Tc1 mouse model of Down's syndrome. *Nature* **2010**, *465*, 813–817. [CrossRef]
6. Martino-Echarri, E.; Fernández-Rodríguez, R.; Rodríguez-Baena, F.J.; Barrientos-Durán, A.; Torres-Collado, A.X.; Plaza-Calonge, M.D.C.; Amador-Cubero, S.; Cortés, J.; Reynolds, L.E.; Hodivala-Dilke, K.M.; et al. Contribution of *ADAMTS1* as a tumor suppressor gene in human breast carcinoma. Linking its tumor inhibitory properties to its proteolytic activity on nidogen-1 and nidogen-2. *Int. J. Cancer* **2013**, *133*, 2315–2324. [CrossRef]
7. Ricciardelli, C.; Frewin, K.M.; Tan, I.D.A.; Williams, E.D.; Opeskin, K.; Pritchard, M.A.; Ingman, W.V.; Russell, D.L. The *ADAMTS1* protease gene is required for mammary tumor growth and metastasis. *Am. J. Pathol.* **2011**, *179*, 3075–3085. [CrossRef]
8. Rocks, N.; Paulissen, G.; Quesada-Calvo, F.; Munaut, C.; Gonzalez, M.-L.A.; Gueders, M.; Hacha, J.; Gilles, C.; Foidart, J.-M.; Noel, A.; et al. *ADAMTS-1* Metalloproteinase Promotes Tumor Development through the Induction of a Stromal Reaction In vivo. *Cancer Res.* **2008**, *68*, 9541–9550. [CrossRef]
9. Fernández-Rodríguez, R.; Rodríguez-Baena, F.J.; Martino-Echarri, E.; Peris-Torres, C.; del Carmen Plaza-Calonge, M.; Rodríguez-Manzaneque, J.C. Stroma-derived but not tumor *ADAMTS1* is a main driver of tumor growth and metastasis. *Oncotarget* **2016**, *7*, 34507–34519. [CrossRef]
10. Casal, C.; Torres-Collado, A.X.; Plaza-Calonge, M.D.C.; Martino-Echarri, E.; Ramón, Y.; Cajal, S.; Rojo, F.; Griffioen, A.W.; Rodríguez-Manzaneque, J.C. *ADAMTS1* contributes to the acquisition of an endothelial-like phenotype in plastic tumor cells. *Cancer Res.* **2010**, *70*, 4676–4686. [CrossRef]
11. Rodríguez-Baena, F.J.; Redondo-García, S.; Peris-Torres, C.; Martino-Echarri, E.; Fernández-Rodríguez, R.; del Carmen Plaza-Calonge, M.; Anderson, P.; Rodríguez-Manzaneque, J.C. *ADAMTS1* protease is required for a balanced immune cell repertoire and tumour inflammatory response. *Sci. Rep.* **2018**, *8*, 13103.
12. Cal, S.; López-Otín, C. ADAMTS proteases and cancer. *Matrix Biol.* **2015**, *44–46*, 77–85. [CrossRef]

13. Maniotis, A.J.; Folberg, R.; Hess, A.; Seftor, E.A.; Gardner, L.M.; Pe'er, J.; Trent, J.M.; Meltzer, P.S.; Hendrix, M.J. Vascular channel formation by human melanoma cells in vivo and in vitro: Vasculogenic mimicry. *Am. J. Pathol.* **1999**, *155*, 739–752. [CrossRef]
14. Kirschmann, D.A.; Seftor, E.A.; Hardy, K.M.; Seftor, R.E.B.; Hendrix, M.J.C. Molecular pathways: Vasculogenic mimicry in tumor cells: Diagnostic and therapeutic implications. *Clin. Cancer Res.* **2012**, *18*, 2726–2732. [CrossRef] [PubMed]
15. Seftor, R.E.B.; Seftor, E.A.; Koshikawa, N.; Meltzer, P.S.; Gardner, L.M.G.; Bilban, M.; Stetler-Stevenson, W.G.; Quaranta, V.; Hendrix, M.J.C. Cooperative interactions of laminin 5 γ2 chain, matrix metalloproteinase-2, and membrane type-1-matrix/metalloproteinase are required for mimicry of embryonic vasculogenesis by aggressive melanoma. *Cancer Res.* **2001**, *61*, 6322–6327. [PubMed]
16. Poltavets, V.; Kochetkova, M.; Pitson, S.M.; Samuel, M.S. The Role of the Extracellular Matrix and Its Molecular and Cellular Regulators in Cancer Cell Plasticity. *Front. Oncol.* **2018**, *8*, 431. [CrossRef]
17. Castet, F.; Garcia-Mulero, S.; Sanz-Pamplona, R.; Cuellar, A.; Casanovas, O.; Caminal, J.; Piulats, J. Uveal Melanoma, Angiogenesis and Immunotherapy, Is There Any Hope? *Cancers* **2019**, *11*, 834. [CrossRef]
18. Folberg, R.; Arbieva, Z.; Moses, J.; Hayee, A.; Sandal, T.; Kadkol, S.H.; Lin, A.Y.; Valyi-Nagy, K.; Setty, S.; Leach, L.; et al. Tumor cell plasticity in uveal melanoma: Microenvironment directed dampening of the invasive and metastatic genotype and phenotype accompanies the generation of vasculogenic mimicry patterns. *Am. J. Pathol.* **2006**, *169*, 1376–1389. [CrossRef]
19. Benton, G.; Arnaoutova, I.; George, J.; Kleinman, H.K.; Koblinski, J. Matrigel: From discovery and ECM mimicry to assays and models for cancer research. *Adv. Drug Deliv. Rev.* **2014**, *79*, 3–18. [CrossRef]
20. Delgado-Bellido, D.; Serrano-Saenz, S.; Fernández-Cortés, M.; Oliver, F.J. Vasculogenic mimicry signaling revisited: Focus on non-vascular VE-cadherin. *Mol. Cancer* **2017**, *16*, 65. [CrossRef]
21. Hendrix, M.J.C.; Seftor, E.A.; Hess, A.R.; Seftor, R.E.B. Vasculogenic mimicry and tumour-cell plasticity: Lessons from melanoma. *Nat. Rev. Cancer* **2003**, *3*, 411–421. [CrossRef] [PubMed]
22. Fridman, R.; Benton, G.; Aranoutova, I.; Kleinman, H.K.; Bonfil, R.D. Increased initiation and growth of tumor cell lines, cancer stem cells and biopsy material in mice using basement membrane matrix protein (Cultrex or Matrigel) co-injection. *Nat. Protoc.* **2012**, *7*, 1138–1144. [CrossRef] [PubMed]
23. Puchalapalli, M.; Zeng, X.; Mu, L.; Anderson, A.; Hix Glickman, L.; Zhang, M.; Sayyad, M.R.; Mosticone Wangensteen, S.; Clevenger, C.V.; Koblinski, J.E. NSG Mice Provide a Better Spontaneous Model of Breast Cancer Metastasis than Athymic (Nude) Mice. *PLoS ONE* **2016**, *11*, e0163521. [CrossRef] [PubMed]
24. Rodríguez-Manzaneque, J.C.; Fernández-Rodríguez, R.; Rodríguez-Baena, F.J.; Iruela-Arispe, M.L. ADAMTS proteases in vascular biology. *Matrix Biol.* **2015**, *44-46C*, 38–45. [CrossRef] [PubMed]
25. Hess, A.R.; Seftor, E.A.; Gruman, L.M.; Kinch, M.S.; Seftor, R.E.B.; Hendrix, M.J.C. VE-cadherin regulates EphA2 in aggressive melanoma cells through a novel signaling pathway: Implications for vasculogenic mimicry. *Cancer Biol. Ther.* **2006**, *5*, 228–233. [CrossRef] [PubMed]
26. Delgado-Bellido, D.; Fernández-Cortés, M.; Rodríguez, M.I.; Serrano-Sáenz, S.; Carracedo, A.; Garcia-Diaz, A.; Oliver, F.J. VE-cadherin promotes vasculogenic mimicry by modulating kaiso-dependent gene expression. *Cell Death Differ.* **2019**, *26*, 348–361. [CrossRef] [PubMed]
27. Hendrix, M.J.C.; Seftor, E.A.; Meltzer, P.S.; Gardner, L.M.G.; Hess, A.R.; Kirschmann, D.A.; Schatteman, G.C.; Seftor, R.E.B. Expression and functional significance of VE-cadherin in aggressive human melanoma cells: Role in vasculogenic mimicry. *Proc. Natl. Acad. Sci. USA* **2001**, *98*, 8018–8023. [CrossRef]
28. Robertson, A.G.; Shih, J.; Yau, C.; Gibb, E.A.; Oba, J.; Mungall, K.L.; Hess, J.M.; Uzunangelov, V.; Walter, V.; Danilova, L.; et al. Integrative Analysis Identifies Four Molecular and Clinical Subsets in Uveal Melanoma. *Cancer Cell* **2017**, *32*, 204–220.e15. [CrossRef]
29. Seftor, E.A.; Meltzer, P.S.; Kirschmann, D.A.; Pe'er, J.; Maniotis, A.J.; Trent, J.M.; Folberg, R.; Hendrix, M.J.C. Molecular determinants of human uveal melanoma invasion and metastasis. *Clin. Exp. Metastasis* **2002**, *19*, 233–246. [CrossRef]
30. Yao, X.; Ping, Y.; Liu, Y.; Chen, K.; Yoshimura, T.; Liu, M.; Gong, W.; Chen, C.; Niu, Q.; Guo, D.; et al. Vascular endothelial growth factor receptor 2 (VEGFR-2) plays a key role in vasculogenic mimicry formation, neovascularization and tumor initiation by Glioma stem-like cells. *PLoS ONE* **2013**, *8*, e57188. [CrossRef]
31. Coussens, L.M.; Fingleton, B.; Matrisian, L.M. Matrix metalloproteinase inhibitors and cancer: Trials and tribulations. *Science* **2002**, *295*, 2387–2392. [CrossRef] [PubMed]

32. Joshi, P.; Kooshki, M.; Aldrich, W.; Varghai, D.; Zborowski, M.; Singh, A.D.; Triozzi, P.L. Expression of natural killer cell regulatory microRNA by uveal melanoma cancer stem cells. *Clin. Exp. Metastasis* **2016**, *33*, 829–838. [CrossRef] [PubMed]
33. Mao, X.G.; Xue, X.Y.; Wang, L.; Zhang, X.; Yan, M.; Tu, Y.Y.; Lin, W.; Jiang, X.F.; Ren, H.G.; Zhang, W.; et al. CDH5 is specifically activated in glioblastoma stemlike cells and contributes to vasculogenic mimicry induced by hypoxia. *Neuro. Oncol.* **2013**, *15*, 865–879. [CrossRef] [PubMed]
34. Lai, C.Y.; Schwartz, B.E.; Hsu, M.Y. CD133+ melanoma subpopulations contribute to perivascular niche morphogenesis and tumorigenicity through vasculogenic mimicry. *Cancer Res.* **2012**, *72*, 5111–5118. [CrossRef]
35. Frank, N.Y.; Schatton, T.; Kim, S.; Zhan, Q.; Wilson, B.J.; Ma, J.; Saab, K.R.; Osherov, V.; Widlund, H.R.; Gasser, M.; et al. VEGFR-1 expressed by malignant melanoma-initiating cells is required for tumor growth. *Cancer Res.* **2011**, *71*, 1474–1485. [CrossRef]
36. Peris-Torres, C.; Serrano, O.; del Carmen Plaza-Calonge, M.; Rodríguez-Manzaneque, J.C. Inhibition of *ADAMTS1* Expression by Lentiviral CRISPR/Cas9 Gene Editing Technology. In *Methods in Molecular Biology*; Humana Press Inc.: New York, NY, USA, 2020; Volume 2043, pp. 13–24.
37. Bueno, C.; Montes, R.; Melen, G.J.; Ramos-Mejia, V.; Real, P.J.; Ayllón, V.; Sanchez, L.; Ligero, G.; Gutierrez-Aranda, I.; Fernández, A.F.; et al. A human ESC model for MLL-AF4 leukemic fusion gene reveals an impaired early hematopoietic-endothelial specification. *Cell Res.* **2012**, *22*, 986–1002. [CrossRef]
38. Canals, F.; Colomé, N.; Ferrer, C.; del Carmen Plaza-Calonge, M.; Rodríguez-Manzaneque, J.C. Identification of substrates of the extracellular protease *ADAMTS1* by DIGE proteomic analysis. *Proteomics* **2006**, *6*, S28–S35. [CrossRef]
39. Barrett, T.; Wilhite, S.E.; Ledoux, P.; Evangelista, C.; Kim, I.F.; Tomashevsky, M.; Marshall, K.A.; Phillippy, K.H.; Sherman, P.M.; Holko, M.; et al. NCBI GEO: Archive for functional genomics data sets—Update. *Nucleic Acids Res.* **2013**, *41*, D991–D995. [CrossRef]
40. Ritchie, M.E.; Phipson, B.; Wu, D.; Hu, Y.; Law, C.W.; Shi, W.; Smyth, G.K. limma powers differential expression analyses for RNA-sequencing and microarray studies. *Nucleic Acids Res.* **2015**, *43*, e47. [CrossRef]
41. Yu, G.; Wang, L.G.; Han, Y.; He, Q.Y. ClusterProfiler: An R package for comparing biological themes among gene clusters. *Omi. A J. Integr. Biol.* **2012**, *16*, 284–287. [CrossRef]
42. Supek, F.; Bošnjak, M.; Škunca, N.; Šmuc, T. REVIGO Summarizes and Visualizes Long Lists of Gene Ontology Terms. *PLoS ONE* **2011**, *6*, e21800. [CrossRef] [PubMed]
43. Grossman, R.L.; Heath, A.P.; Ferretti, V.; Varmus, H.E.; Lowy, D.R.; Kibbe, W.A.; Staudt, L.M. Toward a Shared Vision for Cancer Genomic Data. *N. Engl. J. Med.* **2016**, *375*, 1109–1112. [CrossRef] [PubMed]
44. Goldman, M.; Craft, B.; Hastie, M.; Repečka, K.; McDade, F.; Kamath, A.; Banerjee, A.; Luo, Y.; Rogers, D.; Brooks, A.N.; et al. The UCSC Xena platform for public and private cancer genomics data visualization and interpretation. *bioRxiv* **2019**, 326470.
45. Gao, J.; Aksoy, B.A.; Dogrusoz, U.; Dresdner, G.; Gross, B.; Sumer, S.O.; Sun, Y.; Jacobsen, A.; Sinha, R.; Larsson, E.; et al. Integrative analysis of complex cancer genomics and clinical profiles using the cBioPortal. *Sci. Signal.* **2013**, *6*, l1. [CrossRef]
46. Cerami, E.; Gao, J.; Dogrusoz, U.; Gross, B.E.; Sumer, S.O.; Aksoy, B.A.; Jacobsen, A.; Byrne, C.J.; Heuer, M.L.; Larsson, E.; et al. The cBio cancer genomics portal: An open platform for exploring multidimensional cancer genomics data. *Cancer Discov.* **2012**, *2*, 401–404. [CrossRef]